

DESIGN AND SYNTHESIS OF INHIBITORS OF COLH AND LASB

Dissertation

Zur Erlangung des Grades des Doktors der Naturwissenschaften
der Naturwissenschaftlich-Technischen Fakultät
der Universität des Saarlandes

von

M.Sc. Cansu Kaya

Saarbrücken

2022

Tag des Kolloquiums: 4. Oktober 2022

Dekan: Prof. Dr. Jörn Eric Walter

Berichterstatter: Prof. Dr. Anna K.H. Hirsch
Prof. Dr. Claus-Michael Lehr
Prof. Dr. Ralph Holl

Akad. Mitglied: Dr. Matthias Engel

Vorsitz: Prof. Dr. Alexandra K. Kiemer

Die vorliegende Arbeit wurde von September 2017 bis März 2021 unter Anleitung von Univ.-Prof. Dr. Anna K. H. Hirsch in der Fachrichtung Pharmazeutische und Medizinische Chemie der Naturwissenschaftlich-Technischen Fakultät der Universität des Saarlandes sowie am Helmholtz-Institut für Pharmazeutische Forschung Saarland (HIPS) in der Abteilung Drug Design and Optimization (DDOP) angefertigt.

Empty Page

“I never promised you a rose garden. I never promised you perfect justice [...] and I never promised you peace or happiness. My help is so that you can be free to fight for all of those things. The only reality I offer is challenge and being well is being free to accept it or not at whatever level you are capable. I never promise lies, and the rose garden world of perfection is a lie... and a bore, too!”— Joanne Greenberg, *I Never Promised You a Rose Garden*¹

¹ *I Never Promised You a Rose Garden*, Joanne Greenberg, New American Library, Published in 1964.

Acknowledgements

First and foremost, I would like to express my sincere gratitude to my supervisor Prof. Dr. Anna K. H. Hirsch. I am very thankful for the opportunity that she has given me and her trust along the process. I feel privileged to know her not only as a scientist but also as an open-minded role model.

I would like to express my gratitude to my thesis committee members; Prof. Dr. Claus-Michael Lehr for his kind supervision and also for our nice collaboration in the biodynamers project. I am thankful to Matthias Engel, for the fruitful discussions we had and the support he gave during our committee meetings.

I would like to next thank Dr. Alexander Titz, Dr. Stefanie Wagner as well as current and past members of CBCH group: Dr. Matthew Calvert, Dr. Ghamdan Beshr, Dr. Eva Zahorska, Eike Siebs, Olga Metelkina, Patryca Mala, Varvara Varkova, Joscha Meiers, Saverio Minervini, Océane Monfret and Dirk Hauck for the nice environment we shared inside and outside the lab. I would like to also thank Dr. Martin Empting for the nice discussions and the rest of the Empting group; Ben Zoller and Dr. Philine Kirsch for their friendly company.

A special thanks goes to Dr. Mostafa Hamed without whom this thesis would not be complete. I am forever grateful for his inspiring patience and the kindness he spread full-heartedly in the lab. I would like to also thank Dr. Eleonora Diamanti, Dr. Ravindra Jumde and Dr. Walid Mohammad for providing a supportive environment in the lab and passing their knowledge graciously.

I was lucky to be a part of several interesting projects and these projects would not be successful without our collaborators whom I would like to acknowledge for all the fruitful discussions and thank for the great collaborative work: Dr. Jesko Köhnke and Dr. Asfandyar Sikandar and Dr. Sangeun Lee from HIPS, Prof. Dr. Hans Brandstetter and Dr. Ester Schönauer from University of Salzburg, Prof. Dr. Eugen Proschak and Prof. Dr. Thomas Wichelhaus and their team from University of Frankfurt.

Next, I would like to thank Dr. Jörg Hauptenthal and Dr. Andreas Kany for all the patience and support they provided me in both ColH and LasB projects. I would like to also thank my master student Tizian Rampsporth for his hard work and commitment to the ColH project. I would like to acknowledge all the current/past members of our project group; Dr. Isabell

Walter, Dr. Ravindra Jumde, Dr. Alexander Kiefer, Dr. Christian Schütz, Dr. Greta Bagnolini, Dr. Samir Yahiaoui, Dr. Ahmed Saad, Dr. Virgyl Camberlein, Andreas Klein, Khadidja Si Chaib, Roya Schafei, and Samira Speicher for the friendly environment and fruitful discussions.

A special thanks goes to Dr. Jelena Konstantinović, not only for being a supportive and an inspiring colleague but also for being a good friend along the way. I cannot express my gratitude to her with limited number of words. I am thankful for all of her support through thick and thin in these past years and for our friendship, which I cherish every day. Another special thanks goes to Alaa Alhayek for all her support in the last years not only in scientific context but also as a dear friend. I am grateful for our friendship and the memories we shared.

I would like to mention and thank all my fellow PhDs, whose presence has significantly shaped my journey in Saarbrücken. I would like to thank Federica Mancini for her sincere friendship from the first day I stepped into HIPS. We thought we would end up in Groningen, but I am glad we found each other in Saarbrücken – without her, this journey would be incomplete. I would like to thank Sandra Johannsen for being the single best partner in conferences and for creating the fondest memories of the last three years. I would like to thank Spyros Bousis for providing the ultimate fun whenever he is around and Dr. Henni Ropponen for her valuable friendship and inspiring resilience. Thanks to Dr. Serena Della Volpe for being the Jim to my Pam and for appreciating my sense of humor. Thanks to Yingwen Wu for her positive energy and friendly presence especially through the last period of my PhD. Finally, I would like to also mention and thank my other fellow DDOP- CBCH colleagues; Christina Kosch, Vlad Hapko, Zhoor Hamid, Francesco Fulco, Claudia Petruzzi, Vittoria Nanna, Melissa Guardigni, Anna Fontana, Nadia Varesano, Lara Rosenberger, Komal Daipule, Mario Szeles and Laura Lucaroni for all the joyful memories inside and outside the lab.

This acknowledgement would not be complete without mentioning the residents of Office 2.23. I am grateful that I had Dr. Christian Schütz as an office mate to share my nihilistic jokes while experiencing the ups and downs of doing a PhD. I also would like to thank Dr. Valentin Jakob and Robin Gierse for the warm and welcoming environment they provided in the office. I want to thank the most recent members of our office Daan Wilcox and Ioulia Exapicheidou for their friendly presence in my last days at the office.

I would like to acknowledge and thank other faces from HIPS: Dr. Teresa Röhrig and Dr.

Alwin Hartman from DDOP, Dr. Alexander Popoff and Sebastian Walesch from MINS. Thanks to Dr. Hanzey Yasar, Patrick Carius and Sara Nasr from DDEL department for the nice memories we shared outside the HIPS

A big thanks to our technicians Jeannine Jung, Simone Amann, Tabea Schramm, Dennis Jener and Selina Wolter for all their amazing work. I would like to also acknowledge and thank the other technical staff at HIPS; Frank Jakob, Christian Zeuner, Mark Caspari and Michael Roth and our past and present DDOP-office colleagues Julia Mohr, Lisa Andre, Annette Herkströter and Bahareh Kadkhodazadeh for providing solutions to the everyday problems and making life much easier.

Last but not least, I would like to thank all my friends outside HIPS, Rama Alhassan and Dr. Daisy Blijma, Sandra Lin and Ann Christine Lu for providing a fun and supportive social atmosphere outside work. I would like to also give a shout out my Turkish friends in Turkey and around Europe whose love and support I felt immensely. I also would like to thank Dr. Andreas Corcaci for proofreading my thesis.

Finally, I want to express my deepest gratitude for my family. I feel so lucky to have them and I am grateful for all the support and love they provided during this adventure. Canım ailem, sizleri çok seviyorum ve bana gösterdiğiniz koşulsuz sevgi ve destek ve için sizlere sonsuza dek minnettarım.

-In omnia paratus-

Summary

The rise of antimicrobial resistance presents a serious threat to the public health. Anti-virulence therapy offers an alternative route to combat resistance by reducing the selection pressure on bacteria.

Introduction part describes the recent developments in anti-virulence therapy and the role of proteases in drug discovery. It also overviews the three targets of focus and reports on their recently developed inhibitors.

In the first part, identification of a highly potent α -benzyl-*N*-aryl mercaptoacetamide class inhibitors of LasB from *Pseudomonas aeruginosa* is described. Further modifications of the benzyl group and replacement of the *N*-aryl ring with heterocycles yielded several hit structures. These inhibitors were evaluated *in vitro* and *in vivo* to validate the success of this class in reducing the pathogenicity of the bacteria.

In the next part, a low-micromolar fragment inhibitor of ColH from *Clostridium histolyticum* is identified by screening of a halogen-enriched fragment library. A novel binding mode is rationalized by a co-crystal structure and further synthetic efforts led to a 2-fold improvement in the inhibitory activity.

In the last part, a series of *N*-arylmercaptopropionamide derivatives was investigated as inhibitors of several Metallo-beta-lactamases. Discovery of a highly selective inhibitor demonstrated a strong synergistic effect with a β -lactam antibiotic and showed an *in vivo* effect in a *Galleria mellonella* infection model.

Zusammenfassung

Das Auftreten antibiotikaresistenter Krankheitserreger bedroht die öffentliche Gesundheit. Die Anti-Virulenz-Therapie ermöglicht die Bekämpfung von Resistenzen, indem sie den Selektionsdruck auf Bakterien verringert.

In der Einleitung werden die jüngsten Entwicklungen in der Anti-Virulenz-Therapie und die Rolle von Proteasen in der Arzneimittelentwicklung beschrieben, sowie die drei Zielmoleküle und ihre kürzlich entwickelten Hemmstoffe.

Im ersten Teil wird ein hochpotenter Inhibitor der α -Benzyl-N-Aryl-Mercaptoacetamid-Klasse von LasB aus *Pseudomonas aeruginosa* beschrieben. Modifikationen der Benzylgruppe und Ersatz des N-Arylrings durch Heterocyclen ergaben mehrere Trefferstrukturen. Diese Inhibitoren wurden *in vitro* und *in vivo* untersucht, um deren Erfolg in der Verringerung der Pathogenität der Bakterien zu bestätigen.

Im zweiten Teil wird ein niedrigmikromolarer Fragment-Inhibitor von ColH aus *Clostridium histolyticum* durch Screening einer halogenangereicherten Fragmentbibliothek identifiziert. Ein neuartiger Bindungsmodus wird durch seine ko-kristalline Struktur rationalisiert. Weitere Synthesen verbesserten die hemmende Aktivität um das 2-Fache.

Im letzten Teil wurden N-Arylmercaptopropionamid-Derivate als Inhibitoren verschiedener Metallo-beta-Lactamasen untersucht. Die Entdeckung eines hochselektiven Inhibitors zeigte eine starke synergistische Wirkung mit einem β -Lactam-Antibiotikum und eine *In-vivo*-Wirkung in einem *Galleria-mellonella*-Infektionsmodell.

Özet

Antibiyotiklere dirençli patojenlerin ortaya çıkması halk sağlığı açısından ciddi bir tehdit oluşturmaktadır. Anti-virulans tedavisi, bakteriler üzerindeki seçim baskısını azaltmak ve böylece direnci düşürmek için yeni bir yöntem olarak ortaya çıkmaktadır.

Bu tez, anti-virulans tedavisindeki son gelişmeleri ve proteazların ilaç keşfindeki rolünü açıklayarak başlamaktadır. Ayrıca, odaklanılan üç hedefe genel bir bakış sunmakta ve yakın zamanda geliştirilen inhibitörleri hakkında rapor vermektedir.

Ardından, LasB'nin oldukça güçlü α -benzil-N-aril merkaptosetamid sınıfı inhibitörlerinin tanımlanması anlatılmaktadır. Benzil grubunun daha ileri modifikasyonları ve N-aril halkasının heterosikllerle değiştirilmesi, bu sınıfın bakterilerin patojenitesini azaltmadaki başarısını doğrulamak için in vitro ve in vivo olarak değerlendirilen birkaç hit yapı vermiştir.

Bir sonraki bölümde, halojenle zenginleştirilmiş bir fragman kütüphanesinin taranması, eş-kristal yapısı ile rasyonelleştirilen yeni bir bağlanma modu ile ColH'nin düşük mikromolar fragman inhibitörünü vermiştir. Daha ileri sentetik çabalar, inhibitör aktivitede 2 kat iyileşmeye yol açmıştır.

Son bölümde, çeşitli Metallo-beta-laktamazların inhibitörleri olarak bir dizi N-arilmercaptopropionamid türevi açıklanmaktadır. Oldukça seçici bir inhibitörün keşfi, bir β -laktam antibiyotik ile güçlü bir sinerjik etki göstermiş ve bir *Galleria mellonella* enfeksiyon modelinde in vivo etki göstermiştir.

Publications Included in This Thesis

Publication 1: Kaya C., Hirsch Anna K. H. Targeting extracellular bacterial proteases for the development of novel antivirulence agents. *Chimia* 2022, 76, 402–408, DOI: 10.2533/chimia.2022.402.

Publication 2: Kaya C. *, Walter I. *, Yahiaoui S., Sikandar A., Alhayek A., Konstantinović J., Kany A. M., Hauptenthal J., Köhnke J., Hartmann R., Hirsch A.K.H. *Substrate-inspired Fragment Merging and Growing Affords Efficacious LasB Inhibitors*. *Angew. Chem. Int. Ed.* **2021**, e202112295, : doi.org/10.1002/anie.202112295.

*These authors contributed equally.

Publication 3: Kaya C., Walter I., Alhayek A., Shafiei R., Andreas A., Konstantinović J., Schönauer E., Sikandar A., Hauptenthal J., Brandstetter H., Müller R., Hartmann R. W., Hirsch A.K.H. *Structure-based Design of α -Substituted Mercaptoacetamides as Inhibitors of the Virulence Factor LasB from *P. aeruginosa**. *ACS Infectious Diseases* 2022 8 (5), 1010–1021 DOI: 10.1021/acsinfecdis.1c00628.

Publication 4: Kaya C., Konstantinović J., Kany A.M., Andreas A., Kramer J., Brunst S., Weizel L., Rotter M.J., Frank D., Yahiaoui S., Müller R., Hartmann R.W., Hauptenthal J., Proschak E., Wichelhaus T., Hirsch A.K. *N-Aryl mercaptopropionamides as broad-spectrum inhibitors of metallo-beta-lactamases*. *J. Med. Chem.* 2022, 65, 5, 3913–3922, <https://doi.org/10.1021/acs.jmedchem.1c01755>

Publication 5: Kaya C. Ramsforth T., Schönauer E., Brandstatter H. Hauptenthal J., Hirsch A.K.H. *Fragment-based Design and Synthesis of Inhibitors of Collaganase H(ColH)*. **Manuscript in preparation.**

Publications of the Author Which Are Not Included in This Thesis

Lee S., Kaya C., Jang H., Koch M., Loretz B., Bühler E., Lehr C.M, Hirsch A.K.H. pH-Dependent Morphology and Optical Properties of Lysine-Derived Molecular Biodynamer *Mater. Chem. Front.* (2020), 4, 905–909.

Lee S., Nasr S., Hartwig O., Boes A., Kaya C., Koc M., Loretz B., Buhler E., Hirsch A.K.H., Lehr C.M. Dynaplexes, a new class of pH-responsive dynamic proteoid nanoparticles for safe and efficient mRNA transfection. **Manuscript Submitted.**

Contribution Reports

Publication 2: Substrate-Inspired Fragment Merging and Growing Affords Efficacious LasB Inhibitors

Cansu Kaya*, Isabell Walter*, Samir Yahiaoui, Asfandyar Sikandar, Alaa Alhayek, Jelena Konstantinović, Andreas M. Kany, Jörg Haupenthal, Jesko Köhnke, Rolf W. Hartmann, Anna K. H. Hirsch.

*These authors contributed equally.

Angew. Chemie Int. Ed. **2021**. <https://doi.org/10.1002/anie.202112295>

Contribution: A. M. K., I. W., R. W. H., and A. K. H. H. conceived the study. A. K. H. H. coordinated the study. C. K., I.W., S. Y. and J.K. designed and synthesized the compounds. Jesko K. and A. S. expressed and purified LasB, solved the X-ray crystal structure of one of the compounds. J. K. performed the *in vitro* peptidolytic assay on LasB of *Pseudomonas aeruginosa*. A. A. performed the *in vivo* *Galleria Mellonella* assay. J. H. coordinated the *in vitro* off-target and toxicity evaluation. C. K., A. S. and A. A. prepared the figures in the manuscript. C.K wrote the manuscript together with I.W., who contributed equally. All authors reviewed the results and approved the final version of the manuscript.

Author	Signature
Cansu Kaya	
Isabell Walter	
Samir Yahiaoui	
Asfandyar Sikandar	
Alaa Alhayek	
Jelena Konstantinović	

Andreas M. Kany



29/04/2022

Jörg Haupenthal



Jesko Köhnke



Rolf Hartmann



Anna K. H. Hirsch



Publication 3: Structure-Based Design of α -Substituted Mercaptoacetamides as Inhibitors of the Virulence Factor LasB from *Pseudomonas aeruginosa*

Cansu Kaya, Isabell Walter, Alaa Alhayek, Roya Shafiei, Gwenaëlle Jézéquel, Anastasia Andreas, Jelena Konstantinović, Esther Schönauer, Asfandyar Sikandar, Jörg Haupenthal, Rolf Müller, Hans Brandstetter, Rolf W. Hartmann, Anna K.H. Hirsch

ACS Infectious Diseases 2022 8 (5), 1010–1021 DOI: 10.1021/acscinfecdis.1c00628.

Contribution: R. W. H., and A. K. H. H. conceived the study. A. K. H. H. coordinated the study. C. K., I.W. and G. J. designed and synthesized the compounds. J. K. tested the compounds in in vitro LasB assay. A. S. expressed and purified the LasB. J. H. coordinated the *in vitro* off-target and toxicity evaluation of the compounds. Al. A. and R.S. performed the validation experiments and Al. A performed *Galleria Mellonella* assay. A. A. performed *in vivo* zebrafish embryo toxicity assay under supervision of R. M. C. K. and Al. A. prepared the figures in the manuscript. E.S. performed ColH inhibition assay on selected compounds under supervision of H.B. C.K. performed the docking studies and wrote the manuscript. All authors reviewed the results and approved the final version of the manuscript.

Author	Signature
Cansu Kaya	
Isabell Walter	11.05.2022 
Alaa Alhayek	
Roya Shafiei	
Gwenaëlle Jézéquel	
Anastasia Andreas	

Jelena Konstantinović

Jelena Konstantinović

Esther Schönauer

Esther Schönauer

Asfandyar Sikandar

Asfandyar Sikandar

Jörg Haupenthal

Jörg Haupenthal

Rolf Müller

Rolf Müller

Hans Brandstetter

Hans Brandstetter

Rolf W. Hartmann

Rolf W. Hartmann

Anna K. H. Hirsch

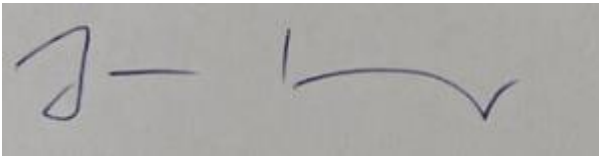
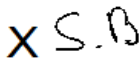
Anna K. H. Hirsch

Publication 4: *N*-Aryl Mercaptopropionamides as Broad-Spectrum Inhibitors of Metallo- β -Lactamases

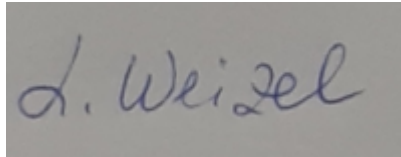
Cansu Kaya, Jelena Konstantinović, Andreas M. Kany, Anastasia Andreas, Jan S. Kramer, Steffen Brunst, Lilia Weizel, Marco J. Rotter, Denia Frank, Samir Yahiaoui, Rolf Müller, Rolf W. Hartmann, Jörg Hauptenthal, Ewgenij Proschak, Thomas A. Wichelhaus, and Anna K. H. Hirsch

J. Med. Chem. 2022, 65, 5, 3913–3922, <https://doi.org/10.1021/acs.jmedchem.1c01755>.

Contribution: A. M. K., S.Y. E.P., R. W. H., and A. K. H. H. conceived the study. A. K. H. H. coordinated the study. C. K., A. M. K. and J. K. designed and synthesized the compounds. J.S.K and S.B. expressed and purified MBLs. L.W. performed the MBL activity assay. M. J. R. synthesized the fluorogenic MBL substrate. E.P. performed molecular modelling studies. D. F. and T.A.W. performed MIC and checkerboard assays as well as time-kill kinetics and *Galleria mellonella* infection model assay. J. H. coordinated the *in vitro* off-target and toxicity evaluation of the compounds. A. A. performed *in vivo* zebrafish toxicity assay under supervision of R. M. C. K., E.P. and T. A. W. prepared the figures in the manuscript. C.K wrote the manuscript. All authors reviewed the results and approved the final version of the manuscript.

Author	Signature
Cansu Kaya	
Jelena Konstantinović	Jelena Konstantinović
Andreas M. Kany	
Anastasia Andreas	
Jan S. Kramer	
Steffen Brunst	 _____ Steffen Brunst

Lilia Weizel



Marco J. Rotter



Denia Frank



Samir Yahiaoui



Rolf Müller



Rolf W. Hartmann



Jörg Haupenthal



Ewgenij Proschak



Thomas A. Wichelhaus



Anna K. H. Hirsch



Abbreviations

SAR	Structure-Activity relationship
TSA	Thermal Shift Assay
MST	Microscale Thermophoresis
ACE	angiotensin-converting enzyme
FDA	Food and Drug Administration
WHO	World Health Organization
CF	cystic fibrosis
eDNA	extracellular DNA
QS	quorum sensing
NDK	nucleoside diphosphate kinase
GTP	guanosine triphosphate
His	histidine
Glu	glutamic acid
Tyr	tyrosine
Gly	glycine
Da	Dalton
EDTA	ethylenediaminetetraacetic acid
CADD	computer assisted drug design
MMPs	matrix metalloprotease
ECM	extracellular matrix
ColG	Collagenase G
ColH	Collagenase H

PBPs	penicillin binding proteins
MDR	Multi-drug resistant
SBLs	serine beta-lactamases
MBLs	Metallo-beta-lactamases
TACE	Tumor necrosis factor- α -converting enzyme
HTS	High-throughput screening
FBDD	Fragment-based drug design
HeFLib	Halogen-enriched fragment library
DSC	Differential scanning calorimetry
T_m	Melting temperature
LD ₅₀	Lethal dose
MST	Microscale Thermophoresis
K_D	Binding constant

Table of Contents

Acknowledgements	vi
Summary.....	ix
Zusammenfassung	x
Özet.....	xi
Publications Included in This Thesis	xii
Publications of the Author Which Are Not Included in This Thesis	xii
Contribution Reports.....	xiii
Abbreviations	xix
Table of Contents	xxi
Chapter 1: Introduction	22
1.1 Targeting Extracellular Bacterial Proteases for the Development of Novel Antivirulence Agents	22
1.2 Aims of the Thesis	30
Chapter 2: Results.....	31
2.1 Substrate-Inspired Fragment Merging and Growing Affords Efficacious LasB inhibitors.....	31
2.2 Structure-Based Design of α -Substituted Mercaptoacetamides as Inhibitors of the Virulence Factor LasB from <i>Pseudomonas aeruginosa</i>	59
2.3 Fragment-Based Design and Synthesis of Inhibitors of ColH	105
2.3.1 Introduction	105
2.3.2 Results and Discussion	106
2.3.3 Experimental Section	113
2.3.4 Conclusions.....	129
2.3.5 Supporting Information	130
2.4 <i>N</i> -Aryl Mercaptopropionamides as Broad-Spectrum Inhibitors of Metallo- β - Lactamases.....	136
Chapter 3: Concluding Remarks and Outlook	169
References.....	175
Appendix: Conference Contributions	178

Chapter 1: Introduction

1.1 Targeting Extracellular Bacterial Proteases for the Development of Novel Antivirulence Agents

Cansu Kaya, Anna K.H. Hirsch

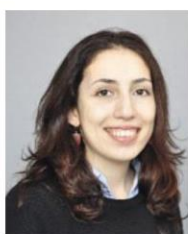
Chimia, 76 (2022) 402–408, DOI: 10.2533/chimia.2022.402.

Targeting Extracellular Bacterial Proteases for the Development of Novel Antivirulence Agents

Cansu Kaya and Anna K. H. Hirsch*

Abstract: As resistance to clinically available antibiotics persistently increases, applying new strategies to target pathogenic bacteria are paramount to design effective drugs. Bacterial proteases play vital roles in cell viability and stress response, contributing to the pathogenicity of the resistant bacteria. Targeting these extracellular enzymes by antivirulence therapy is a prominent strategy in combating multi-drug resistant bacteria. By preventing the colonization and infiltration of the host, this method can lower the selection pressure and reduce resistance development significantly. Here, we review the role of bacterial proteases, the rise of antivirulence therapy and we report on the development of novel antivirulence agents targeting two key virulence factors: elastase B (LasB) from *Pseudomonas aeruginosa* and collagenase H (ColH) from *Clostridium histolyticum*.

Keywords: Anti-virulence therapy · Collagenase · Elastase · Proteases



Cansu Kaya studied chemistry at Bilkent University, Ankara, Turkey, where she also obtained her MSci in Chemistry. She joined Prof. Anna Hirsch's laboratory as a PhD Student in 2017 at the Helmholtz Institute for Pharmaceutical Research Saarland, University of Saarland, where she worked on the design and synthesis of novel antivirulence agents against multi-resistant bacteria. Cansu is currently working as an

Associate Publishing Editor at Springer Nature.



Prof. Anna K. H. Hirsch obtained her MSci from the University of Cambridge and her PhD from the ETH Zurich in 2008 under the supervision of Prof. F. Diederich. After a postdoc in Prof. J.-M. Lehn's group, she became assistant professor at the University of Groningen in 2010 and associate professor in 2015. In 2017, she became head of the department 'Drug Design and Optimization' at the Helmholtz

Institute for Pharmaceutical Research Saarland (HIPS) and full professor at Saarland University. She focuses on target-based anti-infective drug discovery, recognized by numerous prizes such as the Innovation Prize for Medicinal Chemistry of the GdCh/DPhG.

1. Introduction: The Role of Proteases in Drug Discovery

Proteases are important signaling enzymes catalyzing the breakdown of proteins by hydrolyzing peptide bonds.^[1] They control numerous key physiological processes such as cell-cycle progression, cell proliferation, cell death and DNA replication as well as processing of hormones and biologically active peptides. They are able to cleave protein substrates either from the N or C termini (aminopeptidases and carboxypeptidases,

respectively) and/or in the middle of the molecule (endopeptidases).^[2]

Fig. 1 illustrates the substrate binding to a protease where the structure of the active site of the protease determines the substrate specificity.^[3,4]

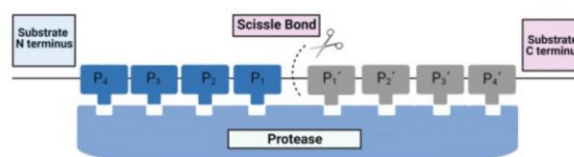


Fig. 1. Schematic representation of the substrate cleavage sites in proteases. Non-primed binding sites are located toward the N terminus, whereas the primed binding sites are toward the C terminus. The figure was adapted from Schechter and Berger and recreated by BioRender.com.^[3]

A great variety of proteases exists that differ in size and structural composition.^[5] Based on their mechanism of catalysis, proteases are classified into six classes; aspartic, glutamic, cysteine, serine and threonine proteases, as well as metalloproteases.^[6] For cysteine, serine and threonine, catalysis involves formation of an acyl-enzyme complex followed by the release of both carboxylate and amine products.^[3] In the case of aspartic, glutamic and metalloproteases, an activated water molecule acts as a nucleophile and attacks a carbonyl group to hydrolyze the peptide substrate.^[7]

As a result of their crucial roles in almost all important biological pathways, proteases constitute attractive target proteins for the treatment of various diseases.^[1] The common strategy for targeting proteases is to identify the active site and to design inhibitors that are able to block it.^[7] Most of the proteases are sequence-specific and therefore, the designed active structures mimic the transition state of the substrate, assuring not to be processed by the enzyme.^[8,9]

*Correspondence: Prof. A. K. H. Hirsch, E-mail: anna.hirsch@helmholtz-hips.de, Helmholtz Institute for Pharmaceutical Research, University of Saarland, Campus E8.1, 66123, Saarbrücken, Germany

Designing inhibitors with selectivity toward a single protease can be challenging if the targeted protease shares a similar catalytic mechanism and substrate specificity with other proteases, but is functionally completely different.^[10] For the discovery of selective protease inhibitors, alternative methods like structure-based drug design or targeting allosteric binding sites are also applied.^[11,12]

There are many successful protease inhibitors on the market (Fig. 2), for the treatment of various diseases such as angiotensin-converting enzyme (ACE) inhibitors (e.g. captopril, **1**)^[11] used for hypertension, and thrombin (serine) protease inhibitors for treating blood coagulation (e.g. dabigatran, **2**).^[13] Clinically approved protease inhibitors are also used for the treatment of diseases caused by viruses like HIV (e.g. ritonavir, **3**)^[6] or hepatitis C.^[14,15]

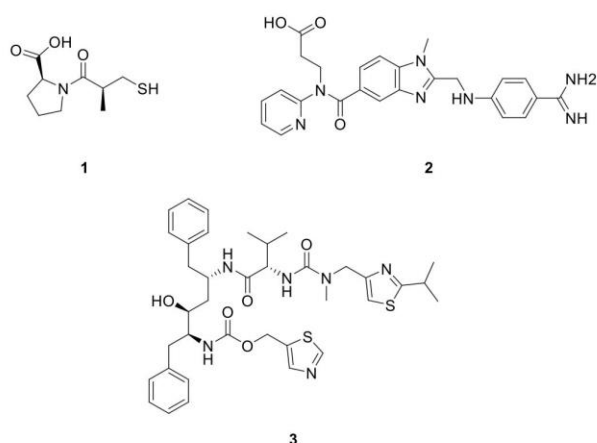


Fig. 2. Structures of the protease inhibitors in clinical use: captopril **1**,^[11] dabigatran **2**,^[13] and ritonavir **3**.^[6]

Considering their versatile functions and the threat imposed by antibiotic-resistant bacteria, proteases are promising targets to develop new antibacterial agents.^[6] Here, we focus on two exemplary ones from a representative Gram-negative and -positive pathogen, namely LasB from *Pseudomonas aeruginosa* and ColH from *Clostridium histolyticum*.

2. Antibiotic Resistance and Antivirulence Therapy

The discovery of antibiotics, starting with penicillin, has saved millions of lives during the 20th century.^[16–18] The term ‘antibiotic’ initially referred to the natural secondary metabolites that were able to inhibit the growth of microorganisms.^[17] Later, its context has been extended to synthetic and semi-synthetic antibacterial agents.^[17] Antibiotics were not only successful in treating serious infections but also played pivotal roles in decreasing morbidity and increasing life expectancy.^[19,20]

As early as the late 1930s, starting with resistance toward sulfonamides, antibiotic-resistant bacteria emerged as a serious threat for the treatment of bacterial infections.^[16] Addition of new classes of antibiotics to the market was not successful in solving this problem as resistance has developed in all cases regardless of the chemical classes that were introduced over the years.^[19,21]

Factors like patient compliance, i.e. stopping the treatment too early or overprescription of antibiotics can activate mutations or gene transfer among bacteria for developing resistance.^[20,22] Moreover, the excessive use of antibiotics in livestock kills the susceptible bacteria causing the rise of more resistant strains.^[16] These strains are transferred to humans by the food supply, leading to serious infections.^[16] All these aspects contribute to the evolution of different ways to maintain or develop resistance.^[23,24]

Several bacteria that are insensitive to multiple drugs have been listed as critical pathogens on the WHO priority list, as they pose a serious threat, especially for immune-compromised patients.^[21,25,26] These are not only responsible for the great share of nosocomial infections but they also represent a reference for possible resistance mechanisms.^[27] Among these pathogens, Gram-negative bacteria such as *P. aeruginosa* and *Acinetobacter baumannii* have been under a special focus since the permeability issues associated with the Gram-negative cell wall represent a particular challenge.^[25,27,28]

In contrast to the rapid emergence of resistant strains witnessed over the past decade, the translation of antibiotics with novel mode of action into clinical practice has not been efficient.^[21,29–31] The efforts for developing novel antibiotics have decreased significantly with most of the newly approved drugs being derivatives of existing classes.^[19] As the current antibiotics target mainly the vital functions in bacteria, this results in a high selection pressure, facilitating more resistance.^[32]

Due to all aforementioned reasons, a ‘post-antibiotic era’ is on the horizon, where the treatment options for many bacterial infections are highly limited.^[33] To combat this issue, an innovative approach should be taken, which requires not only a strong oversight of currently developed drugs but also a consideration of alternative strategies to treat infections.

Antivirulence therapy has emerged as such an alternative strategy, which aims to disarm the bacteria by inhibiting their virulence factors.^[34–36] This method, with a novel mode of action, aims to reduce and reverse the selective pressure, leading to a significant decrease in bacterial resistance (Fig. 3).^[37,38]

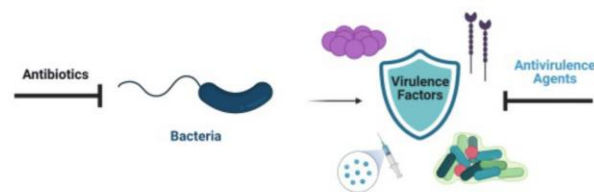


Fig. 3. Schematic representation of the mode of action of conventional antibiotics versus inhibition of virulence factors by antivirulence agents. The figure was adapted from Heras *et al.* and created with Biorender.com.^[40]

Virulence factors are produced by bacteria in order to invade the host cell and to evade the host-immune system.^[33] These include proteases, adhesins, regulators, toxins and siderophores.^[37,39,40] The purpose of targeting virulence factors with so-called ‘pathoblockers’ is to reduce the pathogenicity, thereby enabling the cellular immune response of the host cell to eliminate the bacteria.^[34] This concept is also successful for a vast number of other potential drug targets like key components of quorum-sensing (QS) networks.^[41] Contrary to traditional antibiotics, potential antivirulence drugs can lead to a more effective use of the antibiotics and preserve the host commensal flora.^[42]

Given that each bacterium has its own unique virulence mechanisms, it is likely that the developed antivirulence drugs have a narrow spectrum, which might potentially be a setback.^[40] Furthermore, whether a virulence factor is beneficial for the bacteria or not plays a substantial role in the development of resistance to antivirulence drugs, i.e. the selection of the right target in combination with the right treatment is important for maintaining the efficacy of these drugs.^[43]

The use of antivirulence drugs is in slow progress as most of them are still in pre-clinical development and only a few have made it to the clinic.^[34] Some of these FDA-approved inhibitors

are targeting immunoglobulins.^[34,44] One recent example reaching the market is the antibody drug bezlotoxumab used as a toxin B neutralizer in the treatment of *C. difficile* infections.^[45]

The lack of clinically approved small-molecule drugs proves the urgent need for designing novel inhibitors of virulence factors secreted by pathogenic bacteria. In view of this, zinc-containing metalloproteases, present both in Gram-negative and Gram-positive organisms, have emerged for designing successful inhibitor profiles.^[46]

2.1 *Pseudomonas aeruginosa*

Pseudomonas aeruginosa is an opportunistic Gram-negative bacterium, frequently involved in chronic infections of immunosuppressed patients.^[47] It can be isolated from numerous environments including soil, plants and mammalian tissue.^[48] The World Health Organization (WHO) places carbapenem-resistant *P. aeruginosa* among the most critical pathogens as it is responsible for 10% of hospital-acquired infections, and has a frequent occurrence among cystic-fibrosis (CF) patients.^[26,49,50] It is also responsible for urinary-tract, cornea and wound infections especially in patients with predisposing factors.^[51]

Various mechanisms of resistance are reported for *P. aeruginosa*, including target mutations, disabling compound efflux and inactivation of β -lactam antibiotics by β -lactamases.^[52–55] Another important factor contributing to resistance is the formation of biofilms.^[38,56] Biofilms consist of different components such as extracellular proteins, polysaccharides and extracellular DNA (eDNA) that constitute an effective protection against the host-immune response.^[57–59] *P. aeruginosa* uses QS mechanisms, some of which are partially responsible for the formation and maturation of these biofilms.^[38,58] QS allows bacteria to communicate and coordinate, which adds up to the bacterial infection progress.^[60] Formation of biofilms further favors the adherence to medical devices leading to the rise of nosocomial infections.^[61] It has also been demonstrated that biofilm-like microcolonies are formed in the lungs of CF patients by *P. aeruginosa* exacerbating the effect of infection.^[62,63]

P. aeruginosa produces numerous virulence factors responsible for its pathogenicity.^[51] These can be distinguished by their location either as cell-associated virulence factors, *i.e.* lectins, flagella and biofilms or extracellular virulence factors such as proteases, hemolysins, cytotoxin or pyocyanin.^[62] Cell-associated virulence factors play a crucial role in adhesion and colonization of the bacteria.^[63] For example, lectin inhibitors hinder host-cell invasion and in particular biofilm formation.^[64] As presented previously, quorum sensing is a way for bacteria to manipulate the host immune response by regulation of virulence factors.^[65] Although targeting this network represents a challenge due to the intracellular nature of the QS cascade, recent progress on targeting its key elements, namely the las, rhl and pqs systems, yielded successful inhibitors with favorable pharmacokinetic properties for pulmonary application.^[66–68]

Consequently, extracellular virulence factors represent more attractive targets, as there is no need for crossing the Gram-negative cell wall, which is a highly challenging task due to the presence of two membranes.^[38] Elastases belonging to the protease family are such extracellular targets playing a pivotal role in invasion and evasion of the host immune response, leading to a faster disease progression.^[69–71]

2.2 Elastase (LasB)

LasB is a zinc metalloprotease secreted by *P. aeruginosa*.^[72] Also known as pseudolysin, LasB is encoded by the *lasB* gene and has a mature mass of 33 kDa.^[73,74] The N-terminal domain of the protease consists of antiparallel β -strands, whereas the C-terminal part is predominantly α -helical. The active site is located in between these two domains (Fig. 4).^[75] The overall tertiary structure

of LasB is highly similar to thermolysin from *Bacillus thermoproteolyticus*, which makes it a part of the thermolysin family of enzymes.^[76,77] Accordingly, conserved binding site residues are zinc-coordinating His-140, His-144, and Glu-164, as well as Glu-141, Tyr-155 and His-223.^[76]

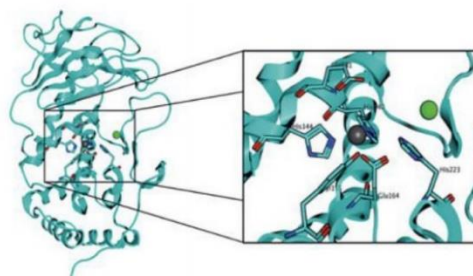


Fig. 4. Apo structure of LasB (PDB code : 1EZM) shown in standard orientation.^[75]

Target-validation experiments have demonstrated LasB as the most abundant extracellular enzyme present in *P. aeruginosa* supernatant with the highest endopeptidase activity, therefore making it a critical anti-infective target.^[78,79] LasB is able to degrade elastin, fibrin and collagen, which are important components of tissue cells and blood vessels, facilitating host colonization.^[72] Moreover, it can degrade surfactant proteins in the lung and it is also involved in the inactivation of human immunoglobulins A and G, cytokines gamma-interferon and tumor necrosis factor alpha.^[80–85]

In addition to these mechanisms of evading host immune response, LasB is also a central player in the formation of biofilms.^[86,87] To date, two mechanisms have been reported for the formation of biofilms that are regulated by LasB.^[86,88] The first one describes a mechanism where LasB activates nucleoside diphosphate kinase (NDK), an enzyme generating guanosine triphosphate (GTP) for the formation of alginate, which is a crucial constituent of the biofilm. The other mechanism is related to the rhamnolipid-regulated biofilm formation, which is controlled by the *lasB* gene. Once they are formed, biofilms are highly resistant to immune response and antibiotics, creating an inflammatory response, which maintains the infection.^[86] Last but not least, LasB is also widely recognized as the key virulence factor in the development of chronic infections in CF patients.^[89]

P. aeruginosa secretes several other proteases, which are also responsible for the infection progress. Aeruginolysin, for example, can also contribute to tissue degradation but the proteolytic capacity of this enzyme is low compared to LasB.^[90,91] LasA, another zinc-metalloprotease secreted by these bacteria with an elastolytic activity, makes elastin tissue more susceptible to LasB by breaking Gly–Gly bonds.^[92,93]

All the aforementioned features of LasB make it an attractive anti-infective drug target, which is attracting more and more attention nowadays.^[94]

2.3 Inhibitors of Elastase (LasB)

As a common trend for all zinc-containing enzymes, most of the inhibitors of LasB contain metal chelators.^[95] In addition to known inhibitors such as ethylenediaminetetraacetic acid (EDTA) and phenanthroline, other chemical classes such as hydroxamates and thiols have also emerged as potent inhibitors of LasB.^[72,96,97]

Cathcart *et al.* demonstrated that P1' amino acid residues in the active site of LasB are responsible for recognition of inhibitors

with a preference for nonpolar and aromatic amino acids.^[68] This observation led to the thiol compound **4** (Fig. 5), which was able to reduce *P. aeruginosa*-induced biofilm formation.^[98]

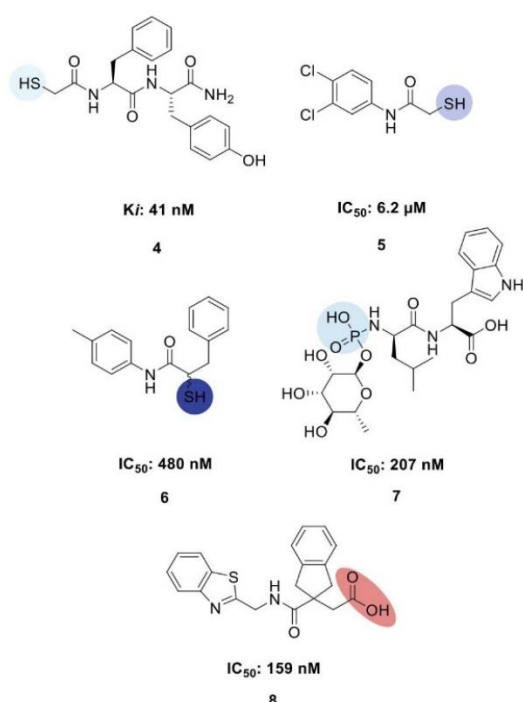


Fig. 5. Structures of selected LasB inhibitors: Peptidic mercaptoacetamide **4**,^[68] *N*-aryl mercaptoacetamide **5**,^[101] α -benzyl *N*-aryl mercaptoacetamide **6**,^[102] phosphoramidon **7**,^[103,104] and a virtual screening hit compound **8**.^[105]

The first nonpeptidic inhibitors of LasB were designed as heterocyclic structures, followed by the introduction of the mercaptoacetamide class.^[99,100] The discovery of the non-peptidic inhibitor compound **5** remains noteworthy as it demonstrated an *in vivo* effect in a *Galleria mellonella* infection model.^[101] Substrate-inspired merging and fragment-growing strategies applied on this structure yielded compound **6** demonstrating a 12-fold increase in potency while maintaining the selectivity and *in vivo* activity, demonstrating the potential for this new scaffold.^[102]

Nevertheless, nonpeptidic inhibitors continue to demonstrate low micromolar activities, whereas peptide-based compounds are active in the sub-micromolar range. A successful example for this observation is phosphoramidon (compound **7**, Fig. 5), a peptidic thermolysin inhibitor.^[103,104]

Recent drug-discovery campaigns with rational approaches involving virtual screening and computer-aided drug design have yielded a series of non-peptidic LasB inhibitors like compound **8** with submicromolar activities and a good selectivity profile.^[105]

The main drawback of zinc-chelating inhibitors of bacterial metalloproteases is the presence of matrix metalloproteases (MMPs) in the human cell, which are essential for important regulatory mechanisms.^[106] These enzymes belong to the M10 family of peptidases and are responsible for degradation of extracellular matrix (ECM) components, regulation of apoptosis and inflammatory processes.^[107–109] More than 20 different MMPs are present in humans, each classified based on their function and the depth of their S1' binding pocket.^[107,110] On the other hand, dysfunction of these enzymes causes various diseases such as cancer,

cardiovascular diseases and inflammation, which makes them attractive targets for treatment of these diseases.^[107,108] Due to these diverse functions, MMPs are often regarded as both targets and anti-targets, creating a challenge for the design of novel, selective metalloprotease inhibitors.^[111]

While designing inhibitors for extracellular metalloenzymes, screening against a series of representative MMPs is essential to assess the selectivity profile of the designed inhibitor. Mercaptoacetamides were reported to be selective over human proteases such as MMP-2 and histone deacetylases (HDACs).^[100] Thiol-containing derivatives were also shown to be successful in terms of selectivity over several MMPs.^[101] For hydroxamate-based inhibitors selectivity, however, remains an issue.^[112,113]

3. Targeting of Clostridial Collagenases

3.1 Introduction to Clostridia Genus

Clostridia are rod-shaped Gram-positive bacteria that are obligate anaerobes and present in soil, waste water or human commensal flora.^[114,115] Among more than 80 different species in this family, a few are known to cause severe diseases.^[115] These include *C. perfringens* and *C. histolyticum*, both causing gas gangrene, *C. tetani* causing tetanus and *C. botulinum* causing botulism.^[115] The strain *C. difficile* is of particular interest as it is responsible for pseudomembranous colitis, which occurs as a consequence of antibiotic use.^[42,116] It also causes severe nosocomial diarrhea.^[115,117] The secretion of toxins and hydrolytic enzymes like collagenases contributes to the pathogenicity of clostridia.^[118] Some of the secreted toxins are known biological warfare agents such as botulinum neurotoxin from *C. botulinum*, which is highly toxic.^[119] In the meantime, collagenases are not only able to invade the host cell directly, but also cause infections by acquiring nutrients and toxin diffusion indirectly.^[118]

An increasing resistance is observed among many strains of clostridia, representing a challenge for treatment of the infections caused by these pathogens.^[120] As extracellular collagenases are becoming highly important antivirulence targets, the next part will focus on virulence factors from *C. histolyticum*.

3.2 Clostridium histolyticum

Clostridium histolyticum produces five different types of toxins.^[115] Among these, β -toxins are the biggest contributors to its pathogenicity as collagenases are crucial for clostridial virulence.^[115] This bacterium uses these extracellular metalloenzymes as a means to invade the host cell and acquire nutrients to evade the immune defense.^[121] Collagenases can then effectively cleave the triple helix collagen into smaller oligopeptides, breaking the connective tissue.^[117,122]

The two types of proteases secreted by this bacterium are encoded by *colH* or *colG* genes.^[123] Collagenase H (ColH) and collagenase G (ColG) are classified as the M9 family of metalloproteases.^[124] Structural studies performed on these enzymes have revealed a similar zinc-binding motif to elastase from *P. aeruginosa*.^[125] A calcium binding site was also discovered close to the zinc-binding site, which proves the necessity of a calcium cation for the peptidolytic and collagenolytic activity.^[126,127]

Contrary to the full collagenase unit ColG, ColH is not able to degrade collagen tissue as a result of bearing an activator and a peptidase domain.^[127,128] Interestingly, the ColG unit shares a greater structural similarity to ColT from *C. tetani* and ColA from *C. perfringens* than to ColH.^[128]

As collagenases play a detrimental role in the progress of bacterial infections caused by *C. histolyticum*, they are considered as essential targets for the development of alternative treatment options for antibiotic resistance.

3.3 Inhibitors of Collagenase H (ColH)

ColH inhibitors also require zinc-chelating groups to maintain their activity by coordination of a zinc cation.^[126] Accordingly, thiols, phosphonamides and hydroxamate motifs with activities ranging from low micromolar to nanomolar are commonly reported for inhibition of ColH.^[129–131] Phosphoramidon has been shown to inhibit ColH as well, but it is not as potent as for LasB.^[129] Interestingly, modified natural coumarin derivatives isolated from *Viola yedonesis* are also potent inhibitors with a nanomolar activity (**9**, Fig. 6).^[131]

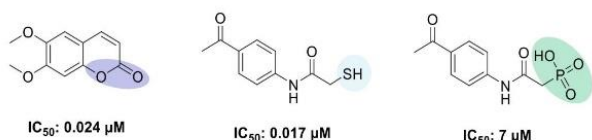


Fig. 6. Structures of selected ColH inhibitors: coumarin derivative **9**,^[131] *N*-aryl mercaptoacetamide derivative **10**,^[132] an alternative zinc binding motif phosphonate derivative **11**.^[133]

Selectivity against human MMPs remains a challenge for ColH inhibitors as most of the existing structures are derived from the established MMP inhibitors.^[134–136] Therefore, efforts for designing novel structural motifs are essential to obtain selective and potent inhibitors.

Schönauer *et al.* introduced *N*-aryl-mercaptoacetamide-based inhibitors that are quite successful in addressing the selectivity issue.^[132] The inhibitor **10** (Fig. 6) with a low nanomolar activity displayed more than 1000-fold selectivity over human MMPs. Building on this exploration, we presented *N*-aryl-mercaptosuccinimide derivatives with an improved chemical stability and lower *in vivo* zebrafish cytotoxicity while demonstrating a significant reduction of collagen degradation in an *ex vivo* pig-skin model.^[137]

The stability issues of thiols triggered the exploration of alternative zinc-binding motifs as inhibitors of ColH.^[138] Inspired by the structure of compound **10**, phosphonate derivative compound **11** showed a low micromolar inhibition of ColH with a good selectivity profile, offering a new direction for inhibitors of this virulence factor.^[132,133] Moreover, the similarity in the substitution pattern of these two structures has provided a better insight into the binding pocket of ColH, indicating a preference for polar and hydrogen-bonding substituents.^[132,133,137]

4. Conclusions and Outlook

In this review, we highlighted the importance of targeting proteases in designing successful inhibitors for antivirulence therapy. We focused on two key bacterial proteases Las B and ColH secreted from the notorious pathogens *P. aeruginosa* and *C. histolyticum*, respectively.

Many peptidic and non-peptidic drug-design inhibitors of LasB have been reported up to date, demonstrating the potential of this virulence factor. In some examples, application of different drug design strategies such as fragment merging/linking or computer-aided drug design accelerated the development of these inhibitors. Nevertheless, selectivity over human metalloproteins and stability of zinc-chelating motifs remain as great challenges that need to be tackled when aiming for inhibitors with a considerable *in vivo* activity.

ColH inhibition has gained more attention lately, as several different inhibitors with successful selectivity profiles and low

micromolar activity have been reported. The discovery of inhibitors with different zinc-binding groups has shown that the efforts for designing and optimizing are not limited to certain scaffolds and there is room for improvement.

Overall, all these efforts underline the importance and the success of antivirulence therapy and various drug-design strategies in the fight against the antimicrobial resistance crisis and increasing the potential of inhibitors to move further into clinical development.

Received: April 11, 2022

- [1] C. López-Otín, J. S. Bond, *J. Biol. Chem.* **2008**, *283*, 30433, <https://doi.org/10.1074/jbc.R800035200>.
- [2] G. S. Salvesen, D. Marcin, *Nat. Rev. Drug Discov.* **2010**, *9*, 690, <https://doi.org/10.1038/nrd3053>.
- [3] B. Turk, *Nat. Rev. Drug Discov.* **2006**, *5*, 785, <https://doi.org/10.1038/nrd2092>.
- [4] E. Harper, A. Berger, *Biochem. Biophys. Res. Commun.* **1972**, *46*, 1956, [https://doi.org/10.1016/0006-291X\(72\)90076-9](https://doi.org/10.1016/0006-291X(72)90076-9).
- [5] J. S. Bond, *J. Biol. Chem.* **2019**, *294*, 1643, <https://doi.org/10.1074/jbc.TM118.004156>.
- [6] E. Culp, G. D. Wright, *J. Antibiot. (Tokyo)* **2017**, *70*, 366, <https://doi.org/10.1038/ja.2016.138>.
- [7] A. A. Agbowuro, W. M. Huston, A. B. Gamble, J. D. A. Tyndall, *Med. Res. Rev.* **2018**, *38*, 1295, <https://doi.org/10.1002/med.21475>.
- [8] T. P. Smyth, *Bioorganic Med. Chem.* **2004**, *12*, 4081, <https://doi.org/10.1016/j.bmc.2004.05.041>.
- [9] R. M. Raju, A. L. Goldberg, E. J. Rubin, *Nat. Rev. Drug Discov.* **2012**, *11*, 777, <https://doi.org/10.1038/nrd3846>.
- [10] I. M. Verhamme, S. E. Leonard, R. C. Perkins, 'Proteases: Pivot points in functional proteomics', **2019**, https://doi.org/10.1007/978-1-4939-8814-3_20.
- [11] G. Abbenante, D. Fairlie, *Med. Chem. (Los Angeles)* **2006**, *1*, 71, <https://doi.org/10.2174/1573406053402569>.
- [12] C. Jensen, P. Herold, H. R. Brunner, *Nat. Rev. Drug Discov.* **2008**, *7*, 399, <https://doi.org/10.1038/nrd2550>.
- [13] W. G. Eisert, N. Huel, J. Stangier, W. Wienen, A. Clemens, J. Van Ryn, *Arterioscler. Thromb. Vasc. Biol.* **2010**, *30*, 1885, <https://doi.org/10.1161/ATVBAHA.110.203604>.
- [14] N. C. Marshall, B. B. Finlay, C. M. Overall, *Mol. Cell. Proteomics* **2017**, *16*, S161, <https://doi.org/10.1074/mcp.O116.066456>.
- [15] D. Leung, G. Abbenante, D. P. Fairlie, *J. Med. Chem.* **2000**, *43*, 305, <https://doi.org/10.1021/jm990412m>.
- [16] C. Lee Ventola, 'The Antibiotic Resistance Crisis Part I: Causes and Threats', *P T.* **2015** Apr; *40*(4): 277–283.
- [17] S. Sengupta, M. K. Chattopadhyay, H. P. Grossart, *Front. Microbiol.* **2013**, *4*, 1, <https://doi.org/10.3389/fmicb.2013.00047>.
- [18] A. Fleming, *Bull. World Health Organ.* **2001**, *79*, 780.
- [19] D. Lydyard, G. L. Jones, B. W. Greatrex, *FEMS Microbiol. Lett.* **2016**, *363*, 1, <https://doi.org/10.1093/femsle/fnw084>.
- [20] D. I. Andersson, N. Q. Balaban, F. Baquero, P. Courvalin, P. Glaser, U. Gophna, R. Kishony, S. Molin, T. Tønjum, *FEMS Microbiol. Rev.* **2021**, *44*, 171, <https://doi.org/10.1093/FEMSRE/FUAA001>.
- [21] 'The antibiotic alarm', *Nature* **2013**, *495*, 141, <https://doi.org/10.1038/495141a>.
- [22] N. Van De Sande-Bruinsma, H. Grundmann, D. Verloof, E. Tiemersma, J. Monen, H. Goossens, M. Ferech, H. Mittermayer, S. Metz, W. Koller, E. Hendrickx, B. Markova, A. Tambic-Andrasevic, I. Francetic, S. Kalenic, D. Bagatzouni, P. Dvorak, P. Urbaskova, D. Monnet, A. Anker Nielsen, P. Naaber, P. Huovinen, P. Paakkari, O. Lyytikäinen, A. Nissinen, P. Maugendre, D. Guillemot, B. Coignard, V. Jarlier, W. Kern, H. Schroeder, W. Witte, K. Heckenbach, H. Giamarellou, A. Antoniadou, A. Tsakris, A. Vatopoulos, G. Ternak, M. Fuzi, K. Kristinsson, E. Smyth, R. Cunney, D. Igoe, O. Murphy, R. Raz, G. Cornaglia, A. Pantosti, P. D'Ancona, S. Berzina, A. Balode, R. Valenteliene, J. Miciuleviciene, R. Hemmer, M. Bruch, M. Borg, P. Zarb, R. Janknegt, M. Filius, H. De Neeling, E. Tiemersma, J. Degener, H. Salvesen Blix, A. Hoiby, G. Simonsen, W. Hryniewicz, P. Grzesiowski, L. Caldeira, M. Canica, I. Codita, V. Foltan, T. Tesar, L. Langsadd, M. Cizman, M. Mueller-Premru, J. Kolman, J. Campos, F. Baquero, O. Cars, G. Skoog, B. Liljequist, G. Kahlmeter, S. Unal, D. Gür, P. Davey, A. Johnson, R. Hill, H. Hughes, M. Coyne, *Emerg. Infect. Dis.* **2008**, *14*, 1722, <https://doi.org/10.3201/eid1411.070467>.
- [23] W. C. Reygaert, *AIMS Microbiol.* **2018**, *4*, 482, <https://doi.org/10.3934/microbiol.2018.3.482>.
- [24] L. B. Rice, *J. Infect. Dis.* **2008**, *197*, 1079, <https://doi.org/10.1086/533452>.

- [25] '2019 Antibacterial agents in clinical development: an analysis of the antibacterial clinical development pipeline. Geneva: World Health Organization; 2019. Licence: CC BY-NC-SA 3.0 IGO. Cataloguing-in-Publication', 2019.
- [26] S. R. Shrivastava, P. S. Shrivastava, J. Ramasamy, *JMS - J. Med. Soc.* **2018**, *32*, 76, https://doi.org/10.4103/jms.jms_25_17.
- [27] Y. X. Ma, C. Y. Wang, Y. Y. Li, J. Li, Q. Q. Wan, J. H. Chen, F. R. Tay, L. N. Niu, *Adv. Sci.* **2020**, *7*, <https://doi.org/10.1002/adv.201901872>.
- [28] World Health Organization, WHO Publ. **2012**, 1.
- [29] M. Lomazzi, M. Moore, A. Johnson, M. Balasegaram, B. Borisch, *BMC Public Health* **2019**, *19*, 1, <https://doi.org/10.1186/s12889-019-7173-7>.
- [30] K. Lewis, *Nature* **2012**, *485*, 439, DOI: 10.1038/485439a.
- [31] L. L. Ling, T. Schneider, A. J. Peoples, A. L. Spoering, I. Engels, B. P. Conlon, A. Mueller, T. F. Schäberle, D. E. Hughes, S. Epstein, M. Jones, L. Lazarides, V. A. Steadman, D. R. Cohen, C. R. Felix, K. A. Fetterman, W. P. Millett, A. G. Nitti, A. M. Zullo, C. Chen, K. Lewis, *Nature* **2015**, *517*, 455, <https://doi.org/10.1038/nature14098>.
- [32] T. Oz, A. Guvenek, S. Yildiz, E. Karaboga, Y. T. Tamer, N. Mumcuayan, V. B. Ozan, G. H. Senturk, M. Cokol, P. Yeh, E. Toprak, *Mol. Biol. Evol.* **2014**, *31*, 2387, <https://doi.org/10.1093/molbev/msu191>.
- [33] D. A. Rasko, V. Sperandio, *Nat. Rev. Drug Discov.* **2010**, *9*, 117, <https://doi.org/10.1038/nrd3013>.
- [34] S. W. Dickey, G. Y. C. Cheung, M. Otto, *Nat. Rev. Drug Discov.* **2017**, *16*, 457, <https://doi.org/10.1038/nrd.2017.23>.
- [35] O. F. Martínez, M. H. Cardoso, S. M. Ribeiro, O. L. Franco, *Front. Cell. Infect. Microbiol.* **2019**, *9*, 1, <https://doi.org/10.3389/fcimb.2019.00074>.
- [36] O. Pacios, L. Blasco, I. Blierot, L. Fernandez-Garcia, A. Bardanca, Mónica González Ambroa, M. López, G. Bou, M. Tomas, *Antibiotics* **2020**, *9*, 1, <https://doi.org/10.3390/antibiotics9020065>.
- [37] A. E. Clatworthy, E. Pierson, D. T. Hung, *Nat. Chem. Biol.* **2007**, *3*, 541, <https://doi.org/10.1038/nchembio.2007.24>.
- [38] S. Wagner, R. Sommer, S. Hinsberger, C. Lu, R. W. Hartmann, M. Empting, A. Titz, *J. Med. Chem.* **2016**, *59*, 5929, <https://doi.org/10.1021/acs.jmedchem.5b01698>.
- [39] B. B. Finlay, S. Falkow, *Microbiol. Mol. Biol. Rev.* **1997**, *61*, 136, <https://doi.org/10.1128/mmb.61.2.136-169.1997>.
- [40] B. Heras, M. J. Scanlon, J. L. Martin, *Br. J. Clin. Pharmacol.* **2015**, *79*, 208, <https://doi.org/10.1111/bcp.12356>.
- [41] P. Piewngam, J. Chiou, P. Chatterjee, M. Otto, *Expert Rev. Anti. Infect. Ther.* **2020**, *18*, 499, <https://doi.org/10.1080/14787210.2020.1750951>.
- [42] G. Taubes, *Science* **2008**, *321*, 356, <https://doi.org/10.1126/science.321.5887.356>.
- [43] R. C. Allen, R. Papat, S. P. Diggle, S. P. Brown, *Nat. Rev. Microbiol.* **2014**, *12*, 300, <https://doi.org/10.1038/nrmicro3232>.
- [44] M. Hentzer, H. Wu, J. B. Andersen, K. Riedel, T. B. Rasmussen, N. Bagge, N. Kumar, M. A. Schembri, Z. Song, P. Kristoffersen, M. Manefield, J. W. Costerton, S. Molin, L. Eberl, P. Steinberg, S. Kjelleberg, N. Høiby, M. Givskov, *EMBO J.* **2003**, *22*, 3803, <https://doi.org/10.1093/emboj/cdg366>.
- [45] M. H. Wilcox, D. N. Gerding, I. R. Poxton, C. Kelly, R. Nathan, T. Birch, O. A. Cornely, G. Rahav, E. Bouza, C. Lee, G. Jenkin, W. Jensen, Y.-S. Kim, J. Yoshida, L. Gabryelski, A. Pedley, K. Eves, R. Tipping, D. Guris, N. Kartsonis, M.-B. Dorr, *N. Engl. J. Med.* **2017**, *376*, 305, DOI: 10.1056/NEJMoa1602615.
- [46] H. Nagase, *Curr. Protoc. Protein Sci.* **2001**, *24*, <https://doi.org/10.1002/0471140864.ps2104s24>.
- [47] M. D. Obritsch, D. N. Fish, R. MacLaren, R. Jung, *Antimicrob. Agents Chemother.* **2004**, *48*, 4606, <https://doi.org/10.1128/AAC.48.12.4606-4610.2004>.
- [48] C. K. Stover, X. Q. Pham, A. L. Erwin, S. D. Mizoguchi, P. Warriner, M. J. Hickey, F. S. L. Brinkman, W. O. Hufnagle, D. J. Kowalk, M. Lagrou, R. L. Garber, L. Goltry, E. Tolentino, S. Westbrook-Wadman, Y. Yuan, L. L. Brody, S. N. Coulter, K. R. Folger, A. Kas, K. Larbig, R. Lim, K. Smith, D. Spencer, G. K. S. Wong, Z. Wu, I. T. Paulsen, J. Relzer, M. H. Saler, R. E. W. Hancock, S. Lory, M. V. Olson, *Nature* **2000**, *406*, 959, <https://doi.org/10.1038/35023079>.
- [49] W. D. Smith, E. Bardin, L. Cameron, C. L. Edmondson, K. V. Farrant, I. Martin, R. A. Murphy, O. Soren, A. R. Turnbull, N. Wierre-Gore, E. W. Alton, J. G. Bundy, A. Bush, G. J. Connett, S. N. Faust, A. Filloux, P. S. Freemont, A. L. Jones, Z. Takats, J. S. Webb, H. D. Williams, J. C. Davies, *FEMS Microbiol. Lett.* **2017**, *364*, 1, <https://doi.org/10.1093/femsle/fnx121>.
- [50] G. Raman, E. E. Avendano, J. Chan, S. Merchant, L. Puzniak, *Antimicrob. Resist. Infect. Control* **2018**, *7*, 1, <https://doi.org/10.1186/s13756-018-0370-9>.
- [51] A. W. Musser, P. R. Beamer, *J. Indiana State Med. Assoc.* **1961**, *54*, 1627.
- [52] P. A. Lambert, *J. R. Soc. Med.* **2002**, *95 Suppl 4*, 22.
- [53] Z. Pang, R. Raudonis, B. R. Glick, T. J. Lin, Z. Cheng, *Biotechnol. Adv.* **2019**, *37*, 177, <https://doi.org/10.1016/j.biotechadv.2018.11.013>.
- [54] J. Botelho, F. Grosso, L. Peixe, *Drug Resist. Updat.* **2019**, *44*, 100640, <https://doi.org/10.1016/j.drup.2019.07.002>.
- [55] W. Ullah, M. Qasim, H. Rahman, Y. Jie, N. Muhammad, *J. Chinese Med. Assoc.* **2017**, *80*, 173, <https://doi.org/10.1016/j.jcma.2016.08.011>.
- [56] P. K. Taylor, A. T. Y. Yeung, R. E. W. Hancock, *J. Biotechnol.* **2014**, *191*, 121, <https://doi.org/10.1016/j.jbiotec.2014.09.003>.
- [57] M. S. Blackledge, R. J. Worthington, C. Melander, *Curr. Opin. Pharmacol.* **2013**, *13*, 699, <https://doi.org/10.1016/j.coph.2013.07.004>.
- [58] T. Rasamiravaka, Q. Labtani, P. Duez, M. El Jaziri, *Biomed Res. Int.* **2015**, *759348*, <https://doi.org/10.1155/2015/759348>.
- [59] H. C. Flemming, J. Wingender, *Nat. Rev. Microbiol.* **2010**, *8*, 623, <https://doi.org/10.1038/nrmicro2415>.
- [60] M. Moses, P. K. Singh, A. L. Schaefer, M. R. Parsek, T. O. Moninger, M. J. Welsh, E. P. Greenberg, *Nature* **2000**, *407*, 762.
- [61] R. Mittal, S. Aggarwal, S. Sharma, S. Chhibber, K. Harjai, *J. Infect. Public Health* **2009**, *2*, 101, <https://doi.org/10.1016/j.jiph.2009.08.003>.
- [62] T. Strateva, I. Mitov, *Ann. Microbiol.* **2011**, *61*, 717, <https://doi.org/10.1007/s13213-011-0273-y>.
- [63] M. Pollack, *Clin. Infect. Dis.* **1984**, *6*, S617, https://doi.org/10.1093/clinids/6.Supplement_3.S617.
- [64] R. Sommer, S. Wagner, K. Rox, A. Varrot, D. Hauck, E. C. Wamhoff, J. Schreiber, T. Ryckmans, T. Brunner, C. Rademacher, R. W. Hartmann, M. Brönstrup, A. Imberty, A. Titz, *J. Am. Chem. Soc.* **2018**, *140*, 2537, <https://doi.org/10.1021/jacs.7b11133>.
- [65] K. P. Rumbaugh, A. Armstrong, 'The Role of Quorum Sensing in Biofilm Development', in 'Antibiofilm Agents', Eds. K. Rumbaugh, I. Ahmad, Springer Series on Biofilms, vol 8. Springer, Berlin, Heidelberg, **2014**, pp. 97, https://doi.org/10.1007/978-3-642-53833-9_6.
- [66] T. Bjarnsholt, M. Givskov, *Anal. Bioanal. Chem.* **2007**, *387*, 409, <https://doi.org/10.1007/s00216-006-0774-x>.
- [67] C. Schütz, D. K. Ho, M. M. Hamed, A. S. Abdelsamie, T. Röhrig, C. Herr, A. M. Kany, K. Rox, S. Schmelz, L. Siebenbürger, M. Wirth, C. Böger, S. Yahiaoui, R. Bals, A. Scrima, W. Blankenfeldt, J. C. Horstmann, R. Christmann, X. Murgia, M. Koch, A. Berwanger, B. Loretz, A. K. H. Hirsch, R. W. Hartmann, C. M. Lehr, M. Empting, *Adv. Sci.* **2021**, *2004369*, 1, <https://doi.org/10.1002/adv.202004369>.
- [68] G. R. A. Cathcart, D. Quinn, B. Greer, P. Harriott, J. F. Lynas, B. F. Gilmore, B. Walker, *Antimicrob. Agents Chemother.* **2011**, *55*, 2670, <https://doi.org/10.1128/AAC.00776-10>.
- [69] B. Wretling, O. R. Pavlovskis, *Clin. Infect. Dis.* **1983**, *5*, S998, https://doi.org/10.1093/clinids/5.Supplement_5.S998.
- [70] Y. Tamura, S. Suzuki, T. Sawada, *Microb. Pathog.* **1992**, *12*, 237, [https://doi.org/10.1016/0882-4010\(92\)90058-V](https://doi.org/10.1016/0882-4010(92)90058-V).
- [71] C. Van Delden, B. H. Iglewski, *Emerg. Infect. Dis.* **1998**, *4*, 551, <https://doi.org/10.3201/eid0404.980405>.
- [72] K. Morihara, H. Tsuzuki, T. Oka, H. Inoue, M. Ebata, *J. Biol. Chem.* **1965**, *240*, 3295, DOI: 10.1016/s0021-9258(18)97217-0.
- [73] E. Kessler, M. Safrin, J. K. Gustin, D. E. Ohman, *J. Biol. Chem.* **1998**, *273*, 30225, <https://doi.org/10.1074/jbc.273.46.30225>.
- [74] E. Kessler, M. Safrin, *J. Bacteriol.* **1988**, *170*, 5241, <https://doi.org/10.1128/jb.170.11.5241-5247.1988>.
- [75] F. X. Gomis-Rüth, T. O. Botelho, W. Bode, *Biochim. Biophys. Acta - Proteins Proteomics* **2012**, *1824*, 157, <https://doi.org/10.1016/j.bbapap.2011.04.014>.
- [76] M. M. Thayer, K. M. Flaherty, D. B. McKay, *J. Biol. Chem.* **1991**, *266*, 2864, [https://doi.org/10.1016/s0021-9258\(18\)49927-9](https://doi.org/10.1016/s0021-9258(18)49927-9).
- [77] O. A. Adekoya, I. Sylte, *Chem. Biol. Drug Des.* **2009**, *73*, 7, <https://doi.org/10.1111/j.1747-0285.2008.00757.x>.
- [78] F. Bastaert, S. Kheir, V. Saint-Criq, B. Villeret, P. M. C. Dang, J. El-Benna, J. C. Sirard, R. Voulhoux, J. M. Sallenave, *Front. Immunol.* **2018**, *9*, 1, <https://doi.org/10.3389/fimmu.2018.01675>.
- [79] V. Saint-Criq, B. Villeret, F. Bastaert, S. Kheir, A. Hatton, A. Cazes, Z. Xing, I. Sermet-Gaudelus, I. Garcia-Verdugo, A. Edelman, J.-M. Sallenave, *Thorax* **2018**, *73*, 49, <https://doi.org/10.1136/thoraxjnl-2017-210298>.
- [80] L. W. Heck, K. Morihara, W. B. McRae, E. J. Miller, *Infect. Immun.* **1986**, *51*, 115, <https://doi.org/10.1128/iai.51.1.115-118.1986>.
- [81] L. W. Heck, P. G. Alarcon, R. M. Kulhavy, K. Morihara, M. W. Mestecky, J. F. Russell, *J. Immunol.* **1990**, *144*, 2253.
- [82] I. A. Holder, R. Wheeler, *Can. J. Microbiol.* **1984**, *30*, 1118, <https://doi.org/10.1139/m84-175>.
- [83] D. R. Galloway, *Mol. Microbiol.* **1991**, *5*, 2315, <https://doi.org/10.1111/j.1365-2958.1991.tb02076.x>.
- [84] M. Parnely, A. Gale, M. Clabaugh, R. Horvat, W. Zhou, *Infect. Immun.* **1990**, *58*, 3009, <https://doi.org/10.1128/iai.58.9.3009-3014.1990>.
- [85] W. I. Mariencheck, J. F. Alcorn, S. M. Palmer, J. R. Wright, *Am. J. Respir. Cell Mol. Biol.* **2003**, *28*, 528, <https://doi.org/10.1165/rmb.2002-0141.OC>.
- [86] H. Yu, X. He, W. Xie, J. Xiong, H. Sheng, S. Guo, C. Huang, D. Zhang, K. Zhang, *Can. J. Microbiol.* **2014**, *60*, 227, <https://doi.org/10.1139/cjm-2013-0667>.
- [87] P. Tielens, F. Roscnau, S. Wilhelm, K. E. Jaeger, H. C. Flemming, J. Wingender, *Microbiology* **2010**, *156*, 2239, <https://doi.org/10.1099/mic.0.037036-0>.

- [88] S. Kamath, V. Kapatral, A. M. Chakrabarty, *Mol. Microbiol.* **1998**, *30*, 933, <https://doi.org/10.1046/j.1365-2958.1998.01121.x>.
- [89] J. F. Poschet, J. C. Boucher, A. M. Firoved, V. Deretic, *Methods Enzymol.* **2001**, *336*, 65, [https://doi.org/10.1016/S0076-6879\(01\)36579-5](https://doi.org/10.1016/S0076-6879(01)36579-5).
- [90] E. Kessler, M. Safrin, 'Elastinolytic and Proteolytic Enzymes', in 'Pseudomonas Methods and Protocols. Methods in Molecular Biology (Methods and Protocols)', Eds: A. Filloux, J. L. Ramos, vol 1149, Humana Press, New York, NY, **2014**, pp. 135, https://doi.org/10.1007/978-1-4939-0473-0_13.
- [91] A. Barrett, N. Rawlings, J. Woessner, 'Handbook of Proteolytic Enzymes, 3rd Edition', Elsevier, **2012**.
- [92] E. Kessler, M. Safrin, W. R. Abrams, J. Rosenbloom, D. E. Ohman, *J. Biol. Chem.* **1997**, *272*, 9884, <https://doi.org/10.1074/jbc.272.15.9884>.
- [93] E. Kessler, M. Safrin, J. C. Olson, D. E. Ohman, *J. Biol. Chem.* **1993**, *268*, 7503, [https://doi.org/10.1016/s0021-9258\(18\)53203-8](https://doi.org/10.1016/s0021-9258(18)53203-8).
- [94] M. J. Everett, D. T. Davies, *Drug Discov. Today* **2021**, *26*, 2108, <https://doi.org/10.1016/j.drudis.2021.02.026>.
- [95] R. Ye, C. Tan, B. Chen, R. Li, Z. Mao, *Front. Chem.* **2020**, *8*, 1, <https://doi.org/10.3389/fchem.2020.00402>.
- [96] J. A. Jacobsen, J. L. Major Jourden, M. T. Miller, S. M. Cohen, *Biochim. Biophys. Acta - Mol. Cell Res.* **2010**, *1803*, 72, <https://doi.org/10.1016/j.bbamer.2009.08.006>.
- [97] A. M. Kany, A. Sikandar, S. Yahiaoui, J. Hauptenthal, I. Walter, M. Empting, J. Köhnke, R. W. Hartmann, *ACS Chem. Biol.* **2018**, *13*, 2449, <https://doi.org/10.1021/acscchembio.8b00257>.
- [98] G. R. Cathcart, B. F. Gilmore, B. Greer, P. Harriott, B. Walker, *Bioorganic Med. Chem. Lett.* **2009**, *19*, 6230, <https://doi.org/10.1016/j.bmlc.2009.08.099>.
- [99] A. L. Garner, A. K. Struss, J. L. Fullagar, A. Agrawal, A. Y. Moreno, S. M. Cohen, K. D. Janda, *ACS Med. Chem. Lett.* **2012**, *3*, 668, <https://doi.org/10.1021/ml300128f>.
- [100] J. Zhu, X. Cai, T. L. Harris, M. Gooyit, M. Wood, M. Lardy, K. D. Janda, *Chem. Biol.* **2015**, *22*, 483, <https://doi.org/10.1016/j.chembiol.2015.03.012>.
- [101] A. M. Kany, A. Sikandar, J. Hauptenthal, S. Yahiaoui, C. K. Maurer, E. Proschak, J. Köhnke, R. W. Hartmann, *ACS Infect. Dis.* **2018**, *4*, 988, <https://doi.org/10.1021/acsinfectdis.8b00010>.
- [102] C. Kaya, I. Walter, S. Yahiaoui, A. Sikandar, A. Alhayek, J. Konstantinovic, A. M. Kany, J. Hauptenthal, J. Köhnke, R. W. Hartmann, A. K. H. Hirsch, *Angew. Chemie Int. Ed.* **2021**, *61*, e202112295, <https://doi.org/10.1002/anie.202112295>.
- [103] N. Nishino, J. C. Powers, *J. Biol. Chem.* **1979**, *255*, 3482.
- [104] K. Morihara, H. Tsuzuki, *Jpn. J. Exp. Med.* **1978**, *48*, 81.
- [105] S. Leiris, D. T. Davies, N. Sprynski, J. Castandet, L. Beyria, M. S. Bodnarchuk, J. M. Sutton, T. M. G. Mullins, M. W. Jones, A. K. Forrest, T. D. Pallin, P. Karunakar, S. K. Martha, B. Parusharamulu, R. Ramula, V. Kotha, N. Pottabathini, S. Pothukanuri, M. Lemonnier, M. Everett, *ACS Med. Chem. Lett.* **2021**, *12*, 217, <https://doi.org/10.1021/acsmchemlett.0c00554>.
- [106] P. G. Jobin, G. S. Butler, C. M. Overall, *Biochim. Biophys. Acta - Mol. Cell Res.* **2017**, *1864*, 2043, <https://doi.org/10.1016/j.bbamer.2017.05.013>.
- [107] D. Sbardella, G. F. Fasciglione, M. Gioia, C. Ciaccio, G. R. Tundo, S. Marini, M. Coletta, *Mol. Aspects Med.* **2012**, *33*, 119, <https://doi.org/10.1016/j.mam.2011.10.015>.
- [108] H. Nagase, R. Visse, G. Murphy, *Cardiovasc. Res.* **2006**, *69*, 562, <https://doi.org/10.1016/j.cardiores.2005.12.002>.
- [109] N. D. Rawlings, A. J. Barrett, A. Bateman, *Nucleic Acids Res.* **2009**, *38*, 227, <https://doi.org/10.1093/nar/gkp971>.
- [110] H. I. Park, Y. Jin, D. R. Hurst, C. A. Monroe, S. Lee, M. A. Schwartz, Q. X. A. Sang, *J. Biol. Chem.* **2003**, *278*, 51646, <https://doi.org/10.1074/jbc.M310109200>.
- [111] A. Dufour, C. M. Overall, *Trends Pharmacol. Sci.* **2013**, *34*, 233, <https://doi.org/10.1016/j.tips.2013.02.004>.
- [112] S. Sjøli, E. Nuti, C. Camodeca, I. Bilotto, A. Rossello, J. O. Winberg, I. Sylte, O. A. Adekoya, *Eur. J. Med. Chem.* **2016**, *108*, 141, <https://doi.org/10.1016/j.ejmech.2015.11.019>.
- [113] O. A. Adekoya, S. Sjøli, Y. Wuxiuier, I. Bilotto, S. M. Marques, M. A. Santos, E. Nuti, G. Cercignani, A. Rossello, J. O. Winberg, I. Sylte, *Eur. J. Med. Chem.* **2015**, *89*, 340, <https://doi.org/10.1016/j.ejmech.2014.10.009>.
- [114] L. R. Lopetuso, F. Scaldaferrri, V. Petito, A. Gasbarrini, *Gut Pathog.* **2013**, *5*, 1, <https://doi.org/10.1186/1757-4749-5-23>.
- [115] C. L. Hatheway, *Clin. Microbiol. Rev.* **1990**, *3*, 66, <https://doi.org/10.1128/cmr.3.1.66-98.1990>.
- [116] J. G. Bartlett, *Ann. N. Y. Acad. Sci.* **2010**, *1213*, 62, <https://doi.org/10.1111/j.1749-6632.2010.05863.x>.
- [117] M. D. Bond, H. E. Van Wart, *Biochemistry* **1984**, *23*, 3077, <https://doi.org/10.1021/bi00308a035>.
- [118] O. Matsushita, A. Okabe, *Toxicol.* **2001**, *39*, 1769, [https://doi.org/10.1016/S0041-0101\(01\)00163-5](https://doi.org/10.1016/S0041-0101(01)00163-5).
- [119] G. A. Senisterra, B. S. Hong, H.-W. Park, M. Vedadi, *J. Biomol. Screening* **2008**, *13*, 337, <https://doi.org/10.1177/1087057108317825>.
- [120] C. J. Alexander, D. M. Citron, J. S. Brazier, E. J. C. Goldstein, *J. Clin. Microbiol.* **1995**, *33*, 3209, <https://doi.org/10.1128/jcm.33.12.3209-3215.1995>.
- [121] U. Eckhard, P. F. Huesgen, H. Brandstetter, C. M. Overall, *J. Proteomics* **2014**, *100*, 102, <https://doi.org/10.1016/j.jpro.2013.10.004>.
- [122] O. Matsushita, C. M. Jung, J. Minami, S. Katayama, N. Nishi, A. Okabe, *J. Biol. Chem.* **1998**, *273*, 3643, <https://doi.org/10.1074/jbc.273.6.3643>.
- [123] O. Matsushita, C. M. Jung, S. Katayama, J. Minami, Y. Takahashi, A. Okabe, *J. Bacteriol.* **1999**, *181*, 923, <https://doi.org/10.1128/jb.181.3.923-933.1999>.
- [124] A. S. Duarte, A. Correia, A. C. Esteves, *Crit. Rev. Microbiol.* **2016**, *42*, 106, <https://doi.org/10.3109/1040841X.2014.904270>.
- [125] M. D. Obritsch, D. N. Fish, R. MacLaren, R. Jung, *Pharmacotherapy* **2005**, *25*, 1353, <https://doi.org/10.1592/phco.2005.25.10.1353>.
- [126] C. M. Jung, O. Matsushita, S. Katayama, J. Minami, J. Sakurai, A. Okabe, *J. Bacteriol.* **1999**, *181*, 2816, <https://doi.org/10.1128/jb.181.9.2816-2822.1999>.
- [127] U. Eckhard, E. Schönauer, H. Brandstetter, *J. Biol. Chem.* **2013**, *288*, 20184, <https://doi.org/10.1074/jbc.M112.448548>.
- [128] U. Eckhard, E. Schönauer, P. Ducka, P. Briza, D. Nüss, H. Brandstetter, *Biol. Chem.* **2009**, *390*, 11, <https://doi.org/10.1515/BC.2009.004>.
- [129] A. Yiotakis, A. Hatgiyannacou, V. Dive, F. Toma, *Eur. J. Biochem.* **1988**, *172*, 761, <https://doi.org/10.1111/j.1432-1033.1988.tb13954.x>.
- [130] V. Dive, A. Yiotakis, A. Nicolaou, F. Toma, *Eur. J. Biochem.* **1990**, *191*, 685, <https://doi.org/10.1111/j.1432-1033.1990.tb19175.x>.
- [131] N. Oshima, Y. Narukawa, T. Takeda, F. Kiuchi, *J. Nat. Med.* **2013**, *67*, 240, <https://doi.org/10.1007/s11418-012-0665-8>.
- [132] E. Schönauer, A. M. Kany, J. Hauptenthal, K. Hüsecken, I. J. Hoppe, K. Voos, S. Yahiaoui, B. Elsässer, C. Ducho, H. Brandstetter, R. W. Hartmann, *J. Am. Chem. Soc.* **2017**, *139*, 12696, <https://doi.org/10.1021/jacs.7b06935>.
- [133] K. Voos, E. Schönauer, A. Alhayek, J. Hauptenthal, A. Andreas, R. Müller, R. W. Hartmann, H. Brandstetter, A. K. H. Hirsch, C. Ducho, *ChemMedChem* **2021**, *16*, 1257, <https://doi.org/10.1002/cmde.202000994>.
- [134] A. Scozzafava, C. T. Supuran, *Eur. J. Med. Chem.* **2000**, *35*, 299, [https://doi.org/10.1016/S0223-5234\(00\)00127-6](https://doi.org/10.1016/S0223-5234(00)00127-6).
- [135] M. A. Santos, S. Marques, M. Gil, M. Tegoni, A. Scozzafava, C. T. Supuran, *J. Enzyme Inhib. Med. Chem.* **2003**, *18*, 233, <https://doi.org/10.1080/1475636031000081134>.
- [136] M. Ilies, M. D. Banciu, A. Scozzafava, M. A. Ilies, M. T. Caproiu, C. T. Supuran, *Bioorganic Med. Chem.* **2003**, *11*, 2227, [https://doi.org/10.1016/S0968-0896\(03\)00113-5](https://doi.org/10.1016/S0968-0896(03)00113-5).
- [137] J. Konstantinovic, S. Yahiaoui, A. Alhayek, J. Hauptenthal, E. Schönauer, A. Andreas, A. M. Kany, R. Müller, J. Köhnke, F. K. Berger, M. Bischoff, R. W. Hartmann, H. Brandstetter, A. K. H. Hirsch, *J. Med. Chem.* **2020**, *63*, 8359, <https://doi.org/10.1021/acsmchem.0c00584>.
- [138] R. E. Galardy, D. Grobely, *Biochemistry* **1983**, *22*, 4556, <https://doi.org/10.1021/bi00288a032>.

License and Terms



This is an Open Access article under the terms of the Creative Commons Attribution License CC BY 4.0. The material may not be used for commercial purposes.

The license is subject to the CHIMIA terms and conditions (<https://chimia.ch/chimia/about>).

The definitive version of this article is the electronic one that can be found at <https://doi.org/10.2533/chimia.2022.402>

1.2 Aims of the Thesis

Targeting virulence factors is an emerging key strategy in designing pathoblockers to combat the rise of resistant bacteria. Nevertheless, to obtain inhibitors of extracellular virulence factors with optimum properties remains a challenging task, as the designed inhibitors face several issues such as lack of selectivity against off-targets or the lack of efficacy *in vivo*.

The main objective of this thesis is to present the design and synthesis of novel inhibitors targeting several key players of antimicrobial resistance.

The first part focuses on the design and synthesis of the inhibitors of virulence factor LasB from Gram-negative *P. aeruginosa*. Previously at the DDOP department, mercaptoacetamides with low micromolar activity were discovered as potent inhibitors of LasB which also demonstrated an *in vivo effect* on a *Galleria mellonella* infection model. To improve the potency of these inhibitors further, a rational design approach was applied based on the crystal structure of the hit structure with LasB. This led to the discovery of alpha-benzylated mercaptoacetamide class with not only a 12-fold improvement in potency, but also with a similar selectivity and an improved *in vivo* profile. To expand the chemical space, a structure–activity relationship (SAR) study on the most potent derivative was employed followed by the introduction of heterocyclic derivatives. The results are outlined in Section 2.1 and Section 2.2.

The second part of the thesis is dedicated to the discovery of fragment-like inhibitors of ColH from Gram-positive *C. histolyticum* with a novel mode of action. Using several biophysical methods, a halogen-containing fragment showing a low micromolar inhibition was identified. The rationalization of the binding mode was performed by an X-ray crystal structure of the fragment hit in complex with peptidase domain of ColH (ColH-PD). A fragment-based design yielded around 35 derivatives, which led to an optimized structure with two-fold improvement in IC₅₀ values and a restored selectivity of ColH over several MMPs. The results are discussed in Section 2.3.

The last part of this thesis focuses on the design and synthesis of broad-spectrum inhibitors of class B1 MBLs. A series of *N*-aryl mercaptopropionamides was discovered to be potent inhibitors of several class B MBLs. Establishment of an SAR study with mainly polar substituents revealed a hit structure restoring the activity of the β -lactam antibiotic imipenem. An *in vivo* effect in a *Galleria mellonella* model demonstrated the potential of these inhibitors as future anti-infectives. The results are summarized in Section 2.4.

Chapter 2: Results

2.1 Substrate-Inspired Fragment Merging and Growing Affords Efficacious LasB inhibitors

Cansu Kaya*, Isabell Walter*, Samir Yahiaoui, Asfandyar Sikandar, Alaa Alhayek, Jelena Konstantinović, Andreas M. Kany, Jörg Haupenthal, Jesko Köhnke, Rolf W. Hartmann, Anna K. H. Hirsch.

*These authors contributed equally.

Angew. Chemie Int. Ed. 2021. <https://doi.org/10.1002/anie.202112295>.

Medicinal Chemistry

How to cite:

International Edition: doi.org/10.1002/anie.202112295

German Edition: doi.org/10.1002/ange.202112295

Substrate-Inspired Fragment Merging and Growing Affords Efficacious LasB Inhibitors

Cansu Kaya⁺, Isabell Walter⁺, Samir Yahiaoui, Asfandyar Sikandar, Alaa Alhayek, Jelena Konstantinović, Andreas M. Kany, Jörg Hauptenthal, Jesko Köhnke, Rolf W. Hartmann, and Anna K. Hirsch*

Abstract: Extracellular virulence factors have emerged as attractive targets in the current antimicrobial resistance crisis. The Gram-negative pathogen *Pseudomonas aeruginosa* secretes the virulence factor elastase B (LasB), which plays an important role in the infection process. Here, we report a sub-micromolar, non-peptidic, fragment-like inhibitor of LasB discovered by careful visual inspection of structural data. Inspired by the natural LasB substrate, the original fragment was successfully merged and grown. The optimized inhibitor is accessible via simple chemistry and retained selectivity with a substantial improvement in activity, which can be rationalized by the crystal structure of LasB in complex with the inhibitor. We also demonstrate an improved *in vivo* efficacy of the optimized hit in *Galleria mellonella* larvae, highlighting the significance of this class of compounds as promising drug candidates.

Alternative binding modes are often observed in the realm of fragment-based drug design.^[1] Despite the potential to significantly accelerate hit-to-lead optimization, there are few examples of successful fragment linking/merging or systematic exploitation of such invaluable sources of structural information. This is presumably due to a number of conditions that need to be met such as the linker composition and the resulting ADMET properties.^[2,3] We

propose that a careful focus on the the structural data of fragments could serve as an important starting point to facilitate optimization via linking/merging, ensuring favorable properties. We explore this hypothesis with simple chemistry using a virulence factor from *Pseudomonas aeruginosa*.

P. aeruginosa is a Gram-negative bacterium that is ranked amongst the most critical pathogens by the World Health Organization.^[4] This opportunistic bacterium causes ≈10% of hospital-acquired infections and has a high incidence in immunocompromised and cystic-fibrosis patients.^[5–8] It has an especially low permeability of the outer membrane, which prevents the entry of antibiotics into the cell.^[9] In addition, its efflux pumps efficiently move undesired antimicrobials out of the cell and its β-lactamases are able to inactivate the corresponding β-lactam antibiotics^[10–13] contributing to the emergence of drug-resistant *P. aeruginosa* strains.^[14,15]

In the search for anti-infectives with novel modes of action, addressing bacterial virulence has become a widely applicable method.^[16–18] Virulence factors are used by pathogenic bacteria and act through several mechanisms, including the invasion of host cells, biofilm formation and the evasion of the host immune response.^[19] Inhibition of virulence factors reduces bacterial virulence and enables clearance of the pathogens by either the host immune system or antibiotics.^[20,21] The main advantages of this strategy is the reduced selective pressure on the bacteria, which decreases the risk of resistance development, and the fact that commensal bacteria remain unaffected.^[20] Among other virulence factors, the secreted metalloprotease LasB has been validated as one of the most important components contributing to the virulence of *P. aeruginosa*.^[22] LasB is thus a particularly attractive target and addressing it circumvents permeation and efflux issues due to its extracellular location.

LasB plays a crucial role in the pathogenic invasion of tissues and is predominantly responsible for acute nosocomial infections.^[19,23] It has the ability to degrade elastin, an important component of lung tissue, blood vessels and skin, which makes it a key target for inhibition. Until now, natural products such as the streptomycetes metalloprotease inhibitor (SMPI) from *Streptomyces nigrescens* TK-23^[24] and phosphoramidon (Pam)^[25] (Figure 1, compound **1**), small peptides containing metal-chelating motifs such as thiol,^[26–28] hydroxamate^[29] or carboxylic acid^[30,31] groups (Figure 1,

[*] C. Kaya,⁺ Dr. I. Walter,⁺ Dr. A. Sikandar, A. Alhayek, Dr. J. Köhnke, Prof. R. W. Hartmann, Prof. A. K. H. Hirsch
 Helmholtz Institute for Pharmaceutical Research Saarland (HIPS)
 Helmholtz Centre for Infection Research (HZI)
 Campus E8.1, 66123 Saarbrücken (Germany)

and
 Department of Pharmacy, Saarland University
 Campus E8.1, 66123 Saarbrücken (Germany)
 E-mail: anna.hirsch@helmholtz-hips.de

Dr. S. Yahiaoui, Dr. J. Konstantinović, Dr. A. M. Kany,
 Dr. J. Hauptenthal
 Helmholtz Institute for Pharmaceutical Research Saarland (HIPS)
 Helmholtz Centre for Infection Research (HZI)
 Campus E8.1, 66123 Saarbrücken (Germany)

[⁺] These authors contributed equally to this work.

© 2021 The Authors. Angewandte Chemie International Edition published by Wiley-VCH GmbH. This is an open access article under the terms of the Creative Commons Attribution License, which permits use, distribution and reproduction in any medium, provided the original work is properly cited.

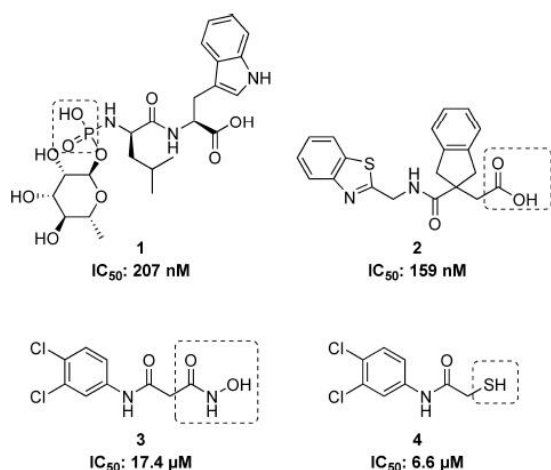


Figure 1. Structures of known LasB inhibitors. Zinc-binding residues are highlighted.

compound **2**), have been reported. However, most of these inhibitors show poor selectivity with respect to mammalian metalloenzymes. The small synthetic molecules with hydroxamate and mercaptoacetamide groups that have been reported by us (Figure 1, compounds **3** and **4**) are promising LasB inhibitors with better selectivity profiles, yet there are still substantial improvements necessary on the way to clinically applicable drugs.^[32, 33]

We set out to exploit alternative binding modes of the parent hit to guide efficient fragment merging and growing and to overcome the above-mentioned limitations of the reported inhibitors. We present the structure-based optimization of a fragment-like LasB inhibitor that resulted in a twelve-fold boost in activity combined with improved in vivo efficacy. The inhibitory potency was determined in vitro whilst ensuring the derivatives displayed no direct antimicrobial activity. Having confirmed the exquisite selectivity using a panel of representative human off-targets, we analyzed the efficacy in vivo in *Galleria mellonella* larvae. A LasB-inhibitor complex crystal structure verified the predicted binding mode.

We recently reported the crystal structure of the hit compound **4** (IC_{50} = 6.6 \pm 0.3 μ M) in complex with LasB.^[32] To our surprise, two molecules of **4** were present in the substrate binding pocket of LasB, which set the stage for rational compound optimization by merging both molecules of **4**. Our attempts to combine these two molecules into one *N*-benzylamide derivative did not provide the desired activity.^[32] In our next attempt to optimize the molecular interactions in the binding pocket, we shifted the benzyl moiety to the alpha position of the amide moiety to create a non-peptidic substrate mimick (Phe side-chain), which afforded the first derivative of the α -alkyl-*N*-aryl mercaptoacetamide class. Compound **7a** displayed a two-fold increase in activity (Table 1).

To explore to which degree the benzyl moiety is responsible for the increase in activity, we further inves-

Table 1: In vitro activities of α -alkyl-*N*-aryl mercaptoacetamides and α -benzyl-*N*-aryl mercaptoacetamides against LasB.^[31]

Compound	R	R ¹	IC ₅₀ [μ M]
4	3,4-di-Cl	H	6.6 \pm 0.3
7a	3,4-di-Cl	Benzyl	2.7 \pm 0.4
7b	3,4-di-Cl	Cyclohexylmethyl	12 \pm 3
7c	3,4-di-Cl	Cyclopropylmethyl	6.3 \pm 1.2
7d	H	Benzyl	1.2 \pm 0.1
7e	2-Me	Benzyl	2.4 \pm 1.0
7f	3-Me	Benzyl	1.0 \pm 0.4
7g	4-Me	Benzyl	0.48 \pm 0.04

[a] Means \pm standard deviations of at least two independent experiments.

tigated the effect of cyclohexylmethyl and cyclopropylmethyl side chains, while maintaining the di-chloro substituent on the *N*-aryl ring. Although the IC_{50} value of compound **7c** remained similar to compound **4** with a relatively small-sized cyclopropylmethyl group, it increased significantly for compound **7b** with a cyclohexylmethyl substituent (Table 1). Therefore, we concluded that both optimal filling of the unoccupied space and the aromaticity of the benzyl group contributed to the activity.

Our next step was to investigate the importance of the di-chloro motif that is engaged in key hydrophobic interactions in the binding pocket. Compared to **7a**, compound **7d** showed a further two-fold improvement in IC_{50} value, which demonstrated that the presence of a di-chloro substituent was not essential for the activity of the α -benzyl-*N*-aryl mercaptoacetamide class.

To elucidate the binding mode of α -substituted mercaptoacetamides, we co-crystallized compound **7d** with LasB (Figure 2A). Full details of the data collection and refinement statistics can be found in the Supporting Information (Table S1). As expected, the compound was found in the

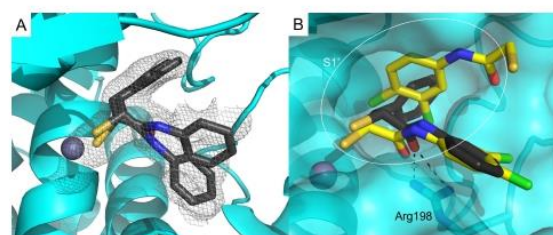


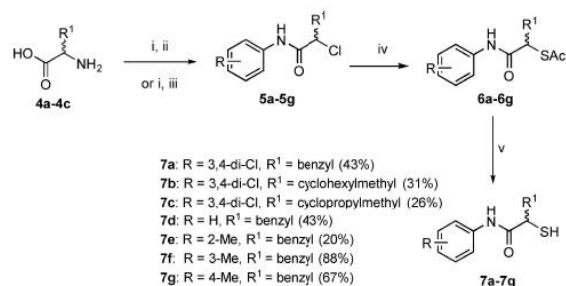
Figure 2. A) Crystal structure of LasB in complex with **7d** (PDB code: 7OC7). Cartoon representation of LasB (cyan) in complex with **7d** (black). The gray isomesh represents the polder map of **7d** contoured at 2 σ . Two different states of **7d** with different occupancies are observed. B) Superposition of LasB (cyan surface) structures in complex with **4** (yellow) or **7d** (black, major conformation shown) showing the phenyl group occupying the S1' binding-site of the enzyme. The active-site Zn²⁺ cation is shown as a gray sphere.

same binding pocket as previously reported for *N*-(3,4-dichlorophenyl) mercaptoacetamide hit **4** and occupied the S1'-S2' pockets with the thiol group coordinating the active-site Zn²⁺ cation (Figure 2B, Figure S1). The *N*-arylacetamide group is stabilized by H-bonding and hydrophobic interactions (Figure S2). The ligand is possibly anchored in the binding pocket by the carbonyl oxygen, which forms a bidentate hydrogen bond with Arg198. The phenyl group of the *N*-arylacetamide occupies the wide, open and solvent-accessible entrance of the S1' binding pocket, which may explain the two different orientations observed for this part of the compound in the crystal structure (Figure 2). The benzyl group lies in the lipophilic S2' binding pocket and is stabilized by numerous hydrophobic interactions (Figure S2).

In contrast to the binding mode of compound **4**, only one molecule of compound **7d** binds to the protein, which leads to the closure of the binding pocket – a phenomenon generally observed for thermolysin-like proteases like LasB upon inhibitor binding.^[33] Our structure-based strategy to move the benzyl moiety from the amide nitrogen to the alpha position proved to be successful, as we were able to occupy the space in the binding pocket with one molecule.^[32]

The LasB-**7d** crystal structure provided a deeper understanding of the potential interactions in the surrounding unoccupied space and paved the way for further optimization. For example, the tolerance of other lipophilic substituent(s), especially in the S1' pocket, is well-documented. As we previously discovered that the hydrophobic di-chloro motif is not essential for the improvement in activity, our next choice for a lipophilic substituent was a sterically less demanding methyl group. We used the crystal structure for a focused, structure-based optimization study. As supported by the docking pose (Figure S3), the presence of a lipophilic methyl substituent in the *para* position most likely leads to further strengthening of the hydrophobic interactions with Leu197, and in combination with the benzyl group in the alpha position, provides optimal interactions in the binding pocket. Taking this into account, we synthesized three regioisomers and all of them proved to be more potent than the initially optimized structure, compound **7a** (Table 1). Expectedly, the introduction of a *para* methyl substituent on the aromatic core of the *N*-arylacetamide group had the most profound effect on activity, confirming the beneficial inhibitor-protein interactions. These interactions account for the submicromolar activity observed for compound **7g** (IC₅₀ = 0.48 ± 0.04 μM).

The synthetic route for all derivatives is shown in Scheme 1. Diazotization and subsequent chlorination of the corresponding commercially available racemic amino acids **4a-4c** yielded α -chloro carboxylic acids. Their coupling with the respective aniline gave the intermediates **5a-5g**. The thioacetate function was introduced via an S_N2 reaction using potassium thioacetate **6a-6g**. Deprotection of the thioacetate under basic conditions afforded final compounds **7a-7g** in 20–88% yield as free thiols.



Scheme 1. Synthetic scheme of α -alkyl/aryl compound class.^[3]

Prior to investigating the in vivo effect of our improved inhibitors, we analyzed their antibacterial activity. A minimum inhibitory concentration (MIC) assay revealed no direct effect on pathogen growth by inhibitor **7d** (Supporting Information, Page S3, MIC > 100 μM). Furthermore, we explored its cytotoxicity towards three human cell lines (Supporting Information, Page S3, IC₅₀ > 100 μM). Given that poor selectivity towards metalloproteases is often an issue, we investigated selectivity of selected inhibitors for LasB over six matrix metalloproteases (MMPs) and additional three human off-targets (Table S2). While the selectivity of the optimized compounds **7d** and **7g** could be maintained compared to the hit compound **4** with the exception of TACE, a slightly reduced cytotoxicity of the novel compounds was shown.

We next analyzed the antivirulence activity of LasB inhibitors in vivo, using a simple model based on *G. mellonella* larvae. This method is used to evaluate the treatment options for *P. aeruginosa*-induced infections and to demonstrate the efficacy of LasB inhibitors in preparation for a murine in vivo pharmacodynamics study.^[32,33] We injected the larvae with the supernatant (s.n.) of *P. aeruginosa* PA14 with or without 0.25 nmol of either **4** or **7g**, incubated them for three days and recorded the survival once per day (Figure 3). Our results showed that PA14 s.n. reduced the survival of larvae by up to 88% after three days of incubation. Compound **4**, which was used as a control, showed virtually no improvement in survival after three

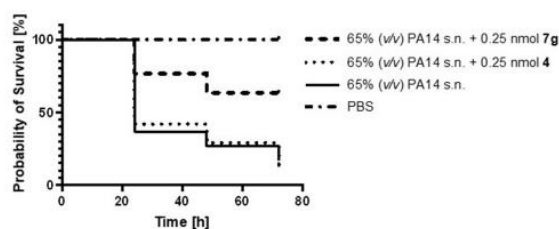


Figure 3. Kaplan-Meier survival analysis of larvae treated with 0.25 nmol compound **4** (dotted) ($p \leq 0.9452$), 0.25 nmol compound **7g** (two dash) ($p \leq 0.0002$) or PA14 s.n. only (solid) ($n=3$). PA14 s.n. was also present during compound treatment. PBS served as a negative control (dot dash). Compounds **7g** and **4** in PBS showed 100% survival. s.n.: supernatant.

days. Treatment of larvae with 0.25 nmol of compound **7g** increased survival up to 60% compared to PBS injected larvae. These results validate our inhibitors as promising candidates to block the pathogenicity of *P. aeruginosa* and confirm that the boost in inhibitory activity in vitro translates to an improved in vivo effect.

In summary, by utilizing structure-guided fragment merging/linking inspired by the natural substrate, we achieved a substantial increase in potency of our LasB inhibitors that translated into in vivo efficacy. We identified compound **7g**, which showed a twelve-fold improvement in activity compared to our best previously reported inhibitor. Encouraged by the excellent in vitro activity of these compounds, we also demonstrated an in vivo effect in a *G. mellonella* model. The survival rate of larvae infected with PA14 supernatant and treated with compound **7g** were significantly improved as compared to our previous inhibitor **4**.

Although structure-guided exploration of the *N*-aryl ring substitution provided us with a strong starting point for lead optimization, systematic variation of the substituent in the α -position (R^1) should be considered to exploit the lipophilicity of the S2' pocket. In addition, compound **7g** only occupies a small fraction (approx. 24%) of the total predicted binding pocket volume, leaving the S2' pocket largely untouched (Figure S4). Therefore, extension of the thiol group in that direction should allow additional ligand-protein interactions, leading to a further improved inhibitory potency. Calculation of Ligand Efficiency (LE) and Lipophilic Ligand Efficiency (LLE) for compound **4** (LE:0.44, LLE:1.67) and our optimized hit **7g** (LE:0.43, LLE:2.37) revealed a slight improvement in LLE with no change in LE, thus representing a successful starting point for further optimization and tuning of this class.

Our work demonstrates the significance of exploiting alternative binding modes to succeed in simple fragment merging. Substrate-inspired design led to an improved potency of previously identified structures accompanied by an enhanced efficacy in vivo, thereby accelerating the translational path. This concept should be applicable to other targets and lays an important foundation for the future development of this class of inhibitors, as they hold the potential to become promising candidates for therapeutic use and to deliver the proof-of-concept of small synthetic molecules targeting virulence factors in the clinic.

Acknowledgments

The authors are grateful for the technical support provided by Simone Amann, Jeannine Jung, Selina Wolter and Dennis Jener. A.K.H. Hirsch gratefully acknowledges funding from the Helmholtz-Association's Initiative and Networking Fund. J. Konstantinović acknowledges funding by the Alexander von Humboldt Foundation. Open Access funding enabled and organized by Projekt DEAL.

Keywords: Antibiotic resistance · Antivirulence · Fragment merging · Mercaptoacetamides · *Pseudomonas aeruginosa*

- [1] A. Bancet, C. Raingeval, T. Lomberget, M. Le Borgne, J. F. Guichou, I. Krimm, *J. Med. Chem.* **2020**, *63*, 11420–11435.
- [2] H. S. Yu, K. Modugula, O. Ichihara, K. Kramschuster, S. Keng, R. Abel, L. Wang, *J. Chem. Theory Comput.* **2021**, *17*, 450–462.
- [3] L. R. de Souza Neto, J. T. Moreira-Filho, B. J. Neves, R. L. B. R. Maidana, A. C. R. Guimarães, N. Furnham, C. H. Andrade, F. P. Silva, *Front. Chem.* **2020**, *8*, 00093.
- [4] World Health Organization, *WHO* **2017**.
- [5] S. S. Magill, J. R. Edwards, W. Bamberg, Z. G. Beldavs, G. Dumyati, M. A. Kainer, R. Lynfield, M. Maloney, L. McAllister-Hollod, J. Nadle, S. M. Ray, D. L. Thompson, L. E. Wilson, S. K. Fridkin, *N. Engl. J. Med.* **2014**, *370*, 1198–1208.
- [6] Y. X. Ma, C. Y. Wang, Y. Y. Li, J. Li, Q. Q. Wan, J. H. Chen, F. R. Tay, L. N. Niu, *Adv. Sci.* **2020**, *7*, 1901872; Correction: Y. X. Ma, C. Y. Wang, Y. Y. Li, J. Li, Q. Q. Wan, J. H. Chen, F. R. Tay, L. N. Niu, *Adv. Sci.* **2020**, *7*, 202000779
- [7] G. Valenza, D. Tappe, D. Turnwald, M. Frosch, C. König, H. Hebestreit, M. Abele-Horn, *J. Cystic Fibrosis* **2008**, *7*, 123–127.
- [8] R. Sordé, A. Pahissa, J. Rello, *Infect. Drug Resist.* **2011**, *4*, 31–41.
- [9] H. Nikaido, F. Yoshimura, *J. Bacteriol.* **1982**, *152*, 636–642.
- [10] K. M. Pos, *Biochim. Biophys. Acta Proteins Proteomics* **2009**, *1794*, 782–793.
- [11] X. Z. Li, P. Plésiat, H. Nikaido, *Clin. Microbiol. Rev.* **2015**, *28*, 337–418.
- [12] D. J. Wolter, P. D. Lister, *Curr. Pharm. Des.* **2012**, *19*, 209–222.
- [13] X. Z. Li, D. M. Livermore, H. Nikaido, *Antimicrob. Agents Chemother.* **1994**, *38*, 1732–1741.
- [14] R. E. W. Hancock, D. P. Speert, *Drug Resist. Updates* **2000**, *3*, 247–255.
- [15] J. M. Thomson, R. A. Bonomo, *Curr. Opin. Microbiol.* **2005**, *8*, 518–524.
- [16] S. W. Dickey, G. Y. C. Cheung, M. Otto, *Nat. Rev. Drug Discovery* **2017**, *16*, 457–471.
- [17] D. A. Rasko, V. Sperandio, *Nat. Rev. Drug Discovery* **2010**, *9*, 117–128.
- [18] S. Wagner, R. Sommer, S. Hinsberger, C. Lu, R. W. Hartmann, M. Empting, A. Titz, *J. Med. Chem.* **2016**, *59*, 5929–5969.
- [19] T. Strateva, I. Mitov, *Ann. Microbiol.* **2011**, *61*, 717–732.
- [20] B. Heras, M. J. Scanlon, J. L. Martin, *Br. J. Clin. Pharmacol.* **2015**, *79*, 208–215.
- [21] A. E. Clatworthy, E. Pierson, D. T. Hung, *Nat. Chem. Biol.* **2007**, *3*, 541–548.
- [22] F. Bastaert, S. Kheir, V. Saint-Criq, B. Villeret, P. M. C. Dang, J. El-Benna, J. C. Sirard, R. Voulhoux, J. M. Sallenave, *Front. Immunol.* **2018**, *9*, 01675.
- [23] P. V. Liu, *J. Infect. Dis.* **1974**, *130*, S94–S99.
- [24] K. Oda, T. Koyama, S. Muraio, *Biochim. Biophys. Acta Enzymol.* **1979**, *571*, 147–156.
- [25] N. Nishino, J. C. Powers, *J. Biol. Chem.* **1980**, *255*, 3482–19.
- [26] G. R. A. Cathcart, D. Quinn, B. Greer, P. Harriott, J. F. Lynas, B. F. Gilmore, B. Walker, *Antimicrob. Agents Chemother.* **2011**, *55*, 2670–2678.
- [27] F. R. Burns, C. A. Paterson, R. D. Gray, J. T. Wells, *Antimicrob. Agents Chemother.* **1990**, *34*, 2065–2069.
- [28] J. Zhu, X. Cai, T. L. Harris, M. Gooyit, M. Wood, M. Lardy, K. D. Janda, *Chem. Biol.* **2015**, *22*, 483–491.
- [29] O. A. Adekoya, S. Sjøli, Y. Wuxiuer, I. Bilto, S. M. Marques, M. A. Santos, E. Nuti, G. Cercignani, A. Rossello, J. O. Winberg, I. Sylte, *Eur. J. Med. Chem.* **2015**, *89*, 340–348.

- [30] E. Kessler, M. Israel, N. Landshman, A. Chechick, S. Blumberg, *Infect. Immun.* **1982**, *38*, 716–723.
- [31] S. Leiris, D. T. Davies, N. Sprynski, J. Castandet, L. Beyria, M. S. Bodnarchuk, J. M. Sutton, T. M. G. Mullins, M. W. Jones, A. K. Forrest, T. D. Pallin, P. Karunakar, S. K. Martha, B. Parusharamulu, R. Ramula, V. Kotha, N. Pottabathini, S. Pothukanuri, M. Lemonnier, M. Everett, *ACS Med. Chem. Lett.* **2021**, *12*, 217–227.
- [32] A. M. Kany, A. Sikandar, J. Hauptenthal, S. Yahiaoui, C. K. Maurer, E. Proschak, J. Köhnke, R. W. Hartmann, *ACS Infect. Dis.* **2018**, *4*, 988–997.
- [33] O. A. Adekoya, I. Sylte, *Chem. Biol. Drug Des.* **2009**, *73*, 7–16.

Manuscript received: September 9, 2021
Accepted manuscript online: November 11, 2021
Version of record online: ■■, ■■

Supporting Information

Substrate-Inspired Fragment Merging and Growing Affords Efficacious LasB Inhibitors

*C. Kaya, I. Walter, S. Yahiaoui, A. Sikandar, A. Alhayek, J. Konstantinović, A. M. Kany, J. Haupenthal, J. Köhnke, R. W. Hartmann, A. K. H. Hirsch**

Table of Contents

General Information.....	S2
Figures and Tables.....	S5
Synthesis of intermediate and final compounds.....	S12
NMR and LC-MS spectra of final compounds.....	S21
References.....	S46

General Information

LasB Inhibition Assay. The purification of LasB from *P. aeruginosa* P14 supernatant and the subsequent performance of the FRET-based *in vitro* inhibition assay were performed as described previously.¹

Antibacterial Activity. Minimum inhibitory concentration (MIC) assays were performed in *P. aeruginosa* PA14 as described previously.¹ The MIC value was higher than 100 μ M for compounds **4**, **7d** and **7g**. For all compounds, at 100 μ M, the bacterial growth was reduced by less than 10%.

Inhibition Assays with human off-targets. Assays focusing on the inhibition of human MMPs and ADAM17 were performed as described previously.^{2,3}

Cytotoxicity Assay. The toxicity of selected compounds towards three cell lines was determined as described previously. Compounds **4**, **7d** and **7g** showed no relevant cytotoxic behaviour against the human hepatoma cell line (HepG2), human embryonic kidney (HEK) 293 cells and adenocarcinomic human alveolar basal epithelial cells (A549) with IC₅₀ values higher than 100 μ M.^{1,4} In detail, while compound **4** showed a very low reduction in the viability of HepG2 (23 \pm 3%) and HEK cells (33 \pm 10%) at 100 μ M, all other inhibition values were found to be below 10%.

X-Ray Crystallography. LasB was expressed and purified as described previously.¹ The protein was concentrated to 12 mg/mL and mixed with compound **7d** at a final concentration of 1 mM. Complex crystals were obtained in 0.1 M sodium acetate pH 4.6, and 15% (w/v) PEG 20,000. Crystals were cryoprotected in glycerol, and diffraction data was collected from single crystals at 100 K at beamline ID30A-3 (ESRF) at a wavelength of 0.967 Å. Data were processed using Xia2 or XDS, and the structure solved using PHASER Molecular Replacement with *P. aeruginosa* elastase (PDB ID 1EZM) as a search model.⁵⁻⁷ The models were manually rebuilt with COOT and refined using PHENIX and Refmac5.⁸⁻¹⁰

Molecular Modeling. Modeling was performed as described previously.¹

Preparation of *P. aeruginosa* supernatant and LasB activity evaluation. A culture of a single colony of PA14 was grown in lysogeny broth medium at 28 °C with constant shaking at 130 rpm for 3 days. Then, the culture was centrifuged at 4 °C, 5000 rpm for 30 minutes. Finally, the supernatant was passed through a membrane filter of 0.2 μ M to sterilize it. The supernatant

was aliquoted and stored at $-80\text{ }^{\circ}\text{C}$ until usage. The LasB activity of the supernatant was evaluated using the FRET-based assay described previously.¹

In vivo Galleria mellonella virulence assay. *G. mellonella* larvae were purchased from BioSystems Technology (Exeter, United Kingdom), stored at $4\text{ }^{\circ}\text{C}$ in the dark and used within 2 weeks. Prior to injection, larvae were immobilized by incubation for 10–15 min on ice. Then, the injection was performed using a LA120 syringe pump (Landgraf Laborsysteme, Langenhagen, Germany) supplied with a 1 mL syringe (B. Braun, Melsungen, Germany) and Sterican $0.30 \times 12\text{ mm}$, $30\text{G} \times 1.5$ sterile needles (B. Braun). The larvae were injected with $10\text{ }\mu\text{L}$ of sample into the last right proleg. The larvae were classified into various groups based on the applied treatment. Two negative control groups supplemented with no injection to control the quality of larvae and a buffer control group injected with sterile PBS were included. A positive control group was also included, and the larvae were administered with 65% (v/v) PA14 supernatant. To test the anti-virulence effect of LasB inhibitors, a mixture of 65% (v/v) PA14 supernatant, LasB inhibitor and $300\text{ }\mu\text{M}$ TCEP were incubated at $37\text{ }^{\circ}\text{C}$ for 30 min and injected into the larvae. All groups were incubated at $37\text{ }^{\circ}\text{C}$ and inspected once per day for 4 days post-treatment and to record mortality. The larvae were considered dead if they are black and do not move when stimulated by contact with the forceps. The survival analysis was performed using GraphPad Prism v8, data were plotted using the Kaplan-Meier method, and statistical significance between groups was calculated with log-rank test.

General Chemistry. All reagents were used from commercial suppliers without further purification. Procedures were not optimized regarding yield. NMR spectra were recorded on a Bruker AV 500 (500 MHz) spectrometer at room temperature. Chemical shifts are given in parts per million (ppm) and referenced against the residual proton, ^1H , or carbon, ^{13}C , resonances of the >99% deuterated solvents as internal reference. Coupling constants (J) are given in Hertz (Hz). Data are reported as follows: chemical shift, multiplicity (s = singlet, d = doublet, t = triplet, dd = doublet of doublets, dt = doublet of triplets, m = multiplet, br = broad and combinations of these) coupling constants and integration. Liquid chromatography-mass spectrometry (LC-MS) was performed on an LC-MS system, consisting of a DionexUltiMate 3000 pump, autosampler, column compartment, and detector (Thermo Fisher Scientific, Dreieich, Germany) and ESI quadrupole MS (MSQ Plus or ISQ EC, Thermo Fisher Scientific, Dreieich, Germany). High-resolution mass spectra were determined by LC-MS/MS using Thermo Scientific Q Exactive Focus Orbitrap LC-MS/MS system. Purity of the final

compounds was determined by LC-MS using the area percentage method on the UV trace recorded at a wavelength of 254 nm and found to be >95%.

Figures and Tables

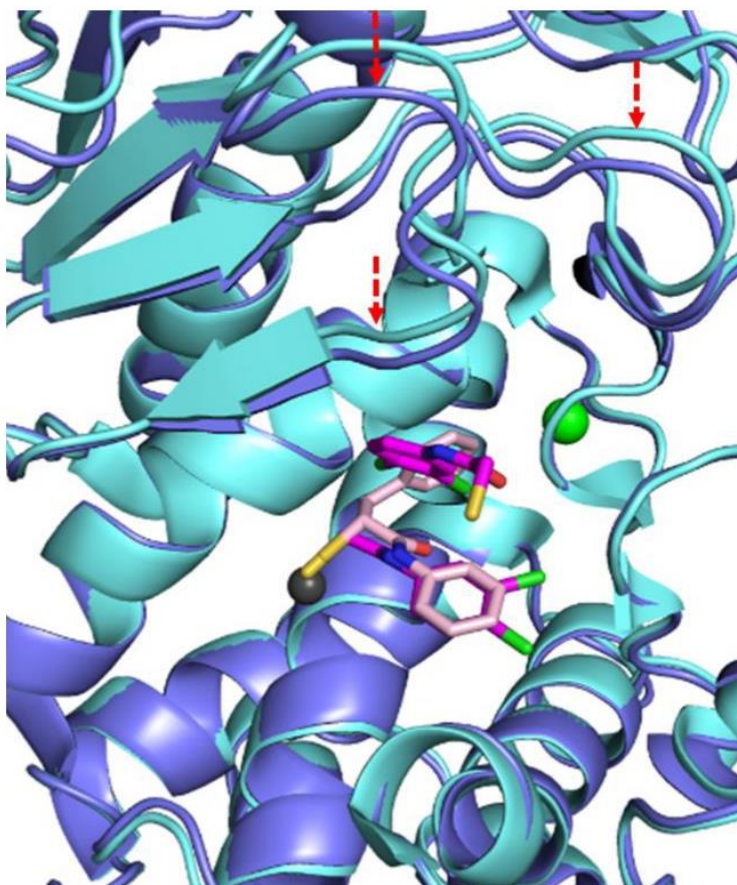


Figure S1. Comparison of compound **7g** and compound **4** binding to LasB. Superposition of the LasB-Compound **4** (aqua; PDB 6f8b) and LasB-**7g** (slate) structures are shown. The movement of loop leading to closure of the binding pocket upon binding to **7g** (light pink sticks) is highlighted by dotted arrows. For simplicity, only the major conformation of **7g** observed in the crystal structure is shown. The color scheme used: **4** (magenta), **7g** (light pink), Zn²⁺ (gray) and Ca²⁺ (green).

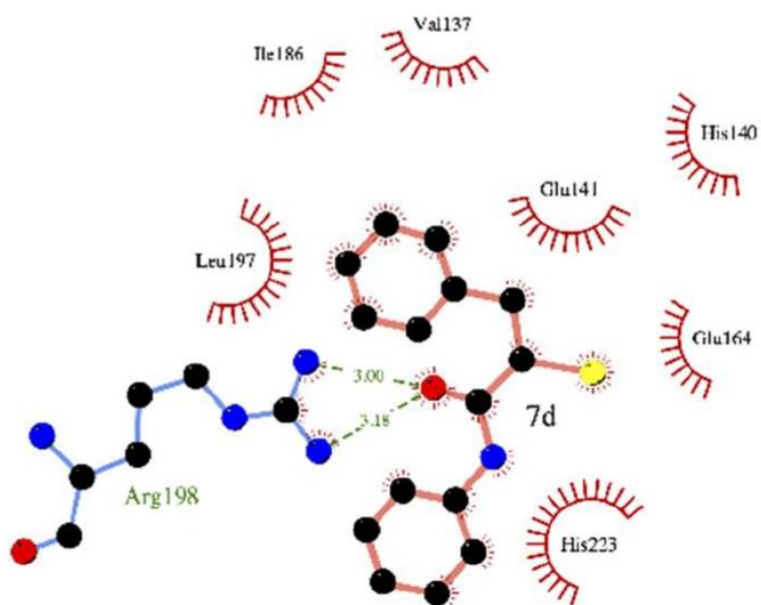


Figure S2. Schematic 2-D representation of LasB-7d complex created with LIGPLOT.

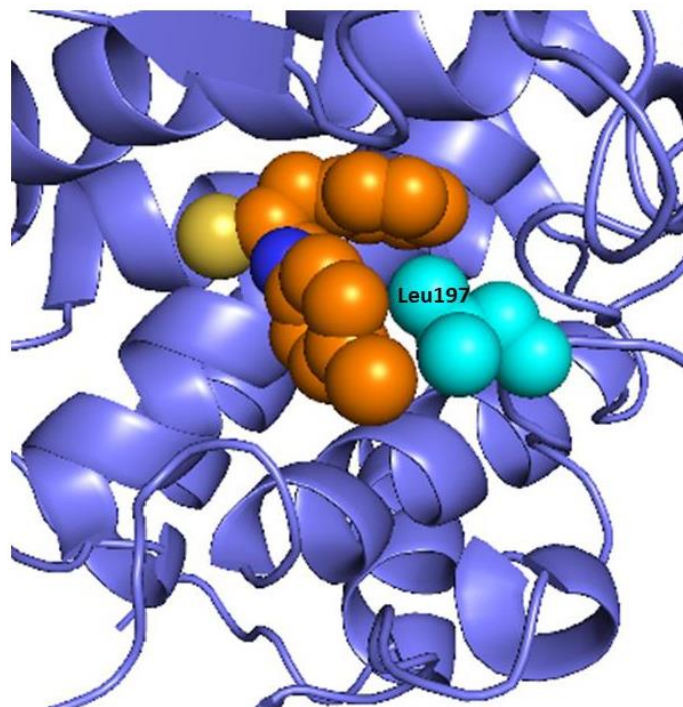


Figure S3. Modelling of *para*-methyl substituted derivative of compound **7d** in the LasB ligand binding pocket.

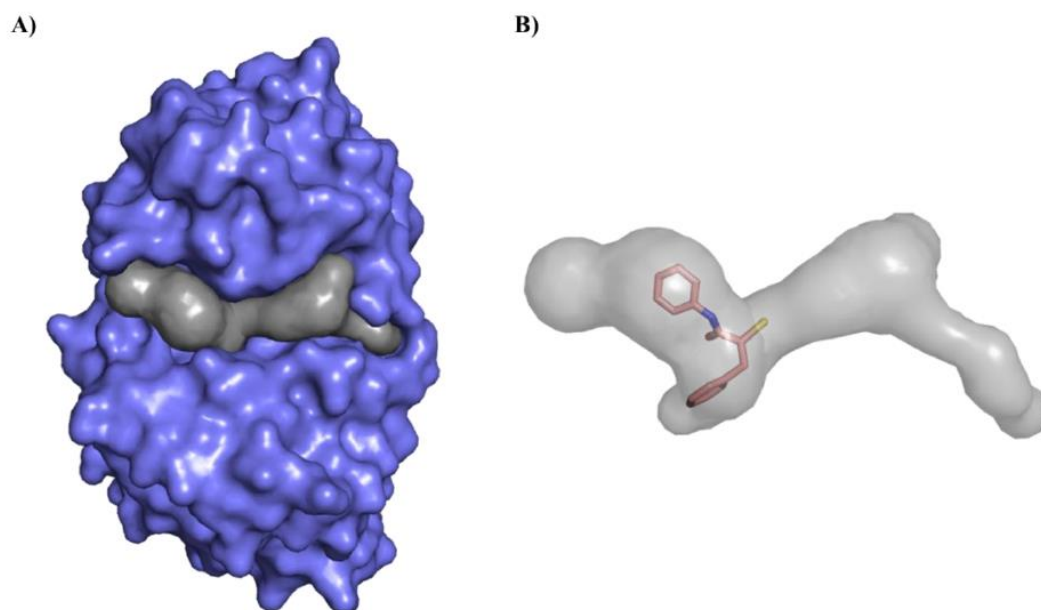


Figure S4. Analysis of putative tunnel identified by CAVER in the structure of LasB in complex with compound **7g**. **A)** LasB (slate) and the computed tunnel (grey) are shown as surface representation. **B)** Surface diagram showing the position of **7g** in the tunnel. Total volume of the tunnel and **7g** was calculated to be approximately 360 \AA^3 and 86 \AA^3 .

Table S1. Data collection and refinement statistics.

LasB_7d	
PDB ID	7OC7
Data collection	
Space group	P 1 2 ₁ 1
Cell dimension	
<i>a</i> , <i>b</i> , <i>c</i> (Å)	39.4, 92.5, 40.76
α , β , γ (°)	90.0, 114.0, 90.0
Wavelength (Å)	0.96768
Resolution	1.95 (2.00 – 1.95) *
<i>R</i> _{sym} or <i>R</i> _{merge}	0.044 (0.141)
<i>R</i> _{pim}	0.029 (0.092)
<i>CC</i> (1/2)	0.99 (0.985)
I / σ I	26.7 (10.2)
Completeness (%)	95.1 (94.1)
Redundancy	6.0 (6.1)
Refinement	
Resolution (Å)	37.21 – 1.95
No. reflection	18485
<i>R</i> _{work} / <i>R</i> _{free}	0.198 / 0.239
No. atoms	2,637
Protein	2,283
Ligands	38
Solvent	316
Protein residues	298
<i>B</i> -factors	17.15
Protein	16.10
Ligands	22.12
Water	24.16

R. m. s deviations	
Bond length (Å)	0.010
Bond angels (°)	0.84
MolProbity score	1.52

*Values in parentheses are for highest-resolution shell.

Table S2. Selectivity of selected inhibitors (n.i. = <10% inhibition).

	4	7d	7g
MMP-1	n.i.	n.i.	n.i.
MMP-2	n.i.	n.i.	n.i.
MMP-3	n.i.	n.i.	n.i.
MMP-7	n.i.	n.i.	n.i.
MMP-8	n.i.	26 ± 4	n.i.
MMP-14	n.i.	n.i.	n.i.
IC₅₀ [μM]			
ADAM17	>100	2.2 ± 0.1	4.8 ± 1.5
HDAC-3	>100	>100	>100
HDAC-8	>100	>100	>100

Synthesis of intermediate and final compounds

General procedure i: Synthesis of chloro acid derivatives 4a–4c from the corresponding amino acid

Amino acid (1.0 eq) was dissolved in 6 N HCl (2 mL/mmol or until mostly dissolved) under nitrogen atmosphere and cooled to -5 °C. NaNO₂ (1.5–2.5 eq) was dissolved in water (0.3 mL/mmol amino acid) and added dropwise slowly. The mixture was stirred overnight while warming to r.t. The reaction mixture was extracted with EtOAc/THF (3:1). The combined organic extracts were washed with saturated aq. NaCl solution and dried over anh. Na₂SO₄ and filtered. The solvent was removed under reduced pressure to afford the product. The crude was used in the next step without further purification.

General procedure ii: Synthesis of derivatives 5a, 5d–5g

The acid (1.0 eq), SOCl₂ (2.0 eq) and a few drops of DMF were heated to 70 °C for 1 h. The cooled mixture was added dropwise to a solution of the corresponding aniline (1.1 eq) in DMF (1 mL/mmol) a cooled to 0 °C. The mixture was stirred at r.t overnight. The reaction was quenched with water and extracted with EtOAc (3x). The combined organic extracts were washed with saturated aq. NaCl solution, dried over anh. Na₂SO₄ and filtered. The solvent was removed under reduced pressure to afford the crude product. The purification was done by column chromatography or flash chromatography.

General procedure iii: Synthesis of derivatives 5b and 5c

2-Chloro-3-cyclohexylpropanoic acid or 2-chloro-3-cyclopropylpropanoic acid (1.2 eq) and EDC·HCl (1.2 eq) were added to a solution of the corresponding aniline (1.0 eq) in DCM. The resultant mixture was stirred at r.t. for 3–4 h. The reaction was monitored with TLC or LC-MS. The solution was washed with 1 M HCl followed by saturated aqueous NaCl solution (1x) then dried over anh. Na₂SO₄. The organic phase was filtered and concentrated under reduced pressure to afford the crude product. The crude was used in the next step without further purification.

General procedure iv: Synthesis of thioacetate derivatives 6a–6g

The amide (1.0 eq) was dissolved in acetone under argon atmosphere. To this solution, CH₃COSK (1.5–2.0 eq) was added, and the reaction was stirred at r.t. for 2–6 h. It was monitored by TLC or LC-MS. The reaction was quenched with water and extracted with EtOAc

(3x). The combined organic extracts were washed with saturated aq. NaCl solution (1x), dried over anh. Na₂SO₄ and filtered. The solvent was removed under reduced pressure to afford the crude product. The purification was done by flash chromatography.

General procedure v: Hydrolysis of thioacetate for derivatives 7a–7g

The thioacetate (1.0 eq) was dissolved in methanol (5 mL/mmol) under argon atmosphere and 2 M aqueous NaOH solution (2.0 eq) or solid NaOH (3.0 eq) was added. The reaction was stirred at r.t. for 1–3 h before quenching with 1 M or 2 M HCl. The reaction was extracted with EtOAc and washed with 0.5 M HCl. The combined organic extracts were washed with saturated aqueous NaCl solution (1x) and then dried over anh. Na₂SO₄. The solvent was removed under reduced pressure to afford the crude product. The purification was done by column chromatography or preparative HPLC (H₂O+0.05%FA/ACN+0.05%FA 95:5 → 5:95).

2-Chloro-3-phenylpropanoic acid (4a)

Compound **4a** was prepared according to **general procedure i**, using DL-phenylalanine (1 g, 6.0 mmol) and NaNO₂ (1.46 g, 21.2 mmol). The crude product was obtained as light yellow oil and used without further purification (1.05 g, 94%). ¹H NMR (500 MHz, CDCl₃) δ ppm: 7.37–7.24 (m, 5H), 4.51 (dd, *J* = 7.8, 6.9 Hz, 1H), 3.42 (dd, *J* = 14.0, 6.7 Hz, 1H), 3.21 (dd, *J* = 14.1, 7.9 Hz, 1H). MS (ESI⁻) *m/z* 183.25 [M-H]⁻, 147.23 [M-H-HCl]⁻.

2-Chloro-N-(3,4-dichlorophenyl)-3-phenylpropanamide (5a)

Compound **5a** was prepared according to **general procedure i**, using compound **4a** (350 mg, 1.90 mmol), SOCl₂ (275 μL, 3.8 mmol) and 3,4-dichloroaniline (339 mg, 2.1 mmol). Purification was done by flash chromatography (Hex/EtOAc, 100:0 to 0:100). The final product was obtained as white solid (388 mg, 62%). ¹H NMR (500 MHz, CDCl₃) δ ppm: 8.03 (s, 1H), 7.71 (d, *J* = 2.5 Hz, 1H), 7.39 (d, *J* = 8.7 Hz, 1H), 7.36–7.23 (m, 6H), 4.68 (dd, *J* = 7.6, 4.5 Hz, 1H), 3.50 (dd, *J* = 14.3, 4.5 Hz, 1H), 3.31 (dd, *J* = 14.3, 7.6 Hz, 1H). ¹³C NMR (126 MHz, CDCl₃) δ ppm: 166.5, 136.2, 135.7, 133.1, 130.7, 129.8, 128.7, 127.6, 122.0, 119.5, 61.8, 41.4. MS (ESI⁺) *m/z* 330.09 [M+H]⁺.

2-Chloro-N-(3',4'-dichlorophenyl)-3-cyclohexylpropanamide (5b).

Compound **5b** was synthesized in two steps. The first step was performed according to **general procedure i**, using DL-3-cyclohexylalanine (260 mg, 1.52 mmol) and NaNO₂ (262 mg, 3.80 mmol). The obtained crude product **4b** was used without further purification. The second step

was achieved according to the **general procedure iii**, using the obtained crude product **4b** from the first step, 3,4-dichloroaniline (205 mg, 1.27 mmol), EDC·HCl (291 mg, 1.52 mmol) and CH₂Cl₂ (10 mL). The reaction was stirred overnight at room temperature. The crude product was purified using column chromatography (100% CH₂Cl₂). The product **5b** was obtained as orange solid (148 mg, 35 % (2 steps)). ¹H NMR (500 MHz, DMSO-*d*₆) δ ppm: 10.64 (s, 1H), 7.99 (d, *J* = 2.5 Hz, 1H), 7.60 (d, *J* = 8.5 Hz, 1H), 7.50 (dd, *J* = 2.5, 8.5 Hz, 1H), 4.58 (dd, *J* = 7.0, 8.5 Hz, 1H), 1.94–1.53 (m, 7H), 1.48–1.31 (m, 1H), 1.26–1.05 (m, 3H), 1.02–0.83 (m, 2H). ¹³C NMR (126 MHz, DMSO-*d*₆) δ ppm: 167.5, 138.5, 131.2, 130.9, 125.6, 120.7, 119.6, 57.1, 41.1, 34.2, 32.6, 31.8, 25.9, 25.6, 25.5. HRMS (ESI⁺) calculated for C₁₅H₁₉Cl₃NO [M+H]⁺ 334.05322, found 334.04984.

2-Chloro-3-cyclopropyl-*N*-(3',4'-dichlorophenyl)propanamide (**5c**).

Compound **5c** was synthesized in two steps. The first step was performed according to the **general procedure i**, using DL-3-cyclopropylalanine (500 mg, 3.87 mmol) and NaNO₂ (668 mg, 9.68 mmol). The obtained crude product **4c** was used in the next step without further purification. The second step was performed according to the **general procedure iii**, using 3,4-dichloroaniline (248 mg, 1.53 mmol), 2-chloro-3-cyclopropylpropanoic acid (273 mg, 1.84 mmol), ClCO₂Et (200 μL, 2.03 mmol), Et₃N (260 μL, 1.84 mmol) and THF (20 mL). The reaction was stirred at room temperature overnight. The crude product was purified using column chromatography (Cyhex/EtOAc, 9:1). The product **5c** was obtained as yellow oil (121 mg, 11% (2 steps)). ¹H NMR (500 MHz, CDCl₃) δ ppm: 8.33 (*br s*, 1H), 7.81 (d, *J* = 2.3 Hz, 1H), 7.44–7.37 (m, 2H), 4.54 (t, *J* = 6.1 Hz, 1H), 2.02 (t, *J* = 6.5 Hz, 2H), 1.04–0.93 (m, 1H), 0.59–0.49 (m, 2H), 0.28–0.15 (m, 2H). ¹³C NMR (126 MHz, CDCl₃) δ ppm: 167.0, 136.3, 132.9, 130.6, 128.3, 121.6, 119.1, 61.6, 40.4, 7.7, 4.74, 3.9. MS (ESI⁺) *m/z* 291.94 [M+H]⁺.

2-Chloro-*N*,3-diphenylpropanamide (**5d**)

Compound **5d** was prepared according to **general procedure ii**, using compound **4a** (934 mg, 5.05 mmol), SOCl₂ (734 μL, 10.1 mmol) and aniline (507 μL, 5.56 mmol). Purification was done by flash chromatography (Hex/EtOAc, 100:0 to 0:100). The product was obtained as white solid (404 mg, 31%). ¹H NMR (500 MHz, DMSO-*d*₆) δ ppm: 7.95 (s, 1H), 7.60–7.52 (m, 2H), 7.38–7.28 (m, 6H), 7.27–7.19 (m, 1H), 7.11–7.04 (m, 1H), 4.76 (t, *J* = 7.5 Hz, 1H), 3.41 (dd, *J* = 13.8, 7.2 Hz, 1H), 3.13 (dd, *J* = 13.9, 7.8 Hz, 1H). MS (ESI⁺) *m/z* 260.08 [M+H]⁺.

2-Chloro-3-phenyl-*N*-(*o*-tolyl)propenamide (**5e**)

Compound **5e** was prepared according to **general procedure ii**, using compound **4a** (259 mg, 1.40 mmol), *o*-toluidine (165 mg, 1.54 mmol), SOCl₂ (203 μL, 2.80 mmol). The crude product was obtained as yellow oil (257 mg, 67%) and used in the next step without further purification. ¹H NMR (500 MHz, CDCl₃) δ ppm: 8.03 (s, 1H), 7.81 (d, *J* = 7.9 Hz, 1H), 7.35–7.25 (m, 5H), 7.23 (t, *J* = 7.7 Hz, 1H), 7.17 (d, *J* = 7.3 Hz, 1H), 7.10 (td, *J* = 7.5, 1.0 Hz, 1H), 4.75 (dd, *J* = 7.6, 4.3 Hz, 1H), 3.54 (dd, *J* = 14.3, 4.3 Hz, 1H), 3.35 (dd, *J* = 14.3, 7.6 Hz, 1H), 2.12 (s, 3H). ¹³C NMR (126 MHz, CDCl₃) δ ppm: 166.2, 136.0, 134.9, 130.7, 130.0, 129.3, 128.6, 127.6, 127.0, 125.8, 122.6, 62.4, 41.6, 17.5. MS (ESI⁺) *m/z* 274.09 [M+H]⁺.

2-Chloro-3-phenyl-*N*-(*m*-tolyl)propenamide (5f)

Compound **5f** was prepared according to **general procedure ii**, using compound **4a** (775 mg, 4.19 mmol), *m*-toluidine (494 mg, 4.61 mmol), SOCl₂ (610 μL, 8.38 mmol). The product was purified using column chromatography (Hex/EtOAc, 100:0 to 0:100). The final product was obtained as yellow oil (510 mg, 44%). ¹H NMR (500 MHz, CDCl₃) δ ppm: 7.95 (s, 1H), 7.28–7.20 (m, 6H), 7.18–7.14 (m, 2H), 6.91 (d, *J* = 7.2 Hz, 1H), 4.60 (dd, *J* = 7.9, 4.4 Hz, 1H), 3.47 (dd, *J* = 14.3, 4.3 Hz, 1H), 3.23 (dd, *J* = 14.4, 7.9 Hz, 1H), 2.28 (s, 3H). MS (ESI⁺) *m/z* 274.07 [M+H]⁺.

2-Chloro-3-phenyl-*N*-(*p*-tolyl)propanamide (5g)

Compound **5g** was prepared according to **general procedure ii**, using compound **4a** (200 mg, 1.08 mmol), SOCl₂ (157 μL, 2.17 mmol) and *p*-toluidine (128 mg, 1.19 mmol). Purification was done by flash chromatography (Hex/EtOAc, 100:0 to 0:100). The final product was obtained as yellow solid (198 mg, 67%). ¹H NMR (500 MHz, CDCl₃) δ ppm: 8.02 (br s, 1H), 7.37–7.26 (m, 7H), 7.15 (d, *J* = 8.2 Hz, 2H), 4.68 (dd, *J* = 7.8, 4.4 Hz, 1H), 3.54 (dd, *J* = 14.3, 4.4 Hz, 1H), 3.31 (dd, *J* = 14.3, 7.8 Hz, 1H), 2.34 (s, 3H). MS (ESI⁺) *m/z* 274.09 [M+H]⁺.

***S*-(1-((3,4-Dichlorophenyl)amino)-1-oxo-3-phenylpropan-2-yl) ethanethioate (6a)**

Compound **6a** was prepared according to **general procedure iv**, using compound **5a** (388 mg, 1.18 mmol) and potassium thioacetate (202 mg, 1.77 mmol) in acetone (10 mL). Purification was done by flash chromatography (Hex/EtOAc 100:0 to 0:100). The final product was obtained as colorless oil (361 mg, 83%). ¹H NMR (500 MHz, CDCl₃) δ ppm: 8.06 (s, 1H), 7.70 (d, *J* = 2.4 Hz, 1H), 7.31 (m, 3H), 7.26 (m, 4H), 4.26 (dd, *J* = 8.4, 7.2 Hz, 1H), 3.42 (dd, *J* = 14.1, 8.5 Hz, 1H), 2.99 (dd, *J* = 14.2, 7.0 Hz, 1H), 2.39 (s, 3H). ¹³C NMR (126 MHz, CDCl₃)

δ ppm: 198.0, 168.7, 137.4, 137.2, 132.9, 130.6, 129.3, 128.8, 127.7, 127.3, 121.6, 119.1, 48.4, 35.6, 30.6. MS (ESI⁺) m/z 369.11 [M+H]⁺, 327.11 [M-Ac+2H]⁺.

2-S-(Acetylthio)-N-(3',4'-dichlorophenyl)-3-cyclohexylpentanamide (6b).

Compound **6b** was synthesized according to **general procedure iv**, using compound **5b** (100 mg, 0.299 mmol), potassium thioacetate (68 mg, 0.60 mmol) and acetone (5 mL). The reaction was stirred at room temperature overnight. The crude product was purified using column chromatography (100% CH₂Cl₂). Compound **6b** was obtained as yellow oil (49 mg, 44%). ¹H NMR (500 MHz, DMSO-*d*₆) δ ppm: 10.59 (s, 1H), 7.98 (*br s*, 1H), 7.57 (d, $J = 8.5$ Hz, 1H), 7.50 (*br d*, $J = 9.0$ Hz, 1H), 4.26 (*br t*, $J = 7.8$ Hz, 1H), 2.36 (s, 3H), 1.87–1.75 (m, 2H), 1.70–1.44 (m, 5H), 1.30–1.04 (m, 4H), 0.99–0.82 (m, 2H). ¹³C NMR (126 MHz, DMSO-*d*₆) δ ppm: 194.3, 169.6, 138.8, 131.1, 130.8, 125.2, 120.6, 119.5, 45.8, 39.5, 35.1, 32.5, 32.3, 30.3, 25.9, 25.6, 25.5. HRMS (ESI⁺) calculated for C₁₇H₂₂Cl₂NO₂S [M+H]⁺ 374.07483, found 374.07126.

2-S-(Acetylthio)-N-(3',4'-dichlorophenyl)-3-cyclopropylpentanamide (6c).

Compound **6c** was synthesized according to the **general procedure iv**, using compound **5c** (118 mg, 0.400 mmol), potassium thioacetate (92 mg, 0.81 mmol) and acetone (4 mL). The reaction was stirred at room temperature overnight. The crude product was purified using column chromatography (Cyhex/EtOAc, 8:2). Compound **6c** was obtained as yellow oil (88 mg, 66%). ¹H NMR (500 MHz, CDCl₃) δ ppm: 8.26 (*br s*, 1H), 7.76 (*br s*, 1H), 7.37–7.30 (m, 2H), 4.10 (t, $J = 7.5$ Hz, 1H), 2.41 (s, 3H), 2.07–1.98 (m, 1H), 1.57–1.53 (m, 1H), 0.88–0.78 (m, 1H), 0.54–0.45 (m, 2H), 0.19–0.12 (m, 2H). ¹³C NMR (126 MHz, CDCl₃) δ ppm: 198.3, 169.2, 137.2, 132.8, 130.4, 127.4, 121.3, 118.9, 47.2, 34.4, 30.4, 9.0, 4.8, 4.7. MS (ESI⁺) m/z 331.98 [M+H]⁺.

S-(1-Oxo-3-phenyl-1-(phenylamino)propan-2-yl) ethanethioate (6d)

Compound **6d** was prepared according to **general procedure iv**, using compound **5d** (242 mg, 0.93 mmol) and potassium thioacetate (118 mg, 1.12 mmol) in acetone (10 mL). Purification was done by flash chromatography (Hex/EtOAc, 100:0 to 0:100). The final product was obtained as colorless oil (127 mg, 46%). ¹H NMR (500 MHz, CDCl₃) δ ppm: 7.96 (*br s*, 1H), 7.46 (d, $J = 8.2$ Hz, 2H), 7.33–7.22 (m, 5H), 7.12–7.07 (m, 2H), 7.09 (t, $J = 7.4$ Hz, 1H), 4.30 (t, $J = 7.7$ Hz, 1H), 3.46 (dd, $J = 14.1, 8.5$ Hz, 1H), 3.01 (dd, $J = 14.1, 7.1$ Hz, 1H), 2.38 (s,

3H). ^{13}C NMR (126 MHz, CDCl_3) δ ppm: 197.3, 168.3, 137.6, 137.6, 129.2, 128.9, 128.6, 127.0, 124.4, 119.8, 48.5, 35.7, 30.4. MS (ESI⁺) m/z 300.17 [M+H]⁺, 258.10 [M-Ac+2H]⁺.

S-(1-Oxo-3-phenyl-1-(*o*-tolylamino)propan-2-yl) ethanethioate (6e)

Compound **6e** was prepared according to **general procedure iv**, using compound **5e** (257 mg, 0.94 mmol) and potassium thioacetate (161 mg, 1.41 mmol) in acetone (10 mL). Purification was done by flash chromatography (Hex/EtOAc, 9:1). The final product was obtained as white solid (149 mg, 51%). ^1H NMR (500 MHz, CDCl_3) δ ppm: 7.85 (d, J = 8.2 Hz, 1H), 7.73 (s, 1H), 7.34–7.26 (m, 4H), 7.23–7.10 (m, 3H), 7.04 (m, 1H), 4.34 (dd, J = 8.5, 7.0 Hz, 1H), 3.54–3.38 (m, 1H), 3.03 (dd, J = 14.1, 7.0 Hz, 1H), 2.38 (s, 3H), 2.14 (s, 3H). ^{13}C NMR (126 MHz, CDCl_3) δ ppm: 197.1, 168.5, 137.8, 135.8, 130.5, 129.4, 128.7, 127.1, 126.8, 125.1, 122.5, 48.5, 35.9, 30.5, 17.7. MS (ESI⁺) m/z 314.17 [M+H]⁺, 272.06 [M-Ac+2H]⁺.

S-(1-Oxo-3-phenyl-1-(*m*-tolylamino)propan-2-yl) ethanethioate (6f)

Compound **6f** was prepared according to **general procedure iv**, using compound **5f** (510 mg, 1.86 mmol) and potassium thioacetate (319 mg, 2.79 mmol) in acetone (10 mL). Purification was done by flash chromatography (Hex/EtOAc, 7:3). The final product was obtained as white powder (300 mg, 51%). ^1H NMR (500 MHz, CDCl_3) δ ppm: 7.91 (s, 1H), 7.31–7.25 (m, 3H), 7.24–7.18 (m, 4H), 7.18–7.12 (m, 1H), 6.88 (d, J = 7.5 Hz, 1H), 4.26 (dd, J = 8.4, 7.2 Hz, 1H), 3.42 (dd, J = 14.1, 8.4 Hz, 1H), 2.97 (dd, J = 14.1, 7.1 Hz, 1H), 2.34 (s, 3H), 2.29 (s, 3H). ^{13}C NMR (126 MHz, CDCl_3) δ ppm: 197.5, 168.4, 139.0, 137.7, 137.6, 129.3, 128.9, 128.7, 127.1, 125.4, 120.5, 116.9, 48.6, 35.8, 30.5, 21.6. MS (ESI⁺) m/z 314.06 [M+H]⁺, 271.99 [M-Ac+2H]⁺.

S-(1-Oxo-3-phenyl-1-(*p*-tolylamino)propan-2-yl) ethanethioate (6g)

Compound **6g** was prepared according to **general procedure iv**, using compound **5g** (190 mg, 0.69 mmol) and potassium thioacetate (119 mg, 1.04 mmol). Purification was done by flash chromatography (Hex/EtOAc, 100:0 to 0:100). The product was obtained as yellow solid (156 mg, 72%). ^1H NMR (500 MHz, CDCl_3) δ ppm: 7.87 (d, J = 11.9 Hz, 1H), 7.32–7.26 (m, 5H), 7.26–7.15 (m, 2H), 7.10 (d, J = 8.2 Hz, 2H), 4.32–4.26 (m, 1H), 3.45 (dd, J = 14.2, 8.4 Hz, 1H), 3.01 (dd, J = 14.0, 7.0 Hz, 1H), 2.37 (s, 3H), 2.31 (s, 3H). ^{13}C NMR (126 MHz, CDCl_3) δ ppm: 197.2, 168.1, 137.6, 135.0, 134.1, 129.4, 129.2, 128.6, 127.0, 119.8, 48.5, 35.8, 30.4, 20.8. MS (ESI⁺) m/z 314.10 [M+H]⁺, 272.04 [M-Ac+2H]⁺.

N-(3,4-Dichlorophenyl)-2-mercapto-3-phenylpropanamide (7a)

Compound **7a** was prepared according to **general procedure v**, using compound **6a** (361 mg, 0.98 mmol) and 2 M NaOH aq. solution (980 μ L, 1.96 mmol). Purification was done by chromatography (Hex/EtOAc, 100:0 to 0:100). The final product was obtained as white solid (138 mg, 43%). ^1H NMR (500 MHz, CDCl_3) δ ppm: 8.06 (br s, 1H), 7.71 (d, $J = 2.0$ Hz, 1H), 7.37 (d, $J = 8.7$ Hz, 1H), 7.31 (dd, $J = 14.6, 6.9$ Hz, 3H), 7.28–7.25 (m, 1H), 7.22 (d, $J = 7.2$ Hz, 2H), 3.72 (dd, $J = 15.3, 6.9$ Hz, 1H), 3.34 (dd, $J = 14.3, 6.6$ Hz, 1H), 3.25 (dd, $J = 13.9, 6.7$ Hz, 1H), 2.11 (d, $J = 9.0$ Hz, 1H). ^{13}C NMR (126 MHz, CDCl_3) δ ppm: 169.8, 137.1, 136.8, 133.0, 130.7, 129.6, 128.8, 128.2, 127.4, 121.8, 119.3, 45.9, 41.5. HRMS (ESI $^-$) m/z calcd. for $\text{C}_{15}\text{H}_{12}\text{Cl}_2\text{NOS}$ $[\text{M}-\text{H}]^-$ 324.00221, found 324.00235.

2-Mercapto-*N*-(3',4'-dichlorophenyl)-3-cyclohexylpropanamide (7b).

Compound **7b** was synthesized according to the **general procedure v**, using compound **6b** (40 mg, 0.11 mmol), sodium hydroxide (13 mg, 0.32 mmol) and MeOH (5 mL). The reaction was stirred at room temperature for 3 h. The crude product was purified using preparative HPLC (CH_3CN (FA 0.05 %)/ H_2O (FA 0.05 %) 5:95 \rightarrow 90:10). The product was obtained as colorless oil (11 mg, 31%). ^1H NMR (500 MHz, $\text{DMSO}-d_6$) δ ppm: 10.39 (s, 1H), 8.00 (d, $J = 2.5$ Hz, 1H), 7.57 (d, $J = 8.5$ Hz, 1H), 7.48 (dd, $J = 2.5, 8.5$ Hz, 1H), 3.53 (dd, $J = 7.0, 8.0$ Hz, 1H), 3.10 (*br s*, 1H), 1.88–1.45 (m, 7H), 1.36–1.03 (m, 4H), 0.96–0.79 (m, 2H). ^{13}C NMR (126 MHz, $\text{DMSO}-d_6$) δ ppm: 171.8, 139.1, 131.1, 130.8, 124.9, 120.4, 119.3, 42.5, 39.2, 35.1, 32.4, 32.4, 26.0, 25.7, 25.6. HRMS (ESI $^+$) calculated for $\text{C}_{15}\text{H}_{20}\text{Cl}_2\text{NOS}$ $[\text{M}+\text{H}]^+$ 332.06427, found 332.06421.

2-Mercapto-*N*-(3',4'-dichlorophenyl)-3-cyclopropylpropanamide (7c).

Compound **7c** was synthesized according to the **general procedure v**, using compound **6c** (88 mg, 0.26 mmol), sodium hydroxide (31 mg, 0.78 mmol) and 5 mL of MeOH. The reaction was stirred at room temperature for 2 h. After extraction, the product was purified column chromatography (Cyhex/EtOAc 8:2). The product was obtained as white solid (20 mg, 26%). ^1H NMR (500 MHz, CDCl_3) δ ppm: 8.21 (*br s*, 1H), 7.68 (s, 1H), 7.13 (s, 2H), 3.44 (q, $J = 7.12$ Hz, 1H), 2.03 (d, $J = 8.54$ Hz, 1H), 1.83–1.68 (m, 2H), 0.80–0.70 (m, 1H), 0.38 (*br d*, $J = 7.93$ Hz, 2H), 0.04 (*br d*, $J = 4.73$ Hz, 2H). ^{13}C NMR (126 MHz, CDCl_3) δ ppm: 170.5, 137.1, 133.1, 130.7, 128.0, 121.6, 119.1, 45.0, 40.5, 8.9, 4.7. HRMS (ESI $^-$) calculated for $\text{C}_{12}\text{H}_{12}\text{Cl}_2\text{NOS}$ $[\text{M}-\text{H}]^-$ 288.00221, found 288.00068.

2-Mercapto-*N*,3-diphenylpropanamide (7d)

Compound **7d** was prepared according to **general procedure v**, using compound **6d** (127 mg, 0.42 mmol) and 2 M NaOH aq. solution (420 μ L, 0.84 mmol). Purification was done by flash chromatography (Hex/EtOAc 100:0 to 0:100). The final product was obtained as white solid (46 mg, 43%). ^1H NMR (500 MHz, CDCl_3) δ ppm: 8.02 (br s, 1H), 7.46 (d, $J = 8.1$ Hz, 2H), 7.36–7.29 (m, 4H), 7.29–7.23 (m, 3H), 7.14 (t, $J = 7.6$ Hz, 1H), 3.72 (dd, $J = 14.8, 6.6$ Hz, 1H), 3.38 (dd, $J = 13.8, 6.5$ Hz, 1H), 3.24 (dd, $J = 13.8, 6.8$ Hz, 1H), 2.11 (d, $J = 8.9$ Hz, 1H). ^{13}C NMR (126 MHz, CDCl_3) δ ppm: 169.5, 137.2, 137.1, 129.3, 129.0, 128.5, 127.1, 124.7, 120.0, 45.7, 41.3. HRMS (ESI⁺) m/z calcd. for $\text{C}_{15}\text{H}_{16}\text{NOS}$ [$\text{M}+\text{H}$]⁺ 258.09471, found 258.09434.

2-Mercapto-3-phenyl-*N*-(*o*-tolyl)propenamide (7e)

Compound **7e** was prepared according to **general procedure v**, using compound **6e** (148 mg, 0.47 mmol) and 2 M NaOH aq. solution (475 μ L, 0.95 mmol) in MeOH (2.5 mL). Purification was done by column chromatography (Hex/EtOAc 7/3). The final product was obtained as white solid (25 mg, 20%). ^1H NMR (500 MHz, CDCl_3) δ ppm: 8.03 (s, 1H), 7.81 (d, $J = 8.0$ Hz, 1H), 7.38–7.24 (m, 5H), 7.22 (t, $J = 7.8$ Hz, 1H), 7.16 (d, $J = 7.3$ Hz, 1H), 7.08 (t, $J = 7.2$ Hz, 1H), 3.79 (dt, $J = 8.8, 6.6$ Hz, 1H), 3.36 (dd, $J = 13.8, 6.4$ Hz, 1H), 3.29 (dd, $J = 13.8, 6.7$ Hz, 1H), 2.11 (t, $J = 4.4$ Hz, 3H), 2.11 (d, $J = 8.7$ Hz, 1H). ^{13}C NMR (126 MHz, CDCl_3) δ ppm: 169.6, 137.4, 135.3, 130.6, 129.7, 129.1, 128.7, 127.3, 126.9, 125.5, 122.5, 46.1, 41.6, 17.7. HRMS (ESI⁺) m/z calcd. for $\text{C}_{16}\text{H}_{18}\text{NOS}$ [$\text{M}+\text{H}$]⁺ 272.11036, found 272.11025.

2-Mercapto-3-phenyl-*N*-(*m*-tolyl)propenamide (7f).

Compound **7f** was prepared according to **general procedure v**, using compound **6f** (298 mg, 0.95 mmol) and 2 M NaOH aq. solution (951 μ L, 2 mmol) in MeOH (5 mL). The final product was obtained as white solid without further purification (227 mg, 88%). ^1H NMR (500 MHz, Acetone- d_6) δ ppm: 9.17 (s, 1H), 7.43 (s, 1H), 7.37 (d, $J = 8.1$ Hz, 1H), 7.30–7.17 (m, 5H), 7.15 (t, $J = 7.8$ Hz, 1H), 6.87 (d, $J = 7.5$ Hz, 1H), 3.76–3.71 (m, 1H), 3.38–3.29 (m, 1H), 3.00 (dd, $J = 13.6, 6.3$ Hz, 1H), 2.54 (d, $J = 9.6$ Hz, 1H), 2.27 (s, 3H). ^{13}C NMR (126 MHz, Acetone- d_6) δ ppm: 171.1, 139.9, 139.7, 139.1, 130.0, 129.4, 129.1, 127.4, 125.2, 120.7, 117.3, 45.1, 43.0, 21.4. HRMS (ESI⁻) m/z calcd. for $\text{C}_{16}\text{H}_{16}\text{NOS}$ [$\text{M}-\text{H}$]⁻ 270.09580, found 270.09560.

2-Mercapto-3-phenyl-*N*-(*p*-tolyl)propenamide (7g).

Compound **7g** was prepared according to **general procedure v**, using compound **6g** (100 mg, 0.32 mmol) and 2 M NaOH aq. solution (320 μ L, 0.64 mmol). Purification was done by flash chromatography (Hex/EtOAc, 100:0 to 0:100). The final product was obtained as white solid (58 mg, 67%). ^1H NMR (500 MHz, CDCl_3) δ ppm: 7.94 (br s, 1H), 7.36–7.29 (m, 4H), 7.28–

7.23 (m, 3H), 7.13 (d, $J = 8.4$ Hz, 2H), 3.70 (dt, $J = 8.8, 6.7$ Hz, 1H), 3.37 (dd, $J = 14.0, 6.4$ Hz, 1H), 3.24 (dd, $J = 13.0, 6.4$ Hz, 1H), 2.31 (s, 3H), 2.10 (d, $J = 8.9$ Hz, 1H). ^{13}C NMR (126 MHz, CDCl_3) δ ppm: 169.5, 137.5, 134.8, 134.6, 129.7, 129.6, 128.7, 127.3, 120.2, 46.0, 41.7, 21.0. HRMS (ESI⁺) m/z calcd. for $\text{C}_{16}\text{H}_{18}\text{NOS}$ $[\text{M}+\text{H}]^+$ 272.11036, found 272.1099.

References

- (1) Kany, A. M.; Sikandar, A.; Hauptenthal, J.; Yahiaoui, S.; Maurer, C. K.; Proschak, E.; Köhnke, J.; Hartmann, R. W. Binding Mode Characterization and Early in Vivo Evaluation of Fragment-Like Thiols as Inhibitors of the Virulence Factor LasB from *Pseudomonas Aeruginosa*. *ACS Infect. Dis.* **2018**, *4* (6), 988–997. <https://doi.org/10.1021/acsinfecdis.8b00010>.
- (2) Schönauer, E.; Kany, A. M.; Hauptenthal, J.; Hüsecken, K.; Hoppe, I. J.; Voos, K.; Yahiaoui, S.; Elsässer, B.; Ducho, C.; Brandstetter, H.; Hartmann, R. W. Discovery of a Potent Inhibitor Class with High Selectivity toward Clostridial Collagenases. *J. Am. Chem. Soc.* **2017**, *139* (36), 12696–12703. <https://doi.org/10.1021/jacs.7b06935>.
- (3) Kany, A. M.; Sikandar, A.; Yahiaoui, S.; Hauptenthal, J.; Walter, I.; Empting, M.; Köhnke, J.; Hartmann, R. W. Tackling *Pseudomonas Aeruginosa* Virulence by a Hydroxamic Acid-Based LasB Inhibitor. *ACS Chem. Biol.* **2018**, *13* (9), 2449–2455. <https://doi.org/10.1021/acscchembio.8b00257>.
- (4) Hauptenthal, J.; Baehr, C.; Zeuzem, S.; Piiper, A. RNase A-like Enzymes in Serum Inhibit the Anti-Neoplastic Activity of siRNA Targeting Polo-like Kinase 1. *Int. J. Cancer* **2007**, *121* (1), 206–210. <https://doi.org/10.1002/ijc.22665>.
- (5) Winter, G. Xia2: An Expert System for Macromolecular Crystallography Data Reduction. *J. Appl. Crystallogr.* **2010**, *43* (1), 186–190. <https://doi.org/10.1107/S0021889809045701>.
- (6) Kabsch, W. XDS. *Acta Crystallogr. Sect. D Biol. Crystallogr.* **2010**, *66*, 125–132. <https://doi.org/10.1107/S0907444909047337>.
- (7) McCoy, A. J.; Grosse-Kunstleve, R. W.; Adams, P. D.; Winn, M. D.; Storoni, L. C.; Read, R. J. Phaser Crystallographic Software. *J. Appl. Crystallogr.* **2007**, *40*, 658–674. <https://doi.org/10.1107/S0021889807021206>.
- (8) Emsley, P.; Lohkamp, B.; Scott, W. G.; Cowtan, K. Features and Development of Coot. *Acta Crystallogr. D. Biol. Crystallogr.* **2010**, *66* (Pt 4), 486–501. <https://doi.org/10.1107/S0907444910007493>.
- (9) Adams, P. D.; Afonine, P. V.; Bunkóczi, G.; Chen, V. B.; Davis, I. W.; Echols, N.; Headd, J. J.; Hung, L.-W.; Kapral, G. J.; Grosse-Kunstleve, R. W.; McCoy, A. J.; Moriarty, N. W.; Oeffner, R.; Read, R. J.; Richardson, D. C.; Richardson, J. S.; Terwilliger, T. C.; Zwart, P. H. PHENIX: A Comprehensive Python-Based System for Macromolecular Structure Solution. *Acta Crystallogr. D. Biol. Crystallogr.* **2010**, *66* (Pt 2), 213–221. <https://doi.org/10.1107/S0907444909052925>.
- (10) Skubák, P.; Murshudov, G. N.; Pannu, N. S. Direct Incorporation of Experimental Phase Information in Model Refinement. *Acta Crystallogr. Sect. D* **2004**, *60* (12 Part 1), 2196–2201. <https://doi.org/10.1107/S09074449040190>.

2.2 Structure-Based Design of α -Substituted Mercaptoacetamides as Inhibitors of the Virulence Factor LasB from *Pseudomonas aeruginosa*

Cansu Kaya, Isabell Walter, Alaa Alhayek, Roya Shafiei, Gwenaëlle Jézéquel, Anastasia Andreas, Jelena Konstantinović, Esther Schönauer, Asfandyar Sikandar, Jörg Haupenthal, Rolf Müller, Hans Brandstetter, Rolf W. Hartmann, Anna K.H. Hirsch

ACS Infectious Diseases 2022 8 (5), 1010–1021 DOI: 10.1021/acsinfecdis.1c00628.

Structure-Based Design of α -Substituted Mercaptoacetamides as Inhibitors of the Virulence Factor LasB from *Pseudomonas aeruginosa*

Cansu Kaya, Isabell Walter, Alaa Alhayek, Roya Shafiei, Gwenaëlle Jézéquel, Anastasia Andreas, Jelena Konstantinović, Esther Schönauer, Asfandyar Sikandar, Jörg Haupenthal, Rolf Müller, Hans Brandstetter, Rolf W. Hartmann, and Anna K.H. Hirsch*



Cite This: *ACS Infect. Dis.* 2022, 8, 1010–1021



Read Online

ACCESS |



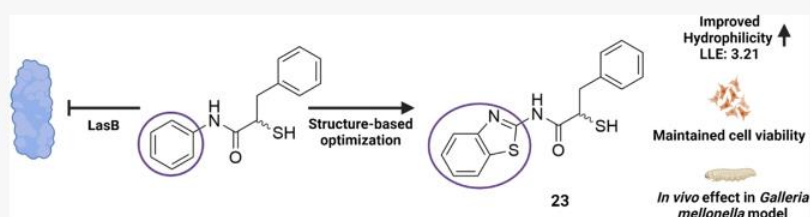
Metrics & More



Article Recommendations



Supporting Information



ABSTRACT: Antivirulence therapy has become a widely applicable method for fighting infections caused by multidrug-resistant bacteria. Among the many virulence factors produced by the Gram-negative bacterium *Pseudomonas aeruginosa*, elastase (LasB) stands out as an important target as it plays a pivotal role in the invasion of the host tissue and evasion of the immune response. In this work, we explored the recently reported LasB inhibitor class of α -benzyl-*N*-aryl mercaptoacetamides by exploiting the crystal structure of one of the compounds. Our exploration yielded inhibitors that maintained inhibitory activity, selectivity, and increased hydrophilicity. These inhibitors were found to reduce the pathogenicity of the bacteria and to maintain the integrity of lung and skin cells in the diseased state. Furthermore, two most promising compounds increased the survival rate of *Galleria mellonella* larvae treated with *P. aeruginosa* culture supernatant.

KEYWORDS: antibiotic resistance, structure-based design, virulence factors, LasB, heterocycles, mercaptoacetamides

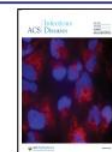
The lack of efficient therapeutics on the market for targeting resistant bacteria calls for the development of novel pathoblockers, agents capable of disarming bacteria by inhibiting their pathogenicity traits rather than killing them directly.^{1,2} *P. aeruginosa* is a Gram-negative bacterium that causes around 10% of hospital-acquired infections and shows a high incidence in immunocompromised patients and in patients with cystic fibrosis.^{3–6} This opportunistic bacterium features several important mechanisms contributing to resistance development. Its efflux pumps can efficiently transport undesired antimicrobials out of the cell, while the secretion of β -lactamases eliminates the effect of β -lactam antibiotics by hydrolyzing their β -lactam ring.^{7–10} Furthermore, its low outer-membrane permeability prevents antibiotics from entering the cell and represents a challenge for the development of effective antibiotics.^{11–13} All these factors underline the urgent need to develop novel therapeutic options for the treatment of infections caused by these bacteria.

Rather than focusing on bacterial viability, combating resistant bacteria by targeting their virulence factors has recently gained more attention.^{14,15} These extracellular proteins are secreted by pathogenic bacteria and play

important roles in various mechanisms, such as biofilm formation, invasion of host cells, and evasion of the immune response, thus contributing to the establishment and the progression of the disease.¹⁶ The development of inhibitors of such targets can facilitate the clearance of the pathogen either by the host immune system or by antibiotics.^{17,18} The main advantages of this method are the reduced selection pressure on the bacteria, which reduces the risk of resistance development by blocking the colonization and infiltration of the host, and the fact that the commensal bacteria remain unaffected.¹⁴ Although only a few small-molecule inhibitors have approached clinical application, numerous *in vitro* and *in vivo* studies support the efficacy of this strategy.^{14,19} One recent successful example is the antibody drug bezlotoxumab,

Received: December 1, 2021

Published: April 22, 2022



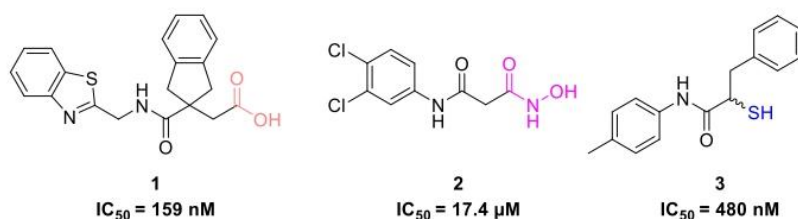


Figure 1. Structures of reported LasB inhibitors.^{33,38,40} Zinc-binding moieties are colored.

which is market-approved and used as a toxin B neutralizer in the treatment of *Clostridium difficile* infections.²⁰

LasB is considered as the key virulence factor secreted by *Pseudomonas aeruginosa*.²¹ It is a zinc-metalloprotease responsible for the pathogenic invasion of tissues and development of acute infections.^{16,22} It can degrade elastin, fibrin, and collagen, which are the vital components of lung tissue, blood vessels, and skin.²³ It is also involved in the inactivation of human immunoglobulins A and G as well as the cytokines gamma-interferon and tumor necrosis factor alpha.^{24–29} All these collective mechanisms of LasB make it an attractive target for an antivirulence-based therapy.

Over the past few years, various inhibitor classes such as natural products,^{29,30} phosphoramidon (Pam),³¹ and several nonpeptidic compounds³² have been reported as inhibitors of LasB. Virtual-screening campaigns also reported fragment-like inhibitors with submicromolar activity (Figure 1, compound 1).³³ Small synthetic molecules such as thiols, hydroxamates, or mercaptoacetamides^{34–39} are commonly reported because of their metal-chelating motifs (Figure 1, compound 2). By successfully applying fragment-merging we recently identified α -benzyl-*N*-aryl mercaptoacetamides as potent LasB inhibitors that are highly selective over a range of human metalloenzymes (Figure 1, compound 3).⁴⁰

The major bottleneck in the development of potent LasB inhibitors is the problem of selectivity with respect to mammalian metalloenzymes, which play a prominent role in metabolism.⁴¹ Matrix metalloproteases (MMPs) are a family of zinc-dependent endopeptidases bearing a Zn²⁺ ion in their catalytic domain, posing a potential selectivity issue for inhibitors with zinc-chelating motifs.⁴² Based on the depth of their S1' binding pocket, MMPs are divided into three classes: deep, intermediate, and shallow. Considering these differences in structure, pre-assessment of selectivity for designed inhibitors is important to obtain potent inhibitors with an acceptable selectivity profile against these off-targets.

We recently reported a successful fragment-merging strategy leading to the discovery of a highly selective and potent class of α -benzyl-*N*-aryl mercaptoacetamides as LasB inhibitors.⁴⁰ Identification of compound 5 in Figure 2 in combination with its X-ray crystal structure with LasB allowed us to

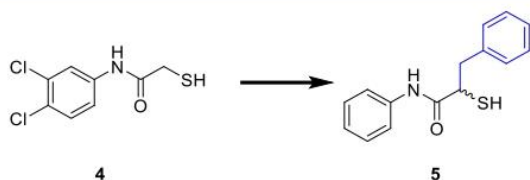


Figure 2. Structure of previously reported LasB inhibitors *N*-aryl mercaptoacetamide 4⁴³ and α -benzyl-*N*-aryl mercaptoacetamide derivative 5.⁴⁰

rationalize the binding mode of this class. A 12-fold boost in potency ($IC_{50} = 0.48 \pm 0.04 \mu M$) observed for inhibitor 3 compared to compound 4 also resulted in an improved *in vivo* effect in a *Galleria mellonella* model, demonstrating the success of this class in reducing bacterial pathogenicity.

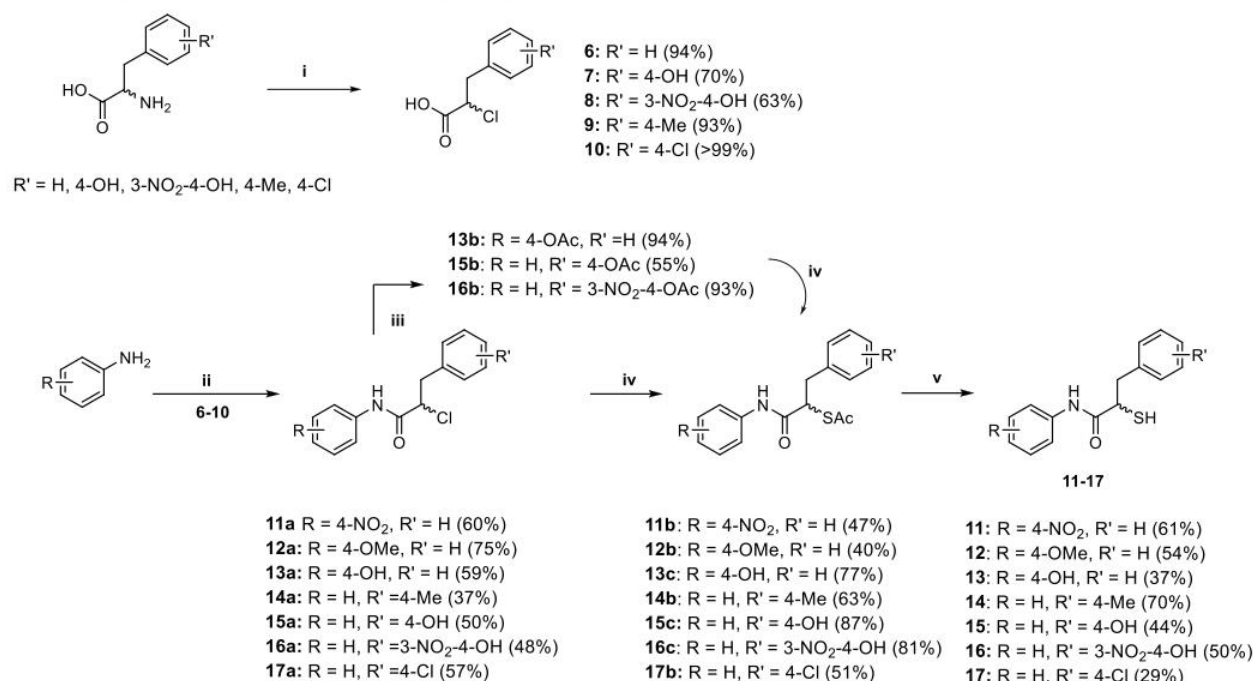
In this work, we embarked on the multiparameter optimization of compound 5 aided by structure-based design. We synthesized seven derivatives by varying the substituents on both aryl rings and nine derivatives in which the *N*-aryl ring was replaced with various heterocycles and evaluated their inhibitory activity against LasB. To demonstrate the potential of the optimized inhibitors, we profiled them in terms of their activity, selectivity, and performance in whole-cell and *in vivo* models. We identified promising inhibitors that maintained efficacy and selectivity compared to compounds 3 and 5. These inhibitors also reduced the pathogenicity of *P. aeruginosa* LasB during the diseased state in lung and skin cell lines. Demonstration of *in vivo* efficacy in a *G. mellonella* model highlights the potential of this class of inhibitors as effective antivirulence agents.

RESULTS AND DISCUSSION

Synthesis and Evaluation of α -Benzyl-*N*-aryl Mercaptoacetamide Derivatives. As we observed a 12-fold improvement in potency by the introduction of a small-sized methyl substituent on the *N*-aryl ring, we first analyzed the effect of other small-sized substituents on activity. Consequently, we synthesized seven derivatives bearing various substituents on both aromatic rings and evaluated their inhibitory activity against LasB. We previously identified the *para*-position to be the most favorable for a methyl group on the *N*-aryl ring. Following this observation, we introduced nitro, methoxy, and hydroxyl groups in the same position. The synthetic route is shown in Scheme 1.

The synthesis started with diazotization and subsequent chlorination of the corresponding commercially available racemic amino acids.⁴⁴ Coupling of the α -chloro carboxylic acid (6–10) with the respective aniline gave the desired amide function (11a–17a). Derivatives containing hydroxyl groups were protected by a reaction with acetic anhydride (13b, 15b, and 16b). The thioacetate function was introduced via an SN2 reaction using potassium thioacetate. The final deprotection of the thioacetate function under basic conditions yielded compounds 11–17 in 29–70% yield as free thiol. The inhibitory activity of the final compounds against LasB was determined as previously reported (Table 1).⁴³

The electron-withdrawing nitro substituent in the *para*-position in compound 11 proved to be less beneficial for the activity compared to the methyl group in compound 3. A slight improvement in potency was achieved through the methoxy group in compound 12. Based on this observation, we synthesized compound 13 with a hydroxyl group, which

Scheme 1. Synthetic Scheme of the α -Benzyl-*N*-aryl Mercaptoacetamide Class^a

^a(i) sodium nitrite, 6 N HCl, 0 °C–r.t., 16 h; (ii) thionyl chloride, DMF, 70 °C, 1 h, aniline derivative, DMF, 0 °C–r.t., 16 h; (iii) Et₃N, DMAP, DCM, acetic anhydride, 0 °C–r.t., 30 min; (iv) potassium thioacetate, acetone, r.t., 5 h; (v) 2 M aq. NaOH solution, MeOH, r.t., 1.5 h.

Table 1. Structures and Inhibitory Activities of α -Benzyl-*N*-aryl Mercaptoacetamide Derivatives 3, 5, and 11–17 against LasB^a

compound	R	R'	IC ₅₀ (μ M)
3	4-Me	H	0.48 \pm 0.04
5	H	H	1.2 \pm 0.1
11	4-NO ₂	H	1.0 \pm 0.1
12	4-OMe	H	0.7 \pm 0.03
13	4-OH	H	0.6 \pm 0.04
14	H	4-Me	2.8 \pm 0.3
15	H	4-OH	7.4 \pm 0.6
16	H	3-NO ₂ -4-OH	2.5 \pm 0.2
17	H	4-Cl	1.1 \pm 0.1

^aMean and SD values of at least two independent experiments.

maintained the activity in a similar range as compounds 11 and 12.

Overall, electron-donating substituents on the *N*-aryl ring proved to be more beneficial for the activity, irrespective of their hydrophilicity (12 and 13), while electron-withdrawing polar substituents such as nitro group in compound 11 did not significantly improve the activity compared to compound 3.

Introduction of various substituents on the benzyl ring in *para*-position yielded mainly unfavorable interactions, with the exception of compound 17. Introducing a methyl group in the *para*-position in compound 14 only led to a twofold decrease

in activity compared to compound 5. The hydrophilic hydroxyl group led to a 15-fold decrease in activity of compound 15 as compared to compound 3. Even though the addition of a strong electron-withdrawing nitro substituent in the *meta*-position in compound 16 compensated for the loss in activity, it remained low in comparison to the modifications on the *N*-aryl ring. Introduction of a *para*-chloro group in compound 17 increased the activity to a similar range compared to the modifications on the *N*-aryl ring, showing a slight increase compared to compound 5.

These observations imply that a chloro substituent seems to be beneficial for the activity; however, a deeper exploration of various regioisomers and combinations with the *N*-aryl ring modifications is necessary for fine-tuning of the activity.

Replacement of the *N*-Aryl Ring with Heterocycles.

The crystal structure of compound 5 allowed us to examine different strategies for further optimization.⁴⁰ We previously discovered that the *N*-arylacetamide group in the S1' pocket is stabilized by H-bonding and hydrophobic interactions. Introduction of a methyl substituent in *para*-position has improved the lipophilic interactions in the S1 pocket (Figure 3). To further improve these core interactions, we performed a molecular-docking study to replace the *N*-aryl ring with various heterocycles. By introducing this, we aimed to exploit the potential interactions such as H-bonding with the surrounding asparagine or arginine residues or π - π interactions with histidine residues.

Heterocycles are utilized in medicinal chemistry for the tuning of various physicochemical properties such as polarity, H-bonding capacity, and solubility. Pyridines, thiazoles, and benzimidazoles are commonly present in many natural products and in anti-infective drugs, providing diverse pharmaceutical applications.^{46,47}

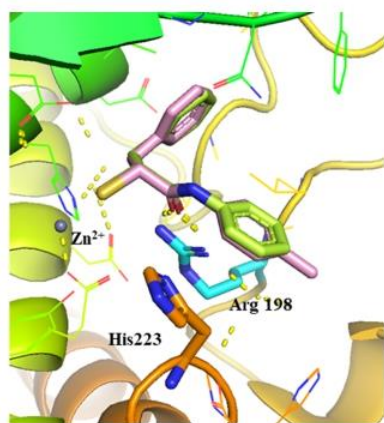


Figure 3. Superimposition of LasB (cyan surface) in complex with compound **5** (lime green, major conformation shown, PDB code: 7OC7) and the modeled pose of hit structure **3** (pink) with key interacting residues. The phenyl group occupies the S1' binding site of the enzyme. The active site Zn²⁺ cation is shown as a gray sphere. The interactions in the binding pocket of LasB are predicted by SeeSAR V.11.1, and all figures are visualized using PyMOL V.2.5 software.⁴⁵

We selected several heterocycles differing in size and substituents and generated docking poses in the binding pocket of LasB using SeeSAR V.11.1, and visualized the interactions with PyMOL V.2.5 software (Figure S1).^{45,48} Figures showing docked compounds as stick representation were generated using PyMOL V.2.5 software. As we previously observed a preference for the *R*-configuration of the ligands in the binding pocket of LasB, all compounds were docked in their *R*-configuration. Predicted interactions in the binding pocket for two selected pyridine and benzothiazole derivatives are shown in Figure 4.

Upon replacement of the *N*-aryl ring with a pyridyl ring, the docking study predicted similar hydrophobic interactions of the benzyl ring with Val137 and Leu197 and a cation- π interaction with Arg198 as in compound **5** (Figure 4A). Additionally, a potential H-bond of the N atom in the ring with Asn112 could be predicted. Introducing a slightly larger benzothiazolyl ring (Figure 4B) led to some additional π - π stacking interactions with His223 residues along with cation- π

interactions with Arg198. In most of the docking poses, the orientation of the heterocyclic compounds did not differ significantly from the crystal structure of **5** in complex with LasB.

Synthesis and Evaluation of α -Benzyl *N*-Heteroaryl Mercaptoacetamide Derivatives. Based on the input from docking, we selected and synthesized nine heterocyclic compounds. The synthetic route is summarized in Scheme 2.

The synthesis of heterocyclic derivatives **18**–**26** was achieved by coupling compound **6** with the corresponding heterocyclic anilines using either ethyl chloroformate or 1-[bis(dimethylamino)methylene]-1*H*-1,2,3-triazolo[4,5-*b*]pyridinium 3-oxide hexafluorophosphate (HATU) as the coupling reagent. Nucleophilic substitution of chlorine yielded the corresponding thioacetate intermediates **18b**–**26b**, which were hydrolyzed under basic conditions to afford free thiol derivatives **18**–**20** and **23**–**26** in moderate-to-good yield (14–84%). For the final compounds **21** and **22**, hydrolysis was performed under acidic conditions, with yields of 29 and 35%, respectively.

IC₅₀ values for all nine derivatives against LasB were determined as reported previously (Table 2).⁴³

Replacement of the *N*-aryl ring with a thiazolyl group in compound **18** maintained the potency in the range of compound **5**. Interestingly, with a relatively small substituent, methyl thiophenyl 3-carboxylate in compound **19**, we observed an almost fivefold drop in IC₅₀ value, presumably caused by unfavorable interactions due to the highly hydrophobic nature of the binding pocket.

We then explored pyridyl analogues in compounds **20**, **21**, and **22**. Compounds **21** and **22** demonstrated a two-fold decrease in potency compared to compound **5**, whereas compound **20** with a 3-pyridyl group did not improve the activity further. Nevertheless, among the three regioisomers, compound **20** demonstrated that the *meta*-position is most favorable for the potency.

Upon the introduction of a larger benzothiazolyl ring in compound **23**, the activity increased two-fold compared to compounds **18** and **20**. The introduction of this ring also proved to be important for the activity when compared to *N*-phenyl derivative **5**. This improvement presumably stems from the additional π - π stacking with the surrounding histidine residues for compound **23**, as predicted by the docking poses. Although similar in size, the benzimidazolyl compound **26** led

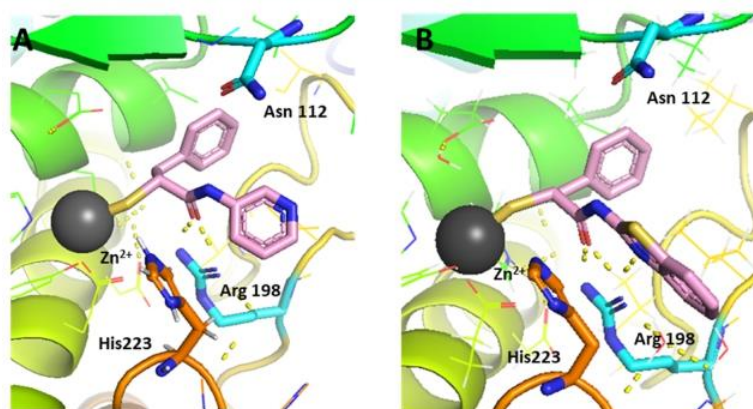
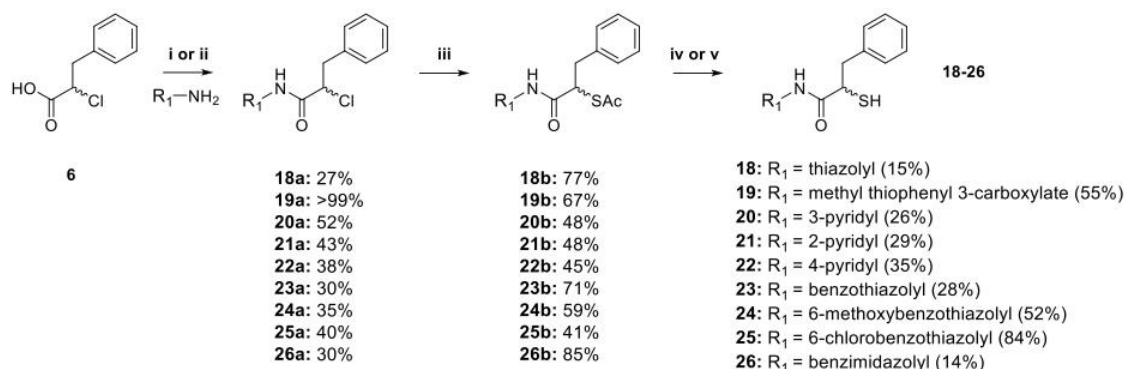


Figure 4. Selected docking poses for (A) 3-pyridine and (B) benzothiazole replacement. The interactions in the binding pocket of LasB (PDB code: 7OC7) are predicted by SeeSAR V.11.1 and visualized using PyMOL V.2.5 software. The dashed lines represent H bonds of less than 2.15 Å.

Scheme 2. Synthetic Scheme of Heterocyclic Derivatives^a

^a(i) Et₃N, ethyl chloroformate, THF, r.t. overnight or (ii) HATU, DIEA, DCM, overnight; (iii) potassium thioacetate, acetone, r.t., 5 h; (iv) 2 M aq. NaOH solution, MeOH, r.t., 1.5 h or (v) AcCl, MeOH, r.t., 30–40 h.

Table 2. Structures and Inhibitory Activities of α -Benzyl-*N*-heteroaryl Mercaptoacetamides 18–26 against LasB^a

Compound	R	IC ₅₀ (μ M)
5		1.2 \pm 0.1
18		1.6 \pm 0.1
19		8.0 \pm 1.1
20		1.2 \pm 0.04
21		3.1 \pm 0.2
22		4.9 \pm 0.5
23		0.7 \pm 0.1
24		1.0 \pm 0.1
25		2.4 \pm 0.2

^aMeans and SD of at least two independent experiments.

to a dramatic decrease in the inhibitory activity. The comparison of interactions of the two structures in the binding pocket of LasB (Figure 5) reveals a slightly different binding mode for compound 26, lacking some key interactions like H-bonding with the surrounding Arg198 residue compared to compound 23. These observations highlight the importance of the correct heterocycle-mediated interactions within the binding pocket for improving potency.

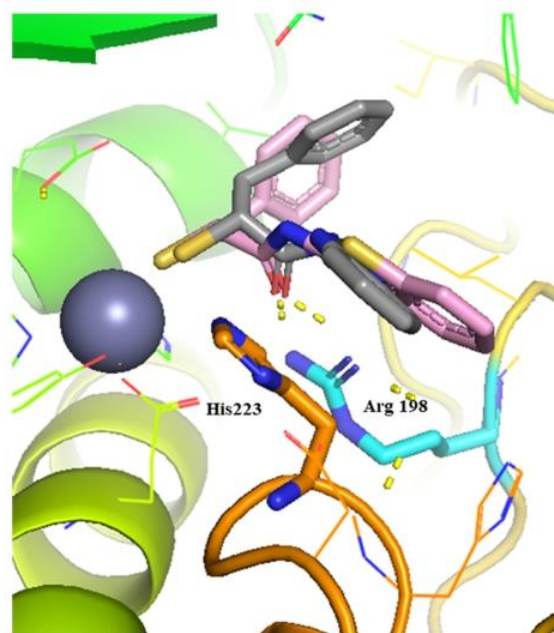


Figure 5. Superimposition of compound 23 (pink) and compound 26 (light gray) in the binding pocket of LasB (PDB code: 7OC7). The active site Zn²⁺ cation is shown as a gray sphere. The dashed lines represent H bonds of less than 2.15 Å.

As much as the ring size, the nature of the substituents also plays a role in the fine-tuning of the activity, as depicted by the threefold decrease in the activity of compound 25 with a chloro-substituted benzothiazolyl ring compared to compound 24 bearing a methoxy group on the benzothiazolyl ring.

Although the replacement of the *N*-aryl ring by heterocycles did not significantly improve the activity compared to compound 5, compound 23 with a benzothiazolyl ring demonstrated an activity in the range similar to that of our previous hit compound 3, while adding a slightly more hydrophilic nature to this class of inhibitors. This observation could be valuable in the future formulation studies of these inhibitors to overcome the potential solubility issues by lowering their log*D* values. Indeed, the calculation of ligand efficiency (LE) and lipophilic ligand efficiency (LLE) of compounds 3 (LE: 0.43, LLE: 2.37) and 23 (LE: 0.48, LLE:

3.21) revealed that we were able to improve the hydrophilicity by maintaining LE and the inhibitory activity in the same range.

To further demonstrate the potential of these inhibitors as pathoblockers against LasB, we selected compounds **12** and **13** along with the two heterocyclic derivatives, compounds **23** and **24**, and evaluated them further in several *in vitro* and *in vivo* assays.

Targeting Other Virulence Factors. We previously demonstrated that the inhibitors of LasB can also act against bacterial collagenases.⁴⁹ Collagenase H (ColH), secreted by the Gram-positive bacterium *C. histolyticum*, is a zinc-containing enzyme that causes tissue destruction by degrading collagen and is involved in various diseases.⁵⁰ Similar to LasB, this extracellular metalloenzyme is capable of invading the host cell and acquiring nutrients to evade the immune defense. Consequently, we evaluated the inhibitory activity of our LasB inhibitors against this virulence factor.

The IC₅₀ values were in the low nanomolar range (Table S1) for several selected α -benzyl-*N*-aryl derivatives, indicating the potential of this class for broad-spectrum inhibition of bacterial metalloproteases.

Among the four selected heterocyclic derivatives, only compound **23** showed a significant inhibition of ColH (K_i : $0.1 \pm 0.01 \mu\text{M}$). This observation is noteworthy, as this compound is also a potent inhibitor of LasB.

Antibacterial Activity. To rule out possible antibacterial activities, we assessed the inhibitory effect of compounds **13** and **23** against *P. aeruginosa* PA14. The minimum inhibitory concentration (MIC) assay showed no reduction of bacterial density up to $100 \mu\text{M}$ for both inhibitors, as expected for antivirulence agents.

Selectivity against MMPs and TACE as Human Off-Targets. Inhibition of human zinc-containing enzymes is described frequently for inhibitors of LasB, hindering the development of selective compounds. MMPs are calcium-dependent zinc-metalloenzymes, playing crucial roles in the human body.⁵¹

To confirm the excellent selectivity we had previously reported for this class of inhibitors, we tested compounds **12**, **13**, and **23** for their activity against six representative MMPs and the three human off-targets, tumor necrosis factor- α -converting enzyme (TACE) or ADAM17, HDAC-3, and HDAC-8 (Table 3).^{52,53} Compound **3** is shown in Table 3 for comparison.

All tested inhibitors demonstrated a high selectivity over MMPs, whereas they showed a relatively low selectivity for TACE (ADAM17), with IC₅₀ values between 2 and $10 \mu\text{M}$. Therefore, optimization strategies to improve selectivity toward this target are still necessary to develop pathoblockers that are closer to a potential therapeutic application.

Cytotoxicity. We next evaluated the cytotoxicity of compounds **13** and **23** against three human cell lines to further support the potential therapeutic use of our compounds. Both inhibitors did not show any toxicity against human hepatoma (HepG2), human embryonic kidney (HEK) 293, and adenocarcinomic human alveolar basal epithelial (A549) cells up to $100 \mu\text{M}$.

In Vivo Zebrafish Embryo Toxicity. In view of their potency, relatively high selectivity, and the lack of cytotoxicity, we next evaluated compounds **12** and **23** in an *in vivo* toxicity study using zebrafish embryos. These embryos possess a high degree of genetic similarity compared to the human genome,

Table 3. Activities of Four LasB Inhibitors against the Selected MMPs (% of inhibition at $100 \mu\text{M}$) and Further Human Off-Targets^a

	3	12	13	23
MMP-1	n.i.	n.i.	n.i.	n.i.
MMP-2	n.i.	n.i.	n.i.	n.i.
MMP-3	n.i.	n.i.	n.i.	n.i.
MMP-7	n.i.	n.i.	n.i.	n.i.
MMP-8	n.i.	12 ± 2	19 ± 4	n.i.
MMP-14	n.i.	n.i.	n.i.	n.i.
		IC ₅₀ (μM)		
ADAM17	4.8 ± 1.5	4.1 ± 0.1	2.3 ± 1.4	10.4 ± 0.2
HDAC-3	>100	>100	>250	>100
HDAC-8	>100	>100	>250	>100

^an.i. = <10% inhibition at $100 \mu\text{M}$. Means and SD of at least two independent experiments.

offering a feasible, medium-throughput *in vivo* toxicity screening.^{54,55} Additionally, the lethality and malformation during the development of embryonic zebrafish can also be assessed with this experiment. A maximum tolerated concentration (MTC) of $\leq 30 \mu\text{M}$ was obtained for compound **23** and $\leq 2 \mu\text{M}$ for compound **12** (Table S2).

Validation of the Effect of LasB Inhibitors. Before validating the effect of selected inhibitors, we examined the cytotoxic effect of LasB-containing culture supernatant *in vitro*. To this end, wild-type (wt) PA14 supernatant and LasB knockout (ΔlasB) PA14 supernatant were investigated on A549 cells and human dermal fibroblasts (NHDF). As shown in Figure S2, the wt PA14 supernatant reduced the viability (determined with MTT assay) and showed a dose-dependent effect on both cell lines. A concentration of 15% (*v/v*) decreased the viability to 10 ± 5 and $40 \pm 5\%$ of A549 and NHDF after 1 day of incubation, respectively. In contrast, the ΔlasB PA14 supernatant exhibited a smaller effect on the viability after 1 day of incubation, as 15% (*v/v*) resulted in a viability of $80 \pm 20\%$ in both cell types. This effect was less prominent on both cell lines after 2 days of incubation. The effect on cell morphology and attachment of both supernatants at 15% (*v/v*) was also examined with bright-field imaging. The wt PA14 supernatant induced cell detachment and rounding, indicating cell death (Figures S3 and S4). On the other hand, 15% (*v/v*) ΔlasB PA14 supernatant showed a negligible effect on cell morphology and attachment of both A549 and NHDF cells. These data underline the role of LasB in inducing cell death.

Due to their high inhibitory activity, low cytotoxicity, and high selectivity over human off-targets, we selected compounds **12**, **13**, **23**, and **24** to verify their effect against LasB in this cell-based assay. A mixture of various concentrations of compounds and 15% (*v/v*) wt PA14 supernatant or ΔlasB PA14 supernatant was prepared and incubated with the cells for 1 day.

Cell viability was assessed by the MTT assay, and live/dead cells were visualized by fluorescence microscopy. The MTT results in Figures 6 and S5 revealed that the selected compounds improved the viability of the cells and reduced the cytotoxic effect of the wt PA14 supernatant in a dose-dependent manner. For instance, compounds **23** and **24** showed an increase of $80 \pm 15\%$ in viability of A549 cells at $50 \mu\text{M}$. This effect was smaller at lower concentrations (Figure 6a). Interestingly, they did not affect the activity of

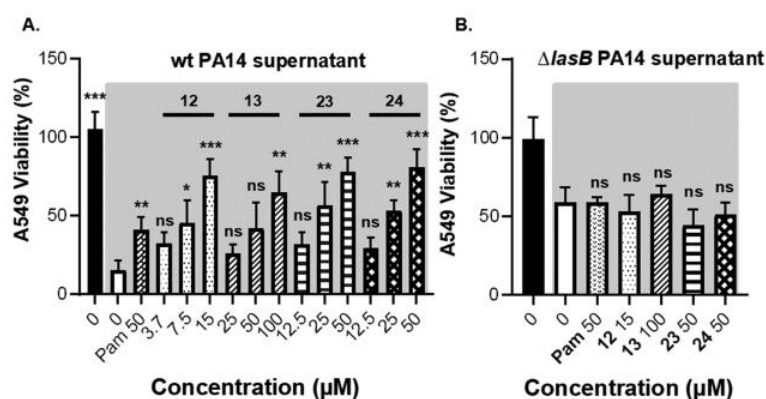


Figure 6. Viability of A549 cells treated with 12, 13, 23, and 24 and 15% (v/v) wt PA14 supernatant or $\Delta lasB$ PA14 supernatant. (A) Dose-dependent effect of the compounds on the viability of A549 cells treated with wt PA14 supernatant; (B) no effect of the compounds on A549 cells treated with $\Delta lasB$ PA14 supernatant. The supernatant-treated groups are shown in gray background. Each graph is a representation of three independent experiments; mean \pm SD. One-way ANOVA was performed for each experiment following Dunnett's multiple comparison test. The mean of each column was compared with the mean of the negative control (ns: not significant, *: $p \leq 0.05$, **: $p \leq 0.01$, ***: $p \leq 0.001$). wt PA14: wild-type *Pseudomonas aeruginosa*, $\Delta lasB$ PA14: LasB knockout *P. aeruginosa*, Pam: phosphoramidon.

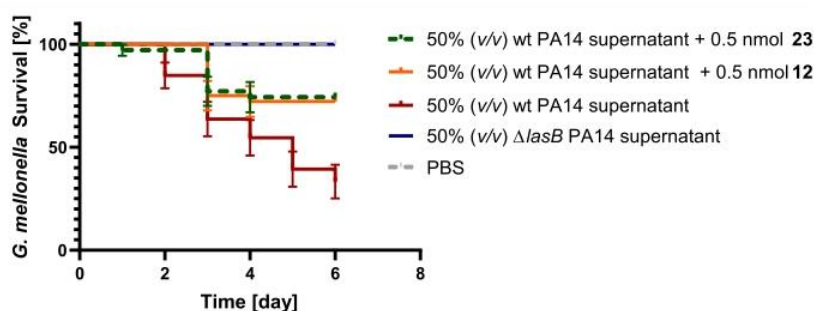


Figure 7. Kaplan–Meier survival analysis of larvae treated with 0.5 nmol of compounds 12 and 23 and 50% (v/v) wt PA14 supernatant. The survival was improved when wt PA14 supernatant-challenged larvae were treated with compounds. Each curve represents the results of three independent experiments. The statistical difference between the groups treated with wt PA14 supernatant and compounds 12 and 23 is $P = 0.0013$ and 0.0016 (log-rank test), respectively. The survival of the group treated with $\Delta lasB$ PA14 supernatant did not change compared to the wt PA14 supernatant-treated group ($P = 0.0001$). The survival of larvae treated with 0.5 nmol of the compounds (in sterile PBS) showed 100% viability. wt PA14: wild-type *Pseudomonas aeruginosa* and $\Delta lasB$ PA14: LasB knockout *P. aeruginosa*.

the $\Delta lasB$ PA14 supernatant, and the viability was similar to that of the control (no inhibitor) (Figure 6b).

Following this, live/dead staining showed an improved cell adhesion and live cell counts in both cell lines when treated with LasB inhibitors and wt PA14 supernatant (Figures S7 and S9), while showing no effect on the viability of the cells when challenged with $\Delta lasB$ PA14 supernatant and treated with our inhibitors (Figures S8 and S10). These data confirm that our compounds are selective and only active against LasB but not against other virulence targets in the supernatant. Moreover, these findings imply that our inhibitors can maintain the integrity of lung and skin cells during the disease state induced by *P. aeruginosa* and may reduce the bacterial propagation through the cells.

***G. mellonella* In Vivo Model.** To analyze the antivirulence activity of LasB inhibitors *in vivo*, we used a simple model based on *G. mellonella* larvae.

We have used this model previously to evaluate the treatment options for *P. aeruginosa*.⁴⁰ We injected the larvae with a mixture of the compounds and wt PA14 supernatant, incubated them for 6 days, and recorded survival once per day (Figure 7). Our results show that wt PA14 supernatant reduced the survival of larvae to $35 \pm 15\%$ after 6 days of

incubation, whereas the $\Delta lasB$ PA14 supernatant resulted in the survival of all larvae. Compared to the larvae treated with wt PA14 supernatant only, 0.5 mmol of compounds 12 and 23 increased the survival from 35 ± 15 to $70 \pm 5\%$ after 6 days compared to the non-treated larvae. Interestingly, the performance of both compounds 12 and 23 was comparable with that of compound 3 with an increase in survival rates up to $\sim 50\%$. These results validate that our inhibitors are potential candidates to block the pathogenicity of *P. aeruginosa*.

Conclusions. In this work, we applied a structure-based optimization approach to extend the chemical space of the recently identified LasB inhibitor class of α -benzyl-*N*-aryl mercaptoacetamides. By exploiting the crystal structure of LasB with the previously reported inhibitor 5, we first explored the effect of different substituents on both sides of the mercaptoacetamide core and synthesized seven derivatives. We then replaced the *N*-aryl ring with nine different heterocycles varying in size and substituents.

Although no notable improvement in potency was observed for these derivatives, we were able to identify three compounds (12, 13, and 23) with a maintained selectivity against selected human off-targets and a preserved low micromolar inhibitory activity against LasB compared to our previous hit compound

3. With no signs of toxicity against human cell lines, these compounds also demonstrated a reduction in the pathogenicity of *P. aeruginosa* and maintained the integrity of lung and skin cells treated with the LasB-containing supernatant.

Inspired by these results, the *in vivo* efficacy of compounds **12** and **23** was further explored using an *in vivo* model based on *G. mellonella* larvae. The survival rate of the larvae challenged with wt PA14 supernatant was slightly increased in the presence of both compounds. This achievement is noteworthy, considering the gain in potency and increased hydrophilicity with this new class of compounds.

In addition to this, the inhibitory effect of this class of inhibitors against the structurally similar target ColH from *C. histolyticum* was also investigated, revealing several inhibitors with submicromolar K_i against this promising target, such as compound **23**.

In view of the current antimicrobial resistance crisis, our results highlight the potential of this class of inhibitors as attractive candidates for becoming effective pathoblockers in reducing bacterial pathogenicity while diminishing potential resistance development. Further optimization strategies on both binding pockets should be explored to ensure an improved physicochemical and pharmacokinetic profile and to address the potential stability issues associated with the free thiol group in this class of inhibitors.

METHODS

General Chemistry. All reagents obtained from commercial suppliers were used without further purification. Procedures were not optimized regarding yield. NMR spectra were recorded on a Bruker AV 500 (500 MHz) spectrometer at room temperature. Chemical shifts are given in parts per million (ppm) and referenced against the residual proton, ^1H , or carbon, ^{13}C , resonances of the >99% deuterated solvents as internal reference. Coupling constants (J) are given in hertz (Hz). Data are reported as follows: chemical shift, multiplicity (s = singlet, d = doublet, t = triplet, dd = doublet of doublets, dt = doublet of triplets, m = multiplet, br = broad), and combinations of these coupling constants and integration. Liquid chromatography–mass spectrometry (LC–MS) was performed on an LC–MS system, consisting of a Dionex-UltiMate 3000 pump, an autosampler, a column compartment, and a detector (Thermo Fisher Scientific, Dreieich, Germany), and an ESI quadrupole MS system (MSQ Plus or ISQ EC, Thermo Fisher Scientific, Dreieich, Germany). Flash chromatography was performed using an automated flash chromatography system CombiFlash Rf+ (Teledyne Isco, Lincoln, NE, USA) equipped with RediSepRf silica columns (Axel Semrau, Sprockhövel Germany) or Chromabond Flash C18 columns (Macherey-Nagel, Düren, Germany). High-resolution mass was determined by LC–MS/MS using a Thermo Scientific Q Exactive Focus Orbitrap LC–MS/MS system. The purity of the final compounds was determined by LC–MS, using the area percentage method on the UV trace recorded at a wavelength of 254 nm, and found to be >95%.

Synthesis of Intermediates and Final Compounds.

General Procedure A: Synthesis of Chloro Acid Derivatives 6–10 from Amino Acid. Amino acid (1.0 equiv) was dissolved in 6 N HCl (2 mL/mmol or until mostly dissolved) under nitrogen atmosphere and cooled to $-5\text{ }^\circ\text{C}$. NaNO_2 (1.5–2.5 equiv) was dissolved in water (0.3 mL/mmol amino acid) and added dropwise slowly. The mixture was stirred overnight while warming to r.t. The reaction mixture was extracted with

EtOAc/THF (3:1). The combined organic extracts were washed with saturated aq. NaCl solution and dried over anhydrous Na_2SO_4 and filtered. The solvent was removed under reduced pressure to obtain the product. The crude was used in the next steps without further purification.

General Procedure B: Synthesis of Derivatives 11a–17a Using Thionyl Chloride. The acid (1.0 equiv), SOCl_2 (2.0 equiv), and a few drops of DMF were heated to $70\text{ }^\circ\text{C}$ for 1 h. The cooled mixture was added dropwise to a solution of the corresponding aniline (1.1 equiv) in DMF (1 mL/mmol) at $0\text{ }^\circ\text{C}$. The mixture was stirred overnight at r.t. The reaction mixture was quenched with water and extracted with EtOAc (3 \times). The combined organic extracts were washed with saturated aqueous NaCl solution and dried over anhydrous Na_2SO_4 and filtered. The solvent was removed under reduced pressure to obtain the crude product. The purification was done by column chromatography or flash chromatography.

General Procedure B-1: Synthesis of Coupling Derivatives 18a and 23a–25a Using Ethylchloroformate as the Coupling Reagent. The acid (1.2 equiv) was dissolved in THF and cooled in an ice bath. Et_3N (1.2 equiv) was added, followed by the addition of ClCO_2Et (1.3 equiv). After 5 min, the ice bath was removed, and the mixture was stirred at r.t. for 30 min. The corresponding amine (1.0 equiv) was slowly added. The reaction was monitored using TLC or LC–MS. After the reaction was completed, volatiles were evaporated under reduced pressure, and the crude product was purified using column chromatography.

General Procedure B-2: Synthesis of Coupling Derivatives 17a, 19a–22a, and 26a Using HATU as the Coupling Reagent. The acid (1.5 equiv) was dissolved in DCM (10 mL) at r.t., and to this DIEA (1.5 equiv) and HATU (1.5 equiv) were added. The corresponding aniline (1 equiv) was then added to this mixture, and the reaction was monitored by LC–MS. The mixture was extracted with saturated aqueous NaCl solution (1 \times) and then dried over anhydrous Na_2SO_4 and filtered. The crude was purified using reverse phase flash chromatography ($\text{H}_2\text{O} + 0.1\text{ }\%$ FA/ACN + 0.1% FA 95:5 \rightarrow 5:95).

General Procedure C: Protection of the Hydroxyl Group in Derivatives 13b, 15b, and 16b. The amide (1.0 equiv), Et_3N (2.0 equiv), and 4-dimethylaminopyridine (0.03 equiv) were dissolved in DCM (5 mL/mmol) and cooled to $0\text{ }^\circ\text{C}$. Acetic anhydride (2.0 equiv) was added dropwise. The solution was warmed to r.t. and stirred for 30 min. The reaction mixture was washed with DCM, washed with saturated aqueous NaCl solution, dried over anhydrous Na_2SO_4 , and filtered. The solvent was removed under reduced pressure to obtain the crude product.

General Procedure D: Synthesis of Thioacetate Derivatives 11b, 12b, 13c, 14b, 15c, 16c, and 17b–26b. The corresponding chloro derivative (1.0 equiv) was dissolved in acetone under argon atmosphere. To this solution, CH_3COSK (1.5–3.0 equiv) was added, and the mixture was stirred for 2–6 h at r.t. It was monitored by TLC or LC–MS. The reaction mixture was quenched with water and extracted with EtOAc (3 \times). The combined organic extracts were washed with saturated aqueous NaCl solution, dried over anhydrous Na_2SO_4 , and filtered. The solvent was removed under reduced pressure to obtain the crude product. The purification was done by flash chromatography.

General Procedure E: Hydrolysis of Thioacetate for Derivatives 11–26. Thioacetate (1.0 equiv) was dissolved in

methanol (5 mL/mmol) under argon atmosphere, and 2 M aqueous NaOH solution (2.0 equiv) or solid NaOH (3.0 equiv) was added. The solution was stirred 1–3 h at r.t. before being quenched with 1 M HCl. The solution was extracted with EtOAc and washed with 0.5 M HCl. The combined organic extracts were washed with saturated aqueous NaCl solution and dried over anhydrous Na₂SO₄ and filtered. The solvent was removed under reduced pressure to obtain the crude product. The purification was done by column chromatography or preparative HPLC (H₂O + 0.05% FA/ACN + 0.05% FA, 95:5 → 5:95). For more polar compounds, instead of quenching the reaction with 1 M HCl, the pH was adjusted to acidic using Amberlite IR-120. After filtration, Amberlite was washed with MeOH (3×), the solvent was evaporated, and the product was purified using preparative HPLC (H₂O + 0.05% FA/ACN + 0.05% FA, 95:5 → 5:95). For compounds **21** and **22**, thioacetate (1.0 equiv) was dissolved in methanol (5 mL/mmol) under argon atmosphere, and acetyl chloride (15 equiv) was added dropwise over 10 h. The mixture was stirred at room temperature for 30–40 h and carefully monitored by LC–MS. Once the conversion was complete, the solvent was removed under reduced pressure to obtain the crude product. Purification was done by preparative HPLC (H₂O + 0.05% FA/ACN + 0.05% FA, 95:5 → 5:95).

2-Chloro-3-phenylpropanoic Acid (6). Compound **6** was prepared according to general procedure A, using DL-phenylalanine (1 g, 6.0 mmol) and NaNO₂ (1.46 g, 21.2 mmol). The crude product was obtained as a yellow oil and used without further purification (1.05 g, 94%). ¹H NMR (500 MHz, CDCl₃): δ ppm 7.37–7.24 (m, 5H), 4.51 (dd, *J* = 7.8, 6.9 Hz, 1H), 3.42 (dd, *J* = 14.0, 6.7 Hz, 1H), 3.21 (dd, *J* = 14.1, 7.9 Hz, 1H). MS (ESI[−]) *m/z*: 183.25 [M − H][−], 147.23 [M − H − HCl][−].

2-Chloro-N-(4-methoxyphenyl)-3-phenylpropanamide (12a). Compound **12a** was prepared according to the general procedure B, using compound **6** (200 mg, 1.08 mmol), SOCl₂ (157 μL, 2.17 mmol), and *p*-anisidine (147 mg, 1.19 mmol). Purification was done by flash chromatography (Hex/EtOAc, 100:0 to 0:100). The product was obtained as a green solid (234 mg, 75%). ¹H NMR (500 MHz, CDCl₃): δ ppm 8.01 (br s, 1H), 7.38–7.24 (m, 7H), 6.90–6.86 (m, 2H), 4.71 (dd, *J* = 7.8, 4.4 Hz, 1H), 3.81 (s, 3H), 3.52 (dd, *J* = 14.3, 4.4 Hz, 1H), 3.32 (dd, *J* = 14.3, 7.6 Hz, 1H). MS (ESI⁺) *m/z*: 290.04 [M + H]⁺.

S-(1-((4-Methoxyphenyl)amino)-1-oxo-3-phenylpropan-2-yl) Ethanethioate (12b). Compound **12b** was prepared according to the general procedure D, using compound **12a** (230 mg, 0.95 mmol) and potassium thioacetate (162 mg, 1.42 mmol). Purification was done by flash chromatography (Hex/EtOAc, 100:0 to 0:100). The product was obtained as a yellow solid (126 mg, 40%). ¹H NMR (500 MHz, CDCl₃): δ ppm 7.81 (br s, 1H), 7.37–7.34 (m, 2H), 7.33–7.23 (m, 5H), 6.86–6.81 (m, 2H), 4.28 (dd, *J* = 8.4, 7.2 Hz, 1H), 3.79 (s, 3H), 3.44 (dd, *J* = 14.0, 8.4 Hz, 1H), 3.01 (dd, *J* = 14.1, 7.1 Hz, 1H), 2.38 (s, 3H). ¹³C NMR (126 MHz, CDCl₃): δ ppm 197.4, 168.3, 156.7, 137.9, 130.9, 129.5, 128.8, 127.2, 114.3, 121.8, 55.7, 48.7, 36.1, 30.7. MS (ESI⁺) *m/z*: 330.08 [M + H]⁺, 288.08 [M − Ac + 2H]⁺.

2-Mercapto-N-(4-methoxyphenyl)-3-phenylpropanamide (12). Compound **12** was prepared according to the general procedure E, using compound **12b** (95 mg, 0.29 mmol) and 2 M NaOH aqueous solution (290 μL, 0.58 mmol) in MeOH (2 mL). Purification was done by flash chromatography (Hex/

EtOAc, 100:0 to 0:100). The final product was obtained as a white solid (45 mg, 54%). ¹H NMR (500 MHz, CDCl₃): δ ppm 7.90 (br s, 1H), 7.37–7.33 (m, 2H), 7.31 (d, *J* = 7.5 Hz, 2H), 7.28–7.23 (m, 3H), 6.89–6.84 (m, 2H), 3.80 (s, 3H), 3.70 (dt, *J* = 8.9, 6.6 Hz, 1H), 3.36 (dd, *J* = 13.7, 6.7 Hz, 1H), 3.24 (dd, *J* = 14.0, 6.4 Hz, 1H), 2.10 (d, *J* = 8.9 Hz, 1H). ¹³C NMR (126 MHz, CDCl₃): δ ppm 169.5, 156.9, 137.5, 130.4, 129.6, 128.7, 127.3, 122.1, 114.3, 55.6, 45.9, 41.7. HRMS (ESI⁺) *m/z*: calcd for C₁₆H₁₈NO₂S [M + H]⁺, 288.10527; found, 288.10453.

N-(Benzo[d]thiazol-2-yl)-2-chloro-3-phenylpropanamide (23a). Compound **23a** was synthesized according to the general procedure B-1, using compound **6** (626 mg, 3.39 mmol), 2-aminobenzothiazole (422 mg, 2.81 mmol), Et₃N (476 μL, 3.39 mmol), and ClCO₂Et (355 μL, 3.72 mmol) in THF (33 mL). The final product was purified using flash chromatography (DCM/MeOH, 100:0 to 95:5). The final product was obtained as an off-white oil (324 mg, 30%). ¹H NMR (500 MHz, CDCl₃): δ ppm 7.86 (d, *J* = 7.9 Hz, 1H), 7.78 (m, 1H), 7.47 (t, *J* = 7.7 Hz, 1H), 7.36 (t, *J* = 7.6 Hz, 1H), 7.32–7.23 (m, 3H), 7.21–7.18 (m, 2H), 4.76–4.70 (m, 1H), 3.56–3.51 (m, 1H), 3.29 (dd, *J* = 14.4, 7.8 Hz, 1H). ¹³C NMR (126 MHz, CDCl₃): δ ppm 167.1, 157.3, 148.2, 135.3, 132.3, 129.6, 128.8, 127.7, 127.72, 126.7, 124.6, 121.7, 121.3, 60.3, 41.2. MS (ESI⁺) *m/z*: 316.98 [M + H]⁺.

S-(1-(Benzo[d]thiazol-2-ylamino)-1-oxo-3-phenylpropan-2-yl) Ethanethioate (23b). Compound **23b** was prepared according to the general procedure D, using compound **23a** (323 mg, 1.02 mmol) and potassium thioacetate (174 mg, 1.53 mmol) in acetone (10 mL). Purification was done by flash chromatography (Hex/DCM, 100:0 to 0:100). The final product was obtained as a yellow solid (257 mg, 71%). ¹H NMR (500 MHz, acetone-*d*₆): δ ppm 11.24 (s, 1H), 8.02–7.88 (m, 1H), 7.69 (d, *J* = 8.1 Hz, 1H), 7.43 (m, 1H), 7.35–7.26 (m, 5H), 7.24–7.17 (m, 1H), 4.72 (dd, *J* = 8.7, 6.9 Hz, 1H), 3.41 (dd, *J* = 13.8, 8.7 Hz, 1H), 3.06 (dd, *J* = 13.8, 6.9 Hz, 1H), 2.36 (s, 3H). ¹³C NMR (126 MHz, CDCl₃): δ ppm 196.2, 169.1, 157.6, 148.4, 136.9, 132.3, 129.3, 128.8, 127.4, 126.5, 124.3, 121.5, 121.2, 47.9, 35.9, 30.5. MS (ESI⁺) *m/z*: 357.01 [M + H]⁺, 314.90 [M − Ac + H]⁺.

N-(Benzo[d]thiazol-2-yl)-2-mercapto-3-phenylpropanamide (23). Compound **23** was prepared according to the general procedure E, using compound **23b** (128 mg, 0.36 mmol) and 2 M NaOH aqueous solution (359 μL, 0.72 mmol) in MeOH (3 mL). Purification was done by flash chromatography (Hex/EtOAc, 7:3). The final product was obtained as a white solid (30 mg, 28%). ¹H NMR (500 MHz, CDCl₃): δ ppm 7.85 (d, *J* = 7.8 Hz, 1H), 7.76 (d, *J* = 8.1, 1H), 7.49–7.44 (m, 1H), 7.39–7.36 (m, 1H), 7.29–7.27 (m, 1H), 7.25–7.15 (m, 4H), 3.87–3.80 (m, 1H), 3.40 (dd, *J* = 14.0, 7.0 Hz, 1H), 3.24 (dd, *J* = 14.0, 6.8 Hz, 1H), 2.26–2.17 (m, 1H). ¹³C NMR (126 MHz, CDCl₃): δ ppm 170.7, 159.0, 145.5, 136.7, 131.0, 129.4, 128.9, 127.5, 127.2, 125.0, 121.9, 120.2, 44.7, 41.1. HRMS (ESI⁺) *m/z*: calcd for C₁₆H₁₅N₂OS₂ [M + H]⁺, 315.06203; found, 315.06178.

■ ASSOCIATED CONTENT

Supporting Information

The Supporting Information is available free of charge at <https://pubs.acs.org/doi/10.1021/acsinfecdis.1c00628>.

Experimental methods; synthesis of intermediates and final compounds; NMR spectra of final compounds; LC–MS spectra of final compounds (PDF)

AUTHOR INFORMATION

Corresponding Author

Anna K.H. Hirsch – Helmholtz Institute for Pharmaceutical Research Saarland (HIPS)—Helmholtz Centre for Infection Research (HZI), 66123 Saarbrücken, Germany; Department of Pharmacy, Saarland University, 66123 Saarbrücken, Germany; Helmholtz International Lab for Anti-Infectives, 66123 Saarbrücken, Germany; orcid.org/0000-0001-8734-4663; Email: anna.hirsch@helmholtz-hips.de

Authors

Cansu Kaya – Helmholtz Institute for Pharmaceutical Research Saarland (HIPS)—Helmholtz Centre for Infection Research (HZI), 66123 Saarbrücken, Germany; Department of Pharmacy, Saarland University, 66123 Saarbrücken, Germany

Isabell Walter – Helmholtz Institute for Pharmaceutical Research Saarland (HIPS)—Helmholtz Centre for Infection Research (HZI), 66123 Saarbrücken, Germany; Department of Pharmacy, Saarland University, 66123 Saarbrücken, Germany

Alaa Alhayek – Helmholtz Institute for Pharmaceutical Research Saarland (HIPS)—Helmholtz Centre for Infection Research (HZI), 66123 Saarbrücken, Germany; Department of Pharmacy, Saarland University, 66123 Saarbrücken, Germany

Roya Shafiei – Helmholtz Institute for Pharmaceutical Research Saarland (HIPS)—Helmholtz Centre for Infection Research (HZI), 66123 Saarbrücken, Germany; Department of Pharmacy, Saarland University, 66123 Saarbrücken, Germany; orcid.org/0000-0001-9783-595X

Gwenaëlle Jézéquel – Helmholtz Institute for Pharmaceutical Research Saarland (HIPS)—Helmholtz Centre for Infection Research (HZI), 66123 Saarbrücken, Germany; orcid.org/0000-0001-8945-8680

Anastasia Andreas – Helmholtz Institute for Pharmaceutical Research Saarland (HIPS)—Helmholtz Centre for Infection Research (HZI), 66123 Saarbrücken, Germany; Department of Pharmacy, Saarland University, 66123 Saarbrücken, Germany

Jelena Konstantinović – Helmholtz Institute for Pharmaceutical Research Saarland (HIPS)—Helmholtz Centre for Infection Research (HZI), 66123 Saarbrücken, Germany

Esther Schönauer – Department of Biosciences and Medical Biology, University of Salzburg, 5020 Salzburg, Austria; orcid.org/0000-0002-2625-9446

Asfandyar Sikandar – Helmholtz Institute for Pharmaceutical Research Saarland (HIPS)—Helmholtz Centre for Infection Research (HZI), 66123 Saarbrücken, Germany

Jörg Hauptenthal – Helmholtz Institute for Pharmaceutical Research Saarland (HIPS)—Helmholtz Centre for Infection Research (HZI), 66123 Saarbrücken, Germany

Rolf Müller – Helmholtz Institute for Pharmaceutical Research Saarland (HIPS)—Helmholtz Centre for Infection Research (HZI), 66123 Saarbrücken, Germany; Department of Pharmacy, Saarland University, 66123 Saarbrücken, Germany; Helmholtz International Lab for Anti-Infectives,

66123 Saarbrücken, Germany; orcid.org/0000-0002-1042-5665

Hans Brandstetter – Department of Biosciences and Medical Biology, University of Salzburg, 5020 Salzburg, Austria

Rolf W. Hartmann – Helmholtz Institute for Pharmaceutical Research Saarland (HIPS)—Helmholtz Centre for Infection Research (HZI), 66123 Saarbrücken, Germany; Department of Pharmacy, Saarland University, 66123 Saarbrücken, Germany; orcid.org/0000-0002-5871-5231

Complete contact information is available at: <https://pubs.acs.org/10.1021/acsinfectdis.1c00628>

Funding

Open Access is funded by the Austrian Science Fund (FWF).

Notes

The authors declare the following competing financial interest(s): The authors declare the following financial interest(s): C.K, I.W., J.K, J.H., R.W.H and A.K.H.H are co-inventors on a pending international patent application (PCT/EP2021/073381) that incorporates compounds and methods outlined in this manuscript.

ACKNOWLEDGMENTS

The authors thank Prof. Dr. Aránzazu Del Campo from Leibniz Institute for New Materials (INM) (Saarbrücken, Germany) for providing the NHDF cells, Khadidja Si Chaib for helping in testing the activity of the supernatant, and Martina Wiesbauer for the determination of ColH activities. They also thank the group of Susanne Häussler (Twincore, Hannover, Germany) for providing the *P. aeruginosa* Δ lasB PA14 strain. The authors are grateful for the technical support provided by Simone Amann, Jeannine Jung, Selina Wolter, and Dennis Jener. A.K.H.H. gratefully acknowledges funding from the Helmholtz Association's Initiative and Networking Fund and by CARB-X. J.K. acknowledges funding by the Alexander von Humboldt Foundation and E.S. by the Austrian Science Fund (P 31843).

ABBREVIATIONS

A549, lung carcinoma cell line; ColH, *Clostridium histolyticum* (*Hathewayia histolytica*) collagenase; DMEM, Dulbecco's modified Eagle's medium; DMAP, 4-dimethylaminopyridine; DCM, dichloromethane; HDAC, histone deacetylase; HEK293, embryonal kidney cell line; HepG2, hepatocellular carcinoma cell line; IC₅₀, the half-maximal inhibitory concentration; LasB, *Pseudomonas aeruginosa* elastase; MIC, minimum inhibitory concentration; MMPs, human matrix metalloproteases; MTC, maximum tolerated concentration; SAR, structure–activity relationship; TACE, tumor necrosis factor- α -converting enzyme; TCEP, Tris(2-carboxyethyl)-phosphine hydrochloride; THF, tetrahydrofuran

REFERENCES

- (1) Mesaros, N.; Nordmann, P.; Plésiat, P.; Roussel-Delvallez, M.; Van Eldere, J.; Glupczynski, Y.; Van Laethem, Y.; Jacobs, F.; Lebecque, P.; Malfroot, A.; Tulkens, P. M.; Van Bambeke, F. *Pseudomonas Aeruginosa: Resistance and Therapeutic Options at the Turn of the New Millennium. Clin. Microbiol. Infect.* **2007**, *13*, 560–578.
- (2) Taubes, G. The Bacteria Fight Back. *Science* **2008**, *321*, 356–361.
- (3) Magill, S. S.; Edwards, J. R.; Bamberg, W.; Beldavs, Z. G.; Dumyati, G.; Kainer, M. A.; Lynfield, R.; Maloney, M.; McAllister-

Hollod, L.; Nadle, J.; Ray, S. M.; Thompson, D. L.; Wilson, L. E.; Fridkin, S. K. Multistate Point-Prevalence Survey of Health Care-Associated Infections. *N. Engl. J. Med.* **2014**, *370*, 1198–1208.

(4) Ma, Y.-X.; Wang, C.-Y.; Li, Y.-Y.; Li, J.; Wan, Q.-Q.; Chen, J.-H.; Tay, F. R.; Niu, L.-N. Considerations and Caveats in Combating ESKAPE Pathogens against Nosocomial Infections. *Adv. Sci.* **2020**, *7*, 1901872.

(5) Valenza, G.; Tappe, D.; Turnwald, D.; Frosch, M.; König, C.; Hebestreit, H.; Abele-Horn, M. Prevalence and Antimicrobial Susceptibility of Microorganisms Isolated from Sputa of Patients with Cystic Fibrosis. *J. Cyst. Fibros.* **2008**, *7*, 123–127.

(6) Sorde, R.; Albert Pahissa, A.; Jordi Rello, J. Management of Refractory *Pseudomonas Aeruginosa* Infection in Cystic Fibrosis. *Infect. Drug Resist.* **2011**, *4*, 31–41.

(7) Pos, K. M. Drug Transport Mechanism of the AcrB Efflux Pump. *Biochim. Biophys. Acta, Proteins Proteomics* **2009**, *1794*, 782–793.

(8) Li, X.-Z.; Plésiat, P.; Nikaido, H. The Challenge of Efflux-Mediated Antibiotic Resistance in Gram-Negative Bacteria. *Clin. Microbiol. Rev.* **2015**, *28*, 337–418.

(9) Wolter, D. J.; Lister, P. D. Mechanisms of β -Lactam Resistance Among *Pseudomonas Aeruginosa*. *Curr. Pharm. Des.* **2012**, *19*, 209–222.

(10) Li, X. Z.; Livermore, D. M.; Nikaido, H. Role of Efflux Pump(s) in Intrinsic Resistance of *Pseudomonas Aeruginosa*: Resistance to Tetracycline, Chloramphenicol, and Norfloxacin. *Antimicrob. Agents Chemother.* **1994**, *38*, 1732–1741.

(11) Pang, Z.; Raudonis, R.; Glick, B. R.; Lin, T.-J.; Cheng, Z. Antibiotic Resistance in *Pseudomonas Aeruginosa*: Mechanisms and Alternative Therapeutic Strategies. *Biotechnol. Adv.* **2019**, *37*, 177–192.

(12) Strateva, T.; Yordanov, D. *Pseudomonas Aeruginosa* - A Phenomenon of Bacterial Resistance. *J. Med. Microbiol.* **2009**, *58*, 1133–1148.

(13) Yoshimura, F.; Nikaido, H. Permeability of *Pseudomonas Aeruginosa* Outer Membrane to Hydrophilic Solutes. *J. Bacteriol.* **1982**, *152*, 636–642.

(14) Dickey, S. W.; Cheung, G. Y. C.; Otto, M. Different Drugs for Bad Bugs: Antivirulence Strategies in the Age of Antibiotic Resistance. *Nat. Rev. Drug Discovery* **2017**, *16*, 457–471.

(15) Rasko, D. A.; Sperandio, V. Anti-Virulence Strategies to Combat Bacteria-Mediated Disease. *Nat. Rev. Drug Discovery* **2010**, *9*, 117–128.

(16) Strateva, T.; Mitov, I. Contribution of an Arsenal of Virulence Factors to Pathogenesis of *Pseudomonas Aeruginosa* Infections. *Am. Microbiol.* **2011**, *61*, 717–732.

(17) Heras, B.; Scanlon, M. J.; Martin, J. L. Targeting Virulence Not Viability in the Search for Future Antibacterials. *Br. J. Clin. Pharmacol.* **2015**, *79*, 208–215.

(18) Clatworthy, A. E.; Pierson, E.; Hung, D. T. Targeting Virulence: A New Paradigm for Antimicrobial Therapy. *Nat. Chem. Biol.* **2007**, *3*, 541–548.

(19) Wagner, S.; Sommer, R.; Hinsberger, S.; Lu, C.; Hartmann, R. W.; Empting, M.; Titz, A. Novel Strategies for the Treatment of *Pseudomonas Aeruginosa* Infections. *J. Med. Chem.* **2016**, *59*, 5929–5969.

(20) Rounds, J.; Strain, J. Bezlotoxumab for Preventing Recurrent Clostridium Difficile Infections. *S. D. Med.* **2017**, *70*, 422–423.

(21) Bastaert, F.; Kheir, S.; Saint-Criq, V.; Villeret, B.; Dang, P. M.-C.; El-Benna, J.; Sirard, J.-C.; Voulhoux, R.; Sallenave, J.-M. *Pseudomonas Aeruginosa* LasB Subverts Alveolar Macrophage Activity by Interfering with Bacterial Killing through Downregulation of Innate Immune Defense, Reactive Oxygen Species Generation, and Complement Activation. *Front. Immunol.* **2018**, *9*, 1675.

(22) Liu, P. V. Extracellular Toxins of *Pseudomonas Aeruginosa*. *J. Infect. Dis.* **1974**, *130*, S94–S99.

(23) Morihara, K.; Tsuzuki, H.; Oka, T.; Inoue, H.; Ebata, M. *Pseudomonas Aeruginosa* Elastase: Isolation, Crystallization and Preliminary Characterization. *J. Biol. Chem.* **1965**, *240*, 3297–3304.

(24) Heck, L. W.; Morihara, K.; McRae, W. B.; Miller, E. J. Specific Cleavage of Human Type III and IV Collagens by *Pseudomonas Aeruginosa* Elastase. *Infect. Immun.* **1986**, *51*, 115–118.

(25) Heck, L. W.; Alarcon, P. G.; Kulhavy, R. M.; Morihara, K.; Russell, M. W.; Mestecky, J. F. Degradation of IgA Proteins by *Pseudomonas Aeruginosa* Elastase. *J. Immunol.* **1990**, *144*, 2253–2257.

(26) Holder, I. A.; Wheeler, R. Experimental Studies of the Pathogenesis of Infections Owing to *Pseudomonas Aeruginosa*: Elastase, an IgG Protease. *Can. J. Microbiol.* **1984**, *30*, 1118–1124.

(27) Galloway, D. R. *Pseudomonas Aeruginosa* Elastase and Elastolysis Revisited: Recent Developments. *Mol. Microbiol.* **1991**, *5*, 2315–2321.

(28) Parmely, M.; Gale, A.; Clabaugh, M.; Horvat, R.; Zhou, W. W. Proteolytic Inactivation of Cytokines by *Pseudomonas Aeruginosa*. *Infect. Immun.* **1990**, *58*, 3009–3014.

(29) Mariencheck, W. I.; Alcorn, J. F.; Palmer, S. M.; Wright, J. R. *Pseudomonas Aeruginosa* Elastase Degrades Surfactant Proteins A and D. *Am. J. Respir. Cell Mol. Biol.* **2003**, *28*, 528–537.

(30) Oda, K.; Koyama, T.; Murao, S. Purification and Properties of a Proteinaceous Metallo-Proteinase Inhibitor from *Streptomyces Nigrescens* TK-23. *Biochim. Biophys. Acta* **1979**, *571*, 147–156.

(31) Nishino, N.; Powers, J. C. *Pseudomonas Aeruginosa* Elastase - Development of a New Substrate, Inhibitors and an Affinity Ligand. *J. Biol. Chem.* **1979**, *255*, 3482–3519.

(32) Fullagar, J. L.; Garner, A. L.; Struss, A. K.; Day, J. A.; Martin, D. P.; Yu, J.; Cai, X.; Janda, K. D.; Cohen, S. M. Antagonism of a Zinc Metalloprotease Using a Unique Metal-Chelating Scaffold: Tropolones as Inhibitors of *P. Aeruginosa* Elastase. *Chem. Commun.* **2013**, *49*, 3197–3199.

(33) Leiris, S.; Davies, D. T.; Sprynski, N.; Castandet, J.; Beyria, L.; Bodnarchuk, M. S.; Sutton, J. M.; Mullins, T. M. G.; Jones, M. W.; Forrest, A. K.; Pallin, T. D.; Karunakar, P.; Martha, S. K.; Parusharamulu, B.; Ramula, R.; Kotha, V.; Pottabathini, N.; Pothukanuri, S.; Lemonnier, M.; Everett, M. Virtual Screening Approach to Identifying a Novel and Tractable Series of *Pseudomonas Aeruginosa* Elastase Inhibitors. *ACS Med. Chem. Lett.* **2021**, *12*, 217–227.

(34) Cathcart, G. R. A.; Quinn, D.; Greer, B.; Harriott, P.; Lynas, J. F.; Gilmore, B. F.; Walker, B. Novel Inhibitors of the *Pseudomonas Aeruginosa* Virulence Factor LasB: A Potential Therapeutic Approach for the Attenuation of Virulence Mechanisms in Pseudomonal Infection. *Antimicrob. Agents Chemother.* **2011**, *55*, 2670–2678.

(35) Burns, F. R.; Paterson, C. A.; Gray, R. D.; Wells, J. T. Inhibition of *Pseudomonas Aeruginosa* Elastase and *Pseudomonas Keratitis* Using a Thiol-Based Peptide. *Antimicrob. Agents Chemother.* **1990**, *34*, 2065–2069.

(36) Zhu, J.; Cai, X.; Harris, T. L.; Gooyit, M.; Wood, M.; Lardy, M.; Janda, K. D. Disarming *Pseudomonas Aeruginosa* Virulence Factor LasB by Leveraging a *Caenorhabditis Elegans* Infection Model. *Chem. Biol.* **2015**, *22*, 483–491.

(37) Adekoya, O. A.; Sjöli, S.; Wuxiuer, Y.; Bilot, I.; Marques, S. M.; Santos, M. A.; Nuti, E.; Cercignani, G.; Rossello, A.; Winberg, J.-O.; Sylte, I. Inhibition of Pseudolysin and Thermolysin by Hydroxamate-Based MMP Inhibitors. *Eur. J. Med. Chem.* **2015**, *89*, 340–348.

(38) Kany, A. M.; Sikandar, A.; Yahiaoui, S.; Hauptenthal, J.; Walter, I.; Empting, M.; Köhnke, J.; Hartmann, R. W. Tackling *Pseudomonas Aeruginosa* Virulence by a Hydroxamic Acid-Based LasB Inhibitor. *ACS Chem. Biol.* **2018**, *13*, 2449–2455.

(39) Pfaff, A. R.; Beltz, J.; King, E.; Ercal, N. Medicinal Thiols: Current Status and New Perspectives. *Mini-Rev. Med. Chem.* **2020**, *20*, 513–529.

(40) Kaya, C.; Walter, I.; Yahiaoui, S.; Sikandar, A.; Alhayek, A.; Konstantinović, J.; Kany, A. M.; Hauptenthal, J.; Köhnke, J.; Hartmann, R. W.; Hirsch, A. K. H. Substrate-inspired Fragment Merging and Growing Affords Efficacious LasB Inhibitors. *Angew. Chem., Int. Ed.* **2021**, *61*, No. e202112295.

(41) Jobin, P. G.; Butler, G. S.; Overall, C. M. New Intracellular Activities of Matrix Metalloproteinases Shine in the Moonlight. *Biochim. Biophys. Acta, Mol. Cell Res.* **2017**, *1864*, 2043–2055.

(42) Agrawal, A.; Romero-Perez, D.; Jacobsen, J. A.; Villarreal, F. J.; Cohen, S. M. Zinc-Binding Groups Modulate Selective Inhibition of MMPs. *ChemMedChem* **2008**, *3*, 812–820.

(43) Kany, A. M.; Sikandar, A.; Haupenthal, J.; Yahiaoui, S.; Maurer, C. K.; Proschak, E.; Köhnke, J.; Hartmann, R. W. Binding Mode Characterization and Early in Vivo Evaluation of Fragment-Like Thiols as Inhibitors of the Virulence Factor LasB from *Pseudomonas aeruginosa*. *ACS Infect. Dis.* **2018**, *4*, 988–997.

(44) Publication, A. (S)-2-Chloroalkanoic Acids of High Enantiomeric Purity From (S)-2-Amino Acids: (S)-2-Chloropropanoic Acid. *Org. Synth.* **1988**, *66*, 151.

(45) Schrödinger, L., DeLano, W. *The PyMOL Molecular Graphics System*, version 2.0; Schrödinger, LLC, 2021. <http://www.pymol.org/pymo>.

(46) Prachayasittikul, S.; Pingaew, R.; Worachartcheewan, A.; Sinthupoom, N.; Prachayasittikul, V.; Ruchirawat, S.; Prachayasittikul, V. Roles of Pyridine and Pyrimidine Derivatives as Privileged Scaffolds in Anticancer Agents. *Mini-Rev. Med. Chem.* **2017**, *17*, 869–901.

(47) Boiani, M.; Gonzalez, M. Imidazole and Benzimidazole Derivatives as Chemotherapeutic Agents. *Mini-Rev. Med. Chem.* **2005**, *5*, 409–424.

(48) SeeSAR v.11.1; BioSolveIT GmbH: Sankt Augustin, Germany, 2021. available from: <http://www.biosolveit.de/seeSAR>.

(49) Konstantinović, J.; Yahiaoui, S.; Alhayek, A.; Haupenthal, J.; Schönauer, E.; Andreas, A.; Kany, A. M.; Müller, R.; Köhnke, J.; Berger, F. K.; Bischoff, M.; Hartmann, R. W.; Brandstetter, H.; Hirsch, A. K. H. N-Aryl-3-Mercaptosuccinimides as Antivirulence Agents Targeting *Pseudomonas aeruginosa* Elastase and Clostridium Collagenases. *J. Med. Chem.* **2020**, *63*, 8359–8368.

(50) Schönauer, E.; Kany, A. M.; Haupenthal, J.; Hüsecken, K.; Hoppe, I. J.; Voos, K.; Yahiaoui, S.; Elsässer, B.; Ducho, C.; Brandstetter, H.; Hartmann, R. W. Discovery of a Potent Inhibitor Class with High Selectivity toward Clostridial Collagenases. *J. Am. Chem. Soc.* **2017**, *139*, 12696.

(51) Sternlicht, M. D.; Werb, Z. How Matrix Metalloproteinases Regulate Cell Behavior. *Annu. Rev. Cell Dev. Biol.* **2001**, *17*, 463–516.

(52) Gooz, M. ADAM-17: The Enzyme That Does It All. *Crit. Rev. Biochem. Mol. Biol.* **2010**, *45*, 146–169.

(53) Roper, S.; Esteller, M. The Role of Histone Deacetylases (HDACs) in Human Cancer. *Mol. Oncol.* **2007**, *1*, 19–25.

(54) MacRae, C. A.; Peterson, R. T. Zebrafish as Tools for Drug Discovery. *Nat. Rev. Drug Discovery* **2015**, *14*, 721–731.

(55) Chakraborty, C.; Sharma, A. R.; Sharma, G.; Lee, S.-S. Zebrafish: A Complete Animal Model to Enumerate the Nanoparticle Toxicity. *J. Nanobiotechnol.* **2016**, *14*, 65.

Recommended by ACS

N-Aryl-3-mercaptosuccinimides as Antivirulence Agents Targeting *Pseudomonas aeruginosa* Elastase and Clostridium Collagenases

Jelena Konstantinović, Anna K. H. Hirsch, *et al.*

MAY 29, 2020

JOURNAL OF MEDICINAL CHEMISTRY

READ 

Comparative Studies to Uncover Mechanisms of Action of N-(1,3,4-Oxadiazol-2-yl)benzamide Containing Antibacterial Agents

George A. Naclerio, Herman O. Sintim, *et al.*

MARCH 17, 2022

ACS INFECTIOUS DISEASES

READ 

N-Aryl Mercaptopropionamides as Broad-Spectrum Inhibitors of Metallo- β -Lactamases

Cansu Kaya, Anna K. H. Hirsch, *et al.*

FEBRUARY 21, 2022

JOURNAL OF MEDICINAL CHEMISTRY

READ 

N-Benzyl Derivatives of Long-Chained 4-Amino-7-chloro-quinolines as Inhibitors of Pyocyanin Production in *Pseudomonas aeruginosa*

Ivana Aleksic, Lidija Senerovic, *et al.*

OCTOBER 24, 2019

ACS CHEMICAL BIOLOGY

READ 

Get More Suggestions >

Supporting Information

Structure-based Design of α -Substituted Mercaptoacetamides as Inhibitors of the Virulence Factor LasB from *Pseudomonas aeruginosa*

Cansu Kaya,^{[1],[2]} Isabell Walter,^{[1],[2]} Alaa Alhayek,^{[1],[2]} Roya Shafiei,^{[1],[2]} Gwenaëlle Jézéquel,^[1] Anastasia Andreas,^{[1],[2]} Jelena Konstantinović,^[1] Esther Schönauer,^[3] Asfandyar Sikandar,^[1] Jörg Haupenthal,^[1] Rolf Müller,^{[1],[2],[4]} Hans Brandstetter,^[3] Rolf W. Hartmann,^{[1],[2]} Anna K.H. Hirsch^{[1],[2],[4]*}

^[1] Helmholtz Institute for Pharmaceutical Research Saarland (HIPS) – Helmholtz Centre for Infection Research (HZI), Campus E8.1, 66123 Saarbrücken, Germany

^[2] Department of Pharmacy, Saarland University, Campus E8.1, 66123 Saarbrücken, Germany

^[3] Department of Biosciences and Medical Biology, University of Salzburg, Hellbrunner Straße, 34, 5020 Salzburg, Austria

^[4] Helmholtz International Lab for Anti-Infectives, Campus E8.1, 66123 Saarbrücken, Germany

Table Of Contents

Experimental Methods	2
Synthesis of Intermediates and Final Compounds.....	4
Tables and Figures	19
NMR Spectra of Final Compounds.....	32
References.....	56

Experimental Methods

LasB Inhibition Assay. The purification of LasB from *P. aeruginosa* P14 supernatant as well as the subsequent performance of the FRET-based *in vitro* inhibition assay was performed as described previously.¹ All samples were run in duplicate for each condition, and experiments were performed independently at least twice.

***In vitro* ColH Inhibition Assay.** The purification of ColH-PD and determination of the inhibitory activities of the selected compounds were performed as described previously.^{2,3} In short, enzyme and inhibitor or buffer control were preincubated for 1 h at RT, before the reactions were initiated by the addition of the quenched fluorescent substrate Mca-Ala-Gly-Pro-Pro-Gly-Pro-Dpa-Gly-Arg-NH₂ (Mca = (7-Methoxycoumarin-4-yl)acetyl; Dpa = *N*-3-(2,4-dinitrophenyl)-*L*-2,3-diaminopropionyl) (FS1-1). The increase in fluorescence was monitored for 2 min 24 s (Excitation: 328 nm, Emission: 392 nm) at 25°C. The final concentrations were 2 nM ColH-PD, 10 μM compound, 250 mM Hepes pH 7.5, 400 mM NaCl, 10 mM CaCl₂, 10 μM ZnCl₂, 2% DMSO, and 2 μM FS1-1. The percentage of enzyme inhibition was calculated in relation to a reference without a compound added, only plus buffer control. For the K_i determination, the concentrations of the compound were optimized according to Murphy.⁴ The apparent inhibition constant (K_i^{app}) value was determined by non-linear fitting to the Morrison equation⁵ following a two-stage regression analysis strategy for tight-binding inhibitors.⁶ Regression analysis was performed using GraphPad Prism 9.0.0 (Graph Pad Software, San Diego, CA, USA). The experiments were performed under first order conditions ($[S_0] \ll K_M$), which resulted in an approximation of the K_i^{app} to the true inhibition constant (K_i), and, therefore, the results are reported as K_i values.

Antibacterial Activity assay. Minimum inhibitory concentration (MIC) assays were performed as described previously.¹ The MIC value was higher than 100 μM for compounds **13** and **23**. At 100 μM, the bacterial growth was reduced by less than 10% for both compounds. All samples were run in duplicate for each condition, and experiments were performed independently at least twice.

Inhibition Assays with human off-targets. Assays focusing on the inhibition of human MMPs and ADAM17 were performed as described previously.^{3,7} All samples were run in duplicate for each condition, and experiments were performed independently at least twice.

Cytotoxicity Assay. The toxicity of selected compounds toward HepG2, A549 and HEK293 cells was determined as described previously.^{1,8} Compounds **13** and **23** showed no relevant cytotoxic behaviour against the human hepatoma cell line (HepG2), human embryonic kidney (HEK) 293 cells and adenocarcinomic human alveolar basal epithelial cells (A549) with IC₅₀ values higher than 100 μM. All samples were run in duplicate for each condition, and experiments were performed independently at least twice.

Docking Studies. Modelling of derivatives of compound **5** in the LasB ligand binding pocket (PDB:7OC7) were performed using SeeSAR V.11.1 (BioSolveIT GmbH, Sankt Augustin, Germany)⁹ software and the interactions are visualized using PyMOL Molecular Graphics System, V. 2.5 Schrödinger, LLC.¹⁰

Zebrafish Experiments. Maximum Tolerated Concentration (MTC) assay was performed with minor modifications according to the procedure described in literature.¹¹ After successful mating of parent fish from the AB wild-type line, embryos were collected, sorted and kept until the next day at 28 °C in 0.3× Danieau's medium [17 mM NaCl, 2 mM KCl, 1.8 mM Ca(NO₃)₂, 1.5 mM HEPES (pH 7.1–7.3), 0.12 mM MgSO₄ and 1.2 μM methylene blue]. The assay was

performed in 96-well plates using zebrafish embryos at 1 day post fertilization (dpf). Compound solutions in 0.3× Danieau's medium were prepared freshly on the day of experiment with a final DMSO concentration of 1% (v/v). Single zebrafish embryos were placed in a 96-well microtiter plate - one embryo per well and ten embryos per condition - and directly incubated in the corresponding compound solutions. The embryos were monitored daily via microscopy until 120 hours post fertilization (hpf) (Table S2). All described experiments were performed with zebrafish embryos younger than 120 hpf and are therefore not classified as animal experiments according to EU Directive 2010/63/EU. Protocols for husbandry and care of adult animals are in accordance with the German Animal Welfare Act (§11 Abs. 1 TierSchG).

Preparation of *P. aeruginosa* culture supernatants and LasB activity evaluation.

The mutant *P. aeruginosa* $\Delta lasB$ PA14 was kindly provided by the Häussler group (Twincore, Hannover, Germany). *P. aeruginosa* $\Delta lasB$ PA14 (parental strain: "*P. aeruginosa* PA14 (DSM 19882)") is a knockout mutant with markerless in-frame deletion (in frame deletion with pEX18Ap (no antibiotic resistance introduction)), as described in Casilag *et al.*¹² Overnight cultures of a single colony of wild-type (wt) and the LasB knockout ($\Delta lasB$) PA14 strains were grown in lysogeny broth medium at 37 °C with constant shaking at 200 rpm. The next day, the culture was centrifuged at 4 °C, 5000 rpm for 30 min. Then, the supernatant was passed through a membrane filter of 0.2 μ m to sterilize it, it was aliquoted and stored at -80 °C until use. LasB activity of both supernatants was evaluated using the FRET-based assay which was described previously (Figure S11).

Cell-based *in vitro* experiments. A549 cells were purchased from Sigma Aldrich and NHDF cells were provided from Leibniz Institute for New Materials (INM) (Saarbrücken, Germany). Both cell lines were cultured in cell culture plates with a 150 X 20 mm diameter. The cells were incubated with Dulbecco's modified Eagle's medium (DMEM) (Gibco) supplemented with 10% (v/v) fetal bovine serum (FBS, Gibco) and 1% (v/v) Penicillin-Streptomycin (Pen-Strep) at 37 °C under 5% CO₂ in a humidified incubator. 50,000 NHDF cells/well and 100,000 A549 cells/well were seeded in 96-well plates (Greiner) and incubated for 24 h at 37 °C and 5% CO₂ so that the cells reached a confluency of 90%. For imaging purposes, the cells were plated on 96 well glass bottom plates (Cellvis). Next, the cells were treated with (0–25%) wt PA14 supernatant or $\Delta lasB$ PA14 supernatant to compare between their cytotoxic effects. 15% of each supernatant was used in the next experiments with compounds. To prevent disulfide formation of our compounds, we added tris(2-carboxyethyl) phosphine (TCEP) as a reducing agent and optimized its concentration in the assay before the evaluation of the compounds. A mixture of PA14 supernatant (*i.e.*, wt or $\Delta lasB$), various concentrations of LasB inhibitors, 40 μ M ZnCl₂, 40 μ M CaCl₂ and 300 μ M TCEP was preincubated for 30 min and directly added to the cells. The optimized concentration of TCEP did not show any toxic effect on cells and did not affect LasB activity. Phosphoramidon was included in the experiments as LasB reference inhibitor. A mixture of DMEM with TCEP, 40 μ M ZnCl₂, 40 μ M CaCl₂ and 1% DMSO was used as a control. To determine the cell viability, we conducted two different assays: an MTT assay and a live/dead staining followed by imaging using a Leica epifluorescence microscope (DMi8, Leica microsystem CMS GmbH). The MTT assay is a method that can be used to determine the metabolic activity of cells, since active cells are able to reduce the MTT dye (3-(4,5-Dimethylthiazol-2-yl)-2,5-Diphenyltetrazolium Bromide) to the purple formazan precipitate which can be dissolved, and its absorbance can be measured. In the MTT assay, the cells were washed twice with 200 μ L of sterile PBS, followed by addition of DMEM containing 5 mg/mL of MTT solution. The cells were incubated at 37 °C, 5% CO₂ for 2 h. In a next step, the MTT solution was carefully removed and 200 μ L of 100% DMSO

was added to dissolve the purple formazan crystals. After this, we measured the absorbance at 550 nm using a PHERastar plate reader (BMG Labtech, Ortenberg, Germany). The viability of the cells was related to untreated control wells/cells. Live/dead staining was performed using fluorescein diacetate (FDA) to stain living cells and propidium iodide (PI) to stain the dead ones. The cells were seeded and incubated with the supernatant as described before. After 1 day of incubation, the cells were washed 3 times with sterile PBS and then 0.03 mg/mL FDA and 0.02 mg/mL PI were added into each well and incubated for 5 min at 37 °C and 5% CO₂. Imaging was performed using 5x magnification to have a general overview about the cell behavior. 20x magnification was used as well to visualize the change in the morphology of the cells in the bright field channel.

Results of a duplicate of three independent experiments were plotted and illustrated using GraphPad Prism V.9 and presented as mean values ± standard deviation. The statistical analysis of variance was performed with ANOVA followed by Dunnett's multiple comparisons test. Statistical significance was calculated by comparing non-treated cell *vs* treated cells and a *P* value less than 0.05 was significant. For image illustration purposes, the brightness and contrast were optimized for all images based on the values of control (no treatment) images for each channel.

***In vivo* Galleria mellonella virulence assay.** *G. mellonella* larvae were purchased from BioSystems Technology (Exeter, United Kingdom), stored at 8 °C in the dark and used within 2 weeks. Prior to injection, larvae were immobilized by incubation for 10–15 min on ice. Then, the injection was performed using an LA120 syringe pump (Landgraf Laborsysteme, Langenhagen, Germany) supplied with a 1 mL syringe (B. Braun, Melsungen, Germany) and Sterican 0.30 × 12 mm, 30G × 1.5 sterile needles (B. Braun). The larvae were injected with 10 μL of sample into the right proleg. The larvae were classified into various groups based on the applied treatment. Two negative control groups supplemented with no injection to control the quality of the larvae and a buffer control group injected with sterile PBS were included. A positive control group was also included, and the larvae were administered with 50% wt PA14 supernatant. To test the anti-virulence effect of LasB inhibitors, a mixture of 50% wt PA14 supernatant, LasB inhibitor and 300 μM TCEP were incubated for 30 min at 37 °C and injected into the larvae. A group of larvae injected with 50% Δ*lasB* PA14 supernatant was also involved. All groups were incubated at 37 °C and inspected once per day for 4 days post-treatment and to record mortality. The larvae were considered dead if they are black and do not move when stimulated by contact with the forceps. The survival analysis was performed using GraphPad Prism V9, data were plotted using the Kaplan–Meier method and statistical significance between groups was calculated with log-rank test. The data of three independent experiments were combined and plotted in the survival curve, thirty larvae in total were included for each condition.

Synthesis of Intermediates and Final Compounds

General procedure A: Synthesis of chloro acid derivatives 6–10 from amino acid

Amino acid (1.0 eq) was dissolved in 6 N HCl (2 mL/mmol or until mostly dissolved) under nitrogen atmosphere and cooled to –5 °C. NaNO₂ (1.5–2.5 eq) was dissolved in water (0.3 mL/mmol amino acid) and added dropwise slowly. The mixture was stirred overnight while warming to r.t. The reaction mixture was extracted with EtOAc/THF (3:1). Combined organic extracts were washed with saturated aq. NaCl solution, dried over anh. Na₂SO₄ and

filtered. The solvent was removed under reduced pressure to obtain the product. The crude is used in the next steps without further purification.

General procedure B: Synthesis of derivatives 11a–17a using thionyl chloride

The acid (1.0 eq), SOCl₂ (2.0 eq) and a few drops of DMF were heated to 70 °C for 1 h. The cooled mixture was added dropwise to a solution of the corresponding aniline (1.1 eq) in DMF (1 mL/mmol) at 0 °C. The mixture was stirred overnight at r.t. The reaction was quenched with water and extracted with EtOAc (3×). Combined organic extracts were washed with saturated aq. NaCl solution, dried over anh. Na₂SO₄ and filtered. The solvent was removed under reduced pressure to obtain the crude product. The purification was done by column chromatography or flash chromatography.

General Procedure B-1: Synthesis of coupling derivatives 18a, 23a–25a using ethylchloroformate as coupling reagent

The acid (1.2 eq) was dissolved in THF and cooled in an ice-bath. Et₃N (1.2 eq) was added, followed by addition of ClCO₂Et (1.3 eq). After 5 minutes, ice-bath was removed, and reaction was stirred at r.t. for 30 minutes. The corresponding amine (1.0 eq) was slowly added. The reaction was monitored using TLC or LC-MS. After the reaction was completed, volatiles were evaporated under reduced pressure and crude product was purified using column chromatography.

General Procedure B-2: Synthesis of coupling derivatives 17a, 19a–22a and 26a using HATU as coupling reagent

The acid (1.5 eq) was dissolved in DCM (10 mL) at r.t. and to this DIEA (1.5 eq) and HATU (1.5 eq) were added. The corresponding aniline (1 eq) was then added to this mixture and the reaction was monitored by LC-MS. The reaction is extracted with saturated aq. NaCl solution (1×) then dried over anh. Na₂SO₄ and filtered. The crude was purified using reverse phase flash chromatography (H₂O+0.1 %FA/ACN+0.1%FA 95:5 → 5:95).

General procedure C: Protection of hydroxyl group in derivatives 13b, 15b and 16b

The amide (1.0 eq), Et₃N (2.0 eq) and 4-dimethylaminopyridine (0.03 eq) were dissolved in DCM (5 mL/mmol) and cooled to 0 °C. Acetic anhydride (2.0 eq) was added dropwise. The solution was warmed to r.t. and stirred for 30 min. The reaction was washed with DCM, washed with saturated aq. NaCl solution, and dried over anh. Na₂SO₄. The solvent was removed under reduced pressure to obtain the crude product.

General procedure D: Synthesis of thioacetate derivatives 11b, 12b, 13c, 14b, 15c, 16c, and 17b–26b

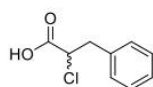
The corresponding chloro derivative (1.0 eq) was dissolved in acetone under argon atmosphere. To this solution, CH₃COSK (1.5–3.0 eq) was added and the reaction was stirred for 2–6 h at r.t. It was monitored by TLC or LC-MS. The reaction was quenched with water and extracted with EtOAc (3×). Combined organic extracts were washed with saturated aq. NaCl solution, dried over anh. Na₂SO₄ and filtered. The solvent was removed under reduced pressure to obtain the crude product. The purification was done by flash chromatography.

General procedure E: Hydrolysis of thioacetate for derivatives 11–26

Thioacetate (1.0 eq) was dissolved in methanol (5 mL/mmol) under argon atmosphere and 2 M aqueous NaOH solution (2.0 eq) or solid NaOH (3.0 eq) was added. The reaction was stirred 1–3 h at r.t. before quenching with 1 M HCl. Reaction was extracted with EtOAc and washed with 0.5 M HCl. Combined organic extracts were washed with saturated aqueous NaCl solution

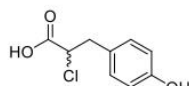
and dried over anh. Na₂SO₄ and filtered. The solvent was removed under reduced pressure to obtain the crude product. The purification was done by column chromatography or preparative HPLC (H₂O+0.05%FA/ACN+0.05%FA, 95:5 → 5:95). For more polar compounds, instead of quenching the reaction with 1 M HCl, pH was adjusted to acidic using Amberlite IR-120. After filtration, Amberlite was washed with MeOH (3×), the solvent was evaporated, and the product was purified using preparative HPLC (H₂O+0.05%FA/ACN+0.05%FA, 95:5 → 5:95). For compounds **21** and **22**, thioacetate (1.0 eq) was dissolved in methanol (5 mL/mmol) under argon atmosphere and acetyl chloride (15 eq) was added dropwise over 10 hours. The mixture was stirred at room temperature for 30–40 hours and carefully monitored by LC-MS. Once the conversion was complete, the solvent was removed under reduced pressure to obtain the crude product. Purification was done by preparative HPLC (H₂O+0.05%FA/ACN+0.05%FA, 95:5 → 5:95).

2-Chloro-3-phenylpropanoic acid (**6**).



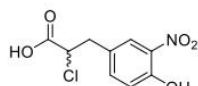
Compound **6** was prepared according to general procedure **A**, using DL-phenylalanine (1 g, 6.0 mmol) and NaNO₂ (1.46 g, 21.2 mmol). The crude product was obtained as yellow oil and used without further purification (1.05 g, 94%). ¹H NMR (500 MHz, CDCl₃) δ ppm: 7.37–7.24 (m, 5H), 4.51 (dd, *J* = 7.8, 6.9 Hz, 1H), 3.42 (dd, *J* = 14.0, 6.7 Hz, 1H), 3.21 (dd, *J* = 14.1, 7.9 Hz, 1H). MS (ESI⁻) *m/z* 183.25 [M-H]⁻, 147.23 [M-H-HCl]⁻. The signals correspond to those reported in literature.¹³

2-Chloro-3-(4-hydroxyphenyl)propanoic acid (**7**).



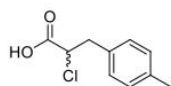
Compound **7** was prepared according to general procedure **A**, using DL-tyrosine (500 mg, 2.76 mmol) and NaNO₂ (286 mg, 4.10 mmol). The product was obtained as off-yellow oil and used without further purification (385 mg, 70%). ¹H NMR (500 MHz, CDCl₃) δ ppm: 7.10 (m, 2H), 6.77 (m, 2H), 4.44 (t, *J* = 7.3 Hz, 1H), 3.35–3.27 (m, 1H), 3.14 (dd, *J* = 14.1, 7.2 Hz, 1H). MS (ESI⁻) *m/z* 199.22 [M-H]⁻, 163.20 [M-H-HCl]⁻. The signals correspond to those reported in literature.¹⁴

2-Chloro-3-(4-hydroxy-3-nitrophenyl)propanoic acid (**8**).



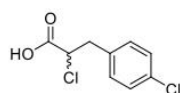
Compound **8** was prepared according to general procedure **A**, using 3-nitro-DL-tyrosine (500 mg, 2.76 mmol) and NaNO₂ (665 mg, 3.5 mmol). The product was obtained as brown oil and used without further purification (344 mg, 63%). ¹H NMR (500 MHz, CDCl₃) δ ppm: 10.53 (br s, 1H), 8.02 (d, *J* = 2.0 Hz, 1H), 7.50 (dd, *J* = 8.5, 2.1 Hz, 1H), 7.14 (d, *J* = 8.7 Hz, 1H), 4.49 (dd, *J* = 7.5, 6.4 Hz, 1H), 3.39 (dd, *J* = 14.4, 6.2 Hz, 1H), 3.22 (dd, *J* = 14.4, 7.9 Hz, 1H). MS (ESI⁻) *m/z* 244.19 [M-H]⁻, 208.22 [M-H-HCl]⁻.

2-Chloro-3-(*p*-tolyl)propanoic acid (**9**).



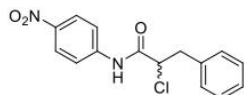
Compound **9** was prepared according to general procedure **A**, using 4-methyl-DL-phenylalanine (200 mg, 1.12 mmol) and NaNO₂ (192 mg, 2.79 mmol). The crude product was obtained as yellow oil and used without further purification (206 mg, 93%). ¹H NMR (500 MHz, CD₃OD) δ ppm: 7.25–7.07 (m, 4H), 4.21 (dd, *J* = 7.8, 5.4 Hz, 1H), 3.27 (dd, *J* = 14.6, 5.3 Hz, 1H), 3.13 (dd, *J* = 14.5, 7.8 Hz, 1H), 2.33 (s, 3H). MS (ESI⁻) *m/z* 197.15 [M-H]⁻ 161.15 [M-H-HCl]⁻. The signals correspond to those reported in literature.¹⁵

2-Chloro-3-(4-chlorophenyl)propanoic acid (**10**).



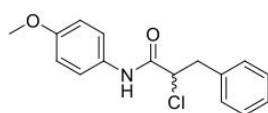
Compound **10** was prepared according to general procedure **A**, using 4-chloro-DL-phenylalanine (500 mg, 2.51 mmol) and NaNO₂ (605 mg, 8.77 mmol). The crude product was obtained as yellow oil and used without further purification (550 mg, 100%). ¹H NMR (500 MHz, CDCl₃) δ ppm: 7.43–7.11 (m, 4H), 4.51 (m, 1H), 3.39 (dd, *J* = 14.1, 6.9 Hz, 1H), 3.21 (dd, *J* = 14.0, 7.7 Hz, 1H). MS (ESI⁻) *m/z* 218.05 [M-H]⁻. The signals correspond to those reported in literature.¹⁶

2-Chloro-*N*-(4-nitrophenyl)-3-phenylpropanamide. (**11a**).



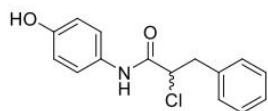
Compound **11a** was prepared according to general procedure **B**, using compound **6** (200 mg, 1.08 mmol), SOCl₂ (157 μL, 2.17 mmol) and 4-nitroaniline (164 mg, 1.19 mmol). Purification was done by flash chromatography (Hex/EtOAc, 100:0 to 0:100). The product was obtained as yellow oil (198 mg, 60%). ¹H NMR (500 MHz, CDCl₃) δ ppm: 8.33 (br s, 1H), 8.26–8.21 (m, 2H), 7.70–7.65 (m, 2H), 7.36–7.24 (m, 5H), 4.73 (dd, *J* = 7.5, 4.6 Hz, 1H), 3.53 (dd, *J* = 14.3, 4.6 Hz, 1H), 3.34 (dd, *J* = 14.3, 7.5 Hz, 1H). MS (ESI⁺) *m/z* 305.11 [M+H]⁺. The signals correspond to those reported in literature.¹⁷

2-Chloro-*N*-(4-methoxyphenyl)-3-phenylpropanamide (**12a**).



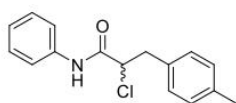
Compound **12a** was prepared according to general procedure **B**, using compound **6** (200 mg, 1.08 mmol), SOCl₂ (157 μL, 2.17 mmol) and *p*-anisidine (147 mg, 1.19 mmol). Purification was done by flash chromatography (Hex/EtOAc, 100:0 to 0:100). The product was obtained as green solid (234 mg, 75%). ¹H NMR (500 MHz, CDCl₃) δ ppm: 8.01 (br s, 1H), 7.38–7.24 (m, 7H), 6.90–6.86 (m, 2H), 4.71 (dd, *J* = 7.8, 4.4 Hz, 1H), 3.81 (s, 3H), 3.52 (dd, *J* = 14.3, 4.4 Hz, 1H), 3.32 (dd, *J* = 14.3, 7.6 Hz, 1H). MS (ESI⁺) *m/z* 290.04 [M+H]⁺. The signals correspond to those described previously.¹⁸

2-Chloro-*N*-(4-hydroxyphenyl)-3-phenylpropanamide (**13a**).



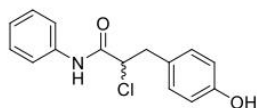
Compound **13a** was prepared according to general procedure **B**, using compound **6** (300 mg, 1.62 mmol), SOCl₂ (239 μL, 3.25 mmol) and 4-aminophenol (195 mg, 1.79 mmol). Purification was done by flash chromatography (Hex/EtOAc, 100:0 to 0:100). The final product was obtained as yellow solid (264 mg, 59%). ¹H NMR (500 MHz, acetone-*d*₆) δ ppm: 9.19 (br s, 1H), 8.24 (s, 1H), 7.41 (d, *J* = 8.8 Hz, 2H), 7.33–7.26 (m, 4H), 7.24–7.20 (m, 1H), 6.76 (d, *J* = 8.8 Hz, 2H), 4.65 (t, *J* = 7.3 Hz, 1H), 3.47 (dd, *J* = 13.7, 7.3 Hz, 1H), 3.16 (dd, *J* = 13.8, 7.2 Hz, 1H). MS (ESI⁺) *m/z* 276.00 [M+H]⁺.

2-Chloro-*N*-phenyl-3-(*p*-tolyl)propanamide (**14a**).



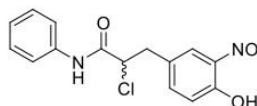
Compound **14a** was prepared according to general procedure **B**, using compound **9** (335 mg, 1.68 mmol), SOCl₂ (244 μL, 3.36 mmol) and aniline (196 μL, 1.85 mmol). Purification was done by flash chromatography (Hex/EtOAc, 100:0 to 0:100). The product was obtained as yellow solid (169 mg, 37%). ¹H NMR (500 MHz, CDCl₃) δ ppm: 8.07 (br s, 1H), 7.49 (br d, *J* = 8.2 Hz, 2H), 7.36 (t, *J* = 7.8 Hz, 2H), 7.20–7.11 (m, 5H), 4.67 (dd, *J* = 7.8, 4.4 Hz, 1H), 3.50 (dd, *J* = 14.3, 4.4 Hz, 1H), 3.28 (dd, *J* = 14.3, 7.8 Hz, 1H), 2.34 (s, 3H). ¹³C NMR (126 MHz, CDCl₃) δ ppm: 166.0, 136.7, 136.5, 132.5, 129.3, 128.9, 128.8, 124.9, 120.0, 61.8, 40.8, 20.8. MS (ESI⁺) *m/z* 274.04 [M+H]⁺.

2-Chloro-3-(4-hydroxyphenyl)-*N*-phenylpropanamide (**15a**).



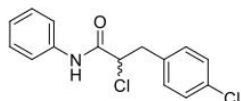
Compound **15a** was prepared according to general procedure **B**, using compound **7** (283 mg, 1.4 mmol), SOCl_2 (205 μL , 2.8 mmol) and aniline (142 μL , 1.55 mmol). Purification was done by flash chromatography (Hex/EtOAc, 100:0 to 0:100). The product was obtained as yellow oil (194 mg, 50%). $^1\text{H NMR}$ (500 MHz, acetone- d_6) δ ppm: 9.36 (br s, 1H), 8.22 (s, 1H), 7.62 (d, $J = 8.1$ Hz, 2H), 7.30 (t, $J = 7.8$ Hz, 2H), 7.14 (d, $J = 8.4$ Hz, 2H), 7.09 (t, $J = 7.0$ Hz, 1H), 6.75 (d, $J = 8.4$ Hz, 2H), 4.61 (t, $J = 7.3$ Hz, 1H), 3.39 (dd, $J = 13.9, 7.8$ Hz, 1H), 3.08 (dd, $J = 13.9, 6.9$ Hz, 1H). $^{13}\text{C NMR}$ (126 MHz, acetone- d_6) δ ppm: 167.4, 157.4, 139.5, 131.5, 129.7, 128.4, 125.0, 120.6, 116.2, 60.9, 40.9. MS (ESI $^+$) m/z 276.08 [M+H] $^+$.

2-Chloro-3-(4-hydroxy-3-nitrophenyl)-N-phenylpropanamide (16a).



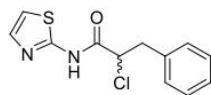
Compound **16a** was prepared according to general procedure **B**, using compound **8** (300 mg, 1.22 mmol), SOCl_2 (218 μL , 3.0 mmol) and aniline (150 μL , 1.65 mmol). Purification was done by flash chromatography (Hex/EtOAc, 100:0 to 0:100). The product was obtained as yellow solid (189 mg, 48%). $^1\text{H NMR}$ (500 MHz, CDCl_3) δ ppm: 10.54 (s, 1H), 8.15 (br s, 1H), 8.07 (d, $J = 2.1$ Hz, 1H), 7.52 (dd, $J = 8.5, 2.1$ Hz, 1H), 7.49 (d, $J = 7.8$ Hz, 2H), 7.37 (t, $J = 7.9$ Hz, 2H), 7.12 (d, $J = 8.7$ Hz, 1H), 7.19 (t, $J = 7.9$ Hz, 1H), 4.69 (dd, $J = 7.4, 4.3$ Hz, 1H), 3.50 (dd, $J = 14.6, 4.7$ Hz, 1H), 3.39 (dd, $J = 14.6, 7.5$ Hz, 1H). $^{13}\text{C NMR}$ (126 MHz, CDCl_3) δ ppm: 165.1, 154.0, 138.8, 136.2, 133.1, 128.9, 127.9, 125.7, 125.2, 120.0, 119.9, 60.8, 39.6. MS (ESI $^+$) m/z 321.16 [M+H] $^+$.

2-Chloro-3-(4-chlorophenyl)-N-phenylpropanamide (17a).



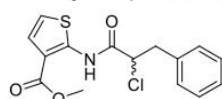
Compound **17a** was prepared according to the general procedure **B-2**, using compound **10** (550 mg, 2.51 mmol), aniline (257 mg, 2.76 mmol), DIEA (641 μL , 3.77 mmol), HATU (1.43 g, 3.77 mmol) in DCM (17 mL). The product was purified by flash column chromatography (Hex/EtOAc, 100:0 to 0:100). The final product was obtained as yellow oil (420 mg, 57%). $^1\text{H NMR}$ (500 MHz, DMSO) δ ppm: 10.31 (s, 1H), 7.55 (d, $J = 7.7$ Hz, 2H), 7.39–7.29 (m, 6H), 7.12–7.06 (m, 1H), 4.72 (t, $J = 7.4$ Hz, 1H), 4.06 (s, 1H), 3.38 (dd, $J = 13.9, 7.8$ Hz, 1H), 3.13 (dd, $J = 13.8, 7.8$ Hz, 1H). $^{13}\text{C NMR}$ (126 MHz, CDCl_3) δ ppm: 166.2, 138.2, 135.8, 131.7, 131.2, 128.9, 128.4, 124.1, 119.5, 59.2, 40.0. MS (ESI $^+$) m/z 294.04 [M+H] $^+$.

2-Chloro-3-phenyl-N-(thiazol-2-yl)propanamide (18a).



Compound **18a** was synthesized according to the general procedure **B-1**, using compound **6** (1.15 g, 6.23 mmol), 2-aminothiazole (517 mg, 5.17 mmol), Et_3N (875 μL , 6.23 mmol) and ClCO_2Et (652 μL , 6.86 mmol) in THF (61 mL). The final product was purified using column chromatography (Hex/EtOAc, 4:1). The final product was obtained as yellow oil (459 mg, 27%). $^1\text{H NMR}$ (500 MHz, acetone- d_6) δ ppm: 11.15 (s, 1H), 7.49–7.40 (t, $J = 3.1$ Hz, 1H), 7.38–7.05 (m, 6H), 4.95 (m, 1H), 3.54 (m, 1H), 3.26 (m, 1H). $^{13}\text{C NMR}$ (126 MHz, acetone- d_6) δ ppm: 167.4, 138.9, 138.8, 137.3, 130.3, 129.3, 128.0, 114.9, 58.9, 41.1. MS (ESI $^+$) m/z 266.84 [M+H] $^+$.

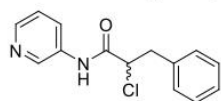
Methyl 2-(2-chloro-3-phenylpropanamido)thiophene-3-carboxylate (19a).



Compound **19a** was prepared according to the general procedure **B-2**, using compound **6** (658 mg, 3.56 mmol), methyl 3-amino-thiophene-2-carboxylate (372 mg, 2.37 mmol), DIEA (619 μL , 3.56 mmol), HATU (1.35 mg, 3.56 mmol) in DCM (25 mL). The product was purified by reverse phase flash column chromatography. The final product was obtained as off-white solid (200 mg, 17%). $^1\text{H NMR}$ (500 MHz, DMSO- d_6) δ ppm: 10.66 (s, 1H), 7.94 (q, $J = 5.4$ Hz, 2H), 7.33–7.27 (m, 4H), 7.27–7.21 (m, 1H), 5.21 (dd, $J = 8.4, 5.5$ Hz, 1H), 3.83 (s, 3H), 3.43 (dd, J

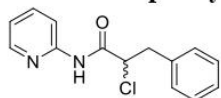
= 14.3, 5.5 Hz, 1H), 3.18 (dd, $J = 14.3, 8.4$ Hz, 1H). ^{13}C NMR (126 MHz, CDCl_3) δ ppm: 166.1, 163.3, 142.5, 136.4, 133.4, 129.4, 128.4, 127.0, 122.0, 111.9, 60.1, 52.3, 40.2. MS (ESI⁺) m/z 324.03 [M+H]⁺.

2-Chloro-3-phenyl-*N*-(pyridin-3-yl)propenamide (20a).



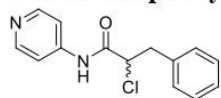
Compound **20a** was prepared according to the general procedure **B-2**, using compound **6** (422 mg, 2.28 mmol), 3-amino-pyridine (143 mg, 1.52 mmol), DIEA (396.9 μL , 2.28 mmol), HATU (866 mg, 2.28 mmol) in DCM (20 mL). The product was purified by reverse phase flash column chromatography. The final product was obtained as yellow oil (312 mg, 52%). ^1H NMR (500 MHz, CDCl_3) δ ppm: 8.57 (s, 1H), 8.45–8.31 (m, 2H), 8.18 (d, $J = 8.1$ Hz, 1H), 7.37 (dd, $J = 8.1, 4.6$ Hz, 1H), 7.34–7.26 (m, 4H), 4.71 (dd, $J = 7.5, 4.9$ Hz, 1H), 4.06 (s, 1H), 3.51 (dd, $J = 14.3, 4.8$ Hz, 1H), 3.31 (dd, $J = 14.3, 7.6$ Hz, 1H). ^{13}C NMR (126 MHz, CDCl_3) δ ppm: 167.2, 144.9, 140.6, 135.7, 134.4, 129.8, 128.8, 128.7, 127.6, 124.4, 61.3, 41.3. MS (ESI⁺) m/z 261.07 [M+H]⁺.

2-Chloro-3-phenyl-*N*-(pyridin-2-yl)propenamide (21a).



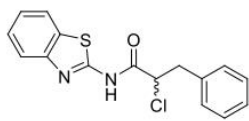
Compound **21a** was prepared according to the general procedure **B-2**, using compound **6** (300 mg, 1.61 mmol), 2-amino-pyridine (166 mg, 1.77 mmol), DIEA (328.0 μL , 1.93 mmol), HATU (733 mg, 1.93 mmol) in DCM (10 mL). The product was purified by reverse phase flash column chromatography. The final product was obtained as yellow oil (180 mg, 43%). ^1H NMR (500 MHz, MeOD) δ ppm: 8.29 (d, $J = 4.6$ Hz, 1H), 8.07 (d, $J = 8.3$ Hz, 1H), 7.84–7.79 (m, 1H), 7.30 (d, $J = 4.3$ Hz, 4H), 7.26–7.21 (m, 1H), 7.18–7.14 (m, 1H), 4.79 (t, $J = 7.3$ Hz, 1H), 4.06 (s, 1H), 3.46 (dd, $J = 13.8, 7.6$ Hz, 1H), 3.22 (dd, $J = 13.8, 7.6$ Hz, 1H). ^{13}C NMR (126 MHz, MEOD) δ ppm: 167.2, 144.9, 140.6, 135.7, 134.4, 129.8, 128.8, 128.7, 127.6, 124.4, 61.3, 41.3. MS (ESI⁺) m/z 261.08 [M+H]⁺.

2-Chloro-3-phenyl-*N*-(pyridin-4-yl)propenamide (22a).



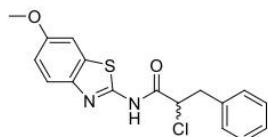
Compound **22a** was prepared according to the general procedure **B-2**, using compound **6** (500 mg, 2.68 mmol), 4-amino-pyridine (277 mg, 2.95 mmol), DIEA (683.0 μL , 4.02 mmol), HATU (1.53 g, 4.02 mmol) in DCM (18 mL). The product was purified by reverse phase flash column chromatography. The final product was obtained as yellow oil (265 mg, 38%). ^1H NMR (500 MHz, CDCl_3) δ ppm: 8.64 (s, 1H), 8.50 (d, $J = 5.6$ Hz, 2H), 7.57 (d, $J = 5.7$ Hz, 2H), 7.35–7.22 (m, 5H), 4.74–4.68 (m, 1H), 4.06 (s, 1H), 3.51 (dd, $J = 14.3, 4.9$ Hz, 1H), 3.29 (dd, $J = 14.3, 7.6$ Hz, 1H). ^{13}C NMR (126 MHz, CDCl_3) δ ppm: 167.4, 149.2, 145.6, 135.5, 129.9, 129.7, 128.7, 127.7, 114.2, 61.2, 41.2. MS (ESI⁺) m/z 261.08 [M+H]⁺.

N-(Benzo[d]thiazol-2-yl)-2-chloro-3-phenylpropanamide (23a).



Compound **23a** was synthesized according to the general procedure **B-1**, using compound **6** (626 mg, 3.39 mmol), 2-aminobenzothiazole (422 mg, 2.81 mmol), Et₃N (476 μL , 3.39 mmol) and ClCO₂Et (355 μL , 3.72 mmol) in THF (33 mL). The final product was purified using flash chromatography (DCM/MeOH, 100:0 to 95:5). Final product was obtained as off-white oil (324 mg, 30%). ^1H NMR (500 MHz, CDCl_3) δ ppm: 7.86 (d, $J = 7.9$ Hz, 1H), 7.78 (m, 1H), 7.47 (t, $J = 7.7$ Hz, 1H), 7.36 (t, $J = 7.6$ Hz, 1H), 7.32–7.23 (m, 3H), 7.21–7.18 (m, 2H), 4.76–4.70 (m, 1H), 3.56–3.51 (m, 1H), 3.29 (dd, $J = 14.4, 7.8$ Hz, 1H). ^{13}C NMR (126 MHz, CDCl_3) δ ppm: 167.1, 157.3, 148.2, 135.3, 132.3, 129.6, 128.8, 127.7, 127.72, 126.7, 124.6, 121.7, 121.3, 60.3, 41.2. MS (ESI⁺) m/z 316.98 [M+H]⁺.

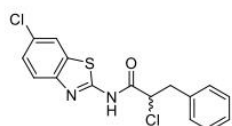
2-Chloro-*N*-(6-methoxybenzo[d]thiazol-2-yl)-3-phenylpropanamide (24a).



Compound **24a** was synthesized according to the general procedure **B-1**, using compound **6** (675 mg, 3.65 mmol), 2-amino-6-methoxybenzothiazole (545 mg, 3.03 mmol), Et₃N (510 μL, 3.65 mmol) and ClCO₂Et (380 μL, 4.01 mmol) in THF (36 mL). The product was purified using column chromatography (DCM/Hex,

3:2). The final product was obtained as yellow oil (450 mg, 35%). ¹H NMR (500 MHz, acetone-*d*₆) δ ppm 11.36 (s, 1H), 7.62 (d, *J* = 8.8 Hz, 1H), 7.53 (d, *J* = 2.6 Hz, 1H), 7.38–7.28 (m, 4H), 7.26–7.22 (m, 1H), 7.04 (dd, *J* = 8.9, 2.6 Hz, 1H), 4.98 (t, *J* = 7.4 Hz, 1H), 3.86 (s, 3H), 3.56 (dd, *J* = 13.9, 7.1 Hz, 1H), 3.27 (dd, *J* = 13.9, 7.7 Hz, 1H). ¹³C NMR (126 MHz, acetone-*d*₆) δ ppm: 168.0, 157.9, 155.8, 143.9, 137.3, 134.4, 130.3, 129.4, 128.0, 122.5, 116.1, 105.0, 59.1, 56.1, 41.0. MS (ESI⁺) *m/z* 346.88 [M+H]⁺.

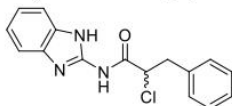
2-Chloro-*N*-(6-chlorobenzo[d]thiazol-2-yl)-3-phenylpropanamide (25a).



Compound **25a** was prepared according to the general procedure **B-1**, using compound **6** (862 mg, 4.66 mmol), 2-amino-6-chlorobenzothiazole (715 mg, 3.86 mmol), Et₃N (656 μL, 4.66 mmol) and ClCO₂Et (489 μL, 5.13 mmol) in THF (46 mL). The product was purified by flash column chromatography (Hex/EtOAc, 7:3). The final

product was obtained as yellow oil (658 mg, 40%). ¹H NMR (500 MHz, CDCl₃) δ ppm: 9.66 (s, 1H), 7.82 (d, *J* = 2.0 Hz, 1H), 7.75–7.67 (m, 1H), 7.45–7.37 (m, 1H), 7.34–7.26 (m, 3H), 7.25–7.20 (m, 2H), 4.77 (dd, *J* = 7.8, 4.6 Hz, 1H), 3.59–3.50 (m, 1H), 3.32 (dd, *J* = 14.4, 7.9 Hz, 1H). ¹³C NMR (126 MHz, CDCl₃) δ ppm: 167.1, 157.3, 147.0, 135.1, 133.6, 130.2, 129.7, 128.8, 127.8, 127.4, 122.3, 121.3, 60.4, 41.2. MS (ESI⁺) *m/z* 350.95 [M+H]⁺.

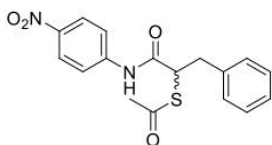
N-(1*H*-Benzo[d]imidazol-2-yl)-2-chloro-3-phenylpropanamide (26a).



Compound **26a** was prepared according to the general procedure **B-2**, using compound **6** (658 mg, 3.56 mmol), 1*H*-benzo[d]imidazol-2-amine (372 mg, 2.37 mmol), DIEA (619 μL, 3.56 mmol), HATU (1.35 mg, 3.56 mmol) in DCM (25 mL). The product was purified by reverse phase

flash column chromatography. The final product was obtained as off-white solid (200 mg, 30%). ¹H NMR (500 MHz, CDCl₃) δ ppm: 7.52–7.46 (m, 2H), 7.34–7.26 (m, 2H), 7.25–7.15 (m, 3H), 7.14–7.10 (m, 2H), 4.70 (t, *J* = 7.1 Hz, 1H), 4.12 (br s, 1H), 3.54–3.42 (m, 1H), 3.33–3.16 (m, 1H). ¹³C NMR (126 MHz, CDCl₃) δ ppm: 170.1, 147.1, 135.6, 129.50, 129.5, 128.8, 128.7, 127.63, 127.6, 123.4, 59.5, 41.2. MS (ESI⁺) *m/z* 300.03 [M+H]⁺.

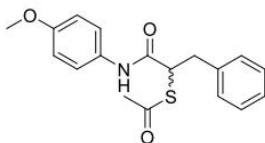
S-(1-((4-Nitrophenyl)amino)-1-oxo-3-phenylpropan-2-yl) ethanethioate (11b).



Compound **11b** was prepared according to general procedure **D**, using compound **11a** (190 mg, 0.78 mmol) and potassium thioacetate (134 mg, 1.17 mmol). Purification was done by flash chromatography (Hex/EtOAc, 100:0 to 0:100). The product was

obtained as yellow oil (127 mg, 47%). ¹H NMR (500 MHz, CDCl₃) δ ppm: 8.45 (br s, 1H), 8.21–8.15 (m, 2H), 7.66–7.61 (m, 2H), 7.33–7.29 (m, 1H), 7.28–7.23 (m, 4H), 4.31 (dd, *J* = 8.5, 7.1 Hz, 1H), 3.46 (dd, *J* = 14.2, 8.5 Hz, 1H), 3.01 (dd, *J* = 14.2, 7.0 Hz, 1H), 2.41 (s, 3H). ¹³C NMR (126 MHz, CDCl₃) δ ppm: 197.9, 168.6, 143.4, 143.1, 136.8, 128.9, 128.4, 126.9, 124.8, 119.0, 48.1, 35.0, 30.2. MS (ESI⁺) *m/z* 345.11 [M+H]⁺, 303.03 [M–Ac+2H]⁺.

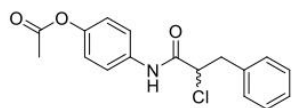
S-(1-((4-Methoxyphenyl)amino)-1-oxo-3-phenylpropan-2-yl) ethanethioate (12b).



Compound **12b** was prepared according to general procedure **D**, using compound **12a** (230 mg, 0.95 mmol) and potassium thioacetate (162 mg, 1.42 mmol). Purification was done by flash chromatography (Hex/EtOAc, 100:0 to 0:100). The product was obtained as yellow

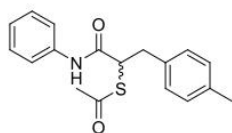
solid (126 mg, 40%). ¹H NMR (500 MHz, CDCl₃) δ ppm: 7.81 (br s, 1H), 7.37–7.34 (m, 2H), 7.33–7.23 (m, 5H), 6.86–6.81 (m, 2H), 4.28 (dd, *J* = 8.4, 7.2 Hz, 1H), 3.79 (s, 3H), 3.44 (dd, *J* = 14.0, 8.4 Hz, 1H), 3.01 (dd, *J* = 14.1, 7.1 Hz, 1H), 2.38 (s, 3H). ¹³C NMR (126 MHz, CDCl₃) δ ppm: 197.4, 168.3, 156.7, 137.9, 130.9, 129.5, 128.8, 127.2, 114.3, 121.8, 55.7, 48.7, 36.1, 30.7. MS (ESI⁺) *m/z* 330.08 [M+H]⁺, 288.08 [M–Ac+2H]⁺.

4-(2-chloro-3-Phenylpropanamido)phenyl acetate (13b).



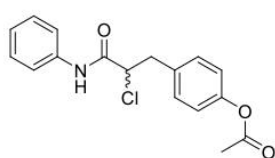
Compound **13b** was prepared according to general procedure **C**, using **13a** (264 mg, 0.96 mmol), Et₃N (266 μL, 1.92 mmol), 4-dimethyl aminopyridine (3.5 mg, 0.03 mmol) and acetic anhydride (181 μL, 1.92 mmol). Purification was done by flash chromatography (Hex/EtOAc, 100:0 to 0:100). The product was obtained as yellow solid (300 mg, 94%). ¹H NMR (500 MHz, acetone-*d*₆) δ ppm: 9.48 (br s, 1H), 7.64 (d, *J* = 8.9 Hz, 2H), 7.31 (m, 2H), 7.28 (m, 2H), 7.23 (m, 1H), 7.07 (d, *J* = 8.9 Hz, 2H), 4.70 (t, *J* = 7.3 Hz, 1H), 3.50 (dd, *J* = 13.9, 7.5 Hz, 1H), 3.19 (dd, *J* = 13.8, 7.2 Hz, 1H), 2.23 (s, 3H). ¹³C NMR (126 MHz, acetone-*d*₆) δ ppm: 169.8, 167.3, 148.1, 137.8, 131.0, 130.4, 129.4, 128.0, 124.0, 123.0, 121.4, 60.6, 41.5, 21.0. MS (ESI⁺) *m/z* 318.07 [M+H]⁺.

S-(1-Oxo-1-(phenylamino)-3-(p-tolyl)propan-2-yl) ethanethioate (14b).



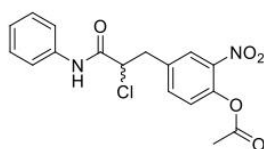
14b was prepared according to general procedure **D**, using **14a** (169 mg, 0.62 mmol) and potassium thioacetate (106 mg, 0.93 mmol). Purification was done via flash chromatography (Hexane/EtOAc, 100:0 to 0:100). The product was obtained as yellow oil (122 mg, 63 %). ¹H NMR (500 MHz, CDCl₃) δ ppm : 7.96 (br s, 1H), 7.48–7.44 (m, 2H), 7.32–7.28 (m, 2H), 7.18–7.14 (m, 2H), 7.13–7.09 (m, 3H), 4.28 (dd, *J* = 8.3, 7.2 Hz, 1H), 3.41 (dd, *J* = 14.1, 8.3 Hz, 1H), 2.97 (dd, *J* = 14.2, 7.2 Hz, 1H), 2.38 (s, 3H), 2.32 (s, 3H). ¹³C NMR (126 MHz, CDCl₃) δ ppm: 197.4, 168.4, 137.7, 136.6, 134.5, 129.3, 129.1, 129.0, 124.4, 119.8, 48.6, 35.3, 30.4, 21.1. MS (ESI⁺) *m/z* 314.10 (M+H)⁺, 272.03 (M–Ac+2H)⁺.

4-(2-Chloro-3-oxo-3-(phenylamino)propyl)phenyl acetate (15b).



15b was prepared according to general procedure **C**, using **15a** (180 mg, 0.65 mmol), Et₃N (180 μL, 1.30 mmol), 4-dimethylaminopyridine (2.4 mg, 0.02 mmol) and acetic anhydride (123 μL, 1.30 mmol). Purification was done by flash chromatography (Hex/EtOAc, 100:0 to 0:100). The final product was obtained as white solid (114 mg, 55%). ¹H NMR (500 MHz, acetone-*d*₆) δ ppm: 9.44 (br s, 1H), 7.62 (d, *J* = 8.9 Hz, 2H), 7.35 (d, *J* = 8.4 Hz, 2H), 7.31 (t, *J* = 7.9 Hz, 2H), 7.10 (m, 1H), 7.05 (d, *J* = 8.4 Hz, 2H), 4.71 (t, *J* = 7.3 Hz, 1H), 3.50 (dd, *J* = 13.9, 7.5 Hz, 1H), 3.20 (dd, *J* = 13.8, 7.2 Hz, 1H), 2.23 (s, 3H). ¹³C NMR (126 MHz, acetone-*d*₆) δ ppm: 169.7, 167.3, 151.1, 139.5, 135.2, 131.4, 129.7, 128.1, 122.7, 120.7, 60.6, 40.8, 21.0. MS (ESI⁺) *m/z* 318.07 [M+H]⁺.

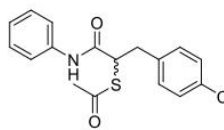
4-(2-Chloro-3-oxo-3-(phenylamino)propyl)-2-nitrophenyl acetate (16b).



16b was prepared according to general procedure **C**, using **16a** (189 mg, 0.59 mmol), Et₃N (164 μL, 1.18 mmol), 4-dimethylaminopyridine (2.0 mg, 0.02 mmol) and acetic anhydride (112 μL, 1.18 mmol). Purification was done by flash chromatography (Hex/EtOAc, 100:0 to 0:100). The final product was obtained as yellow solid (200 mg, 93%). ¹H NMR (500 MHz, acetone-*d*₆) δ ppm: 9.50 (br s, 1H), 8.15 (d, *J* = 2.0 Hz, 1H), 7.77 (dd, *J* = 8.4, 2.0 Hz, 1H), 7.62 (d, *J* = 8.2 Hz, 2H), 7.36 (d, *J* = 8.2 Hz, 1H), 7.32 (t, *J* = 7.9 Hz, 2H), 7.11 (t, *J* = 7.4 Hz, 1H), 4.84 (t, *J* = 7.2 Hz, 1H), 3.63 (dd, *J* =

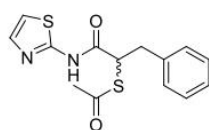
14.1, 6.6 Hz, 1H), 3.37 (dd, $J = 14.1, 7.9$ Hz, 1H), 2.31 (s, 3H). ^{13}C NMR (126 MHz, acetone- d_6) δ ppm: 169.1, 166.9, 143.8, 142.7, 139.3, 137.3, 130.6, 129.8, 127.3, 126.2, 125.2, 120.7, 60.1, 40.2, 20.8. MS (ESI $^+$) m/z 362.12 [M+H] $^+$, 321.06 [M-Ac+2H] $^+$.

S-(3-(4-Chlorophenyl)-1-oxo-1-(phenylamino)propan-2-yl) ethanethioate (17b).



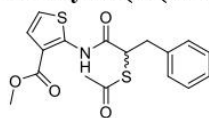
Compound **17b** was prepared according to general procedure **D**, using compound **17a** (200 mg, 0.68 mmol) and potassium thioacetate (233 mg, 2.04 mmol) in acetone (7 mL). Purification was done by column chromatography (Hex/EtOAc, 100:0 to 0:100). The final product was obtained as yellow solid (115 mg, 51%). ^1H NMR (500 MHz, CDCl_3) δ ppm: 7.99 (s, 1H), 7.44 (d, $J = 7.7$ Hz, 2H), 7.31–7.17 (m, 6H), 7.09 (t, $J = 7.4$ Hz, 1H), 4.27–4.22 (m, 1H), 3.40 (dd, $J = 14.1, 8.5$ Hz, 1H), 2.95 (dd, $J = 14.2, 7.0$ Hz, 1H), 2.36 (s, 3H). ^{13}C NMR (125 MHz, CDCl_3) δ ppm: 197.2, 168.2, 137.6, 136.2, 133.0, 130.8, 129.1, 128.8, 124.7, 120.0, 48.3, 35.2, 30.5. MS (ESI $^+$) m/z 334.07 [M+H] $^+$.

S-(1-Oxo-3-phenyl-1-(thiazol-2-ylamino)propan-2-yl) ethanethioate (18b).



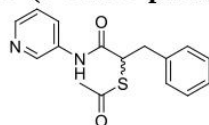
Compound **18b** was prepared according to general procedure **D**, using compound **18a** (336 mg, 1.26 mmol) and potassium thioacetate (215 mg, 1.90 mmol) in acetone (13 mL). Purification was done by flash chromatography (Hex/EtOAc, 3:1). The final product was obtained as white powder (300 mg, 77%). ^1H NMR (500 MHz, acetone- d_6) δ ppm: 11.41 (s, 1H), 7.46–7.37 (m, 1H), 7.3–7.23 (m, 4H), 7.22–7.17 (m, 1H), 7.15 (d, $J = 3.5$ Hz, 1H), 4.66 (dd, $J = 8.8, 6.7$ Hz, 1H), 3.38 (dd, $J = 13.7, 8.9$ Hz, 1H), 3.02 (dd, $J = 13.7, 6.7$ Hz, 1H), 2.05 (d, $J = 2.2$ Hz, 3H). ^{13}C NMR (126 MHz, acetone- d_6) δ ppm: 194.6, 169.2, 158.5, 138.6, 138.4, 130.0, 129.2, 127.7, 114.5, 61.7, 49.1, 38.6. MS (ESI $^+$) m/z 306.90 [M+H] $^+$, 264.90 [M-Ac+H] $^+$.

Methyl 2-(2-(acetylthio)-3-phenylpropanamido)thiophene-3-carboxylate (19b).



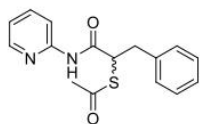
Compound **19b** was prepared according to general procedure **D**, using compound **19a** (172 mg, 0.53 mmol) and potassium thioacetate (112 mg, 0.79 mmol) in acetone (12 mL). Purification was done by column chromatography (Hex/EtOAc, 6:1). The final product was obtained as yellow solid (129 mg, 67%). ^1H NMR (500 MHz, CDCl_3) δ ppm: 10.46 (s, 1H), 8.10 (d, $J = 5.5$ Hz, 1H), 7.44 (d, $J = 5.4$ Hz, 1H), 7.30–7.26 (m, 2H), 7.26–7.20 (m, 3H), 4.45 (t, $J = 7.7$ Hz, 1H), 3.89 (s, 3H), 3.43 (dd, $J = 14.2, 7.6$ Hz, 1H), 3.07 (dd, $J = 14.2, 7.7$ Hz, 1H), 2.37 (s, 3H). ^{13}C NMR (126 MHz, CDCl_3) δ ppm: 194.6, 168.3, 164.4, 143.9, 137.5, 131.5, 129.3, 128.7, 127.1, 122.7, 111.5, 52.2, 49.1, 36.8, 30.5. MS (ESI $^+$) m/z 364.05 [M+H] $^+$, 322.03 [M-Ac+H] $^+$.

S-(1-Oxo-3-phenyl-1-(pyridin-3-ylamino)propan-2-yl) ethanethioate (20b).



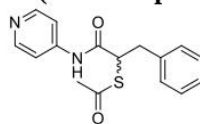
Compound **20b** was prepared according to general procedure **D**, using compound **20a** (326 mg, 1.25 mmol) and potassium thioacetate (264 mg, 1.88 mmol) in acetone (12 mL). Purification was done by column chromatography (DCM/MeOH, 98:2). The final product was obtained as yellow solid (179 mg, 48%). ^1H NMR (500 MHz, CDCl_3) δ ppm: 8.59 (s, 1H), 8.53–8.21 (m, 2H), 8.17 (d, $J = 8.5$ Hz, 1H), 7.39–7.27 (m, 5H), 7.25–7.20 (m, 1H), 4.37–4.30 (m, 1H), 3.43 (dd, $J = 14.1, 8.5$ Hz, 1H), 3.01 (dd, $J = 14.1, 7.0$ Hz, 1H), 2.39 (s, 3H). ^{13}C NMR (126 MHz, CDCl_3) δ ppm: 197.5, 169.3, 144.0, 140.0, 137.4, 129.8, 129.3, 128.8, 128.7, 128.4, 127.3, 124.3, 48.5, 35.9, 30.6. MS (ESI $^+$) m/z 301.06 [M+H] $^+$, 260.98 [M-Ac+2H] $^+$.

S-(1-Oxo-3-phenyl-1-(pyridin-2-ylamino)propan-2-yl) ethanethioate (21b).



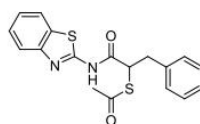
Compound **21b** was prepared according to general procedure **D**, using compound **21a** (170 mg, 0.65 mmol) and potassium thioacetate (115 mg, 1.01 mmol) in acetone (5 mL). Purification was done by column chromatography (DCM/MeOH, 98:2). The final product was obtained as yellow solid (179 mg, 48%). ¹H NMR (500 MHz, CDCl₃) δ ppm: 8.59 (s, 1H), 8.53–8.21 (m, 2H), 8.17 (d, *J* = 8.5 Hz, 1H), 7.39–7.27 (m, 5H), 7.25–7.20 (m, 1H), 4.37–4.30 (m, 1H), 3.43 (dd, *J* = 14.1, 8.5 Hz, 1H), 3.01 (dd, *J* = 14.1, 7.0 Hz, 1H), 2.39 (s, 3H). ¹³C NMR (126 MHz, CDCl₃) δ ppm: 197.5, 169.3, 144.0, 140.0, 137.4, 129.8, 129.3, 128.8, 128.7, 128.4, 127.3, 124.3, 48.5, 35.9, 30.6. MS (ESI⁺) *m/z* 301.09 [M+H]⁺, 260.98 [M–Ac+2H]⁺.

S-(1-Oxo-3-phenyl-1-(pyridin-4-ylamino)propan-2-yl) ethanethioate (22b).



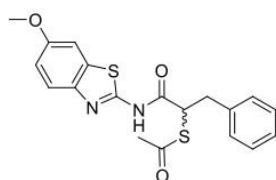
Compound **22b** was prepared according to general procedure **D**, using compound **22a** (120 mg, 0.46 mmol) and potassium thioacetate (158 mg, 1.38 mmol) in acetone (5 mL). Purification was done by column chromatography (DCM/MeOH, 98:2). The final product was obtained as yellow solid (62 mg, 45%). ¹H NMR (500 MHz, CDCl₃) δ ppm: 8.42 (d, *J* = 3.7 Hz, 2H), 7.44 (d, *J* = 6.4 Hz, 1H), 7.31–7.20 (m, 5H), 4.34–4.29 (m, 1H), 3.41 (dd, *J* = 14.1, 8.5 Hz, 1H), 2.98 (dd, *J* = 14.1, 7.0 Hz, 1H), 2.37 (s, 3H). ¹³C NMR (126 MHz, CDCl₃) δ ppm: 197.5, 169.3, 149.9, 145.3, 137.4, 129.6, 129.2, 128.7, 127.2, 113.9, 48.5, 35.7, 30.4. MS (ESI⁺) *m/z* 301.09 [M+H]⁺.

S-(1-(Benzo[d]thiazol-2-ylamino)-1-oxo-3-phenylpropan-2-yl) ethanethioate (23b).



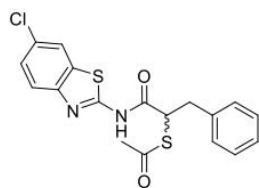
Compound **23b** was prepared according to general procedure **D**, using compound **23a** (323 mg, 1.02 mmol) and potassium thioacetate (174 mg, 1.53 mmol) in acetone (10 mL). Purification was done by flash chromatography (Hex/DCM, 100:0 to 0:100). The final product was obtained as yellow solid (257, 71%). ¹H NMR (500 MHz, acetone-*d*₆) δ ppm: 11.24 (s, 1H), 8.02–7.88 (m, 1H), 7.69 (d, *J* = 8.1 Hz, 1H), 7.43 (m, 1H), 7.35–7.26 (m, 5H), 7.24–7.17 (m, 1H), 4.72 (dd, *J* = 8.7, 6.9 Hz, 1H), 3.41 (dd, *J* = 13.8, 8.7 Hz, 1H), 3.06 (dd, *J* = 13.8, 6.9 Hz, 1H), 2.36 (s, 3H). ¹³C NMR (126 MHz, CDCl₃) δ ppm: 196.2, 169.1, 157.6, 148.4, 136.9, 132.3, 129.3, 128.8, 127.4, 126.5, 124.3, 121.5, 121.2, 47.9, 35.9, 30.5. MS (ESI⁺) *m/z* 357.01 [M+H]⁺, 314.90 [M–Ac+H]⁺.

S-(1-((6-Methoxybenzo[d]thiazol-2-yl)amino)-1-oxo-3-phenylpropan-2-yl) ethanethioate (24b).



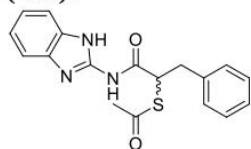
Compound **24b** was prepared according to general procedure **D**, using compound **24a** (377 mg, 1.08 mmol) and potassium thioacetate (186 mg, 1.63 mmol) in acetone (10 mL). Purification was done by flash chromatography (Hex/DCM, 100:0 to 0:100). The final product was obtained as yellow solid (250 mg, 59%). ¹H NMR (500 MHz, CDCl₃) δ ppm: 7.64 (d, *J* = 8.9 Hz, 1H), 7.32–7.26 (m, 3H), 7.26–7.18 (m, 3H), 7.03 (dd, *J* = 8.9, 2.5 Hz, 1H), 4.44 (t, *J* = 7.7 Hz, 1H), 3.88–3.85 (m, 3H), 3.46 (dd, *J* = 14.2, 7.9 Hz, 1H), 3.06 (dd, *J* = 14.2, 7.6 Hz, 1H), 2.38 (s, 3H). ¹³C NMR (126 MHz, CDCl₃) δ ppm: 196.3, 168.8, 157.04, 155.5, 142.5, 136.9, 133.5, 129.3, 128.82, 127.4, 121.8, 115.5, 104.2, 56.0, 47.8, 35.8, 30.5. MS (ESI⁺) *m/z* 386.88 [M+H]⁺, 345.00 [M–Ac+H]⁺.

S-(1-((6-Chlorobenzo[d]thiazol-2-yl)amino)-1-oxo-3-phenylpropan-2-yl) ethanethioate (25b).



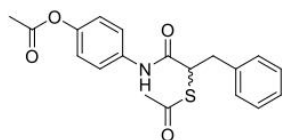
Compound **25b** was prepared according to general procedure **D**, using compound **25a** (658 mg, 1.87 mmol) and potassium thioacetate (325 mg, 2.80 mmol) in acetone (5 mL). Purification was done by flash chromatography (Hex/EtOAc, 7:3). The final product was obtained as yellow solid (300 mg, 41%). ^1H NMR (500 MHz, CDCl_3) δ ppm: 9.61 (s, 1H), 7.79 (d, $J = 2.1$ Hz, 1H), 7.69 (d, $J = 8.6$ Hz, 1H), 7.40 (dd, $J = 8.7, 2.1$ Hz, 1H), 7.35–7.29 (m, 2H), 7.25–7.22 (m, 3H), 4.45 (t, $J = 7.7$ Hz, 1H), 3.49 (dd, $J = 14.2, 8.0$ Hz, 1H), 3.08 (dd, $J = 14.2, 7.5$ Hz, 1H), 2.42 (s, 3H). ^{13}C NMR (126 MHz, CDCl_3) δ ppm: 196.8, 171.3, 169.0, 157.4, 147.3, 136.8, 129.3, 128.9, 127.5, 127.1, 122.2, 121.1, 47.6, 35.4, 30.5. MS (ESI $^+$) m/z 390.93 [M+H] $^+$, 348.98 [M–Ac+H] $^+$.

S-(1-((1H-Benzo[d]imidazol-2-yl)amino)-1-oxo-3-phenylpropan-2-yl) ethanethioate (26b).



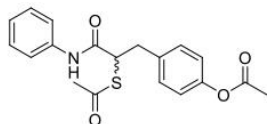
Compound **26b** was prepared according to general procedure **D**, using compound **26a** (172 mg, 0.53 mmol) and potassium thioacetate (112 mg, 0.79 mmol) in acetone (12 mL). Purification was done by column chromatography (Hex/EtOAc 6:1). The final product was obtained as yellow solid (136 mg, 85%). ^1H NMR (500 MHz, CDCl_3) δ ppm: 12.06 (s, 1H), 11.62 (s, 1H), 7.42 (br s, 2H), 7.33–7.14 (m, 5H), 7.07 (dd, $J = 5.9, 3.0$ Hz, 2H), 3.93 (d, $J = 6.3$ Hz, 1H), 3.34 (s, 3H), 3.27 (d, $J = 9.0$ Hz, 1H), 2.99 (dd, $J = 13.7, 6.4$ Hz, 1H). MS (ESI $^+$) m/z 340.08 [M+H] $^+$, 297.03 [M–Ac+H] $^+$.

4-(2-(Acetylthio)-3-phenylpropanamido)phenyl acetate (13c).



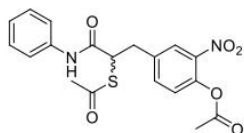
Compound **13c** was prepared according to general procedure **D**, using compound **13b** (280 mg, 0.88 mmol) and potassium thioacetate (151 mg, 1.32 mmol) in acetone (10 mL). Purification was done by flash chromatography (Hex/EtOAc, 100:0 to 0:100). The final product was obtained as yellow solid (244 mg, 77%). ^1H NMR (500 MHz, acetone- d_6) δ ppm: 9.32 (br s, 1H), 7.58 (d, $J = 8.8$ Hz, 2H), 7.30–7.24 (m, 3H), 7.22–7.18 (m, 2H), 7.03 (d, $J = 8.9$ Hz, 2H), 4.41 (dd, $J = 9.3, 6.0$ Hz, 1H), 3.35 (dd, $J = 13.6, 9.3$ Hz, 1H), 2.95 (dd, $J = 13.6, 6.0$ Hz, 1H), 2.34 (s, 3H), 2.22 (s, 3H). ^{13}C NMR (126 MHz, CDCl_3) δ ppm: 195.0, 169.8, 169.0, 147.9, 139.1, 137.2, 130.1, 129.3, 127.7, 122.9, 121.2, 50.4, 39.3. MS (ESI $^+$) m/z 358.13 [M+H] $^+$, 282.03 [M–HSAc+H] $^+$.

4-(2-(Acetylthio)-3-oxo-3-(phenylamino)propyl)phenyl acetate (15c).



Compound **14c** was prepared according to general procedure **D**, using compound **14b** (130 mg, 0.41 mmol) and potassium thioacetate (70 mg, 0.61 mmol). Purification was done via flash chromatography (Hex/EtOAc, 100:0 to 0:100). The product was obtained as yellow oil (125 mg, 87%). ^1H NMR (126 MHz, CDCl_3) δ ppm: 7.97 (s, 1H), 7.46 (d, $J = 7.9$ Hz, 2H), 7.33–7.26 (m, 4H), 7.11 (br d, $J = 7.3$ Hz, 1H), 7.02 (d, $J = 8.4$ Hz, 2H), 4.29–4.25 (m, 1H), 3.45 (dd, $J = 14.2, 8.5$ Hz, 1H), 2.99 (dd, $J = 14.2, 7.0$ Hz, 1H), 2.39 (s, 3H), 2.29 (s, 3H). MS (ESI $^+$) m/z 358.10.08 [M+H] $^+$, 316.10 [M–Ac+2H] $^+$.

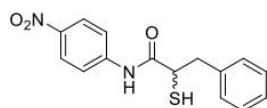
4-(2-(Acetylthio)-3-oxo-3-(phenylamino)propyl)-2-nitrophenyl acetate (16c).



Compound **16c** was prepared according to general procedure **D**, using compound **16b** (185 mg, 0.51 mmol) and potassium thioacetate (87 mg, 0.76 mmol). Purification was done by flash chromatography (Hex/EtOAc, 100:0 to 0:100). The product was obtained as yellow oil (166 mg, 81%). ^1H NMR (500 MHz, acetone- d_6) δ ppm: 9.36 (br s, 1H),

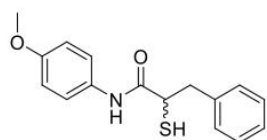
8.09 (d, $J = 1.7$ Hz, 1H), 7.71 (dd, $J = 8.2, 1.8$ Hz, 1H), 7.56 (d, $J = 8.2$ Hz, 2H), 7.32 (d, $J = 8.4$ Hz, 1H), 7.28 (t, $J = 7.9$ Hz, 2H), 7.07 (t, $J = 7.4$ Hz, 1H), 4.51 (dd, $J = 8.7, 6.6$ Hz, 1H), 3.50 (dd, $J = 13.8, 8.8$ Hz, 1H), 3.12 (dd, $J = 13.7, 6.4$ Hz, 1H), 2.35 (s, 3H), 2.30 (s, 3H). ^{13}C NMR (126 MHz, acetone- d_6) δ ppm: 194.8, 169.1, 168.5, 143.6, 142.6, 139.6, 138.5, 137.0, 129.7, 127.1, 126.1, 124.9, 120.5, 49.8, 38.0, 20.7. MS (ESI $^+$) m/z 402.09 [M+H] $^+$.

2-Mercapto-*N*-(4-nitrophenyl)-3-phenylpropanamide (11).



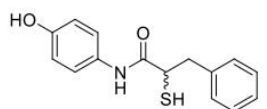
Compound **11** was prepared according to general procedure **E**, using compound **11b** (95 mg, 0.28 mmol) and 2 M NaOH aq. solution (280 μL , 0.56 mmol) in MeOH (2 mL). Purification was done by flash chromatography (Hex/EtOAc, 100:0 to 0:100). The final product was obtained as colorless oil (52 mg, 61%). ^1H NMR (500 MHz, CDCl_3) δ ppm: 8.35 (br s, 1H), 8.24–8.20 (m, 2H), 7.69–7.64 (m, 2H), 7.34–7.27 (m, 3H), 7.25–7.22 (m, 2H), 3.77 (dt, $J = 9.1, 6.6$ Hz, 1H), 3.37 (dd, $J = 13.9, 6.4$ Hz, 1H), 3.28 (dd, $J = 13.9, 6.9$ Hz, 1H), 2.15 (d, $J = 9.0$ Hz, 1H). ^{13}C NMR (126 MHz, CDCl_3) δ ppm: 170.2, 144.1, 143.1, 137.0, 129.6, 128.9, 127.5, 125.2, 119.4, 46.0, 41.4. HRMS (ESI $^-$) m/z calcd. for $\text{C}_{15}\text{H}_{13}\text{N}_2\text{O}_3\text{S}$ [M-H] $^-$ 301.06523, found 301.06518.

2-Mercapto-*N*-(4-methoxyphenyl)-3-phenylpropanamide (12).



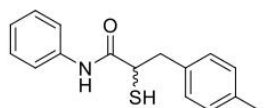
Compound **12** was prepared according to general procedure **E**, using compound **12b** (95 mg, 0.29 mmol) and 2 M NaOH aq. solution (290 μL , 0.58 mmol) in MeOH (2 mL). Purification was done by flash chromatography (Hex/EtOAc, 100:0 to 0:100). The final product was obtained as white solid (45 mg, 54%). ^1H NMR (500 MHz, CDCl_3) δ ppm: 7.90 (br s, 1H), 7.37–7.33 (m, 2H), 7.31 (d, $J = 7.5$ Hz, 2H), 7.28–7.23 (m, 3H), 6.89–6.84 (m, 2H), 3.80 (s, 3H), 3.70 (dt, $J = 8.9, 6.6$ Hz, 1H), 3.36 (dd, $J = 13.7, 6.7$ Hz, 1H), 3.24 (dd, $J = 14.0, 6.4$ Hz, 1H), 2.10 (d, $J = 8.9$ Hz, 1H). ^{13}C NMR (126 MHz, CDCl_3) δ ppm: 169.5, 156.9, 137.5, 130.4, 129.6, 128.7, 127.3, 122.1, 114.3, 55.6, 45.9, 41.7. HRMS (ESI $^+$) m/z calcd. for $\text{C}_{16}\text{H}_{18}\text{NO}_2\text{S}$ [M+H] $^+$ 288.10527, found 288.10453.

N-(4-Hydroxyphenyl)-2-mercapto-3-phenylpropanamide (13).



Compound **13** was prepared according to general procedure **E**, using compound **13c** (240 mg, 0.67 mmol) and 2M NaOH aq. solution (1.05 mL, 2.1 mmol) in MeOH (2 mL). Purification was done by flash chromatography (Hex/EtOAc, 100:0 to 0:100). The final product was obtained as white solid (68 mg, 37%). ^1H NMR (500 MHz, acetone- d_6) δ ppm: 9.05 (br s, 1H), 8.22 (s, 1H), 7.38 (d, $J = 8.8$ Hz, 2H), 7.32–7.17 (m, 5H), 6.75 (d, $J = 9.3$ Hz, 2H), 3.70 (td, $J = 8.9, 6.5$ Hz, 1H), 3.32 (dd, $J = 13.5, 8.8$ Hz, 1H), 2.99 (dd, $J = 13.6, 6.3$ Hz, 1H), 2.50 (d, $J = 9.5$ Hz, 1H). ^{13}C NMR (126 MHz, acetone- d_6) δ ppm: 170.6, 154.7, 139.8, 132.0, 130.1, 129.1, 127.4, 122.1, 116.0, 45.2, 43.3. HRMS (ESI $^-$) m/z calcd. for $\text{C}_{15}\text{H}_{14}\text{NO}_2\text{S}$ [M-H] $^-$ 272.07507, found 272.07520.

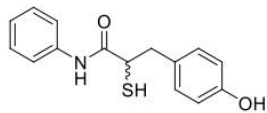
2-Mercapto-*N*-phenyl-3-(*p*-tolyl)propenamide (14).



Compound **14** was prepared according to general procedure **E**, using compound **14b** (90 mg, 0.29 mmol) and 2 M NaOH aq. solution (290 μL , 0.58 mmol) in MeOH (5 mL). Purification was done by flash chromatography (Hex/EtOAc, 100:0 to 0:100). The product was obtained as white solid (55 mg, 70%). ^1H NMR (500 MHz, CDCl_3) δ ppm: 8.02 (br s, 1H), 7.48 (br d, $J = 7.8$ Hz, 2H), 7.34 (t, $J = 7.9$ Hz, 2H), 7.17–7.09 (m, 5H), 3.70 (dt, $J = 8.6, 6.7$ Hz,

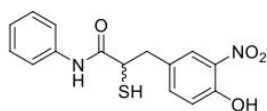
1H), 3.33 (dd, $J = 13.9, 6.7$ Hz, 1H), 3.21 (dd, $J = 13.8, 6.8$ Hz, 1H), 2.33 (s, 3H), 2.09 (d, $J = 8.9$ Hz, 1H). ^{13}C NMR (126 MHz, CDCl_3) δ ppm: 169.6, 137.3, 136.8, 134.1, 129.3, 129.3, 129.0, 124.7, 120.0, 46.0, 41.0, 21.1. HRMS (ESI⁺) m/z calcd. for $\text{C}_{16}\text{H}_{18}\text{NOS}$ [$\text{M}+\text{H}$]⁺ 272.11036, found 272.10971.

3-(4-Hydroxyphenyl)-2-mercapto-*N*-phenylpropanamide (15).



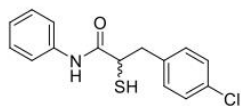
Compound **15** was prepared according to general procedure **E**, using compound **15c** (120 mg, 0.34 mmol) and 2 M NaOH aq. solution (340 μL , 0.68 mmol) in MeOH (2 mL). Purification was done by flash chromatography (Hex/EtOAc, 100:0 to 0:100). The final product was obtained as white solid (41 mg, 44%). ^1H NMR (500 MHz, Acetone- d_6) δ ppm: 9.21 (br s, 1H), 8.16 (br s, 1H), 7.59 (d, $J = 8.2$ Hz, 2H), 7.09 (d, $J = 8.4$ Hz, 2H), 7.27 (t, $J = 7.9$ Hz, 2H), 7.05 (t, $J = 7.3$ Hz, 1H), 6.72 (d, $J = 8.4$ Hz, 2H), 3.67 (dd, $J = 8.7, 6.1$ Hz, 1H), 3.24 (dd, $J = 13.7, 8.9$ Hz, 1H), 2.91 (dd, $J = 13.7, 6.1$ Hz, 1H), 2.48 (br s, 1H). ^{13}C NMR (126 MHz, Acetone- d_6) δ ppm: 171.5, 157.1, 140.1, 131.1, 130.4, 129.6, 124.5, 120.3, 116.0, 45.6, 42.5. HRMS (ESI⁺) m/z calcd. for $\text{C}_{15}\text{H}_{16}\text{NO}_2\text{S}$ [$\text{M}+\text{H}$]⁺ 274.08962, found 274.08893.

3-(4-Hydroxy-3-nitrophenyl)-2-mercapto-*N*-phenylpropanamide (16).



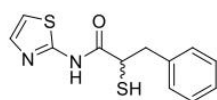
Compound **16** was prepared according to general procedure **E**, using compound **16c** (160mg, 0.40 mmol) and 2 M NaOH aq. solution (600 μL , 1.2 mmol) in MeOH (10 mL). Purification was done by flash chromatography (Hex/EtOAc, 100:0 to 0:100). The final product was obtained as light green solid (70 mg, 50%). ^1H NMR (500 MHz, acetone- d_6) δ ppm: 10.33 (s, 1H), 9.33 (br s, 1H), 8.06 (d, $J = 2.0$ Hz, 1H), 7.63 (dd, $J = 8.5, 2.1$ Hz, 1H), 7.58 (d, $J = 8.1$ Hz, 2H), 7.28 (t, $J = 7.9$ Hz, 2H), 7.12 (d, $J = 8.5$ Hz, 1H), 7.06 (t, $J = 7.3$ Hz, 1H), 3.79 (dd, $J = 8.9, 7.0$ Hz, 1H), 3.36 (dd, $J = 13.7, 8.4$ Hz, 1H), 3.07 (dd, $J = 13.8, 6.6$ Hz, 1H), 2.60 (d, $J = 9.8$ Hz, 1H). ^{13}C NMR (126 MHz, acetone- d_6) δ ppm: 170.9, 154.2, 139.8, 139.6, 134.7, 132.1, 129.6, 126.1, 124.6, 120.5, 120.3, 44.9, 41.4. HRMS (ESI⁻) m/z calcd. for $\text{C}_{15}\text{H}_{13}\text{N}_2\text{O}_4\text{S}$ [$\text{M}-\text{H}$]⁻ 317.06015, found 317.06003.

3-(4-Chlorophenyl)-2-mercapto-*N*-phenylpropanamide (17).



Compound **17** was prepared according to general procedure **E**, using compound **17b** (28 mg, 0.08 mmol) and 2 M NaOH aq. solution (17 μL , 0.17 mmol) in MeOH (2 mL). Purification was done by preparative HPLC. The final product was obtained as white solid (7 mg, 29%). ^1H NMR (500 MHz, acetone- d_6) δ ppm: 9.26 (s, 1H), 7.57 (d, $J = 8.2$ Hz, 2H), 7.32–7.24 (m, 6H), 7.05 (t, $J = 7.4$ Hz, 1H), 3.77–3.70 (m, 1H), 3.33 (dd, $J = 13.6, 8.6$ Hz, 1H), 3.00 (dd, $J = 13.7, 6.4$ Hz, 1H), 2.56 (d, $J = 9.6$ Hz, 1H). ^{13}C NMR (125 MHz, acetone- d_6) δ ppm: 171.0, 139.9, 138.6, 132.8, 132.0, 129.5, 129.1, 124.6, 120.2, 45.0, 42.2. HRMS (ESI⁺) m/z calcd. for $\text{C}_{15}\text{H}_{15}\text{ClNOS}$ [$\text{M}+\text{H}$]⁺ 292.0557, found 292.0554.

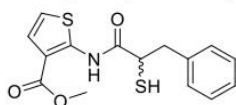
2-Mercapto-3-phenyl-*N*-(thiazol-2-yl)propanamide (18).



Compound **18** was prepared according to general procedure **E**, using compound **18b** (219 mg, 0.71 mmol) and 2 M NaOH aq. solution (714 μL , 1.43 mmol) in MeOH (5 mL). Purification was done by column chromatography (Hex/EtOAc, 7:3). The final product was obtained as white solid (25 mg, 15%). ^1H NMR (500 MHz, DMSO- d_6) δ ppm: 12.18 (s, 1H), 7.46 (d, $J = 3.5$ Hz, 1H), 7.30–7.24 (m, 2H), 7.24–7.16 (m, 4H), 3.90 (t, $J = 7.6$ Hz, 1H), 3.26 (dd, $J = 13.7, 8.8$ Hz, 1H), 2.97 (dd, $J = 13.7, 6.6$ Hz, 1H), 2.53–2.51 (m, 1H). ^{13}C NMR (126 MHz,

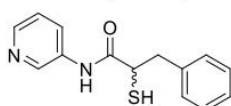
DMSO-*d*₆) δ ppm: 170.6, 157.7, 138.3, 137.8, 129.0, 128.3, 126.6, 113.8, 41.7, 40.6. HRMS (ESI⁻) *m/z* calcd. for C₁₂H₁₁N₂OS₂ [M-H]⁻ 263.03182, found 263.03189.

Methyl 2-(2-mercapto-3-phenylpropanamido)thiophene-3-carboxylate (19).



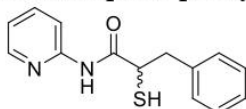
Compound **19** was prepared according to general procedure **E**, using compound **19b** (129 mg, 0.52 mmol) and solid NaOH (40 mg, 1.03 mmol) in MeOH (3 mL). Purification was done by preparative HPLC. The final product was obtained as white solid (94 mg, 82%). ¹H NMR (500 MHz, DMSO-*d*₆) δ ppm: 10.45 (s, 1H), 7.91 (dd, *J* = 13.1, 5.4 Hz, 2H), 7.36–7.09 (m, 5H), 4.06 (t, *J* = 7.4 Hz, 1H), 3.82 (s, 3H), 3.27 (dd, *J* = 13.9, 7.4 Hz, 1H), 2.97 (dd, *J* = 13.9, 7.4 Hz, 1H), 2.52–2.51 (m, 1H). ¹³C NMR (126 MHz, DMSO-*d*₆) δ ppm: 170.0, 163.2, 143.2, 138.2, 133.1, 129.2, 128.3, 126.6, 122.2, 111.0, 52.2, 43.6, 40.7. HRMS (ESI⁺) *m/z* calcd. for C₁₅H₁₆NO₃S₂ [M+H]⁺ 322.05661, found 322.05664.

2-Mercapto-3-phenyl-N-(pyridin-3-yl)propanamide (20).



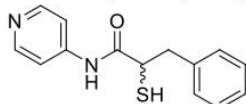
Compound **20** was prepared according to general procedure **E**, using compound **20b** (108 mg, 0.35 mmol) and solid NaOH (28 mg, 0.71 mmol) in MeOH (2 mL). Purification was done by preparative HPLC. The final product was obtained as white solid (24 mg, 26%). ¹H NMR (500 MHz, DMSO-*d*₆) δ ppm: 10.25 (s, 1H), 8.65 (d, *J* = 2.4 Hz, 1H), 8.25 (dd, *J* = 4.7, 1.5 Hz, 1H), 7.97 (dd, *J* = 8.3, 1.0 Hz, 1H), 7.33 (dd, *J* = 8.3, 4.7 Hz, 1H), 7.30–7.17 (m, 5H), 3.79–3.72 (m, 1H), 3.25 (dd, *J* = 13.7, 8.7 Hz, 1H), 3.17 (d, *J* = 5.2 Hz, 1H), 2.98–2.93 (m, 1H). ¹³C NMR (126 MHz, DMSO-*d*₆) δ ppm: 171.1, 144.5, 140.8, 138.5, 135.5, 129.0, 128.3, 126.6, 126.2, 123.7, 43.1, 41.1. HRMS (ESI⁻) *m/z* calcd. for C₁₄H₁₃N₂OS [M-H]⁻ 257.07540, found 257.07547.

2-Mercapto-3-phenyl-N-(pyridin-2-yl)propanamide (21).



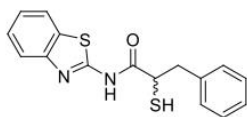
Compound **21** was prepared according to general procedure **E**, using compound **21b** (20 mg, 0.07 mmol), acetyl chloride (94 μ L, 1.33 mmol) in MeOH (3 mL). Purification was done by preparative HPLC. The final product was obtained as white solid (5 mg, 29%). ¹H NMR (500 MHz, acetone-*d*₆) δ ppm: 9.53 (s, 1H), 8.23 (dd, *J* = 4.8, 0.9 Hz, 1H), 8.18 (d, *J* = 8.3 Hz, 1H), 7.75 (td, *J* = 8.8, 1.8 Hz, 1H), 7.32–7.24 (m, 4H), 7.21–7.16 (m, 1H), 7.09–7.04 (m, 1H), 4.06–3.97 (m, 1H), 3.38 (dd, *J* = 13.7, 8.5 Hz, 1H), 3.04 (dd, *J* = 13.7, 6.4 Hz, 1H), 2.58 (d, *J* = 9.7 Hz, 1H). ¹³C NMR (126 MHz, acetone-*d*₆) δ ppm: 172.0, 152.9, 148.9, 139.6, 138.8, 130.1, 129.1, 127.4, 120.4, 114.3, 44.7, 42.7. HRMS (ESI⁺) *m/z* calcd. for C₁₄H₁₅N₂OS⁺ [M+H]⁺ 259.0900, found 259.0905.

2-Mercapto-3-phenyl-N-(pyridin-4-yl)propanamide (22).



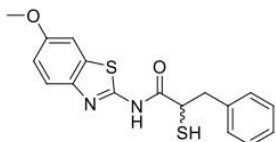
Compound **22** was prepared according to general procedure **E**, using compound **22b** (13 mg, 0.04 mmol) and acetyl chloride (49 μ L, 0.69 mmol) in MeOH (2 mL). Once the conversion was complete, the solvent was removed under reduced pressure to obtain the crude product. Purification was done by preparative HPLC. The final product was obtained as white solid (4 mg, 35%). ¹H NMR (500 MHz, acetone-*d*₆) δ ppm: 9.76 (s, 1H), 8.42 (m, 2H), 7.58 (d, *J* = 4.6 Hz, 2H), 7.32–7.16 (m, 5H), 3.85–3.76 (m, 1H), 3.35 (dd, *J* = 13.7, 8.7 Hz, 1H), 3.02 (dd, *J* = 13.7, 6.4 Hz, 1H), 2.66 (d, *J* = 7.4 Hz, 1H). ¹³C NMR (126 MHz, acetone-*d*₆) δ ppm: 172.5, 151.1, 146.8, 139.5, 130.1, 129.2, 127.5, 114.2, 45.0, 42.5. HRMS (ESI⁺) *m/z* calcd. for C₁₄H₁₅N₂OS⁺ [M+H]⁺ 259.0900, found 259.0896.

N-(Benzo[d]thiazol-2-yl)-2-mercapto-3-phenylpropanamide (23).



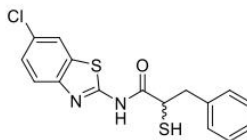
Compound **23** was prepared according to general procedure **E**, using compound **23b** (128 mg, 0.36 mmol) and 2 M NaOH aq. solution (359 μ L, 0.72 mmol) in MeOH (3 mL). Purification was done by flash chromatography (Hex/EtOAc, 7:3). The final product was obtained as white solid (30 mg, 28%). ^1H NMR (500 MHz, CDCl_3) δ ppm: 7.85 (d, $J = 7.8$ Hz, 1H), 7.76 (d, $J = 8.1$, 1H), 7.49–7.44 (m, 1H), 7.39–7.36 (m, 1H), 7.29–7.27 (m, 1H), 7.25–7.15 (m, 4H), 3.87–3.80 (m, 1H), 3.40 (dd, $J = 14.0, 7.0$ Hz, 1H), 3.24 (dd, $J = 14.0, 6.8$ Hz, 1H), 2.26–2.17 (m, 1H). ^{13}C NMR (126 MHz, CDCl_3) δ ppm: 170.7, 159.0, 145.5, 136.7, 131.0, 129.4, 128.9, 127.5, 127.2, 125.0, 121.9, 120.2, 44.7, 41.1. HRMS (ESI⁺) m/z calcd. for $\text{C}_{16}\text{H}_{15}\text{N}_2\text{OS}_2$ $[\text{M}+\text{H}]^+$ 315.06203, found 315.06178.

2-Mercapto-*N*-(6-methoxybenzo[d]thiazol-2-yl)-3-phenylpropanamide (24).



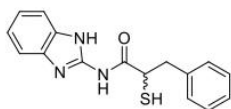
Compound **24** was prepared according to general procedure **E**, using compound **24b** (225 mg, 0.58 mmol) and 2 M NaOH aq. solution (582 μ L, 1.64 mmol) in MeOH (3 mL). Purification was done by column chromatography (Hex/EtOAc, 3:1). The final product was obtained as white solid (104 mg, 52%). ^1H NMR (500 MHz, $\text{DMSO-}d_6$) δ ppm: 12.33 (s, 1H), 7.62 (d, $J = 8.8$ Hz, 1H), 7.57 (d, $J = 2.6$ Hz, 1H), 7.31–7.13 (m, 5H), 7.02 (dd, $J = 8.8, 2.6$ Hz, 1H), 3.91 (dd, $J = 8.5, 6.8$ Hz, 1H), 3.80 (s, 3H), 3.37 (br s, 1H), 3.28 (dd, $J = 13.8, 8.5$ Hz, 1H), 2.98 (dd, $J = 13.8, 6.7$ Hz, 1H). ^{13}C NMR (126 MHz, $\text{DMSO-}d_6$) δ ppm: 171.4, 156.2, 155.7, 142.6, 138.3, 132.8, 129.1, 128.3, 126.7, 121.3, 115.0, 104.7, 55.7, 41.9, 40.5. HRMS (ESI⁻) m/z calcd. for $\text{C}_{17}\text{H}_{15}\text{N}_2\text{O}_2\text{S}_2$ $[\text{M}-\text{H}]^-$ 343.05804, found 343.05835.

***N*-(6-Chlorobenzo[d]thiazol-2-yl)-2-mercapto-3-phenylpropanamide (25).**



Compound **25** was prepared according to general procedure **E**, using compound **25b** (105 mg, 0.27 mmol) and 2 M NaOH aq. solution (270 μ L, 0.54 mmol) in MeOH (2 mL). Purification was done by preparative HPLC. The final product was obtained as white solid (78 mg, 84%). ^1H NMR (500 MHz, $\text{DMSO-}d_6$) δ ppm: 12.54 (br s, 1H), 8.13 (d, $J = 2.2$ Hz, 1H), 7.72 (d, $J = 8.6$ Hz, 1H), 7.45 (dd, $J = 8.6, 2.2$ Hz, 1H), 7.34–7.13 (m, 5H), 3.95–3.91 (m, 1H), 3.30–3.25 (m, 1H), 3.00 (dd, $J = 13.8, 6.9$ Hz, 1H), 2.52–2.51 (m, 1H). ^{13}C NMR (126 MHz, $\text{DMSO-}d_6$) δ ppm: 171.9, 158.6, 147.4, 138.2, 133.2, 129.03, 128.3, 127.7, 126.7, 126.6, 121.8, 121.5, 41.9, 40.3. HRMS (ESI⁻) m/z calcd. for $\text{C}_{16}\text{H}_{12}\text{ClN}_2\text{OS}_2$ $[\text{M}-\text{H}]^-$ 349.02305, found 349.02304.

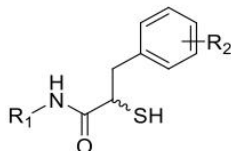
***N*-(1*H*-Benzo[d]imidazol-2-yl)-2-mercapto-3-phenylpropanamide (26).**



Compound **26** was prepared according to general procedure **E**, using compound **26b** (120 mg, 0.35 mmol) and solid NaOH (27 mg, 0.70 mmol) in MeOH (2 mL). Purification was done by preparative HPLC. The final product was obtained as white solid (85 mg, 80%). ^1H NMR (500 MHz, $\text{DMSO-}d_6$) δ ppm: 12.06 (s, 1H), 11.64 (s, 1H), 7.42 (s, 2H), 7.33–7.14 (m, 5H), 7.13–7.04 (m, 2H), 3.93 (d, $J = 5.9$ Hz, 1H), 3.31–3.26 (m, 1H), 3.26 (br s, 1H), 2.99 (dd, $J = 13.7, 6.4$ Hz, 1H). ^{13}C NMR (126 MHz, $\text{DMSO-}d_6$). HRMS (ESI⁻) m/z calcd. for $\text{C}_{16}\text{H}_{16}\text{N}_3\text{OS}$ $[\text{M}-\text{H}]^-$ 298.10085, found 298.10069.

Tables and Figures

Table S1. K_i values for six selected compounds against ColH-PD and % inhibition of ColH-PD at 1 μ M concentration of six selected compounds. K_i values and residual activities are determined as described previously.³



Compound	R ₁	R ₂	K_i (μ M)
3	Ph	4-Me	0.05 \pm 0.01
5	Ph	H	0.4 \pm 0.04
12	4-OMe-Ph	H	0.04 \pm 0.01
13	4-OH-Ph	H	0.1 \pm 0.02
23	benzothiazolyl	H	0.1 \pm 0.01
24	6-methoxybenzothiazolyl	H	28 \pm 1
Compound	R ₁	R ₂	% inh. of ColH-PD @1 μ M
11	4-NO ₂ -Ph	H	88 \pm 2
14	Ph	4-Me-Ph	69 \pm 3
15	Ph	4-OH	63 \pm 2
16	Ph	3-NO ₂ -4-OH	74 \pm 5
18	thiazolyl	H	34 \pm 3
24	6-chlorobenzothiazolyl	H	73 \pm 2

Table S2. Zebrafish embryotoxicity results for compounds **12** and **23**.

Compound	Concentration (μ M)	2 dpf	3 dpf	4 dpf	5 dpf	Survival rate %
12	100	all dead	-	-	-	0
	50	imp. dev., turbid body	all dead	-	-	0
	30	imp. dev.	all dead	-	-	0
	2	OK	OK	OK	OK	100
23	100	imp. dev.	5 imp. dev.	5 imp. dev.	5 imp. dev.	0
	50	imp. dev.	5 imp. dev.	5 imp. dev.	5 imp. dev.	50
	30	OK	OK, 3 imp. dev.	OK, 3 imp. dev.	OK, 3 imp. dev.	70
	2	OK	OK	OK	OK	100
Danieau's ctrl	-	OK	OK, 1 malf., 1 dead	OK	OK	80
DMSO ctrl	1%	OK	OK, 1 malf.	OK	OK	100

malf. = body curvature

impaired dev. = impaired development, pericardial edema

No toxicity signs were observed for compound **12** at a concentration of 2 μ M. However, all concentrations above (30 μ M, 50 μ M, and 100 μ M) have led to a toxicity of 100%.

30% of larvae showed toxicity signs, such as impaired body development and pericardial edema, when incubated with compound **23** at a concentration of 30 μ M. The two highest concentrations (50 μ M and 100 μ M) were lethal for all larvae resulting in a survival rate of 0%.

A comparable ratio of malformation was also found in the control groups (with only Danieau's medium or 1% DMSO). Therefore, observed body malformation in larvae incubated in compound can be considered as not related to compound treatment.

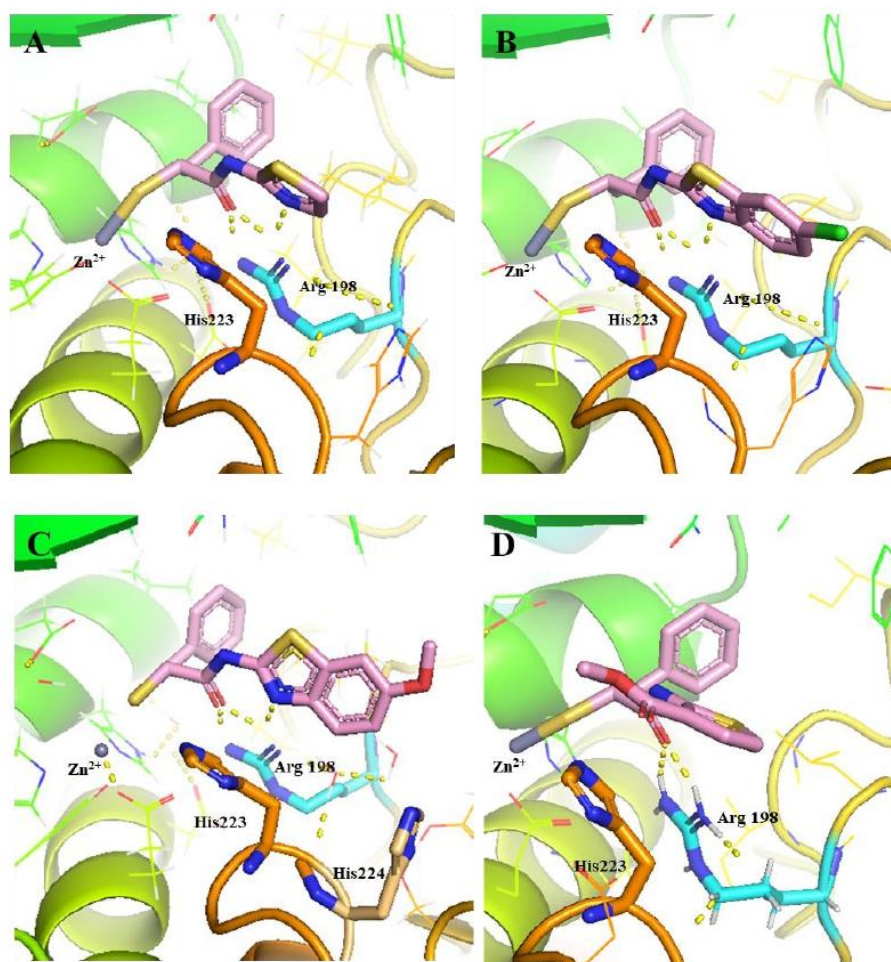


Figure S1. Docking poses for **A)** Thiazole, **B)** 6-chlorobenzothiazolyl, **C)** 6-methoxybenzothiazolyl and **D)** Methyl thiophenyl 3-carboxylate replacement in the LasB ligand binding pocket. The interactions in the binding pocket of LasB are predicted by SeeSAR V.11.1 and visualized using PyMOL V.2.5 softwares..¹⁰ The dashed lines represent H-bonds of less than 2.15 Å .

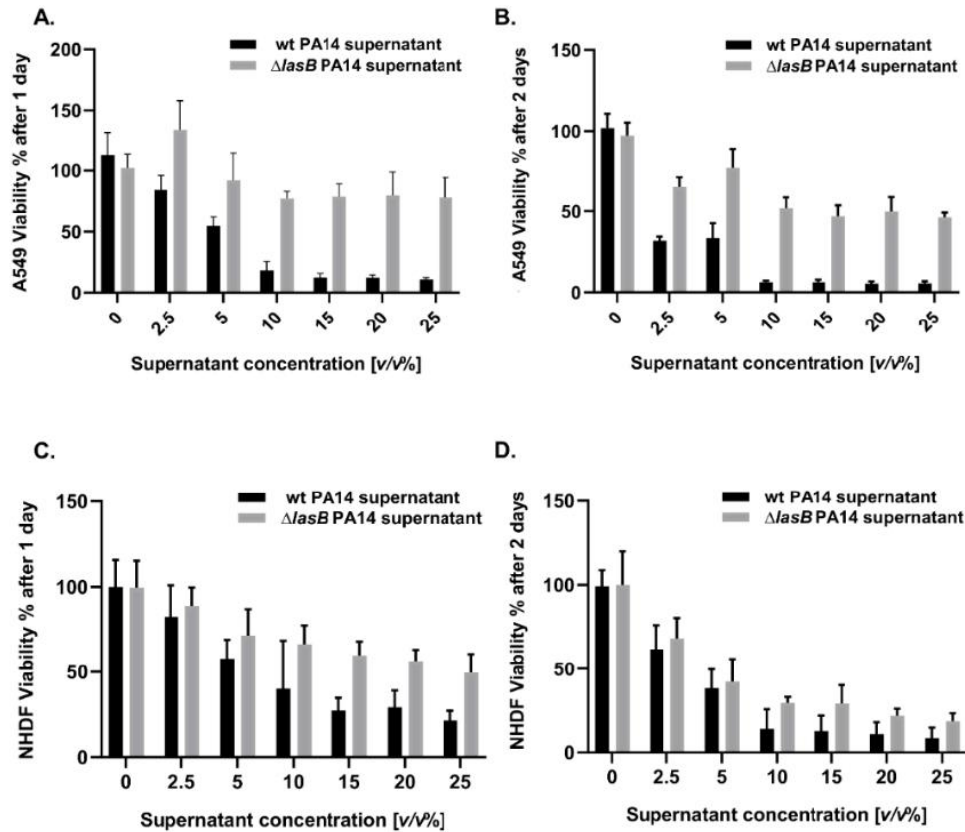


Figure S2. Illustration of the dose-dependent cytotoxic effect of wt PA14 and $\Delta lasB$ PA14 supernatant on normal human dermal fibroblast (NHDF) and adenocarcinomic human alveolar basal epithelial (A549) cells. **A)** wt PA14 supernatant reduces the viability of A549 cells after 24 h incubation compared with $\Delta lasB$ PA14 supernatant. **B)** wt PA14 supernatant effect on the cell viability after 48 h incubation with A549 cells, the viability is further minimized. **C)** wt PA14 supernatant effect on NHDF cell after 24 h incubation, its cytotoxic effect on NHDF cells is less than on A549 cells **D)** The cytotoxic effect of wt supernatant after 48 h incubation with NHDF cells is improved. This confirms that LasB is one of the major virulence factors present in the supernatant. The low cytotoxic effect observed with the $\Delta lasB$ PA14 supernatant might be due to effect of other extracellular toxins than LasB such as phospholipase, LasA, phytotoxic factors and exotoxins.¹⁹ Each graph is a representation of three independent experiments, mean \pm SD. The percentage shows the amount of supernatant in the whole volume of Dulbecco's Modified Eagle Medium (DMEM) and cells. PA14: wild-type *Pseudomonas aeruginosa*, Δ PA14: LasB knockout *P. aeruginosa*.

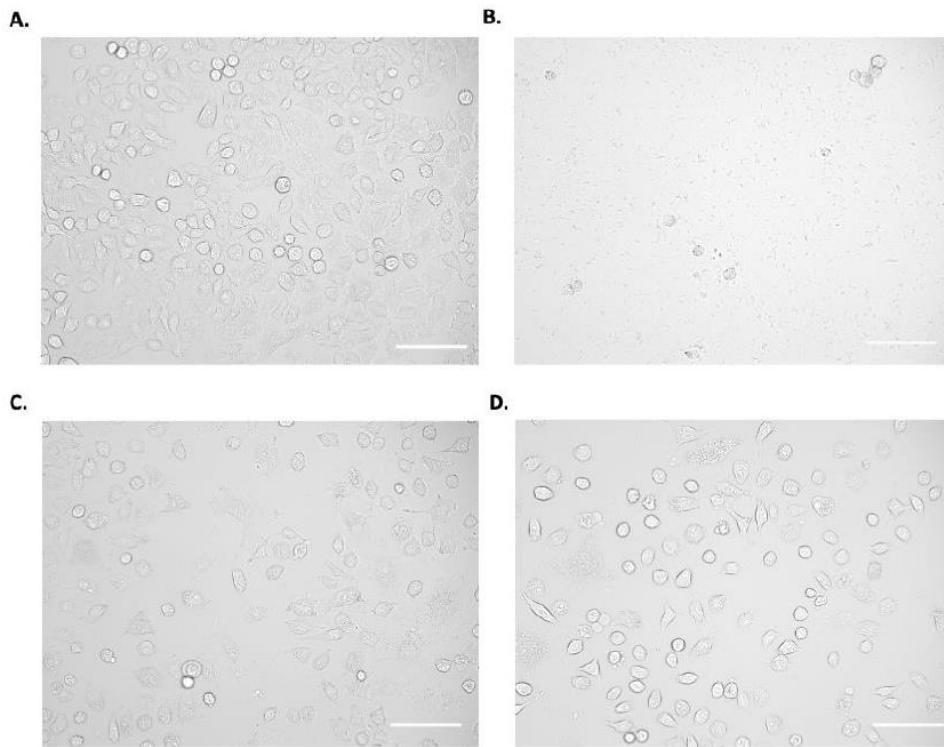


Figure S3. Visualization of differently treated adenocarcinomic human alveolar basal epithelial (A549) cells. **A)** Untreated cells; **B)** Cells treated with 15% (v/v) wt PA14 supernatant, cell density significantly reduced compared with untreated cells; **C)** A549 cells treated with 15% (v/v) $\Delta lasB$ PA14 supernatant; cell density is still high, and the morphology of the cells did not change; **D)** Cells challenged with wt PA14 supernatant and treated with Pam; their cell integrity and morphology were maintained. Images were generated with 20X objective by Leica Las X and modified with the software Fiji ImageJ (Scale bar: 100 μm). wt PA14: wild-type *P. aeruginosa*, $\Delta lasB$ PA14: LasB knockout *P. aeruginosa*. Pam: phosphoramidon.

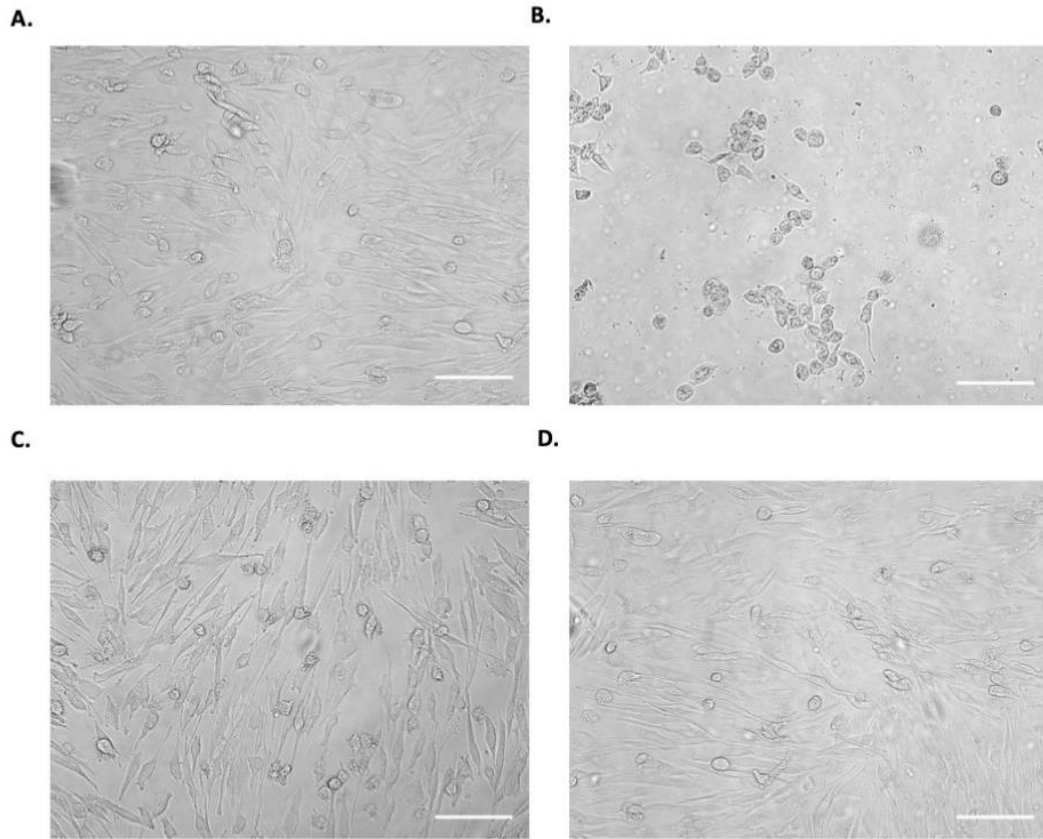


Figure S4. Visualization of differently treated normal human dermal fibroblast (NHDF) cells. **A)** Untreated cells; **B)** Cells treated with 15% (v/v) wt PA14 supernatant, cell density significantly reduced compared with untreated cells; **C)** Cells treated with 15% (v/v) $\Delta lasB$ PA14 supernatant; the cell density is still high, and the morphology of the cells did not change; **D)** Cells challenged with wt PA14 supernatant and treated with Pam; their cell integrity and morphology were maintained. Images were generated with 20X objective by Leica Las X and modified with the software Fiji ImageJ (Scale bar: 100 μm). wt PA14: wild-type *P. aeruginosa*, $\Delta lasB$ PA14: LasB knockout *P. aeruginosa*, Pam: phosphoramidon.

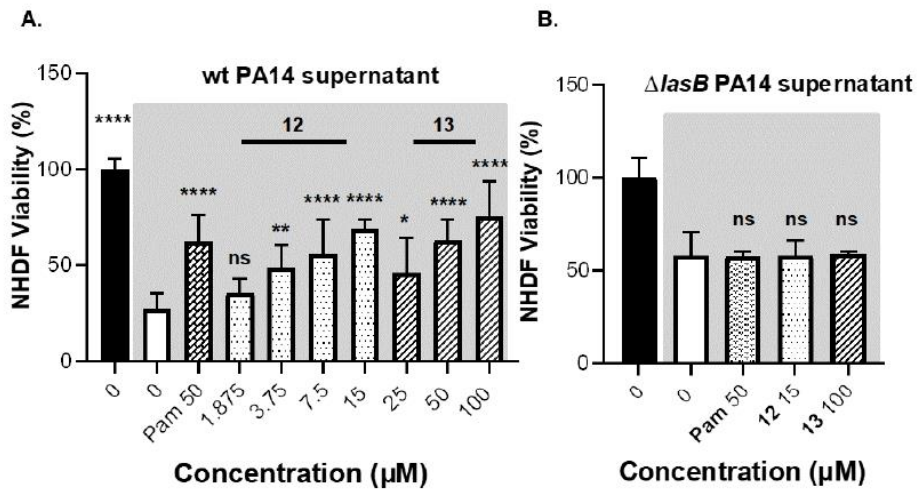


Figure S5. Viability of normal human dermal fibroblast (NHDF) cells treated with **12** and **13** and 15% (v/v) wt PA14 or $\Delta lasB$ PA14 supernatant. **A)** Concentrations-dependent effects of compounds on the viability of NHDF cells treated with wt PA14 supernatant; **(c) B)** Viability of NHDF cells treated with $\Delta lasB$ PA14 supernatant and the highest tested concentration of compound that was used with PA14 supernatant. Each graph is a representation of three independent experiments \pm SD. One-way ANOVA was performed for each experiment following Dunnett's multiple comparisons test and moreover, the mean of each column was compared with the mean of the negative control (ns: not significant, *: $p \leq 0.05$, **: $p \leq 0.01$, ****: $p \leq 0.0001$). wt PA14: wild-type *Pseudomonas aeruginosa*, $\Delta lasB$ PA14: LasB knockout *P. aeruginosa*, Pam: phosphoramidon.

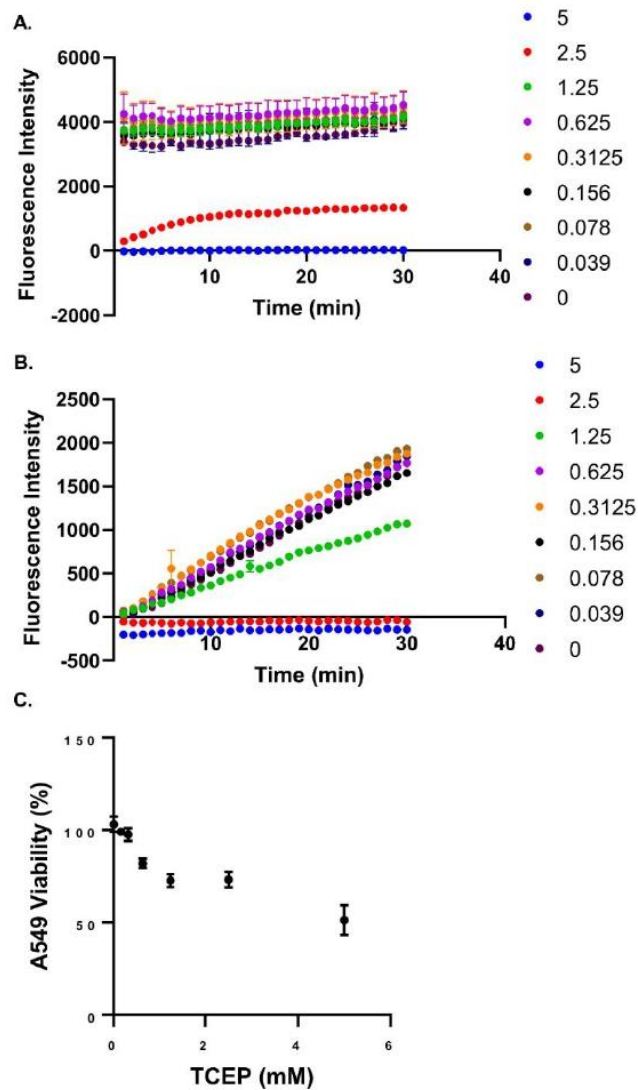


Figure S6. Effect of a reducing agent on LasB activity. **A)** Activity of LasB presented in 10% (v/v) wt PA14 supernatant incubated with different concentrations (mM) of TCEP. Similar to pure LasB high concentration of TCEP (*i.e.*, 5 and 2.5 mM) inhibited the activity of LasB in the supernatant. **B)** Effect of various concentrations (mM) of TCEP on 0.3 nM pure LasB. The activity was completely lost with 5 mM and 2.5 mM while at 0.6 mM and lower concentrations no inhibition was detected, similar to no TCEP conditions. **C)** Effect of TCEP concentrations on viability of A549 cells. 0.3 mM TCEP showed no effect on cell viability while higher concentrations showed a reduction in the cell viability, which was evaluated with MTT assay. Each curve represents a mean \pm SD of two independent experiments. wt PA14: wild-type *Pseudomonas aeruginosa*, TCEP: Tris(2-carboxyethyl)phosphine hydrochloride.

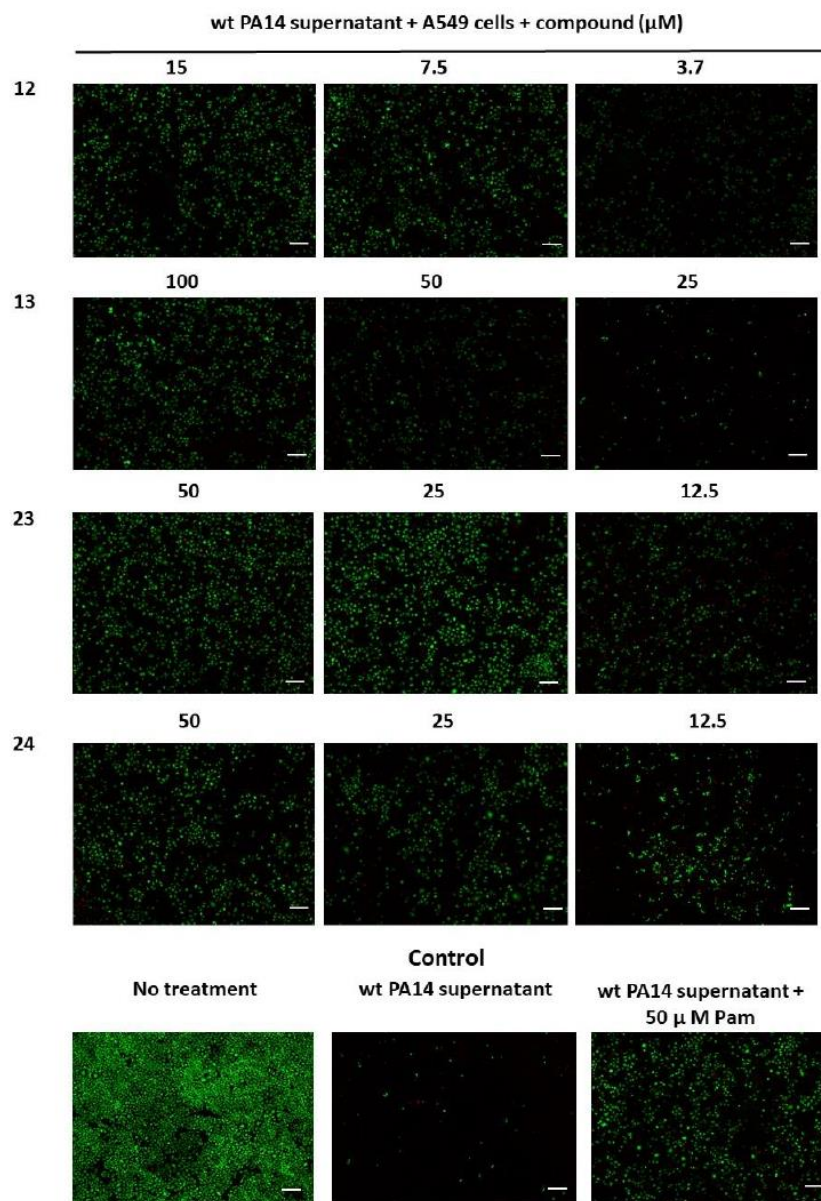


Figure S7. Visualization of the effects of compounds **12**, **13**, **23** and **24** on wt PA14 supernatant treated adenocarcinomic human alveolar basal epithelial (A549) cells. Live/dead staining was carried out with fluoresceine diacetate and propidium iodide. Living cells are shown in green and dead cells in red. Red signal in some cases was lost because the detached cells were washed away after the rinsing step with PBS (scale bar: 200 μm). wt PA14: wild-type *Pseudomonas aeruginosa*, Pam: phosphoramidon.

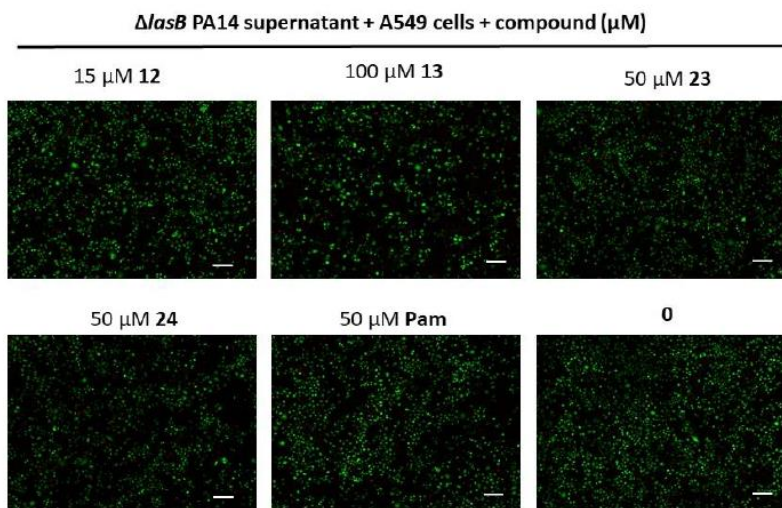


Figure S8. Visualization of effect of compounds **12**, **13**, **23** and **24** on $\Delta lasB$ PA14 supernatant applied adenocarcinomic human alveolar basal epithelial (A549) cells. Live/dead staining was carried out with fluoresceine diacetate and propidium iodine. Live cells are showed in green and dead cells in red. Scale bar: 200 μm . Red signal in some cases was lost because the detached cells were washed away after the rinsing step with PBS. $\Delta lasB$ PA14: LasB knockout *Pseudomonas aeruginosa*, Pam: phosphoramidon.

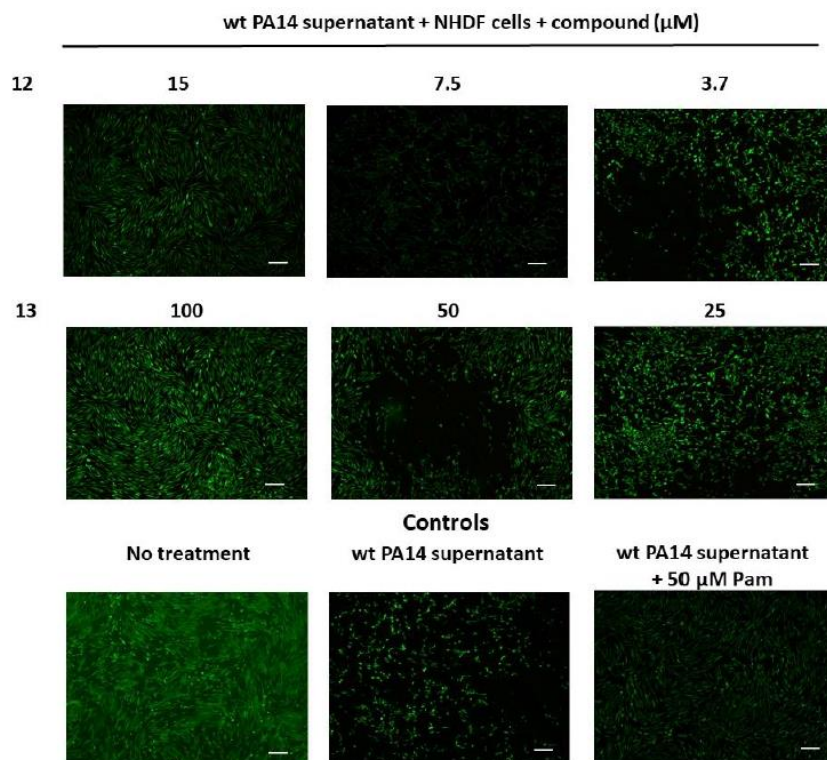


Figure S9. Visualization of the effects of compounds **12** and **13** on wt PA14 supernatant treated human dermal fibroblasts (NHDF) cells. Live/dead staining was carried out with fluoresceine diacetate and propidium iodine. Living cells are shown in green and dead cells in red (Scale bar: 200 μm). Red signal in some cases was lost because the detached cells were washed away after the rinsing step with PBS. wt PA14: wild-type *Pseudomonas aeruginosa*, Pam: phosphoramidon.

$\Delta lasB$ PA14 supernatant + NHDF cells + Compound (μM)

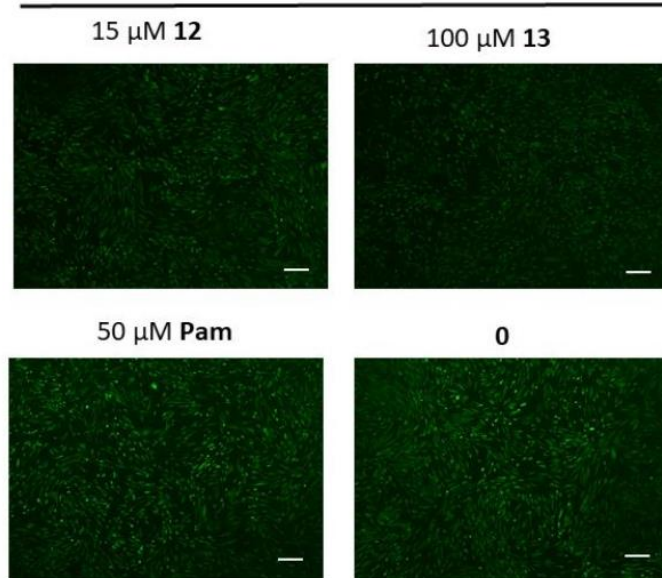


Figure S10. Visualization of effect of compounds **12** and **13** on $\Delta lasB$ PA14 supernatant applied human dermal fibroblasts (NHDF) cells. Live/dead staining was carried out with fluoresceine diacetate and propidium iodine. Live cells are shown in green and dead cells in red. Scale bar: 200 μm . Red signal in some cases was lost because the detached cells were washed away after the rinsing step with PBS. $\Delta lasB$ PA14: LasB knockout *Pseudomonas aeruginosa*, Pam: phosphoramidon.

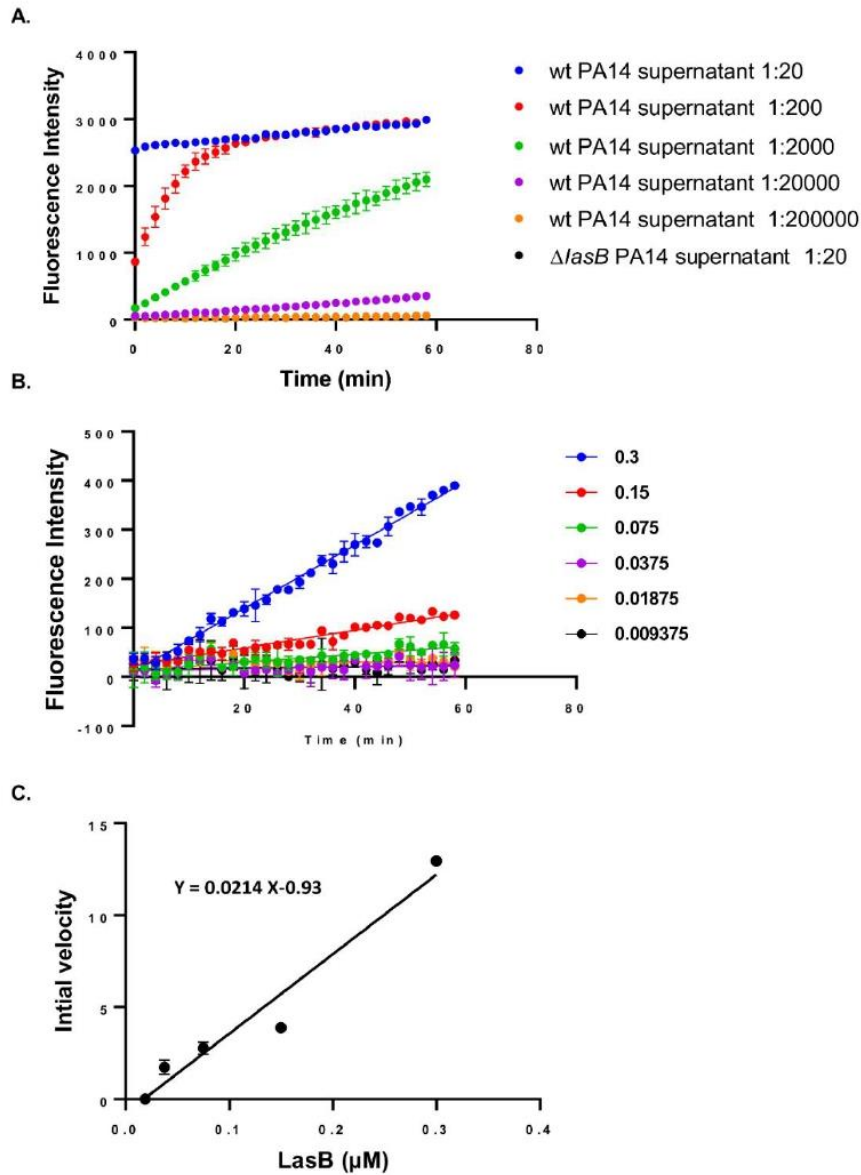


Figure S11. Supernatant evaluation with LasB activity assay. **A)** The activity of serially diluted wt PA14 and $\Delta lasB$ PA14 supernatants **B)** The activity of various concentrations of pure LasB. **C)** The calibration curve that was created from the initial velocity that we calculated from graph B. The calibration curve estimates that 100% supernatant has 0.88 μM of LasB. wt PA14: wild-type *Pseudomonas aeruginosa*, $\Delta lasB$ PA14: LasB knockout *Pseudomonas aeruginosa*.

References

- (1) Kany, A. M.; Sikandar, A.; Hauptenthal, J.; Yahiaoui, S.; Maurer, C. K.; Proschak, E.; Köhnke, J.; Hartmann, R. W. Binding Mode Characterization and Early in Vivo Evaluation of Fragment-Like Thiols as Inhibitors of the Virulence Factor LasB from *Pseudomonas Aeruginosa*. *ACS Infect. Dis.* **2018**, *4* (6), 988–997. <https://doi.org/10.1021/acsinfecdis.8b00010>.
- (2) Eckhard, U.; Schönauer, E.; Brandstetter, H. Structural Basis for Activity Regulation and Substrate Preference of Clostridial Collagenases G, H, and T. *J. Biol. Chem.* **2013**, *288* (28), 20184–20194. <https://doi.org/10.1074/jbc.M112.448548>.
- (3) Schönauer, E.; Kany, A. M.; Hauptenthal, J.; Hüsecken, K.; Hoppe, I. J.; Voos, K.; Yahiaoui, S.; Elsässer, B.; Ducho, C.; Brandstetter, H.; Hartmann, R. W. Discovery of a Potent Inhibitor Class with High Selectivity toward Clostridial Collagenases. *J. Am. Chem. Soc.* **2017**, *139* (36), 12696–12703. <https://doi.org/10.1021/jacs.7b06935>.
- (4) Murphy, D. J. Determination of Accurate KI Values for Tight-Binding Enzyme Inhibitors: An in Silico Study of Experimental Error and Assay Design. *Anal. Biochem.* **2004**, *327* (1), 61–67. <https://doi.org/10.1016/j.ab.2003.12.018>.
- (5) Morrison, J. F. Kinetics of the Reversible Inhibition of Enzyme-Catalysed Reactions by Tight-Binding Inhibitors. *Biochim. Biophys. Acta - Enzymol.* **1969**, *185* (2), 269–286. [https://doi.org/10.1016/0005-2744\(69\)90420-3](https://doi.org/10.1016/0005-2744(69)90420-3).
- (6) Kuzmič, P.; Elrod, K. C.; Cregar, L. M.; Sideris, S.; Rai, R.; Janc, J. W. High-Throughput Screening of Enzyme Inhibitors: Simultaneous Determination of Tight-Binding Inhibition Constants and Enzyme Concentration. *Anal. Biochem.* **2000**, *286* (1), 45–50. <https://doi.org/10.1006/abio.2000.4685>.
- (7) Kany, A. M.; Sikandar, A.; Yahiaoui, S.; Hauptenthal, J.; Walter, I.; Empting, M.; Köhnke, J.; Hartmann, R. W. Tackling *Pseudomonas Aeruginosa* Virulence by a Hydroxamic Acid-Based LasB Inhibitor. *ACS Chem. Biol.* **2018**, *13* (9), 2449–2455. <https://doi.org/10.1021/acscchembio.8b00257>.
- (8) Hauptenthal, J.; Baehr, C.; Zeuzem, S.; Piiper, A. RNase A-like Enzymes in Serum Inhibit the Anti-Neoplastic Activity of SiRNA Targeting Polo-like Kinase 1. *Int. J. Cancer* **2007**, *121* (1), 206–210. <https://doi.org/10.1002/ijc.22665>.
- (9) SeeSAR v.11.1, BioSolveIT GmbH, Sankt Augustin, G. 2021. Available from: <Http://Www.Biosolveit.de/SeeSAR>.
- (10) Schrödinger, L., & DeLano, W. (2020). P. R. from <http://www.pymol.org/pymo>. The PyMOL Molecular Graphics System, Version 2.0 Schrödinger, LLC. 2021.
- (11) Chakraborty, C.; Sharma, A. R.; Sharma, G.; Lee, S. S. Zebrafish: A Complete Animal Model to Enumerate the Nanoparticle Toxicity. *J. Nanobiotechnology* **2016**, *14* (1), 1–13. <https://doi.org/10.1186/s12951-016-0217-6>.
- (12) Casilag, F.; Lorenz, A.; Krueger, J.; Klawonn, F.; Weiss, S.; Häussler, S. The LasB Elastase of *Pseudomonas Aeruginosa* Acts in Concert with Alkaline Protease AprA To Prevent Flagellin-Mediated Immune Recognition. *Infect. Immun.* **2016**, *84* (1), 162–171. <https://doi.org/10.1128/IAI.00939-15>.

- (13) Tanasova, M.; Yang, Q.; Olmsted, C. C.; Vasileiou, C.; Li, X.; Anyika, M.; Borhan, B. An Unusual Conformation of α -Haloamides Due to Cooperative Binding with Zincated Porphyrins. *European J. Org. Chem.* **2009**, No. 25, 4242–4253. <https://doi.org/10.1002/ejoc.200900089>.
- (14) Vijayakumar, V. N.; Jayaprakasam, R. Nanoliquid Crystals: A Study of Permeability and Optical Measurements in Nematic Phase. *Macromol. Symp.* **2016**, 361 (1), 112–116. <https://doi.org/10.1002/masy.201400260>.
- (15) Zhuze, A. L.; Jošt, K.; Kasafirek, E.; Rudinger, J. Amino Acids and Peptides. XLV. Analogues of Oxytocin with O-Ethyltyrosine, p-Methylphenylalanine, and p-Ethylphenylalanine Replacing Tyrosine. *Collect. Czechoslov. Chem. Commun.* **1964**, 29 (11), 2648–2662. <https://doi.org/10.1135/cccc19642648>.
- (16) Schmidt, R. R. Synthesis and Herbicidal Activity of d (+) and l (–) Methyl-2-Chloro-3-(4-Chlorophenyl)-Propionate. **1976**, 1, 7–9.
- (17) Hydrochloride, N.; Lee, W. W.; Tong, G. L.; Martinez, A. P.; Weinstein, B.; Schelstraete, M. G. M.; Baker, B. R.; Goodman, L.; Baker, S. Synthesis of N, N-Bis (2-Chloroethyl) -DL-Phenylalanine Hydrochloride. **1963**, 275 (1953), 1954–1957.
- (18) Vora, H. U.; Rovis, T. Nucleophilic Carbene and HOAt Relay Catalysis in an Amide Bond Coupling: An Orthogonal Peptide Bond Forming Reaction. *J. Am. Chem. Soc.* **2007**, 129 (45), 13796–13797. <https://doi.org/10.1021/ja0764052>.
- (19) Liu, P. V. Extracellular Toxins of *Pseudomonas Aeruginosa*. *J. Infect. Dis.* **1974**, 130 (November), S94–S99. <https://doi.org/10.1093/infdis/130.Supplement.S94>.

2.3 Fragment-Based Design and Synthesis of Inhibitors of ColH

2.3.1 Introduction

Growing antibiotic resistance among notorious bacteria represents a significant risk to public health.¹ Development of antibiotics with high efficacy, low susceptibility and novel modes of action is urgently needed for the treatment of the persistent infections caused by these pathogens.^{2,3}

An outside-the-box strategy to overcome resistance is through the inhibition of extracellular virulence factors secreted by pathogenic bacteria.⁴ By designing pathoblockers that can inhibit these targets, the aim is not to harm the bacteria but to disarm them by blocking the colonization of pathogens. Adjunctive treatments in combination with low-dose antibiotics can then eliminate the bacteria and enable a cellular immune response to be developed. The main advantage of this method is to reduce the selection pressure and to keep the commensal bacteria unaffected.⁵

Clostridia are Gram-positive, obligately anaerobic bacteria present in soil, wastewater, and human commensal flora.^{6,7} Some cause severe diseases with high mortality rates such as gas gangrene (by *C. perfringens* and *C. histolyticum*), tetanus (by *C. tetani*) and botulism (by *C. botulinum*).⁷ An increasing amount of resistance among many strains of clostridia are reported, representing a challenge for the treatment of these diseases.⁸ *Clostridium histolyticum* uses clostridial collagenases to invade the host cell and acquire nutrients to evade the immune defense.⁹ These enzymes efficiently degrade collagen tissue during the infection state.¹⁰ Given their vital and diverse roles in the diseased state and their extracellular position, bacterial collagenases are regarded as prominent targets for inhibition. As a result, much focus has been dedicated to the design and synthesis of inhibitors of collagenases, in particular collagenase H (ColH) from *C. histolyticum*.

Along with the identification of natural coumarin derivatives isolated from *Viola yedonesis* as inhibitors of ColH (compound **1**, Figure 1)¹¹, small non-peptidic structures like compound **2** containing a free thiol¹², carboxylate¹³ or hydroxamate¹⁴ motifs with activities ranging from low micromolar to nanomolar were also reported as potent inhibitors of ColH.

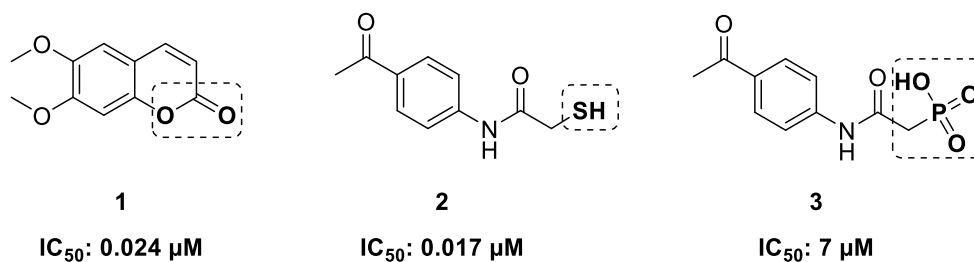


Figure 1. Structures of recently reported ColH inhibitors **1**¹¹, **2**¹⁵, and **3**¹⁶. Zinc-binding groups are shown in circles.

The common major drawback for ColH inhibitors is the selectivity issues with respect to mammalian matrix metalloenzymes that show a great structural homology to these bacterial proteases. Most recently, exploration of other zinc-binding motifs such as phosphonates yielded compound **3** with low micromolar activity addressing this problem have been identified.¹⁶

Fragment-based drug design (FBDD) is a powerful method to discover potent small molecule inhibitors of critical drug targets.¹⁷⁻¹⁹ It also opens up the possibility to access new chemical classes and new binding modes as starting points. Low-binding affinity fragments can be identified from compound libraries using different biophysical methods and can be further optimized to drug-like structures.²⁰ The initial applications of this method were mostly performed on kinases, playing vital roles in human metabolism.²¹ Vemurafenib, targeting protein kinase B-RAF, was the first example demonstrating the potential of the fragment-based approach.²² Encouraged by the identification of several drug candidates over the years using this method, the target range has been broadened to metalloproteins and to ion channels.

In this work, we report a successful application of fragment-based approach on metalloprotease ColH yielding a small halogen-containing fragment with a low-micromolar IC₅₀ value. Rationalization of the binding of this small inhibitor to the target protein revealed a novel binding mode as the fragment did not coordinate to the zinc cation. Furthermore, the fragment demonstrated a promising selectivity over selected human off-targets and a low cytotoxicity. After exploring the different growing directions and analyzing 35 derivatives differing in size and substituents, we identified a fragment with two-fold increase in potency.

2.3.2 Results and Discussion

Screening of a Halogen-enriched fragment Library using Differential Scanning Calorimetry Method. Our fragment-based design strategy started with the screening of a halogen-enriched fragment library (HeFLib) containing 148 fragments. Halogen bonds offer an alternative to classical polar interactions and have gained a lot of attention recently due to their presence in many protein–ligand interactions.²³ Therefore, our choice of starting library offered a diverse set of potential interactions as the fragments contained various halogen atoms. We used differential scanning calorimetry (DSC) to screen the fragment library.^{24,25} This method measures the degree of denaturation of a protein in the presence of a fluorescence dye such as Sypro Orange.¹⁹ As the stability of most proteins decreases when the melting temperature (T_m) is increased due to unfolding, a compound binding to a protein is expected to increase the T_m and can thus be considered as a positive hit.

All fragments were screened against the target protein with a single final concentration of 1 mM each fragment and 5 μ M of the protein. We considered a 2 °C increase in the T_m of ColH-PD to be significant and selected 21 fragments showing an increase in $T_m \geq 2$ °C for a concentration-dependent DSC screening.

Among the selected fragments, six demonstrated a concentration-dependent affinity for the protein at three final concentration points 5 mM, 1 mM, and 0.2 mM (Table S1). The same final concentrations of protein and fluorescent dye were used as in single-point screening.

Next, we measured the inhibition of the protein at single point concentration in the presence of these six fragments in a FRET-based inhibition assay (Table S2) to confirm the binding of these compounds. Only compound **4** (Figure 2) showed an inhibition of the target. Encouraged by these results, we then determined its IC_{50} value which revealed a micromolar inhibition of ColH-PD, with an IC_{50} value of 117 ± 5 μ M. The observed potency is quite significant for such a low-molecular weight molecule as reflected by a calculated ligand efficiency (LE) of 0.46.

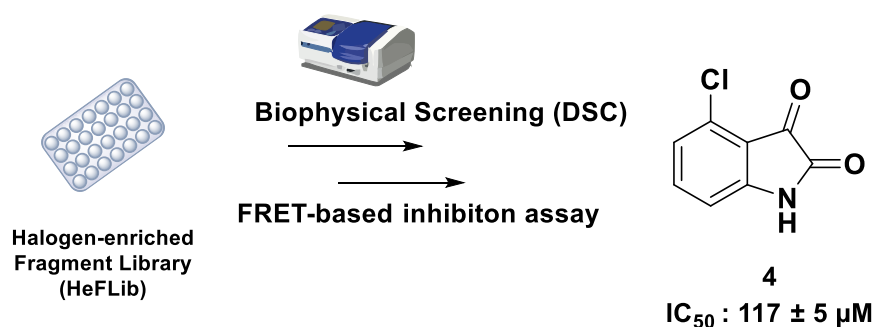


Figure 2. Schematic representation of screening of a fragment library using different biophysical methods and identification of fragment **4** as an inhibitor of ColH-PD. Calculated Ligand Efficiency: 0.46.

Selectivity against MMPs and cytotoxicity against human cell-lines. Since selectivity for ColH over human metalloproteases is a notorious issue in designing potent inhibitors, an early investigation of these properties can serve as a good basis for further development. As a result, in the next step we explored the selectivity of the identified fragment **4** against several human off-targets.

We selected six matrix metalloproteases representing different sub-classes and evaluated the fragment at 500 μM and 100 μM against these targets (Table 1). Our fragment did not show any inhibition of the selected MMPs.

Table 1. Selectivity of fragment **4** against six selected MMPs.

	% Inhibition					
Conc (μM)	MMP-1	MMP-2	MMP-3	MMP-7	MMP-8	MMP-14
500	9.6	10.2	10.7	9.8	4.8	12.9
100	5.6	5.4	4.1	14.3	-1.3	-1.3

We also checked its cytotoxicity against two human cell lines HEPG2 ($\text{LD}_{50} \leq 100 \mu\text{M}$) and HEK 293 ($\text{LD}_{50} \leq 100 \mu\text{M}$). These results served as a good basis for further optimization.

Co-crystallization of the fragment with ColH-PD. To elucidate the binding mode of the fragment **4** and to get a deeper understanding of the potential interactions in the surrounding unoccupied space, we co-crystallized it with ColH-PD.

The interacting amino acid residues in the binding pocket are shown in Figure 3. π - π stacking of the five-membered and six-membered rings of the fragment with surrounding Trp471 as well as π -lone pair and π -CH interactions of the five-membered ring and chlorine atom with Trp471 and surrounding water molecules are well-documented. Carbonyl groups in the fragment also contribute to H-bonding with surrounding Glu430 residue.

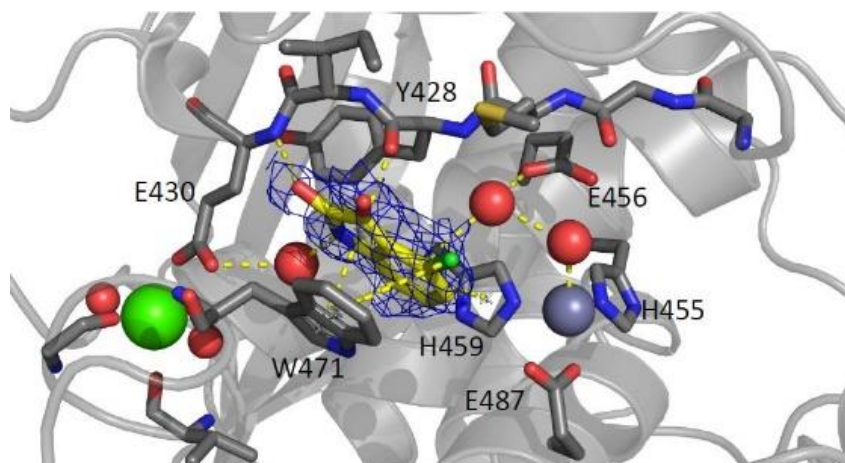


Figure 3. Peptidase domain of ColH in complex with fragment **4**. Close-up view of the active site in ball-and-stick representation. The inhibitor (yellow) is shown in sticks with the maximum likelihood weighted $2F_o-F_c$ electron density map contoured at 1σ . The catalytic zinc ion (dark gray), calcium ion (green), and water molecule (red) are shown as spheres. The edge strain (shown in dark gray sticks) is indicated on top.

The crystal structure also revealed that the fragment was not complexed to the zinc cation, which was a notable finding considering coordination to the zinc cation is critical for metalloprotease inhibitor efficacy. It also demonstrated that the low micromolar activity reported with our fragment was not due to zinc coordination.

Encouraged by the small size of the fragment and its newly discovered binding mode, we investigated its potential growth vectors. Our aim was to grow the fragment in the binding pocket further and improve the interactions in the binding pocket with small modifications.

Based on these different directions, we designed a total of 33 fragment molecules with various modifications differing in size and substituents. Figure 4 depicts three fragment-growing directions identified and type of reactions used in each direction. In Part A of the core structure, Suzuki coupling or bromination yielded various derivatives, whereas in Part B, the reactions were mostly focused on reduction or carbonyl transformation. For Part C, we relied on substitution reactions or alkyne transformation.

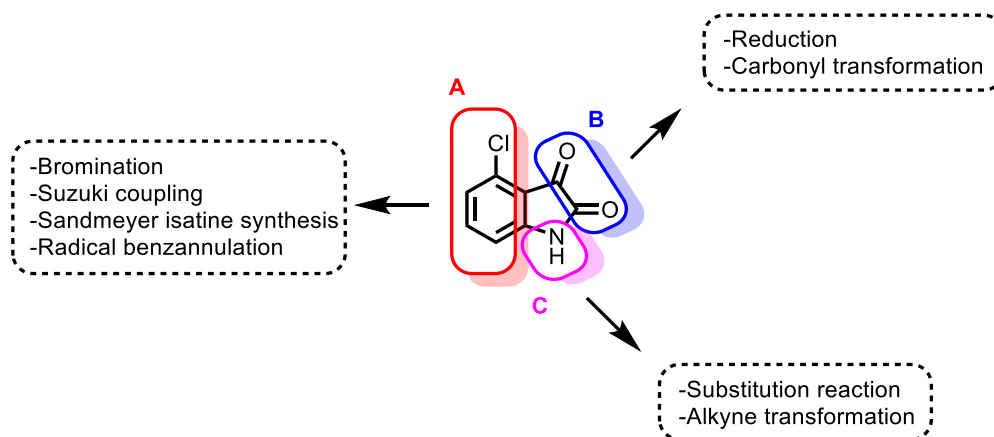


Figure 4. Schematic representation of three growing directions (A, B and C) for fragment **4** and different reactions used for fragment optimization.

Figure 5 represents all fragments that we either designed and synthesized or purchased commercially. As fragments **15**, **16**, and **18–23** were commercially available, these fragments were purchased and evaluated without further purification. We synthesized fragments **5–15** containing modifications on part A, fragments **24–32** with modifications on part B and fragments **33–39** containing modifications on part C using the reactions shown in Figure 4 with low to moderate yields. The synthetic route for each fragment is shown in detail in experimental section 2.3.3. We docked each fragment derivative in the binding pocket of the protein using SeeSAR V.11.1 to investigate its potential interactions.

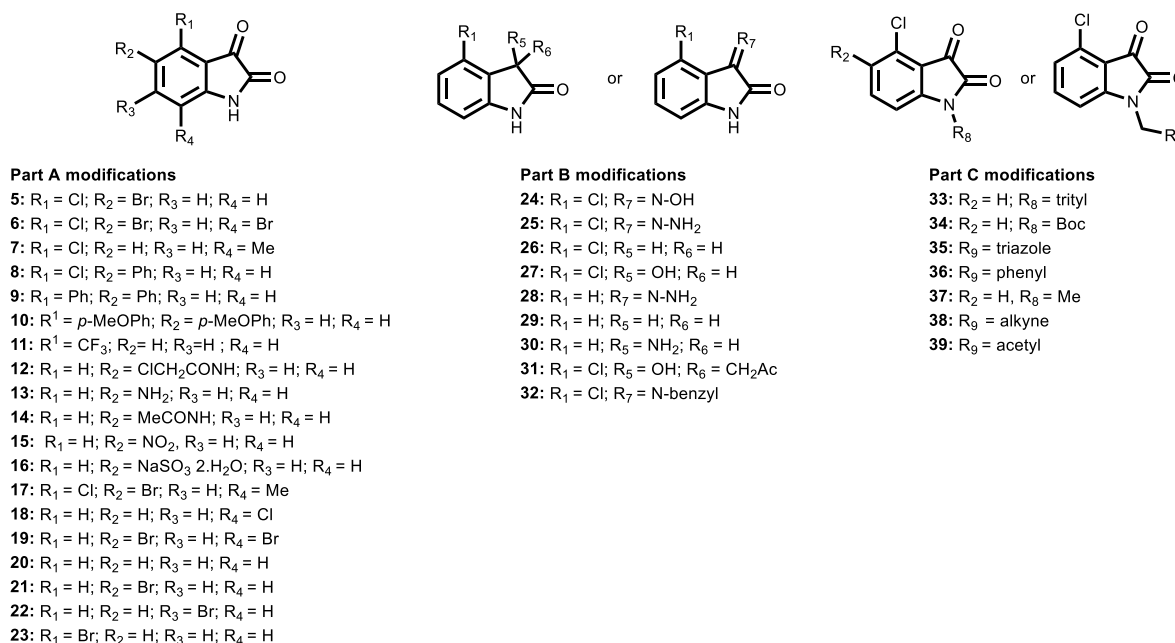
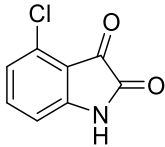
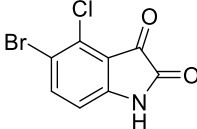
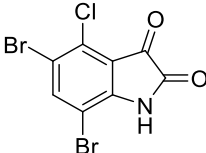
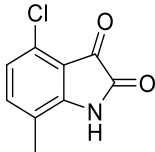


Figure 5: Chemical structures of the designed 33 fragments highlighting the modifications made on each part.

To quantify the effect the modifications on fragment **4** have on its potency, we measured the percent residual activity of ColH-PD in the presence of 10 μM or 100 μM final concentration of all fragments. The residual activities for each fragment are shown in Tables S2, S3 and S4. The measurement of residual activity of ColH-PD was performed as described in the experimental section.

Only the three fragments **5**, **6**, and **7** caused a decrease to $\leq 50\%$ residual activity of the protein. We therefore selected these three compounds for IC_{50} determination. Table 2 shows the measured IC_{50} values, which were determined using a FRET-based inhibition assay as described in the experimental section.

Table 2. IC_{50} values of compounds **4**, **5**, **6** and **7** against ColH-PD.^[a]

Compound	Structure	IC_{50} (μM)
4		117 ± 5
5		$128 \pm 8^*$
6		$44 \pm 2^*$
7		$155 \pm 14^*$

^[a]All measurements were performed in triplicate.

Addition of a bromine group *ortho* to the 4-chloro substituent in compound **5** did not yield any change in the activity, whereas an additional bromine in *para* position with compound **6** increased the potency two-fold compared to compound **4**. This improvement can be rationalized by additional Π -alkyl interactions of the bromine in *para* position with His459, Tyr428 and Trp471 residues, which compounds **4** and **5** cannot provide. The methyl group in compound **7**, however, interrupts a H-bond network between His459 and Glu430 residues that

is mediated *via* two water molecules by displacing one of the waters, which could explain the observed decrease in potency of this fragment.

The results in Table 2 were also in accordance with the residual activity measured in the presence of several other fragments in Tables S1, S2 and S3. For example, fragments **18** and **20** causing around 70% residual activity of the protein highlighted the importance of having a chlorine atom on the isatin core in the correct position. On the other hand, the fragments **19** and **23** containing a one or two bromine atoms caused less than $\leq 50\%$ residual activity, which was consistent with the potential interactions the bromine atom demonstrated with the surrounding residues in fragment **6**. We also observed that fragments **21** (5-bromoisatin) and **22** (6-bromoisatin) demonstrate the importance of the position of the bromine atom.

In the next step, we sought to confirm the binding of fragment **6** further by determining its K_D value using Microscale Thermophoresis (MST). This method is based on identifying the temperature changes in fluorescence intensity, which can be influenced by binding interactions of a suitable ligand with a fluorescently labeled target protein under IR laser.²⁶

Figure 6 shows the fitted curve plotting the normalized fluorescence against concentration of the ligand. K_D of fragment **6** is calculated from this binding curve using the nonlinear function of the law of mass ($K_D: 66.83 \pm 7.91 \mu\text{M}$ ($n=2$)).²⁷

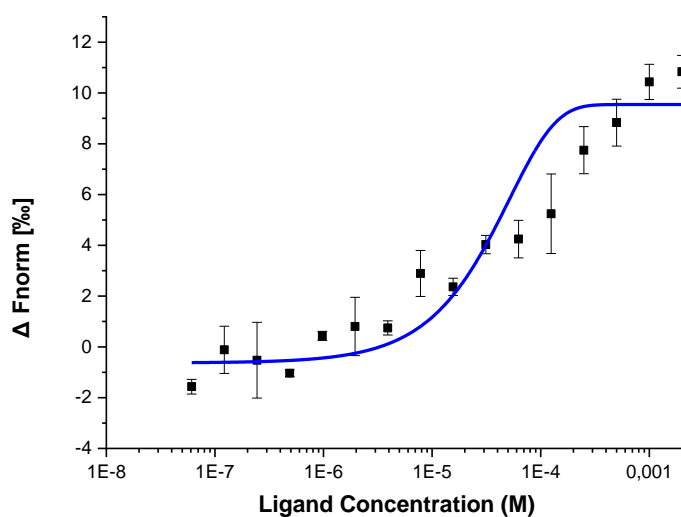


Figure 6. K_D fit curve obtained with MST for compound **6** (His-Tag Col-PD concentration 50 nM, fragment **6** concentration range 2 mM to 6.0×10^{-5} mM). $K_D: 66.83 \pm 7.91 \mu\text{M}$ ($n=2$).

The calculated K_D value of fragment **6** was in the low micromolar range, which is in accordance with the IC_{50} value. This result also supported our observation concerning the potency of the fragment against ColH-PD.

The identification of fragments **4** and **6** with low affinity for ColH has demonstrated that the direction A of the 4-chloroisatin core is crucial for growing of the fragment. Therefore, further modifications should be explored to introduce common zinc-binding motifs such as thiols or phosphonates into this part of the core structure to gain more potency while fine-tuning the selectivity against human off-targets.

2.3.3 Experimental Section

General Chemistry. All starting reagents, including fragments **15**, **16**, and **18–23**, that were purchased from commercial suppliers were used without further purification. Procedures were not optimized regarding yield. NMR spectra were recorded on a Bruker AV 500 (500 MHz) spectrometer at room temperature. Chemical shifts are given in parts per million (ppm) and referenced against the residual proton, 1H , or carbon, ^{13}C , resonances of the >99% deuterated solvents as internal reference. Coupling constants (J) are given in hertz (Hz). Data are reported as follows: chemical shift, multiplicity (s = singlet, d = doublet, t = triplet, dd = doublet of doublets, dt = doublet of triplets, m = multiplet, br = broad), and combinations of these coupling constants and integration. Liquid chromatography–mass spectrometry (LC–MS) was performed on an LC–MS system, consisting of a Dionex-UltiMate 3000 pump, an autosampler, a column compartment, and a detector (Thermo Fisher Scientific, Dreieich, Germany), and an ESI quadrupole MS system (MSQ Plus or ISQ EC, Thermo Fisher Scientific, Dreieich, Germany). Flash chromatography was performed using an automated flash chromatography system CombiFlash Rf+ (Teledyne Isco, Lincoln, NE, USA) equipped with RediSepRf silica columns (Axel Semrau, Sprockhövel, Germany) or Chromabond Flash C18 columns (Macherey-Nagel, Düren, Germany). Preparative HPLC of the compounds were performed with the solvent system ($H_2O + 0.05\% FA/ACN + 0.05\% FA 95:5 \rightarrow 5:95$). High-resolution mass was determined by LC–MS/MS using a Thermo Scientific Q Exactive Focus Orbitrap LC–MS/MS system. The purity of the final compounds was determined by LC–MS, using the area percentage method on the UV trace recorded at a wavelength of 254 nm, and found to be >95%.

Inhibition Assays with Human Off-Targets. Assays focusing on the inhibition of human MMPs were performed as described previously.^{14,15}

Cytotoxicity Assay. The toxicity of selected compounds towards three cell lines was determined as described previously.²⁸ Fragment 4 showed no relevant cytotoxic behaviour against the human hepatoma cell line (HepG2) and human embryonic kidney (HEK 293) cells.

Screening of Halogen-Enriched Fragment Library by Differential Scanning Calorimetry Assay. All experiments were performed in a 96-well PCR plate (Thermoscientific). The final volume per well was 25 μ L, consisting of 18.75 μ L of protein buffer 10 mM HEPES, pH: 7.5, 10 mM NaCl, 1 mM CaCl₂, 3 mM NaH₃, 2.5 μ L of SYPRO orange dye, 2.5 μ L of ColH-PD enzyme and 5 % final DMSO (1.25 μ L). The plates were centrifuged for 2 min. at room temperature, and the melting temperature of the protein was measured using a Real-time PCR machine (Step One plus, Applied Biosystemd). The conditions of the experiment were adjusted using Step One 2.3 software. The starting temperature, the ending temperature and the heating rate were set as 20 °C, 95 °C and 0.5 °C / min, respectively. The melting curves were analyzed using Protein Thermal Shift 1.3 software. Initially, the final concentration of the ColH-PD and SYPRO orange 5000x dye (Sigma-Aldrich) were optimized by screening different concentrations of ColH-PD (10 and 5 mg/mL) at different dye concentrations (50X, 25X, 10X). Most suitable final protein and dye concentrations were determined as 5 μ M and 50X, respectively. The T_m of the ColH-PD under these conditions was found 45.5 °C.

These concentrations were used to screen the HeFLib containing of 148 fragments in two 96-well plates with 100 mM final concentration in DMSO. The DSC plates were incubated at room temperature, and the melting curves were measured for each plate twice in final concentrations of 5 μ M protein, 1 mM of fragments and 50x dye as described above (25 μ L total volume, 5 % final DMSO). As positive control, compound *N*-(4-acetylphenyl)-2-mercaptoacetamide was used in 4 μ M final concentration. As a negative control, rifampicin was included at 100 μ M and 20 μ M final concentrations.

Fragments showing a shift in the $T_m \geq 2$ °C were selected further for concentration-dependent DSC measurements. Three different final concentrations (5 mM, 1 mM, 0.2 mM) of the selected fragments were used against the same protein (5 μ M) and dye (50x) concentration. The plates were incubated at room temperature and the melting curves were measured for each plate twice. The melting curves were analyzed using Protein Thermal Shift 1.3 software. The shift in T_m measured for ColH-PD in presence of fragments showing concentration dependency is shown in Table S1.

FRET-based ColH-PD Inhibition Assay. In the prescreening assay, ColH-PD was pretreated with the compounds for 1 h at room temperature. The reaction was initiated by the addition of 2 μ M FS1-1. The final concentrations were 25 nM ColH-PD, 100 μ M compound or 100 μ M 4-chloroisatin as control, 250 mM Hepes pH 7.5, 400 mM NaCl, 10 mM CaCl₂, 10 μ M ZnCl₂, and 2% DMSO. The increase in fluorescence was monitored for 2 min (Excitation: 328 nm, Emission: 392 nm) at 25 °C. The percentage of enzyme inhibition was calculated with respect to a reference without addition of any compound, only plus buffer control. The initial velocities were calculated via linear regression. For IC₅₀ measurements, the experiments were performed as described above, employing eight different compound concentrations. The compound concentrations were chosen to be evenly distributed above and below the estimated IC₅₀. IC₅₀ values were determined by nonlinear regression. When necessitated by solubility or compound limitations, IC₅₀ values were determined by linear interpolation. Then compound concentrations were chosen to cover a narrow residual activity window of 50 \pm 10% to ensure linearity. All experiments were performed in triplicate and repeated at least three times. Regression analysis was performed using GraphPad Prism 5 (Graph Pad Software, San Diego, CA, USA).

Crystallization of Fragment 4 with ColH-PD. Prior to crystallization, 9 mg/mL ColH-PD were preincubated with 5 mM 4-chloroisatin in 7 mM Hepes pH 7.5, 74 mM NaCl, 0.74 mM CaCl₂, and 8.7% DMSO for 30 min. at RT and then clarified by centrifugation for 30 min. at 13,000 g. The co-crystal was grown using the sitting drop vapor diffusion method by mixing 0.4 μ L protein-inhibitor solution with 0.4 μ L crystallization buffer. The crystallization buffer contained 0.1 M Hepes/MOPS pH 7.3, 0.02 M 1,6-hexanediol, 0.02 M 1-butanol, 0.02 M 1,2-propanediol, 0.02 M 2-propanol, 0.02 M 1,4-butanediol, 0.02 M 1,3-propanediol, 12.5% v/v MPD, 12.5% PEG 1000, and 12.5% w/v PEG 3350. The drop was streak-seeded from crystals of unliganded ColH-PD.²⁹ Crystals appeared within days. The crystals were cryoprotected with MiTeGen LV Cryo-oil (MiTeGen, Ithaca, NY) and immediately flash-frozen in liquid nitrogen. X-ray diffraction data were collected on beamline ID23-1 at the European Synchrotron Radiation Facility (ESRF) in Grenoble, France. The data set was indexed, integrated and scaled using XDS and AIMLESS.^{30,31} Molecular replacement was performed with PHASER65 using as search model PDB entry 5O7E (ligand deleted). Ligand coordinates and restraints were generated using the Grade Web Server.³² Final structures were obtained by several refinement cycles using PHENIX interspersed together with model building in WinCoot.^{33,34} PyMOL

version 4.0.0 was used for figure generation (The PyMOL Molecular Graphics System, Version 4.0.0 Schrödinger, LLC).

Determination of K_D by Microscale Thermophoresis (MST). To evaluate the binding affinity of compound **6**, an MST was established and performed on a Monolith NT.115 device. The protein (HIS-tagged ColH) was labeled with a red fluorescent dye NT-647 using a procedure provided by Nano Temper, including 30 min. incubation time with a ratio of 2:1 of fluorescent dye to protein. The samples were prepared by incubation of the labelled protein with the fragment in 10 mM Hepes, 100 mM NaCl, 1 mM CaCl₂, 5% glycerol, 3 mM NaN₃, %0.05 Tween20, 5% DMSO buffer solution with a pH of 7.2 for 25 minutes. The final concentration of the protein was 50 nM, while the concentration of the fragment was ranging from 2 mM to 6.0x10⁻⁵ mM. The fragment was screened in duplicate at a temperature of 25 °C with an LED power of 40%–60% using standard capillaries. MST on time was 20 sec. and off time was 4 sec. for all measurements. A negative control was measured in triplicate, containing the labeled protein only. As positive control, the initial hit for ColH (*N*-(4-acetylphenyl)-2-mercaptoacetamide) at a final concentration of 625 nM (2 times of its dissociation constant (K_D)) was measured as well. Data were evaluated using the MO Affinity Analysis software (version 2.3, Nano Temper Technologies), and the K_D curve was plotted by OriginLab V.7.0.

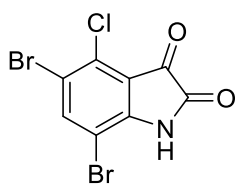
Synthesis of Fragment Derivatives

Bromo-4-chloroindoline-2,3-dione (**5**)

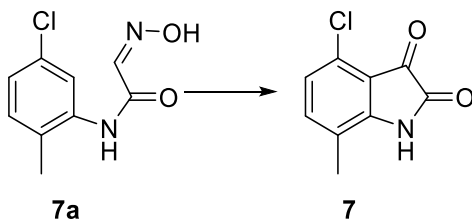


4-chloroisatin (506 mg, 2.79 mmol) was dissolved in MeOH (70 mL) and cooled to 0 °C. *N*-bromosuccinimide (881 mg, 4.95 mmol) was added portion-wise and the orange solution was stirred for 22 h at room temperature. The reaction mixture was concentrated *in vacuo* and dissolved in EtOAc. The organic layer was washed with dist. water and sat. aq. NaCl solution, was dried over MgSO₄, filtered and the solvent was removed under reduced pressure. The dark orange crude was adsorbed on silica and purified via flash chromatography (Hexane / EtOAc) to obtain the desired product as orange crystals (243 mg, 0.93 mmol, 33%). ¹H NMR (500 MHz, DMSO-*d*₆) δ ppm: 10.27 (s, 1H, -NH), 7.85 (d, ³*J*_{HH} = 8.4 Hz, 1H, H6), 6.81 (d, ³*J*_{HH} = 8.4 Hz 1H, H7). ¹³C NMR (126 MHz, DMSO-*d*₆) δ ppm: 180.4 (s, C3), 158.3 (s, C2), 151.1 (s, C4), 141.3 (s, C6), 130.8 (s, C7a), 116.4 (s, C3a), 115.5 (s, C5) 112.5 (s, C7). HRMS (ESI⁺) *m/z* calcd. for C₈H₄BrClNO₂ [M+H]⁺ 259.91085 found 259.90955. MP: 275.4 °C

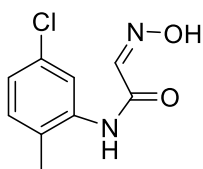
5,7-Dibromo-4-chloroindoline-2,3-dione (**6**)



The compound was obtained as a side product of the synthesis of 5-bromo-4-chloroisatin (**5**). The product was isolated as red crystals (20.3 mg, 0.06 mmol, 2%) after purification by flash chromatography (Hexane / EtOAc). ^1H NMR (500 MHz, $\text{DMSO-}d_6$) δ ppm: 11.56 (s, 1H, -NH), 8.23 (s, 1H, H6). ^{13}C NMR (126 MHz, $\text{DMSO-}d_6$) δ ppm: 179.8 (s, C3), 158.8 (s, C2), 149.9 (s, C4), 142.2 (s, C6), 130.1 (s, C7a), 117.9 (s, C3a), 115.9 (s, C5) 103.9 (s, C7). HRMS (ESI⁺) m/z calcd. for $\text{C}_8\text{H}_3\text{Br}_2\text{ClNO}_2$ $[\text{M}+\text{H}]^+$ 337.80476 found 337.80499. MP: 157.2 °C.

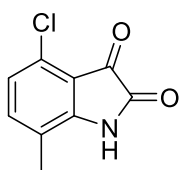


***N*-(5-Chloro-2-methylphenyl)-2-(hydroxyimino)acetamide (7a)**



Chloral hydrate (1.16g, 6.99 mmol) was dissolved in dist. water (12.5 mL), and Na_2SO_4 (4.51g, 31.75 mmol) was added. The solution was heated to 35 °C, and a suspension of 5-chloro-2-methylaniline (502 mg, 3.54 mmol), hydroxylamine hydrochloride (988 mg, 14.22 mmol) and con. HCl solution (0.37 mL) in dist. water (15 mL) was added dropwise. The colorless solution was heated to 80 °C for 2 h. The brown suspension was filtrated and washed with cold water to obtain the product as light brown solid (575 mg, 2.72 mmol, 77 %). ^1H NMR (500 MHz, $\text{DMSO-}d_6$) δ ppm: 12.28 (s, -OH), 9.55 (s, -NH), 7.69 (s, 1H, -CH(NOH)), 7.64 (d, $^4J_{\text{HH}} = 2.1$ Hz, 1H, H2), 7.27 (d, $^3J_{\text{HH}} = 8.3$ Hz, 1H, H5), 7.17 (dd, $^4J_{\text{HH}} = 2.2$ Hz, $^3J_{\text{HH}} = 8.3$ Hz, 1H, H4), 2.20 (s, 3H, - CH_3). ^{13}C NMR (126 MHz, $\text{DMSO-}d_6$) δ ppm: 160.5 (s, -NH-C(O)-), 143.8 (s, -CH(NOH)), 136.9 (s, -CCl-), 131.9 (s, C5), 130.3 (s, C6), 130.0 (s, -C-NH-), 125.2 (s, C4), 124.0 (s, C2), 17.2 (s, - CH_3). HRMS (ESI⁺) m/z calcd. for $\text{C}_9\text{H}_{10}\text{ClN}_2\text{O}_2$ $[\text{M}+\text{H}]^+$ 213.04253 found 213.04170.

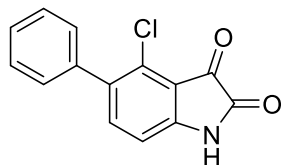
4-Chloro-7-methylindoline-2,3-dione (7)



Compound **7a** (200 mg, 0.94 mmol) was dissolved in conc. H_2SO_4 (4.5 mL) and was heated to 60 °C for 30 min. The red solution was then heated to 80 °C for 15 min. and was allowed to cool to 70 °C afterwards. The purple solution was diluted with ice water (20 mL) and was cooled down to 0 °C for 1 h. An orange precipitate formed, which was collected and dried under high vacuum to afford the product as brown-orange solid (140 mg, 0.71 mmol, 76%). ^1H NMR (500 MHz, $\text{DMSO-}d_6$) δ

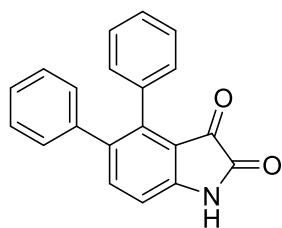
ppm: 11.24 (s, 1H, -NH), 7.40 (dd, $^4J_{\text{HH}} = 0.6$ Hz, $^3J_{\text{HH}} = 8.2$ Hz, 1H, H6), 6.98 (d, $^3J_{\text{HH}} = 8.2$ Hz 1H, H5), 2.16 (s, 3H, -CH₃). ¹³C NMR (126 MHz, DMSO-*d*₆) δ ppm: 181.6 (s, C3), 159.1 (s, C2), 150.6 (s, -CCl-), 140.0 (s, C6), 128.3. HRMS (ESI⁺) *m/z* calcd. for C₉H₇ClNO₂ [M+H]⁺ 196.01598 found 196.02667. MP: 282.3 °C

4-Chloro-5-phenylindoline-2,3-dione (8)



An oven-dried pressure tube was charged with compound **6** (50.0 mg, 0.19 mmol), phenylboronic acid (46.0 mg, 0.38 mmol) and Na₂CO₃ (84.8 mg, 0.80 mmol). Pd(tBu₃P)₂ (9.71 mg, 10 mol %) was added briefly afterwards and the pressure tube was sealed, evacuated, and backfilled with Ar (3x). Dried and degassed 1,4-dioxane (4.5 mL) was added and the reaction mixture was placed in an oil bath, preheated to 85 °C. The dark red suspension was stirred for 18 h, quenched with dist. water and acidified to pH = 2 using 2 N HCl solution. The orange suspension was extracted with EtOAc (3x), dried over Na₂SO₄, filtered, and concentrated in vacuo. The crude product was purified using reversed phase flash chromatography (H₂O+0.1% FA/MeCN+0.1% FA). The product was isolated as orange solid (14.6 mg, 0.056 mmol, 29%). ¹H NMR (500 MHz, DMSO-*d*₆) δ ppm: 11.28 (s, -NH), 7.58 (d, $^3J_{\text{HH}} = 8.0$ Hz, 1H H6), 7.47 (t, $^3J_{\text{HH}} = 7.0$ Hz, 2H, Phenyl H-*meta*), 7.40 (m, 3H, Phenyl H-*ortho*, H-*para*), 6.93 (d, $^3J_{\text{HH}} = 8.0$ Hz, 1H, H7). ¹³C NMR (126 MHz, DMSO-*d*₆) δ ppm: 181.4 (s, C3), 158.7 (s, C2), 151.4 (s, C4), 139.9 (s, C6), 137.5 (s, C7a), 134.8 (s, C5), 129.4 (s, Phenyl C-*ortho*), 129.3 (s, -CCl-C-C-CH-) 128.4 (s, Phenyl C-*meta*), 127.9 (s, Phenyl C-*para*), 115.5 (s, C3a), 111.2 (s, C7). HRMS (ESI⁺) *m/z* calcd. for C₁₄H₉ClNO₂ [M+H]⁺ 258.03163 found 258.03076. MP: 229.1 °C

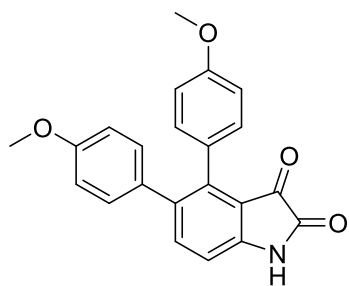
4,5-Diphenylindoline-2,3-dione (9)



Compound **5** (48.2 mg, 0.18 mmol), phenylboronic acid (73.6 mg, 0.60 mmol) and Na₂CO₃ (70.5 mg, 0.66 mmol) were dissolved in MeCN (3 mL) and dist. water (1.5 mL) in a Schlenk tube. The dark red solution was degassed by flushing nitrogen through it for 30 min. Then Pd(PPh₃)₄ (21.9 mg, 10 mol%) was added and the reaction mixture was placed into an oil bath, preheated to 85 °C. The suspension was stirred for 18 h at 85 °C until it was allowed to cool down to room temperature. The light brown suspension was diluted with dist. water and EtOAc and was filtered. The aqueous phase was acidified to pH = 3 using 2 N HCl solution and was extracted with EtOAc three times. The organic layers were dried over MgSO₄, filtered and the solvent was removed under reduced pressure. The orange crude was

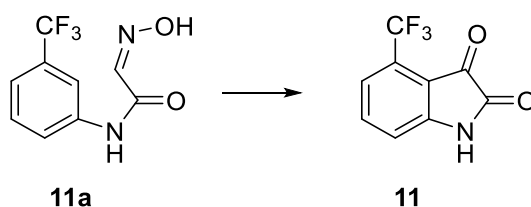
purified using reversed phase flash chromatography (H₂O+0.1% FA/MeCN+0.1% FA). The product was isolated as dark orange crystals (3 mg, 0.010 mmol, 5%). ¹H NMR (500 MHz, DMSO-*d*₆) δ ppm: 8.20 (s, -NH), 7.59 (d, ³J_{HH} = 8.1 Hz, 1H, H6), 7.26 (m, 3H, Phenyl_(pos.4) H-*meta*, Phenyl_(pos.4) H-*para*), 7.18 (m, 3H, Phenyl_(pos.5) H-*meta*, Phenyl_(pos.5) H-*para*), 7.08 (d, ³J_{HH} = 7.2 Hz, 2H, Phenyl_(pos.4) H-*ortho*), 7.00 (m, 2H, Phenyl_(pos.5) H-*ortho*), 6.97 (d, ³J_{HH} = 8.1 Hz, 1H, H7). ¹³C NMR (126 MHz, DMSO-*d*₆) δ ppm: 181.7 (s, C3), 158.6 (s, C2), 148.7 (s, C7a), 141.7 (s, C4), 140.0 (s, C6), 139.4 (s, Phenyl_(pos.5)-C), 138.5 (s, C5), 134.6 (s, Phenyl_(pos.4)-C), 130.0 (s, Phenyl_(pos.4) C-*ortho*), 129.8 (s, Phenyl_(pos.5) C-*ortho*), 128.2 (s, Phenyl_(pos.4) C-*para*), 128.1 (s, Phenyl_(pos.5) C-*meta*), 127.9 (s, Phenyl_(pos.4) C-*meta*), 127.1 (s, Phenyl_(pos.5) C-*para*), 115.1 (s, C3a), 111.4 (s, C7).

4,5-Bis(3-methoxyphenyl)indoline-2,3-dione (10)



Compound **5** (100 mg, 0.38 mmol), 3-(methoxy)phenylboronic acid (116 mg, 0.76 mmol) and Na₂CO₃ (161 mg, 1.51 mmol) were dissolved in MeCN (6mL) and dist. H₂O (3 mL) in a Schlenk tube. The dark red solution was degassed by flushing nitrogen through it for 20 min. [Pd(PPh₃)₄] (65.9 mg, 15 mol %) was added and the reaction mixture was stirred in a preheated oil bath at 80 °C for 18 h. Again 3-(methoxy)phenylboronic acid (100 mg, 0.7 mmol) and Na₂CO₃ (100 mg, 0.9 mmol) was added, and the suspension was stirred for another 18 h. The brown suspension was diluted with water, filtrated, and acidified to pH = 3 using 2 N HCl solution. The orange suspension was extracted with EtOAc three times, and the combined organic layers were washed with sat. aq. NaCl solution, dried over MgSO₄, filtered and concentrated in vacuo. The orange crude was adsorbed on silica and purified using reversed phase flash chromatography (H₂O+0.1% FA / MeCN+0.1% FA) to obtain the product as orange solid (1.6 mg, 0.004 mmol, 1%). ¹H NMR (500 MHz, DMSO-*d*₆) δ ppm: 8.20 (s, -NH), 7.60 (d, ³J_{HH} = 8.0 Hz, 1H, H6), 7.17 (t, ³J_{HH} = 8.0 Hz, 1H, Phenyl_(pos.4) H-*meta*), 7.11 (t, ³J_{HH} = 8.0 Hz, 1H, mPhenyl_(pos.5) H-*meta*), 6.95 (d, ³J_{HH} = 8.1 Hz, 1H, H7), 6.83 (dd, ⁴J_{HH} = 2.4 Hz, ³J_{HH} = 8.2 Hz, 1H, mPhenyl_(pos.4) H-*para*), 6.73 (dd, ⁴J_{HH} = 2.4 Hz, ³J_{HH} = 8.2 Hz, 1H, mPhenyl_(pos.5) H-*para*), 6.70 (d, ³J_{HH} = 7.5 Hz, 1H, Phenyl_(pos.4) H-*ortho* (-CH-CH-C-)), 6.64 (d, ³J_{HH} = 7.5 Hz, 1H, mPhenyl_(pos.5) H-*ortho* (-CO-CH-C-)), 6.62 (s, 1H, mPhenyl_(pos.4) H-*ortho* (-CO-CH-C-)), 6.52 (s, 1H, mPhenyl_(pos.5) H-*ortho* (-CO-CH-C-)), 3.65 (s, mPhenyl_(pos.5) -OCH₃), 3.59 (s, mPhenyl_(pos.4) -OCH₃). ¹³C NMR (126 MHz, DMSO-*d*₆) δ ppm: 181.6 (s, C3), 158.9 (s, C2), 159.2 (s, 2C, -C-O-CH₃), 149.0 (s, C7a), 141.4 (s, C4), 140.7 (s, mPhenyl_(pos.4)-C), 139.8 (C6),

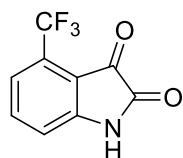
138.1 (s, mPhenyl_(pos.5)-C), 136.0 (s, mPhenyl_(pos.4)-C), 129.2 (s, mPhenyl_(pos.5) C-meta), 129.0 (s, mPhenyl_(pos.4) C-meta), 122.5 (s, mPhenyl_(pos.4) C-ortho (-CH-CH-C-)), 122.1 (s, mPhenyl_(pos.5) C-ortho (-CH-CH-C-)), 115.8 (s, C3a), 115.2 (s, mPhenyl_(pos.4) C-ortho (-CO-CH-C-)), 115.1 (s, mPhenyl_(pos.5) C-ortho (-CO-CH-C-)), 114.5 (s, mPhenyl_(pos.4) C-para), 113.2 (s, mPhenyl_(pos.5) C-para), 111.4 (s, C7), 55.4 (s, mPhenyl_(pos.4) -OCH₃), 55.3 (s, mPhenyl_(pos.5) -OCH₃).



2-(Hydroxyimino)-N-(3-(trifluoromethyl)phenyl)acetamide (11a)

Chloral hydrate (349 mg, 2.11 mmol) was dissolved in dist. water (5 mL) and Na₂SO₄ (1.58 g, 11.2 mmol) was added. The solution was stirred at 35 °C until a solution of 3-(trifluoromethyl)aniline (0.15 mL, 1.20 mmol), hydroxylamine hydrochloride (319 mg, 4.59 mmol) and conc. HCl solution (0.15 mL) in dist. water (5 mL) was added dropwise. The solution was heated to 80 °C for 2 h. A yellow precipitate formed, which was filtrated and washed with cold water to obtain the desired product (199 mg, 0.86 mmol, 72%). ¹H NMR (500 MHz, DMSO-*d*₆) δ ppm: 12.28 (s, -OH), 10.50 (s, -NH), 8.17 (s, 1H, H2), 7.92 (d, ³J_{HH} = 8.2 Hz, 1H, H6), 7.65 (s, 1H, -CH(NOH)), 7.57 (t, ³J_{HH} = 8.0 Hz, 1H, H5), 7.44 (d, ³J_{HH} = 8.0 Hz, 1H, H4). ¹³C NMR (126 MHz, DMSO-*d*₆) δ ppm: 160.8 (s, -NH-C(O)-), 143.8 (s, -CH(NOH)), 139.2 (s, C1), 130.0 (s, C5), 129.4 (q, ²J_{CF} = 31.6 Hz, C3), 124.1 (q, ¹J_{CF} = 271.4 Hz -CF₃), 123.4 (s, C6), 120.2 (q, ³J_{CF} = 4.0 Hz, C4), 115.9 (q, ³J_{CF} = 4.0 Hz, C2). ¹⁹F(¹H) (470 MHz, DMSO-*d*₆) δ ppm: -61.32 (s, 3F, -CF₃). HRMS (ESI⁺) m/z calcd. for C₉H₈F₃N₂O₂ [M+H]⁺ 233.05324 found 233.05229.

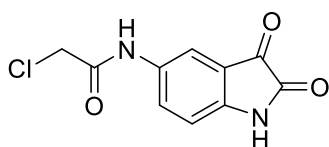
4-(Trifluoromethyl)indoline-2,3-dione (11)



Compound **11a** (169 mg, 0.73 mmol) was dissolved in conc. H₂SO₄ (3.5 mL) and heated to 60 °C for 30 min. The red solution was then heated to 80 °C for 15 min. and was allowed to cool to 70 °C afterwards. The red solution was diluted with ice water (20 mL) and was cooled down to 0 °C for 1 h. The suspension was then extracted with EtOAc (3x), the combined organic layers were washed with sat. aq. NaCl solution, dried over MgSO₄, filtered and the solvent was removed under reduced pressure. The

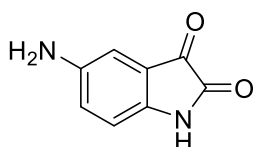
crude was co-evaporated two times with toluene and dried in high vacuum overnight. The dry crude was then dissolved in 2 N NaOH solution and was heated to 60 °C for 1 h. The reaction mixture was neutralized using acetic acid and the aqueous phase was extracted with EtOAc (3x). The combined organic layers were washed with sat. aq. NaCl solution, dried over MgSO₄, filtered, and concentrated in *vacuo*. The crude was purified using column chromatography (Hexane / EtOAc, 1:1) to obtain the desired product as bright orange solid (29.3 mg, 0.14 mmol, 19 %). ¹H NMR (500 MHz, DMSO-*d*₆) δ ppm: 11.30 (s, -NH), 7.75 (t, ³J_{HH} = 8.1 Hz, 1H, H6), 7.36 (d, ³J_{HH} = 8.1 Hz, 1H, H5), 7.20 (d, ³J_{HH} = 8.1 Hz, 1H, H7). ¹³C NMR (126 MHz, DMSO-*d*₆) δ ppm: 180.5 (s, C3), 158.2 (s, C2), 152.5 (s, C7a), 138.3 (s, C6), 125.2 (q, ²J_{CF} = 34.4 Hz, C4), 122.3 (q, ¹J_{CF} = 272.0 Hz -CF₃), 119.2 (q, ³J_{CF} = 5.7 Hz, C5), 116.8 (s, C7), 113.7 (s, C3a). ¹⁹F(¹H) (470 MHz, DMSO-*d*₆) δ ppm: - 61.36 (s, 3F, -CF₃). HRMS (ESI⁻) m/z calcd. for C₉H₃F₃NO₂ [M-H]⁻ 214.01214 found 214.01134.

2-Chloro-N-(2,3-dioxindolin-5-yl)acetamide (12)



Chloroacetic acid (77 mg, 0.34 mmol) was dissolved in DMF (3 mL). To this mixture, EDC.HCl (66 mg, 0.34 mmol) and HOBT (46 mg, 0.34 mmol) were added, and the solution was stirred at room temperature until it is clear. Compound **13** (42 mg, 0.22 mmol) was added to the reaction, and it was stirred at room temperature overnight. Next day, DMF was evaporated and then the mixture was dissolved in DCM and washed with sat. aq. NaCl solution twice. The organic phase was dried over MgSO₄, filtered, and concentrated in *vacuo*. The crude was purified using reverse phase HPLC to yield orange solid (34 mg, 0.14 mmol, 66%). ¹H NMR (500 MHz, DMSO-*d*₆) δ ppm: 11.00 (s, 1H), 10.38 (s, 1H), 7.79 (d, *J* = 2.1 Hz, 1H), 7.66 (dd, *J* = 8.5, 2.2 Hz, 1H), 6.91 (d, *J* = 8.4 Hz, 1H), 4.24 (s, 2H). ¹³C NMR (126 MHz, DMSO-*d*₆) δ ppm: 184.4, 164.7, 159.6, 146.7, 133.7, 129.2, 117.8, 115.6, 112.6, 43.4. HRMS (ESI⁻) m/z calcd. for C₁₀H₆ClN₂O₃ 237.00724 [M-H]⁻ found 237.00723.

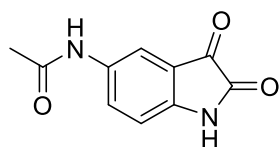
5-Aminoindoline-2,3-dione (13)



5-nitroisatin (500 mg, 2.6 mmol) was dissolved in warm EtOH (10 mL). The emulsion was warmed up to reflux and Fe powder (430 mg, 7.8 mmol) was added. Then, HCl (2 mL) was added dropwise. After 30 min. at reflux, the reaction was stopped. NaHCO₃ solution was added until pH is 8. The mixture was extracted with EtOAc (3x), and the combined organic layers were washed with sat. aq. NaCl solution, dried over MgSO₄, filtered, and concentrated in *vacuo*. The crude was purified using

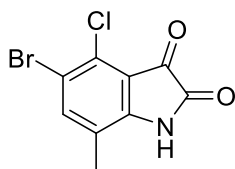
column chromatography (DCM / MeOH, 95:5) to obtain the desired product as orange solid (420 mg, 2.59 mmol, 99%). ¹H NMR (500 MHz, DMSO-*d*₆) δ ppm: 10.62 (s, 1H), 6.81 (dd, *J* = 8.3, 2.5 Hz, 1H), 6.70 (d, *J* = 2.4 Hz, 1H), 6.63 (d, *J* = 8.3 Hz, 1H), 5.09 (s, 2H). ¹³C NMR (126 MHz, DMSO-*d*₆) δ ppm: 185.5, 159.5, 144.0, 140.9, 123.6, 118.2, 112.8, 109.1, 39.5.

***N*-(2,3-Dioxindolin-5-yl)acetamide (14)**



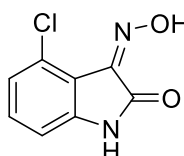
5-aminoisatin (134 mg, 0.72 mmol) was dissolved in THF (2 mL) and flushed with Ar. To this solution, Et₃N (44 μL, 0.43 mmol) was added dropwise. The mixture was cooled to 0 °C and acetyl chloride (22 μL, 0.28 mmol) was added slowly. After 1 h, THF is evaporated, and the crude is washed with DCM. The combined organic layers were washed with sat. aq. NaCl solution, dried over MgSO₄, filtered, concentrated *in vacuo*. The crude was purified using reverse phase HPLC to yield orange solid (20 mg, 0.01 mmol, 43%) ¹H NMR (500 MHz, DMSO-*d*₆) δ ppm: 10.96 (s, 1H), 10.03 (s, 1H), 7.79 (d, *J* = 5.0 Hz, 1H), 7.64 (dd, *J* = 8.4, 2.2 Hz, 1H), 6.87 (d, *J* = 8.4 Hz, 1H), 2.03 (s, 1H). ¹³C NMR (126 MHz, DMSO-*d*₆) δ ppm: 184.6, 168.3, 159.6, 146.1, 134.7, 128.7, 117.6, 115.1, 112.4, 39.5, 23.8.

5-Bromo-4-chloro-7-methylindoline-2,3-dione (17)



Compound **7** (49.9 mg, 0.25 mmol) was suspended in MeOH (5 mL) and THF (1 mL) and *N*-bromosuccinimide (68.3 mg, 0.38 mmol) was added. The reaction mixture was stirred at room temperature for 20 h. The orange solution was diluted with DCM, washed with water, and sat. aq. NaCl solution, dried over Na₂SO₄, filtered, and concentrated *in vacuo*. The crude was adsorbed on silica gel and purified by flash chromatography (Hexane / EtOAc). The product was obtained as dark orange solid (32.5 mg, 0.12 mmol, 47%). ¹H NMR (500 MHz, DMSO-*d*₆) δ ppm: 11.33 (s, 1H, -NH), 7.82 (d, ⁴*J*_{HH} = 0.7 Hz, 1H, H6), 2.17 (s, 3H, -CH₃). ¹³C NMR (126 MHz, DMSO-*d*₆) δ ppm: 181.2 (s, C3), 158.9 (s, C2), 150.1 (s, -CCl-), 142.1 (s, C6), 128.2 (s, C7a), 122.6 (s, C5), 115.8 (s, C3a), 115.2 (s, C7) 14.9 (s, -CH₃). HRMS (ESI⁺) *m/z* calcd. for C₉H₆BrClNO₂ [M+H]⁺ 271.91194 found 271.91202. MP: 272.1 °C

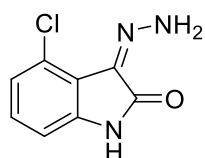
4-Chloro-3-(hydroxyimino)indolin-2-one (24)



4-chloroisatin (100 mg, 0.55 mmol) and hydroxylamine hydrochloride (45.9 mg, 0.66 mmol) were dissolved in dist. water (8 mL) and heated to 100 °C for 30 min. NaOAc (136 mg, 1.66 mmol) was added, and the orange suspension

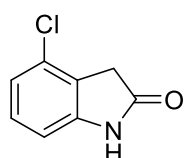
was stirred for another 30 min. at 100 °C. The reaction mixture was allowed to cool down to room temperature, was diluted with dist. water, acidified with 2N HCl solution, extracted with EtOAc and dried over MgSO₄. The solvent was filtered and removed under reduced pressure. The orange solid was adsorbed on silica and purified *via* flash column chromatography (Hexane / EtOAc) to obtain the product as orange solid (65.0 mg, 0.33 mmol, 60%). ¹H NMR (500 MHz, DMSO-*d*₆) δ ppm: 13.49 (s, 1H), 11.20 (s, -NH_E), 10.91 (s, 1H, -NH_Z), 7.54 (t, ³J_{HH} = 8.0 Hz, 1H, H_{6E}), 7.30 (t, ³J_{HH} = 8.3 Hz, 1H, H_{6Z}), 7.06 (d, ³J_{HH} = 8.3 Hz, 1H, H_{5E}), 7.04 (d, ³J_{HH} = 8.3 Hz, 1H, H_{5Z}), 6.85 (d, ³J_{HH} = 8.0 Hz, 1H, H_{7E}), 6.81 (d, ³J_{HH} = 7.8 Hz, 1H, H_{7Z}). ¹³C NMR (126 MHz, DMSO-*d*₆) δ ppm: 158.0 (s, C₂), 143.8 (s, C₄), 142.8 (s, C₃), 139.0 (s, C_{6E}), 131.7 (s, C_{6Z}), 127.1 (s, C_{7a}), 123.6 (s, C_{5E}), 123.0 (s, C_{5Z}), 116.6 (s, C_{3a}), 111.0 (s, C_{7E}), 108.9 (s, C_{7Z}). E/Z ratio: 1 : 4.76 (determined by NMR) HRMS (ESI⁺) m/z calcd. for C₈H₆ClN₂O₂ [M+H]⁺ 197.01123 found 197.01067. MP: 232.2 °C.

4-Chloro-3-hydrazineylideneindolin-2-one (25)



4-chloroisatin (99.5 mg, 0.55 mmol) was dissolved in MeOH (5 mL) and hydrazine (1 M solution in THF) (0.83 mL, 0.83 mmol) was added dropwise. The solution was heated to reflux for 3 h. The solvent was removed under reduced pressure and the crude was partially dissolved in ethanol (7 mL). The suspension was heated to 61 °C, cooled down and left overnight at 4 °C. A precipitate is formed which was filtrated to isolate the product as light orange solid (21.1 mg, 0.11 mmol, 20%). ¹H NMR (500 MHz, DMSO-*d*₆) δ ppm: 10.96 (s, 1H), 10.94 (d, ²J_{HH} = 15.0 Hz, 1H), 9.95 (d, ²J_{HH} = 15.0 Hz, 1H), 7.14 (t, ³J_{HH} = 7.9 Hz, 1H), 6.99 (dd, ⁴J_{HH} = 0.8 Hz, ³J_{HH} = 8.2 Hz, 1H, H₅), 6.84 (dd, ⁴J_{HH} = 0.8 Hz, ³J_{HH} = 7.9 Hz, 1H, H₇). ¹³C NMR (126 MHz, DMSO-*d*₆) δ ppm: 162.5 (s, C₂), 140.0 (s, C₄), 127.8 (s, C₆), 125.0 (s, C₃), 124.4 (s, C_{7a}), 122.6 (s, C₅), 118.7 (s, C_{3a}), 108.8 (s, C₇). HRMS (ESI⁺) m/z calcd. for C₈H₇ClN₃O [M+H]⁺ 196.0272 found 196.02667.

4-Chloroindolin-2-one (26)



4-chloroisatin (151 mg, 0.83 mmol) was suspended in *t*-BuOH (5 mL) and hydrazine (1 M solution in THF) (0.99 mL, 0.99 mmol) was added dropwise. The solution was stirred at 35 °C for 45 min. and was heated to 80 °C for 2 h afterwards. Et₃N (0.12 mL, 0.86 mmol) was added at the same temperature and the solution was stirred at 100 °C for 16 h. The brown suspension was concentrated in *vacuo*, diluted with EtOAc, and washed with dist. water and sat. aq. NaCl solution. The organic layer was dried over MgSO₄, filtered and the solvent was removed under reduced pressure. The brown oily

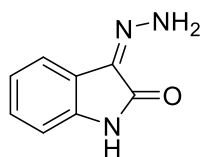
residue was purified by flash chromatography (Hexane/EtOAc) and *via* column chromatography (DCM / MeOH, 9:1) to isolate the desired product as orange solid (10.1 mg, 0.06 mmol, 7%). ¹H NMR (500 MHz, DMSO-*d*₆) δ ppm: 10.59 (s, 1H), 7.20 (t, ³J_{HH} = 8.1 Hz, 1H), 6.98 (d, ³J_{HH} = 8.1 Hz, 1H), 6.78 (d, ³J_{HH} = 7.8 Hz, 1H), 3.50 (s, 2H). ¹³C NMR (126 MHz, DMSO-*d*₆) δ ppm: 175.2, 145.1, 129.5, 128.9, 124.2, 121.0, 108.3, 35.6. HRMS (ESI⁺) *m/z* calcd. for C₈H₆ClN [M+H]⁺ 168.02107 found 168.02051.

4-Chloro-3-hydroxyindolin-2-one (27)



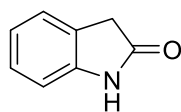
4-chloroisatin (100 mg, 0.55 mmol) was suspended in THF (2 mL), and zinc dust (180 mg, 2.75 mmol) was added. After 5 min., 4.4 mL of 8 M NH₄Cl solution was added dropwise, and the red suspension was stirred for 20 minutes at room temperature. The reaction mixture was filtered, washed with THF, and concentrated in vacuo. The crude aqueous phase was diluted with EtOAc, acidified with 2 N HCl solution and was extracted EtOAc (3x). The combined organic layers were dried over MgSO₄, filtered and the solvent was removed under reduced pressure. The product was isolated as yellow solid (80.3 mg, 0.43 mmol, 79%). ¹H NMR (500 MHz, DMSO-*d*₆) δ ppm: 10.44 (s, 1H, -NH), 7.23 (t, ³J_{HH} = 7.9 Hz, 1H, H6), 6.95 (d, ³J_{HH} = 8.2 Hz, 1H, H5), 6.74 (d, ³J_{HH} = 7.7 Hz, 1H, H7), 6.23 (d, ³J_{HH} = 8.60 Hz, 1H, -OH), 4.87 (d, ³J_{HH} = 8.60 Hz 1H, H3). ¹³C NMR (126 MHz, DMSO-*d*₆) δ ppm: 177.1 (s, C2), 144.5 (s, C7a), 130.9 (s, C6), 130.8 (s, C4), 126.2 (s, C3a), 121.8 (s, C5), 108.5 (s, C7), 69.0 (s, C3). HRMS (ESI⁺) *m/z* calcd. for C₈H₇ClNO₂ [M+H]⁺ 184.01598 found 183.99681.

3-Hydrazineylideneindolin-2-one (28)



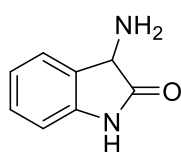
Isatin (2.21 g, 15.0 mmol) was suspended in MeOH (37 mL), and 55% aqueous solution of hydrazine (2.6 mL) was added. The solution was heated to reflux for 3 h. The suspension was filtrated and was washed with dist. water, cold MeOH and cold Et₂O. The product was dried under high vacuum to obtain the product as brown solid (2.07 g, 12.9 mmol, 86%). ¹H NMR (500 MHz, DMSO-*d*₆) δ ppm: 10.68 (s, 1H, -NH), 10.53 (d, ²J_{HH} = 14.5 Hz, 1H, -NH₂), 9.5 (d, ²J_{HH} = 14.5 Hz, 1H, -NH₂), 7.35 (d, ³J_{HH} = 7.5 Hz, 1H, H4) 7.15 (td, ⁴J_{HH} = 1.1 Hz, ³J_{HH} = 7.7 Hz, 1H, H6), 6.97 (td, ⁴J_{HH} = 1.1 Hz, ³J_{HH} = 7.6 Hz, 1H, H5), 6.84 (d, ³J_{HH} = 7.7 Hz, 1H, H7). ¹³C NMR (126 MHz, DMSO-*d*₆) δ ppm: 162.8 (s, C2), 138.6 (s, C3), 127.1 (s, C6), 126.2 (s, C7a), 122.3 (s, C3a), 121.3 (s, C5), 117.4 (s, C4), 110.0 (s, C7). HRMS (ESI⁺) *m/z* calcd. for C₈H₈N₃O [M+H]⁺ 162.06619 found 162.06566.

Indolin-2-one (29)



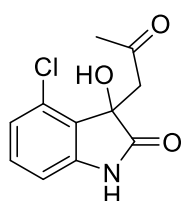
Compound **29** (2.04 g, 12.6 mmol) was added to a solution of freshly prepared NaOEt (3.7 eq.) in EtOH (30.5 mL) and the red reaction mixture was stirred for 3.5 h under reflux. The solution was quenched with 10 % HCl solution and was extracted with DCM three times. The combined organic layers were concentrated in vacuo, diluted with DCM again and were washed with sat. aq. NaCl solution. The organic solvent was dried over MgSO₄, filtered and the solvent was removed under reduced pressure. The crude product was purified via column chromatography (DCM / MeOH, 24:1) to obtain the product as brown solid (1.28 g, 9.61 mmol, 76%). ¹H NMR (500 MHz, DMSO-*d*₆) δ ppm: 10.37 (s, 1H, -NH), 7.20 (d, ³J_{HH} = 7.4 Hz, 1H, H7), 7.16 (t, ³J_{HH} = 7.5 Hz, 1H, H5), 6.92 (t, ³J_{HH} = 7.4 Hz, 1H, H6), 6.81 (d, ³J_{HH} = 7.6 Hz, 1H, H4), 3.46 (s, 2H, H3). ¹³C NMR (126 MHz, DMSO-*d*₆) δ ppm: 176.4 (s, C2), 143.7 (s, C7a), 127.4 (s, C6), 125.8 (s, C3a), 124.4 (s, C4), 121.1 (s, C5), 109.1 (s, C7), 35.7 (s, C3). HRMS (ESI⁺) *m/z* calcd. for C₈H₇NO₂ [M+H]⁺ 134.06004 found 134.05965.

3-Aminoindolin-2-one (30)



Compound **25** (50.0 mg, 0.25 mmol) was dissolved in THF (5 mL) and palladium on activated charcoal (10%) (6 mg, 20 mol%) was added. The suspension was stirred for 18 h under hydrogen atmosphere at room temperature. The reaction mixture was filtered afterwards, and the solvent was removed under reduced pressure to isolate the product as orange solid (18.9 mg, 0.13 mmol, 52%). ¹H NMR (500 MHz, DMSO-*d*₆) δ ppm: 10.91 (s, 1H, -NH), 9.02 (s, 2H, -NH₂), 7.62 (d, ³J_{HH} = 7.5 Hz, 1H, H4), 7.33 (t, ³J_{HH} = 7.8 Hz, 1H, H5), 7.06 (t, ³J_{HH} = 7.6 Hz, 1H, H5), 6.92 (d, ³J_{HH} = 7.8 Hz, 1H, H7), 4.95 (s, 1H, H3). ¹³C NMR (126 MHz, DMSO-*d*₆) δ ppm: 173.0 (s, C2), 143.0 (s, C7a), 130.3 (s, C6), 125.8 (s, C4), 123.3 (s, -C3a), 122.1 (s, C5), 110.29 (s, C7), 51.2 (s, C3). HRMS (ESI⁻) *m/z* calcd. for : C₈H₇N₂O [M-H]⁻ 147.05639 found 146.92238.

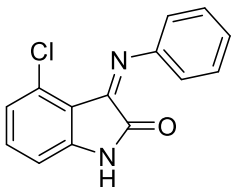
4-Chloro-3-hydroxy-3-(2-oxopropyl)indolin-2-one (31)



4-chloroisatin (54.6 mg, 0.30 mmol) and K₂CO₃ (41.6 mg, 0.30 mmol) were dissolved in acetone (6 mL) and stirred for 18 h at room temperature. The beige suspension was filtrated and concentrated in vacuo. The crude was adsorbed on silica and purified via flash chromatography (Hexane / EtOAc) to obtain the product as colourless solid (37.1 mg, 0.15 mmol, 50%). ¹H NMR (500 MHz, DMSO-*d*₆) δ ppm: 10.46 (s, 1H, -NH), 7.19 (t, ³J_{HH} = 8.0 Hz, 1H, H6), 6.88 (dd, ⁴J_{HH} = 0.8 Hz, ³J_{HH} = 8.2

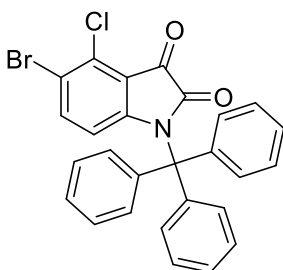
Hz, 1H, H5), 6.75 (dd, $^4J_{\text{HH}} = 0.8$ Hz, $^3J_{\text{HH}} = 7.7$ Hz, 1H, H7), 6.13 (s, 1H, -OH), 3.64 (d, $^2J_{\text{HH}} = 17.3$ Hz 1H, -CH₂-), 3.16 (d, $^2J_{\text{HH}} = 17.3$ Hz 1H, -CH₂-), 1.99 (s, 3H, -CH₃). ¹³C NMR (126 MHz, DMSO-*d*₆) δ ppm: 205.1 (s, -CH₂-C(O)-), 177.3 (s, C2), 144.9 (s, C7a), 130.8 (s, C6), 129.7 (s, C4), 127.4 (s, C3a), 122.1 (s, C5), 108.4 (s, C7), 73.3 (s, C3), 48.5 (s, CH₂), 30.2 (s, -CH₃). HRMS (ESI⁺) *m/z* calcd. for C₁₁H₁₁ClNO₃ [M+H]⁺ 240.0422 found 240.04128.

4-Chloro-3-(phenylimino)indolin-2-one (32)



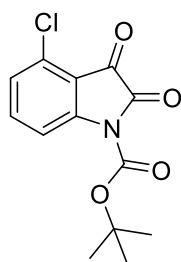
4-chloroisatin (181 mg, 1 mmol) was dissolved in methanol (40 mL). Aniline (92 mg, 1 mmol) and glacial acetic acid (1 mL) were added in respective order and the reaction was refluxed for 6 h. Afterwards, it was left stirring overnight at room temperature. Next day, the mixture was filtered the solid was washed with cold methanol to obtain the final product (100 mg, 0.39 mmol, 39%). ¹H NMR (500 MHz, DMSO-*d*₆) δ ppm: 11.08 (s, 1H), 7.43 (t, *J* = 8.1 Hz, 1H), 7.30 (t, *J* = 7.7 Hz, 2H), 7.11–7.07 (m, 2H), 6.94 (d, *J* = 7.9 Hz, 4H), 6.82 (d, *J* = 7.7 Hz, 2H). HRMS (ESI⁺) *m/z* calcd. for C₁₄H₁₀ClN₂O [M+H]⁺ 257.04761 found 257.04749.

5-Bromo-4-chloro-1-tritylindoline-2,3-dione (33)



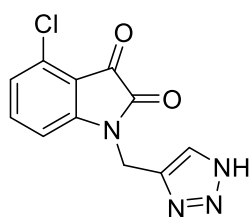
A pressure tube was charged with compound **6** (97.8 mg, 0.38 mmol), K₂CO₃ (93.3 mg, 0.68 mmol) and THF (5 mL). The sealed tube was placed in an oil bath preheated to 40 °C and was heated to 60 °C for 1 h. The reaction was quenched with water, extracted with EtOAc and the organic layers were washed with sat. aq. NaCl solution, dried over Na₂SO₄, filtered, and concentrated in vacuo. The crude product was adsorbed on Celite and purified by flash chromatography (Hexane / EtOAc) to obtain the product as yellow solid (104 mg, 0.21 mmol, 56%). ¹H NMR (500 MHz, DMSO-*d*₆) δ ppm: 7.65 (d, $^3J_{\text{HH}} = 7.5$ Hz, 1H, H6), 7.48 (d, $^3J_{\text{HH}} = 7.5$ Hz, 6H, Trityl H-*ortho*), 7.30 (t, 6H, $^3J_{\text{HH}} = 7.3$ Hz Trityl H-*meta*), 7.23 (t, $^3J_{\text{HH}} = 7.5$ Hz, 3H, Trityl H-*para*), 6.24 (d, $^3J_{\text{HH}} = 8.8$ Hz, 1H, H7). ¹³C NMR (126 MHz, DMSO-*d*₆) δ ppm: 178.8 (s, C3), 158.0 (s, C2), 151.2 (s, -CCl-), 141.1 (s, -C-C-CH), 139.0 (s, C6), 130.6 (s, C7a), 129.0 (s, Trityl C-*ortho*), 127.9 (s, Trityl C-*meta*), 127.1 (s, Trityl C-*para*), 117.8 (s, C3a) 117.0 (s, C7), 116.5 (s, -CBr-), 74.6 (s, -C-C-CH).

Tert-butyl 4-chloro-2,3-dioxindoline-1-carboxylate (34)



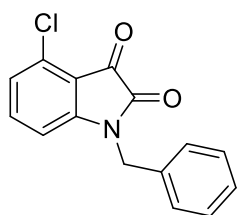
4-chloroisatin (100 mg, 0.55 mmol) was dissolved in a heat dried Yang flask under N₂ atmosphere in dry THF (5 mL) and was cooled to 0 °C. Boc₂O (240.4 mg, 1.10 mmol) was dissolved in another heat dried Yang flask in dry THF (5 mL) under inert conditions and was added dropwise to the solution of 4-chloroisatin. The yellow solution was allowed to warm to room temperature and was stirred for 2 h. The reaction was quenched with water and THF was removed under reduced pressure. The aqueous phase was extracted with EtOAc, (3x), dried over MgSO₄, filtered and the solvent was removed under reduced pressure. The yellow crude was adsorbed on silica and purified via flash column chromatography (Hexane / EtOAc) to obtain the desired product as yellow crystals (82 mg, 0.29 mmol, 53%). ¹H NMR (500 MHz, DMSO-*d*₆) δ ppm: 7.91 (d, ³J_{HH} = 8.2 Hz, 1H, H7), 7.71 (t, ³J_{HH} = 8.4 Hz, 1H, H6), 7.34 (d, ³J_{HH} = 8.3 Hz, 1H, H5), 1.58 (s, 9H, -CH₃). ¹³C NMR (126 MHz, DMSO-*d*₆) δ ppm: 177.1 (s, C2), 155.4 (s, -C(O)-O-C-), 148.8 (s, -CCl-), 148.0 (s, C3), 138.2 (s, C6), 131.1 (s, C7a), 126.1 (s, C5), 116.7 (s, C3a) 115.1 (s, C7), 84.3 (s, -C-CH₃)₃, 27.7 (s, -CH₃). HRMS (ESI⁺) m/z calcd. for C₁₃H₁₃ClNO₄ [M+H]⁺ 282.05276 found 282.27792. MP: 157.2 °C

1-(1,2,3-Triazol-4-yl)methyl)-4-chloroindoline-2,3-dione (35)



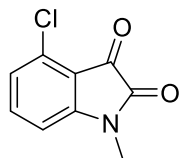
Compound **38** (75.0 mg, 0.34 mmol), NaN₃ (33.2 mg, 0.51 mmol) and NaOAc (67.4 mg, 0.34 mmol) were dissolved in dist. water (5 mL) and MeCN (5 mL) in a reaction tube. CuSO₄ · 5H₂O (42.4 mg, 0.17 mmol) was added to the orange solution and the sealed pressure tube was placed in an oil bath preheated to 60 °C. After 18 h, the brown suspension was allowed to cool down to room temperature, was filtered, washed with MeCN, MeOH and EtOAc and was concentrated in *vacuo*. The residue was diluted with dist. water, acidified using 2N HCl solution and was extracted three times with EtOAc. The organic layers were collected, washed with sat. aq. NaCl solution, and dried over MgSO₄. After filtration, the solvent was removed under reduced pressure and the brown crude was purified *via* column chromatography (Hexane / EtOAc, 3:7). The yellow oil was then recrystallized from chloroform to obtain the desired product as orange crystals (4.6 mg, 0.018 mmol, 5%). ¹H NMR (500 MHz, DMSO-*d*₆) δ ppm: 7.87 (s, 1H, -C-CH-), 7.62 (t, ³J_{HH} = 8.0 Hz, 1H, H6), 7.16 (d, ³J_{HH} = 7.9 Hz, 1H, H7), 7.13 (d, ³J_{HH} = 8.0 Hz, 1H, H5), 5.11 (s, 2H, -CH₂-). ¹³C NMR (126 MHz, DMSO-*d*₆) δ ppm: 181.0 (s, C3), 157.9 (s, C2), 153.0 (s, C4), 139.4 (s, C6), 132.8 (s, C7a), 131.6 (s, -CH₂-C-CH-), 125.6 (s, C5), 124.0 (s, -CH₂-C-CH-), 115.7 (s, C3a), 110.8 (s, C7), 36.0 (s, -CH₂-). HRMS (ESI⁺) m/z calcd. for C₁₁H₈ClN₄O₂ [M+H]⁺ 263.03303 found 263.03198. MP: 185.0 °C.

1-Benzyl-4-chloroindoline-2,3-dione (36)



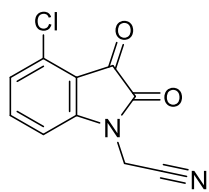
4-Chloroisatin (100 mg, 0.55 mmol) and K_2CO_3 (149 mg, 1.07 mmol) were dissolved in MeCN (10 mL) in a sealed pressure tube. Benzyl bromide (0.10 mL, 0.84 mmol) was added, and the reaction mixture was stirred for 16 h at 85 °C. The orange suspension was diluted with EtOAc, washed with dist. water, and sat. aq. NaCl solution, dried over $MgSO_4$, filtered, and concentrated in vacuo. The crude was purified via flash chromatography (Hexane / EtOAc) to isolate the desired product as orange solid (122 mg, 0.45 mmol, 83%). 1H NMR (500 MHz, $DMSO-d_6$) δ ppm: 7.54 (t, $^3J_{HH} = 8.1$ Hz, 1H, H6), 7.43 (d, $^3J_{HH} = 7.4$ Hz, 2H, Phenyl H-*ortho*), 7.34 (t, $^3J_{HH} = 7.4$ Hz, 2H, Phenyl H-*meta*), 7.28 (t, $^3J_{HH} = 7.3$ Hz, 1H, Phenyl H-*para*), 7.11 (d, $^3J_{HH} = 8.1$ Hz, 1H, H5), 6.89 (d, $^3J_{HH} = 8.0$ Hz 1H, H7), 4.91 (s, 2H, -CH₂-). ^{13}C NMR (126 MHz, $DMSO-d_6$) δ ppm: 179.9 (s, C3), 157.7 (s, C2), 151.6 (s, -CCl-), 138.4 (s, C6), 135.3 (s, C7a), 131.0 (s, -CH₂-C-), 128.6 (s, Phenyl C-*meta*), 127.5 (s, Phenyl C-*para*), 127.3 (s, Phenyl C-*ortho*), 124.2 (s, C5), 114.8 (s, C3a), 109.8 (s, C7), 43.0 (s, -CH₂-). HRMS (ESI⁺) m/z calcd. for $C_{15}H_{11}ClNO_2$ [M+H]⁺ 272.04728 found 272.04608.

4-Chloro-1-methylindoline-2,3-dione (37)



4-chloroisatin (100 mg, 0.55 mmol) was dissolved in DMF (10 mL) and K_2CO_3 (228 mg, 3 mmol) was added followed by iodomethane (93 mg, 1.2 mmol). The reaction was stirred at room temperature and monitored with TLC until the starting material was consumed. The solvent was removed, and the mixture was washed with DCM and sat. aq. NaCl solution, dried over $MgSO_4$, filtered, and concentrated in vacuo. The crude was purified via flash chromatography (P. Ether / EtOAc, 20:1) to isolate the desired product as orange solid (50 mg, 0.25 mmol, 47%). 1H NMR (500 MHz, $CDCl_3$) δ ppm: 7.51 (t, $J = 8.0$ Hz, 1H), 7.08 (d, $J = 8.2$ Hz, 1H), 6.80 (d, $J = 7.9$ Hz, 1H), 3.27 (s, 3H). ^{13}C NMR (126 MHz, $CDCl_3$) δ ppm: 138.63 134.5, 125.6, 108.2, 26.6. HRMS (ESI⁻) m/z calcd. for $C_9H_5ClNO_2$ [M+H]⁺ 196.01598 found 196.01681.

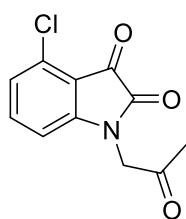
2-(4-Chloro-2,3-dioxindolin-1-yl)acetonitrile (38)



An oven dried pressure tube was charged with 4-chloroisatin (250 mg, 1.38 mmol), K_2CO_3 (387 mg, 2.80 mmol), NaI (38.6 mg, 0.26 mmol) and dry THF (20 mL), was sealed and heated to 50 °C under argon atmosphere. Bromoacetonitrile (0.15 mL, 2.15 mmol), dissolved in dry THF (5 mL) was added dropwise and the dark red solution was stirred for 24 h at the same temperature. The

suspension was filtered, concentrated in *vacuo*, and dissolved in EtOAc. The organic mixture was washed with dist. water and sat. aq. NaCl solution, dried over MgSO₄, filtered and the solvent was removed under reduce pressure. The brown residue was adsorbed on Celite and purified *via* column chromatography (Hexane / EtOAc 7:3 to 5:5) to obtain the product as yellow oil (64.8 mg, 0.29 mmol, 21 %). ¹H NMR (500 MHz, DMSO-*d*₆) δ ppm: 7.65 (t, ³*J*_{HH} = 8.1 Hz, 1H, H6), 7.22 (d, ³*J*_{HH} = 8.3 Hz, 1H, H5), 7.00 (d, ³*J*_{HH} = 8.1 Hz, 1H, H7), 4.70 (s, 2H, -CH₂-). ¹³C NMR (126 MHz, DMSO-*d*₆) δ ppm: 177.8 (s, C3), 156.1 (s, C2), 149.1 (s, -CCl-), 139.4 (s, C6), 135.0 (s, C7a), 127.2 (s, C5), 115.2 (s, C3a), 112.6 (s, -CN), 108.7 (s, C7), 27.9 (s, -CH₂-).

4-Chloro-1-(2-oxopropyl)indoline-2,3-dione (39)



Compound **38** (50,0 mg, 0.23 mmol) and Hg(OAc)₂ (36.6 mg, 0.11 mmol) were suspended in dist. water (1 mL) and MeOH (1.8 mL) in a sealed pressure tube. While stirring, conc. H₂SO₄ was added, and the orange suspension was heated to 60 °C for 18 h. The reaction mixture was diluted with water and the precipitate was collected to obtain the desired product as orange solid (24.6 mg,

0.10 mmol, 43%). ¹H NMR (500 MHz, DMSO-*d*₆) δ ppm: 7.62 (t, ³*J*_{HH} = 8.1 Hz, 1H, H6), 7.16 (d, ³*J*_{HH} = 8.1 Hz, 1H, H5), 7.05 (d, ³*J*_{HH} = 8.1 Hz, 1H, H7), 4.73 (s, 2H, -CH₂-), 2.25 (s, 3H, -CH₃). ¹³C NMR (126 MHz, DMSO-*d*₆) δ ppm: 201.6 (s, -C(O)-CH₃), 179.7 (s, C3) 157.4 (s, C2), 152.1 (s, -CCl-), 139.3 (s, C6), 131.1 (s, C7a), 124.7 (s, C5), 114.2 (s, C3a), 110.3 (s, C7), 49.4 (s, -CH₂-), 27.4 (s, -CH₃). HRMS (ESI⁺) *m/z* calcd. for C₁₁H₉ClNO₃ [M+H]⁺ 238.02655 found 238.0257.

2.3.4 Conclusions

In this work, we successfully applied a fragment-based approach to an extracellular target and after utilizing several biophysical methods identified two fragments **4** and **6** demonstrating low micromolar activity against ColH.

The co-crystal structure of fragment **4** revealed an exceptional binding mode as the fragment did not coordinate to the zinc cation. Exploration of different modifications yielded fragment **6** with a two-fold increase in potency. We further confirmed binding of this fragment to ColH-PD by a *K*_D determination by MST.

Our findings highlight the importance of fragment-based approaches in designing and obtaining potent and selective small-molecule inhibitors of important targets. Nevertheless, it should be stated that FBDD is not an amenable to all drug targets and there are limitations to

its application. For example, the necessity for using high concentrations of small fragments brings certain challenges such as identifying false-positive fragments.

Nevertheless, our results pave the way for considering extracellular metalloproteases as potential targets for fragment-based approaches. Exploration of such targets would not only extend the knowledge of FBDD methodology, but also underline the versatility of the antivirulence strategy in combating antibiotic resistance.

2.3.5 Supporting Information

Tables and Figures

Table S1. Concentration-dependent thermal shift assay screening results of selected fragments (n=2).

Fragment	Shift in ΔT_m (°C)		
	5 mM	1 mM	0.2 mM
F1	2.9 ± 0.6	1.2 ± 0.1	1.0 ± 0.2
F2	2.7 ± 0.4	1.4 ± 0.2	0.8 ± 0.1
F3	3.0 ± 0.4	1.2 ± 0.1	0.8 ± 0.1
F4	4.0 ± 0.2	1.7 ± 0.2	0.8 ± 0.1
F5	1.9 ± 0.4	1.9 ± 0.1	1.2 ± 0.1
F6	3.6 ± 0.4	1.5 ± 0.1	0.1 ± 0.6

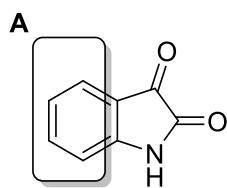
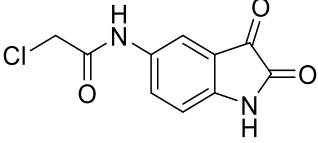
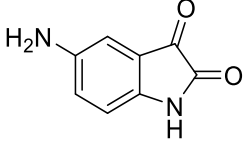
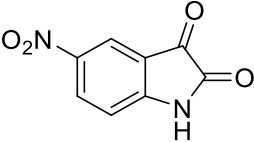
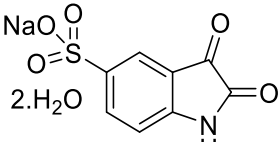
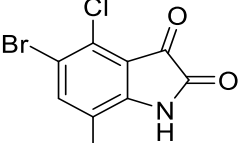
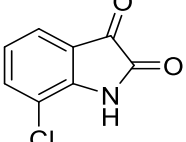
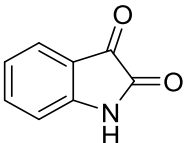
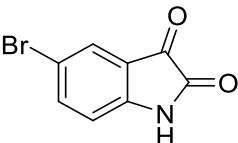


Table S2. Residual activity of ColH-PD (%) at 100 μ M and 10 μ M (n =3) of fragment **4** derivatives with modifications in position A.

Compound	Chemical Structure	Residual activity of ColH-PD (%) at 100 μ M
5		50 \pm 2
6		25 \pm 1
7		46 \pm 2
8		71 \pm 4
9		86 \pm 1
10		57 \pm 3
11		70 \pm 2

Compound	Chemical Structure	Residual activity of ColH-PD (%) at 10 μ M
12		82 \pm 2
13		77 \pm 3
14		83 \pm 2
15		91 \pm 9
16		98 \pm 8
17		57 \pm 4
18		68 \pm 4
19		40 \pm 2
20		70 \pm 4
21		60 \pm 2

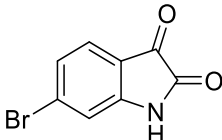
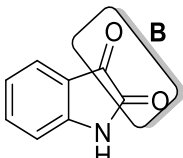
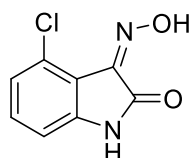
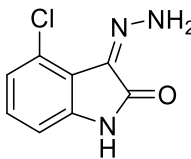
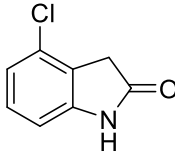
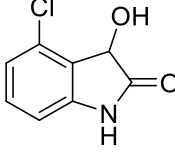
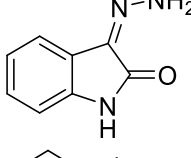
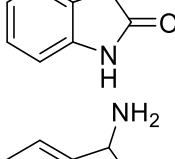
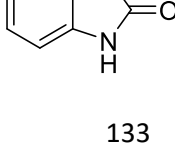
22		88 ± 5
23		42 ± 2
		

Table S3. Residual activity of ColH-PD (%) at 100 μM (n =3) of fragment 4 derivatives with modifications in position B.

Fragment	Chemical Structure	Residual activity of ColH-PD (%) at 100 μM
24		69 ± 2
25		88 ± 4
26		87 ± 2
27		75 ± 3
28		74 ± 2
29		91 ± 3
30		90 ± 2

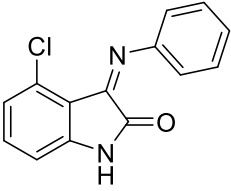
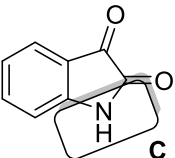
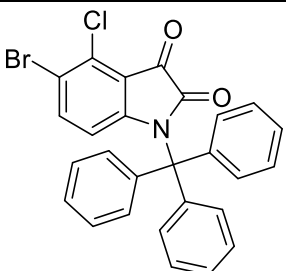
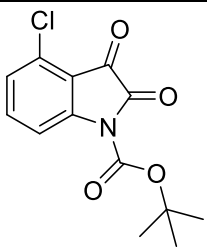
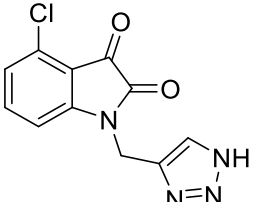
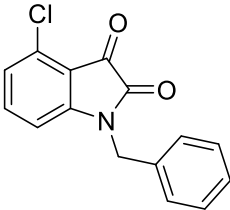
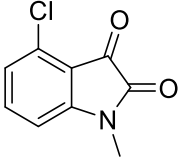
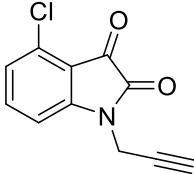
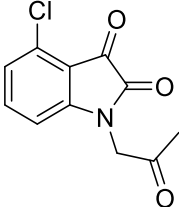
31		97 ± 5
32		56 ± 3
		

Table S4. Residual activity of ColH-PD (%) at 100 μ M (n =3) of fragment 4 derivatives with modifications in position C.

Fragment	Chemical Structure	Residual activity of ColH-PD (%) at 100 μ M
33		96 ± 5
34		94 ± 3
35		82 ± 5

36		86 ± 3
37		95 ± 3
38		73 ± 5
39		70 ± 5

2.4 *N*-Aryl Mercaptopropionamides as Broad-Spectrum Inhibitors of Metallo- β -Lactamases

Cansu Kaya, Jelena Konstantinović, Andreas M. Kany, Anastasia Andreas, Jan S. Kramer, Steffen Brunst, Lilia Weizel, Marco J. Rotter, Denia Frank, Samir Yahiaoui, Rolf Müller, Rolf W. Hartmann, Jörg Hauptenthal, Ewgenij Proschak, Thomas A. Wichelhaus, and Anna K. H. Hirsch

J. Med. Chem. 2022, 65, 5, 3913–3922, <https://doi.org/10.1021/acs.jmedchem.1c01755>.

N-Aryl Mercaptopropionamides as Broad-Spectrum Inhibitors of Metallo- β -Lactamases

Cansu Kaya, Jelena Konstantinović, Andreas M. Kany, Anastasia Andreas, Jan S. Kramer, Steffen Brunst, Lilia Weizel, Marco J. Rotter, Denia Frank, Samir Yahiaoui, Rolf Müller, Rolf W. Hartmann, Jörg Haupenthal, Ewgenij Proschak, Thomas A. Wichelhaus, and Anna K. H. Hirsch*

Cite This: *J. Med. Chem.* 2022, 65, 3913–3922

Read Online

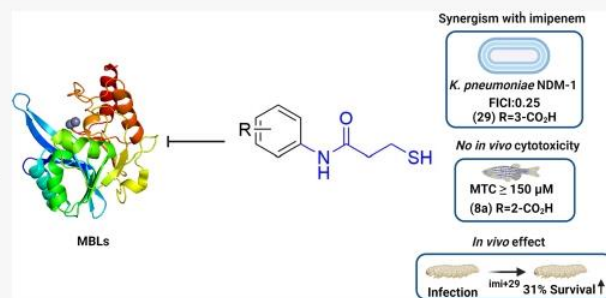
ACCESS |

Metrics & More

Article Recommendations

Supporting Information

ABSTRACT: Drug-resistant pathogens pose a global challenge to public health as they cause diseases that are extremely difficult to cure. Metallo- β -lactamases (MBLs) are a diverse set of zinc-containing enzymes that catalyze the hydrolysis of β -lactam drugs, including carbapenems, which are considered as the last resort to fight severe infections. To restore the activity of current β -lactam antibiotics and to offer an orthogonal strategy to the discovery of new antibiotics, we have identified a series of polar N-aryl mercaptopropionamide derivatives as potent inhibitors of several class B1 MBLs. We have identified a hit structure with high selectivity restoring the effect of imipenem and reducing minimum inhibitory concentration (MIC) values up to 256-fold in resistant isolates from *Escherichia coli*. Furthermore, the combination of imipenem with our inhibitor showed *in vivo* efficacy in a *Galleria mellonella* model, increasing the survival rate of infected larvae by up to 31%.



INTRODUCTION

Antibiotic resistance is a global health issue that is exceedingly limiting the possible treatments for many infectious diseases.^{1,2} The extensive misuse and overuse of antibiotics have caused many bacteria to evolve numerous mechanisms of resistance including gene mutations, target modifications, secretion of extracellular hydrolytic enzymes capable of evading antibacterial agents, and β -lactamases that are found mostly in the periplasm.³ Infections due to Gram-negative pathogens such as *Pseudomonas aeruginosa* and *Escherichia coli* are often treated with β -lactam antibiotics, which remain the most effective therapeutic agents to date.^{4,5} The expression of β -lactamases—enzymes that inhibit the effect of these drugs by hydrolyzing the β -lactam ring—therefore represents an enormous threat.^{2,6}

Based on their catalytic mechanism, the molecular classification initiated by Ambler divides β -lactamases into four categories.⁷ Classes A, C, and D comprise serine β -lactamases (SBLs), which cleave the β -lactam ring by nucleophilic attack of the catalytic serine residue. Compounds such as avibactam, clavulanic acid, sulbactam, or tazobactam can inhibit most of these enzymes.^{8–10} Class B contains metallo- β -lactamases (MBLs) bearing one or two zinc cations in the active site. MBLs are found to hydrolyze the core of β -lactam antibiotics by a nucleophilic water molecule.⁸ Based on their sequence identity, β -lactamases belonging to class B are further divided into B1, B2, and B3.^{11,12} Class B1 MBLs (B1MBLs) contain the largest number of clinically relevant

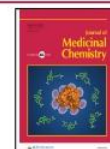
members, including Verona integron-encoded MBL (VIM), imipenemase (IMP), and New Delhi MBL (NDM).^{6,13}

The threat arising from multidrug-resistant pathogens can be tackled through the design of novel β -lactamase inhibitors, which usually do not have an intrinsic antibacterial activity but could extend the life of currently used β -lactam antibiotics.^{14,15} In contrast to the success of SBL inhibitors, there is a lack of clinically approved MBL inhibitors.^{16–18} Although a great number of chemical scaffolds has been reported over the years to target these metalloenzymes, factors such as shallow active sites or the lack of sequence similarity among various members pose a setback to develop potent broad-spectrum inhibitors of MBLs.^{19–23} Another serious challenge is to achieve selectivity of the designed inhibitors over several human metalloenzymes, which are involved in crucial metabolic pathways.^{24,25}

Although thiols are well-known for their chemical instability, they are the most investigated class of zinc-chelating agents to address a metalloenzyme.^{26–29} Following the discovery of thiomandelic acid (**1**, Figure 1)³⁰ as a broad-spectrum inhibitor of MBLs, structural studies of thiol-containing

Received: October 10, 2021

Published: February 21, 2022



drugs revealed the inhibitory potential of compounds like DL-captopril (**2**, Figure 1).^{31,32}

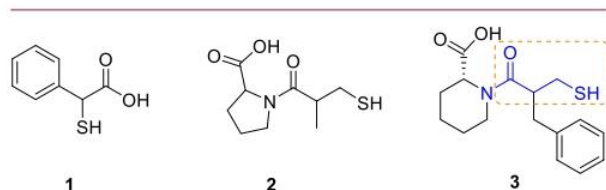


Figure 1. Chemical structures of known MBL inhibitors, thiomandelic acid **1**,³⁰ DL-captopril **2**,³¹ and piperidine derivative **3**.²⁸

In our recent work, we conducted a structure–activity relationship (SAR) study to extend the chemical space of the successful DL-captopril core.³³ A series of bioorthogonal methods revealed compound **3** (Figure 1) as a broad-spectrum inhibitor of three different B1MBLs (NDM, VIM, and IMP).³³ Following this discovery, a series of *N*-mercaptoacetamides were identified as dual inhibitors of several B1MBLs and the extracellular virulence factor elastase (LasB) secreted from *P. aeruginosa*.³⁴ Compound **4** (Figure 2) was identified as the hit

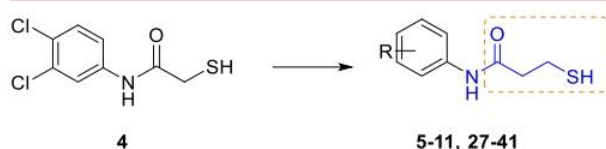


Figure 2. Structure of the dual inhibitor *N*-aryl mercaptoacetamide derivative³⁴ and the merged inhibitor *N*-aryl mercaptopropionamide. The common chemical motif found in compound **3** is indicated with an orange circle.

structure with a low micromolar inhibition against LasB (IC_{50} : $6.6 \pm 0.3 \mu\text{M}$) and displayed broad-spectrum inhibition of selected B1MBLs (IC_{50} (NDM-1): $0.6 \pm 0.04 \mu\text{M}$, IC_{50} (IMP-7): $0.9 \pm 0.1 \mu\text{M}$, IC_{50} (VIM-1): $2.2 \pm 0.2 \mu\text{M}$).³⁴

In this work, our objective was to present a merged inhibitor design, inspired by the structural similarity of MBL inhibitor **3**, bearing a piperidine moiety and the dual inhibitor *N*-aryl mercaptoacetamide derivative **4**.^{34,35} We envisaged that this structural motif could lead to inhibitors that can serve as successful anti-infectives to restore the activity of antibiotics against B1MBLs.

We designed and synthesized a series of *N*-aryl mercaptopropionamide derivatives and determined their inhibitory activity against clinically relevant B1MBLs produced by *E. coli*. Considering different factors such as inhibitory activity, $\log D_{7.4}$, and minimum inhibitory concentrations (MICs), we identified a hit structure showing a strong synergistic effect with imipenem by reducing MIC values up to 256-fold. Our most advanced inhibitor also showed an *in vivo* effect in a *Galleria mellonella* infection model, demonstrating the potential of this class of compounds as successful MBL inhibitors.

RESULTS AND DISCUSSION

In our previous work, we have shown the piperidine derivative to be beneficial against several different MBLs (**3**, Figure 1).³³ This was supported by an X-ray crystal structure of compound **3** with VIM-2 and the demonstration of a 32-fold decrease in MIC among imipenem-resistant *E. coli* isolates producing three

MBLs (NDM-1, VIM-1, and IMP-7).³³ Given that the virulence factor LasB also requires a zinc cation for its activity, compound **4**, which is a highly potent and selective inhibitor of LasB, also exhibited broad-spectrum inhibition of several MBLs, as expected.^{34,35}

Encouraged by the low micromolar activities of compound **4** against B1MBLs and given the fact that the thiol group in compound **3** is in β position, we designed a merged inhibitor scaffold (Figure 2) with an additional methylene spacer.

The first derivative of the new class of *N*-aryl mercaptopropionamides demonstrated up to eightfold improvement in activity against some of the MBLs. Broad-spectrum inhibitory activity of these compounds against all three enzymes along with the ease of modification of the *N*-aryl ring in various positions made this structural motif a valuable candidate for future evaluation. Consequently, we explored various functional groups and their effect on the activity toward clinically relevant B1MBLs. We synthesized 22 compounds, some of which have highly polar groups, with the aim to improve permeation of the bacterial cell wall.

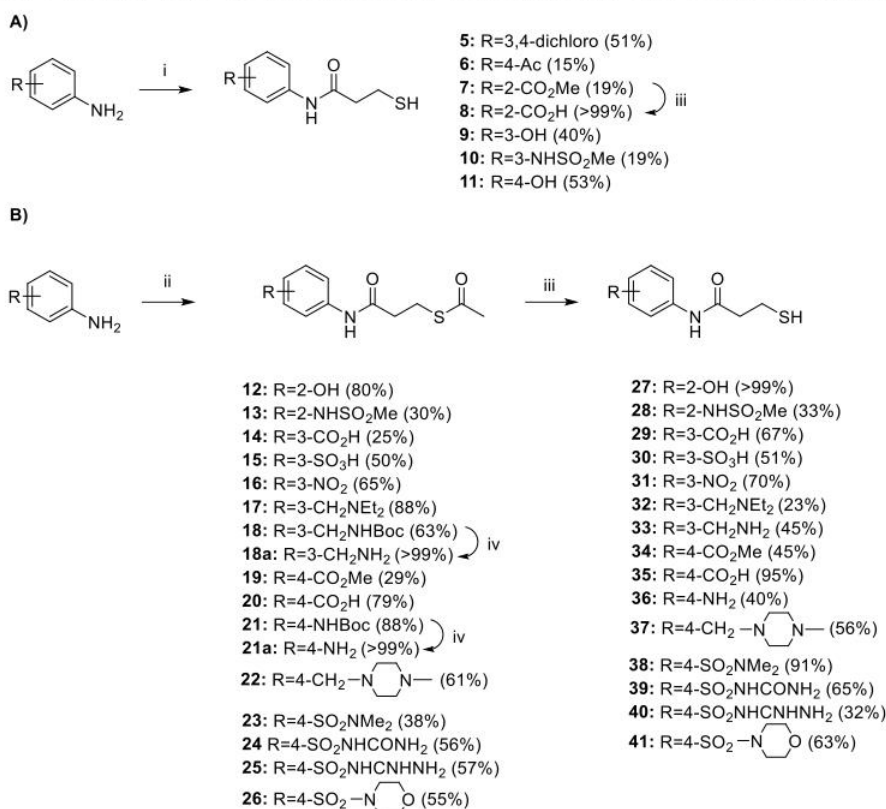
The outer membrane of Gram-negative bacteria hinders the uptake of many molecules. β -Lactamases are usually restricted to the periplasmic space in Gram-negative organisms, which represents a challenge when targeting these enzymes. A low $\log D_{7.4}$ value for a given inhibitor is therefore crucial for antibacterial agents targeting Gram-negative pathogens, as it facilitates penetration through the outer membrane.³⁶ By introducing more hydrophilic substituents, we aimed to investigate the effect of increased polarity and decreased $\log D_{7.4}$ on their activity.

Synthesis of *N*-Aryl Mercaptopropionamides. The overall synthetic route for mercaptopropionamide derivatives is outlined in Scheme 1. Following route A, neat reaction of the corresponding anilines with commercially available 3-mercapto-propionic acid at 120 °C afforded final compounds **5–11** in 15–99% yield. For the synthesis of compounds **27–41**, route B was followed, circumventing the problem of solubility and stability observed for some of the aniline derivatives when route A was used. For the activation of 3-(acetylthio)-mercapto-propionic acid, we used three different coupling reagents. Activation with EDC-HCl followed by the reaction with the corresponding aniline afforded compounds **12–14**, **16–18**, and **19–23** in 25–88% yield. A coupling reaction using HATU in the presence of diisopropylethylamine furnished compounds **24** and **25**, while activation of 3-(acetylthio) mercapto-propionic acid with ethylchloroformate in the presence of trimethylamine gave compounds **15** and **26** in moderate yield (50–57%). BOC deprotection of intermediate compounds **18a** and **21a** was achieved in the presence of TFA in dichloromethane (DCM) at room temperature. Hydrolysis of thioacetate using sodium hydroxide in methanol at room temperature provided final compounds **27–41** and hydrolysis of methyl ester provided compound **8** in 23–99% yield.

SARs of *N*-Aryl Mercaptopropionamides against Various B1MBLs. The inhibitory activity of all final compounds against three B1MBLs (Table 1) was determined in a kinetic fluorescence-based *in vitro* assay as described previously.⁵ All compounds were preincubated with the protein for 30 min before addition of the substrate.³²

Inspired by the structure of compound **3**, we first evaluated the effect of the carboxylic acid motif on the activity. Although the *para* derivative **35** did not show inhibition of IMP-7, it

Scheme 1. Reaction Scheme for the Synthesis of *N*-Aryl Mercaptopropionamides; (A) (i) 3-Mercaptopropionic Acid, Neat, Overnight, 120 °C; (B) (ii) 3-(Acetylthio)Mercaptopropionic Acid, EDC·HCl, DCM, Overnight, r.t. or 3-(Acetylthio)Mercaptopropionic Acid, ClCO₂Et, Et₃N, THF, Overnight, 0 °C to r.t. or 3-(Acetylthio)Mercaptopropionic Acid, HATU, DIEA, DCM, Overnight; (iii) 2 M NaOH, MeOH, 2–3 h, r.t; and (iv) TFA, DCM, Overnight, r.t.



showed the highest activity against VIM-1 and NDM-1 among all three regioisomers. *ortho*- and *meta*- derivatives (8 and 29) showed comparable activities toward all three targets.

The sulfonamide group is a substituent known to interact with various types of MBLs.³⁷ Examination of two isomers showed the *meta* position in compound 10 to be the most beneficial for activity for the three targets. Another commonly used motif, the hydroxyl group in compounds 9, 11, and 27, however, did not show a significant difference between the three regioisomers. All three derivatives displayed micromolar activities against NDM-1 and IMP-7 and sub-micromolar inhibition against VIM-1. In addition to the improvement in potency, we also aimed to improve the physicochemical profile of our MBL inhibitors. In view of this, we explored two heterocyclic substituents on the *N*-aryl ring, such as piperazine (37) and morpholine (41). Although we did not observe a substantial improvement in potency, VIM-1 activities were essentially preserved compared to the other two targets.

Accumulation studies performed in Gram-negative bacteria like *E. coli* provided some insights into understanding the desired molecular properties for inhibitors targeting these pathogens. Along with other parameters such as rotatable bonds (≤ 5) and globularity (≤ 0.25), the entry rules state that compounds with an ionizable nitrogen, especially primary amines, have a strong potential to accumulate in Gram-negative bacteria.^{38,39} To fulfill this criterion, we included two primary amines (33 and 36) and two tertiary amines (32 and 37). Again, all three derivatives, especially compound 36,

demonstrated a high inhibitory activity against VIM-1. However, considering the significantly lower activity on the other two enzymes, these compounds are much less suitable as broad-spectrum inhibitors. One interesting observation in this regard is that an electron-withdrawing nitro group in compound 31 in the *meta* position had an almost equal effect as a primary amine in the *para* position in compound 36.

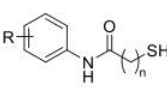
Notably, boosting hydrophilicity further with substituents such as sulfonic acid 30, sulfaguanidine 39, and sulfonyleurea 40 did not change the inhibitory effect significantly.

Overall, increasing the polarity of the substituents on the *N*-aryl ring did not have a significant effect on the activity against IMP-7 and NDM-1. Nevertheless, it yielded somewhat more potent inhibitors of VIM-1 such as compounds 35, 36, and 40. Although a general trend in VIM-1 inhibition is well-documented, most of the designed inhibitors show a broad-spectrum inhibition of the isolated enzymes. However, taking factors such as hydrophilicity and/or permeability into consideration for further stages, compounds 8, 29, 30, 35, 39, and 40 appear to be the most suitable candidates for further evaluation.

Evaluation of Inhibitory Activities against LasB.

Encouraged by the activity of our previous hit compound 4 against the zinc-containing virulence factor LasB, we evaluated the inhibitory potency of four *N*-arylmercaptpropionamides against this protease. None of the selected compounds (5, 29, 34, and 39) showed considerable inhibition of the enzyme at a concentration of 100 μ M (Table S1).

Table 1. Structures and Inhibitory Activities of *N*-Aryl Mercaptopropionamide Derivatives 3–11 and 27–41 against Three MBLs^a



Cp.	n	R	IC ₅₀ [μM]			
			NDM-1	IMP-7	VIM-1	logD _{7.4}
3	-	-	0.7 ± 0.05	4.6 ± 0.8	0.9 ± 0.1	0.49
4	1	3,4-di-Cl	0.6 ± 0.04	0.9 ± 0.1	2.2 ± 0.2	-
5	2	3,4-di-Cl	1.3 ± 0.0	5.0 ± 0.6	0.1 ± 0.0	5.34
6	2	4-Ac	1.5 ± 0.3	5.5 ± 0.1	0.4 ± 0.1	1.35
7	2	2-CO ₂ Me	1.3 ± 0.2	1.0 ± 0.1	>10	1.95
8	2	2-CO ₂ H	3.4 ± 0.1	4.1 ± 0.3	2.2 ± 0.2	-0.92
9	2	3-OH	2.7 ± 0.5	1.4 ± 0.2	0.1 ± 0.0	0.41
10	2	3-NHSO ₂ Me	2.2 ± 0.3	1.3 ± 0.0	1.3 ± 0.0	0.62
11	2	4-OH	4.0 ± 1.1	3.4 ± 0.7	0.2 ± 0.0	0.32
27	2	2-OH	2.2 ± 0.4	3.3 ± 0.4	0.2 ± 0.0	1.14
28	2	2-NHSO ₂ Me	7.0 ± 0.3	>10	1.9 ± 0.2	1.10
29	2	3-CO ₂ H	4.0 ± 0.0	6.4 ± 0.6	1.2 ± 0.0	-0.96
30	2	3-SO ₃ H	1.3 ± 0.0	3.6 ± 0.3	1.6 ± 0.1	-1.35
31	2	3-NO ₂	2.5 ± 0.2	2.6 ± 0.1	0.1 ± 0.0	2.21
32	2	3-CH ₂ NEt ₂	6.5 ± 0.4	5.5 ± 0.7	0.8 ± 0.1	0.24
33	2	3-CH ₂ NH ₂	5.5 ± 0.8	5.1 ± 0.3	1.0 ± 0.1	0.28
34	2	4-CO ₂ Me	2.8 ± 0.1	1.1 ± 0.7	0.1 ± 0.0	1.95
35	2	4-CO ₂ H	1.0 ± 0.4	>10	0.6 ± 0.0	-1.65
36	2	4-NH ₂	6.5 ± 0.5	2.1 ± 0.3	0.5 ± 0.0	-0.31
37	2	4-CH ₂ -N ₄	6.4 ± 0.6	5.8 ± 0.4	1.5 ± 0.1	0.28
38	2	4-SO ₂ NMe ₂	2.8 ± 0.1	2.1 ± 0.2	0.8 ± 0.0	1.70
39	2	4-SO ₂ NHCONH ₂	8.6 ± 0.2	12.6 ± 2.8	2.0 ± 0.1	-1.69
40	2	4-SO ₂ NHCNHNH ₂	2.1 ± 0.1	3.3 ± 0.4	0.5 ± 0.0	-0.50
41	2	4-SO ₂ -N ₄ O	2.5 ± 0.2	7.1 ± 1.4	1.7 ± 0.3	1.52

^aExperimental log *D*_{7.4} values are also shown for compounds 3, 5–11, and 27–41. Means and SD of at least two independent experiments. n.i. = no inhibition if inhibition <20% at 10 μM.

Table 2. Selectivity of Five Selected MBL Inhibitors against Six MMPs^a

cpd.	% inhibition at 100 μM						TACE
	MMP-1	MMP-2	MMP-3	MMP-7	MMP-8	MMP-14	
5	n.i.	14 ± 11	n.i.	n.i.	22 ± 29	18 ± 8	n.d.
8	n.i.	n.i.	17 ± 11	11 ± 4	n.i.	77 ± 7 ¹	n.i.
29	n.i.	n.i.	n.i.	n.i.	n.i.	61 ± 11 ²	n.i.
39	n.i.	88 ± 10 ³	n.i.	32 ± 7	n.i.	73 ± 6 ⁴	n.i.
40	n.i.	n.i.	n.i.	n.i.	n.i.	n.i.	32 ± 6

^aMeans and SD of at least two independent experiments. n.d. = not determined, n.i. = <10% inhibition; IC₅₀ values: ¹12 ± 3 μM, ²68 ± 20 μM, ³64 ± 6 μM, ⁴31 ± 3 μM.

Antibacterial Activities and MIC values. After evaluating the inhibitory activities of the compounds, the next step was the determination of their intrinsic antibacterial activity. Our MBL inhibitors should per se not harm the pathogens. Indeed, MIC assays with eight selected structures (5, 8, 29, 30, 33, and 38–40) did not reveal antibacterial effects against different MBL-expressing *E. coli* and *P. aeruginosa* isolates (Table S2).

Selectivity against Human Matrix Metalloproteases and TACE as Human Off-Targets. Human matrix metalloproteases (MMPs) are calcium-dependent zinc metalloproteases playing pivotal roles in numerous biochemical processes in humans.⁴⁰ To evaluate selectivity against these off-targets, the selectivity profile for five inhibitors was determined. We chose six MMPs containing two members of each class as representatives to provide information on the existing pocket

types.^{41–43} Even though a total of 26 of the 30 measured values indicated no or only low inhibition of these human proteases (Table 2), we determined IC₅₀ values for the four cases with the highest percent (%) inhibition at 100 μM. Notably, the lowest IC₅₀ value was 12 ± 3 μM (compound 8 toward MMP-14), which was still up to fivefold higher than the measured inhibition of MBLs.

Moreover, we investigated the selectivity of four inhibitors (8, 29, 39, and 40) against the human off-target tumor necrosis factor-α-converting enzyme, TACE (ADAM17). None of the selected compounds showed an inhibition of >50% at a concentration of 100 μM.

Cytotoxicity Assays. To support the promising selectivity observed for our inhibitors, we investigated their cytotoxicity against three human cell lines—HepG2 (hepatocellular carcinoma), HEK293 (embryonal kidney), and A549 (lung

carcinoma) cells. Five selected compounds (5, 8, 29, 39, and 40) showed no toxicity (<10% inhibition) at a concentration of 100 μ M, representing a good starting point for further *in vivo* studies.

In Vivo Toxicity in a Zebrafish Model. Encouraged by the high selectivity and low cytotoxicity, we subjected compounds 8, 39, and 40 to an *in vivo* toxicity study in zebrafish larvae. As zebrafish have a high genetic homology to humans, this valuable *in vivo* method can provide information on the type of toxicity encountered.⁴⁴ Furthermore, it can also evaluate lethality and malformation during the development of embryonic zebrafish.⁴⁵ In this experiment, our three selected inhibitors showed no *in vivo* toxicity with a maximum tolerated concentration (MTC) of $\geq 150 \mu$ M (Table S3).

Evaluation of Synergistic Effects between β -Lactam Antibiotics and Our MBL Inhibitors. MBLs pose a serious threat by efficiently inactivating β -lactam antibiotics including carbapenems, which are often regarded as the last line of drugs against infections caused by resistant pathogens.²³ Since the discovery of MBL inhibitors against carbapenem-resistant strains, combination therapy is a commonly employed method to treat these infections offering an alternative to the discovery of novel antibiotics.⁴⁶ The combination of a β -lactamase inhibitor with a β -lactam antibiotic can help maintain the activity of these drugs and improve their success in the clinic.

To assess the ability of our inhibitors to restore the antibacterial activity of a given β -lactam *in vitro*, we employed antibacterial susceptibility testing for selected structures. Our choice of accompanying β -lactam antibiotic was imipenem (imi), a broad-spectrum member of the carbapenem family.

Given that the penetration through the Gram-negative cell wall requires low log $D_{7.4}$ values, our strategy was to select those derivatives that are not only potent inhibitors of BIMBLs but also demonstrate a relatively low log $D_{7.4}$ value. Therefore, we first determined the lipophilicity of all compounds in an HPLC–MS based assay (Tables 1 and S4) and selected seven compounds (8, 29, 30, 33, 35, 39, and 40) to be tested in combination with imipenem at different concentrations against *E. coli* producing the three BIMBLs NDM-1, VIM-1, and IMP-1 (Tables S5–S7).

Our results showed that both inhibitors 8 and 29 demonstrate a synergistic effect with imipenem against *E. coli* producing NDM-1. They also showed concentration dependency and reduced the MIC values at their highest concentration up to 64-fold (8) and 256-fold (29) (Table S5). Table 3 illustrates the susceptibility effect on *E. coli* producing NDM-1 when compound 29 is combined with imipenem over several concentrations.

These results are in accordance with the experimental log $D_{7.4}$ of these inhibitors, as these values are among the five lowest values (Table 1). Given that the concentration needed to achieve an MIC value below 1 mg/L is in the range where we observed toxicity for MMP-14 (Table 2), we will particularly focus on this off-target during further development of the compounds.

Although compound 39 showed the lowest experimental log $D_{7.4}$ value among other selected structures, the lack of a synergistic effect observed for this structure can be attributed to its low inhibitory potency against selected MBLs (Table 1). On the other hand, for compounds 33 and 40 showing a good inhibitory profile, the poor MIC results overall can be explained by their relatively higher log $D_{7.4}$ values, potentially diminishing the possibility of penetration for these inhibitors.

Table 3. MIC (mg/L) of Imipenem in the Presence of Increasing Concentrations of Compound 29 in *E. coli* Producing NDM-1^a

inhibitor concentration (29)	imipenem MIC (mg/L) (fold change vs imi)
	128
+2 μ g/mL	128 (1)
+4 μ g/mL	128 (1)
+8 μ g/mL	64 (2)
+16 μ g/mL	64 (2)
+32 μ g/mL	8 (16)
+64 μ g/mL	2 (64)
+128 μ g/mL	≤ 0.5 (256)

^aAt 128 μ g/mL, the MIC value was determined to be ≤ 0.5 , and the significant fold change (≥ 4) is indicated in bold.

Despite having low log $D_{7.4}$ values and high inhibitory activities, surprisingly, compounds 30 and 35 were not able to demonstrate an effect in any of the isolates. The high inhibitory activity of compound 35 can be rationalized through different binding modes (Figure S1). Based on its low log $D_{7.4}$ value and its effect in reducing the MIC value for imipenem, we selected compound 29 for further evaluation.

To determine whether our inhibitor shows a synergistic effect on different isolates, we evaluated the intrinsic antimicrobial activity of compound 29 against 11 additional clinical isolates expressing various carbapenemases (MBL and non-MBL) (Table S8). After confirming that it does not harm these pathogens, we evaluated the MIC value of imipenem in combination with compound 29 at a fixed concentration of 128 mg/L against these isolates (Table 4). The change

Table 4. MIC (mg/L) of Imipenem (imi) in Combination with Compound 29 against 11 Selected Clinical Isolates Expressing Various MBLs^a

isolates	MIC (mg/L)	
	imi	imi + 29 (fold change vs imi)
<i>E. coli</i> NDM-7 (T2239)	32	2 (16)
<i>K. pneumoniae</i> NDM-1 (T2301)	16	0.5 (32)
<i>E. cloacae</i> NDM-1 (T2311)	8	1 (8)
<i>S. marcescens</i> NDM-1 (T2352)	256	4 (64)
<i>E. coli</i> NDM-5 (T2351)	8	2 (4)
<i>P. aeruginosa</i> VIM-1 (T2357)	256	256 (1)
<i>E. cloacae</i> VIM-1 (T2353)	4	2 (2)
<i>P. aeruginosa</i> IMP-1 (T2325)	16	16 (1)
<i>E. cloacae</i> GIM-1 (T2218)	2	2 (1)
<i>A. baumannii</i> OXA-23 (T2434)	32	32 (1)
<i>E. coli</i> KPC-2 (T2435)	4	4 (1)

^aThe median of three experiments is given. Compound 29 was tested at a single concentration of 128 mg/L. Significant fold change (≥ 4) is indicated in bold.

observed in MIC values for all transformants is shown in Table 4. With regards to clinical isolates, the effect of compound 29 focusing mostly on NDM-1 is noteworthy, reducing the MIC value up to 64-fold in *Serratia marcescens*. However, this effect is not observed for *P. aeruginosa* isolates, and MIC values remained unaffected.

After establishing a successful *in vitro* profile for our most promising structure 29 with different isolates, we evaluated its ability to rescue the effect of imipenem in a two-dimensional checkerboard analysis against a clinical *Klebsiella pneumoniae*

isolate producing NDM-1. A fractional inhibitory concentration index (FICI) value of 0.25 indicated the synergism of the hit compound **29** when combined with imipenem, verifying the rescue effect of our inhibitor (Figure 3).

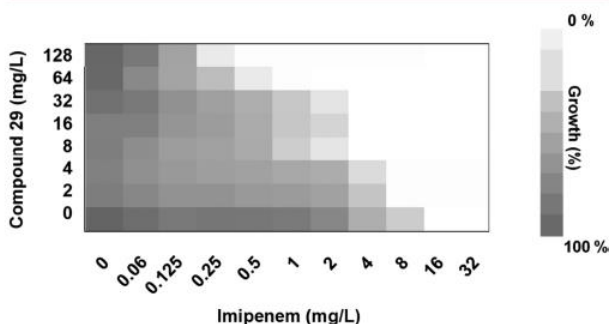


Figure 3. Compound **29** rescues the activity of imipenem. Microdilution checkerboard analysis showing the combined effect of compound **29** and imipenem against NDM-1-producing clinical isolate *K. pneumoniae* (T2301) over different concentrations. Data are means of three experiments.

Time-kill assays can monitor the effect of various concentrations of an inhibitor over time with respect to the different growth stages of the bacteria and provide more information on synergism.⁴⁷ Therefore, we evaluated the effect of 128 mg/L compound **29** in a time-kill analysis on resistant *K. pneumoniae* producing NDM-1 (T2301) over 24 h (Figure 4). As expected, same as the control group with nontreated

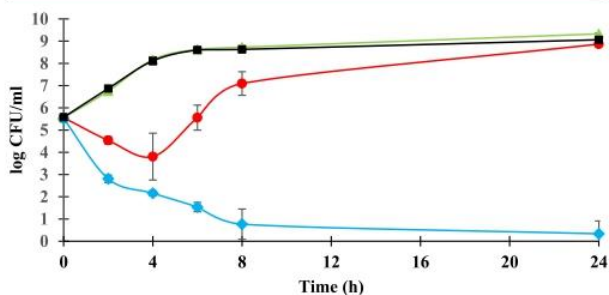


Figure 4. Time-kill kinetics involving imipenem-resistant *K. pneumoniae* producing NDM-1 (T2301). ■ (black), growth control; ▲ (green), +**29** (128 mg/L); ● (red), +imi (0.5× MIC; 8 mg/L); ◆ (blue), +imi (0.5× MIC; 8 mg/L) +**29** (128 mg/L). Curves represent mean values from three different experiments. Error bars indicate standard deviation.

bacteria, bacteria treated with 128 mg/L compound **29** were unaffected as the inhibitor lacks intrinsic antimicrobial activity. Even though imipenem (0.5× MIC; 8 mg/L) can reduce the growth by itself, this effect is significantly lowered after 4 h due to the presence of MBLs. When bacteria are treated with 8 mg/L imipenem in combination with 128 mg/L compound **29**, a significant reduction in growth over 24 h is observed. These results indicate the potential of our inhibitor **29**, exerting a pronounced synergistic effect.

Demonstration of an *In Vivo* Effect in a *G. mellonella* Infection Model. The *G. mellonella* infection model is a commonly used method to evaluate treatment options for infections caused by pathogenic bacteria and to demonstrate the *in vivo* efficacy of inhibitors.^{48,49} Owing to its potency,

selectivity, and strong synergistic effect in combination with imipenem, as demonstrated in several different isolates, we subjected compound **29** to such an *in vivo* infection study (Figure 5). Survival kinetics were determined based on the differences between treated and untreated larvae.

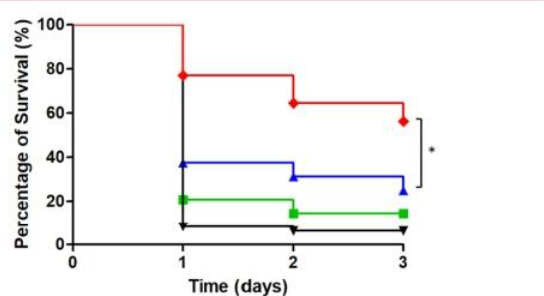


Figure 5. Kaplan–Meier survival curves of *G. mellonella* larvae infected with imipenem-resistant *K. pneumoniae* producing NDM-1 (T2301) and treated with imipenem (imi; 0.12 μg) and compound **29** (38.4 μg) in monotherapy or combination therapy. The curves represent pooled data from three independent experiments using 16 *G. mellonella* larvae in each experiment. **P* = <0.001. Error bars indicate standard deviation.

In this experiment, *G. mellonella* larvae are infected with imipenem-resistant *K. pneumoniae* producing NDM-1 (T2301). The survival rate of the larvae was measured over three days. After one day, it dropped below 20% for both control groups receiving no treatment (green) and treated only with compound **29** (black). This was expected since compound **29** does not exert an antimicrobial effect by itself. The treatment of larvae with imipenem (blue) increased the survival rate only up to 25% over the course of three days, as the effect of the antibiotic was significantly diminished by the predicted accumulation of MBLs. Combination of the inhibitor **29** (3.84 μg/μL) with imipenem (0.01 μg/μL) showed a significant increase in the percentage of survival of larvae after three days up to 56%. These results validate our hit structure as a promising anti-infective to restore the activity of β-lactam antibiotics against MBLs. It also confirms that the boost in hydrophilicity along with synergism between our inhibitor and selected antibiotic successfully translates to an *in vivo* effect.

CONCLUSIONS

In this study, we identified a series of *N*-aryl mercaptopropionamides with low micromolar inhibitory activities against three clinically relevant B1MBLs. Our objective was to provide a new anti-infective β-lactam/β-lactamase inhibitor combination to combat MBL-resistant pathogens. To improve Gram-negative cell–wall penetration, we decreased the lipophilicity of our inhibitors with additional hydrophilic substituents. The overall efficacy of this class of compounds is supported by their high selectivity over selected off-targets and their lack of toxicity, as represented by an *in vivo* toxicity study in zebrafish.

We estimated the penetration efficacy of our inhibitors based on their experimental log $D_{7.4}$ values. This estimate along with inhibitory activities served as a rational selection criterion as to which inhibitors should be further evaluated. Consequently, we identified hit compound **29** with a good log $D_{7.4}$ value that restored imipenem activity by significantly reducing MIC

values for several resistant MBL-producing bacteria including clinical isolates.

The synergistic effect and the time-kill studies of inhibitor **29** also translated to an *in vivo* effect in *K. pneumoniae* producing NDM-1 in a *G. mellonella* infection model. The survival of *G. mellonella* larvae increased up to 56% after three days when treated with imipenem in combination with compound **29**.

To the best of our knowledge, our hit structure proves to be the most advanced in terms of incorporating several different factors such as inhibition of several MBLs and high selectivity that can address the challenges associated with thiol-based MBL inhibitors. As there is an increasing need for novel anti-infective combinations to treat MBL-resistant pathogens, further exploration of combination therapy with different β -lactams and transformants is highly desirable to achieve optimum performance of these inhibitors. Further animal studies should be explored to prove the eligibility of these compounds for clinical studies. Conceivably, this structural motif has the potential to fill the increasing void for clinically approved MBL inhibitors in the battle against the emerging resistant bacteria worldwide.

EXPERIMENTAL SECTION

Chemistry. All reagents were received from commercial suppliers without further purification. Procedures were not optimized regarding yield. NMR spectra were recorded on a Bruker AV 500 (500 MHz) spectrometer. Chemical shifts are given in parts per million (ppm) and referenced against the residual proton, ^1H , or carbon, ^{13}C , with resonances of the >99% deuterated solvents as an internal reference. Coupling constants (J) are given in Hertz (Hz). Data are reported as follows: chemical shift, multiplicity (s = singlet, d = doublet, t = triplet, q = quartet, m = multiplet, dt = doublet of triplets, and br = broad and combinations of these) coupling constants, and integration. Liquid chromatography–mass spectrometry was performed on an LC–MS system, consisting of a Dionex UltiMate 3000 pump, autosampler, column compartment and detector (Thermo Fisher Scientific, Dreieich, Germany), and ESI quadrupole MS (MSQ Plus or ISQ EC, Thermo Fisher Scientific, Dreieich, Germany). High-resolution mass was determined by LC–MS/MS using a Thermo Scientific QExactive Focus Orbitrap LC–MS/MS system. The purity of all synthesized compounds was determined by LC–MS using the area percentage method on the UV trace recorded at a wavelength of 254 nm and found to be >95%.

General Procedure A-1: Synthesis of Thioacetate Derivatives 12–14, 16–18, and 19–23 Using EDC·HCl as a Coupling Reagent. 3-(Acetylthio)propionic acid (1.2–1.5 equiv) was placed in a vial and dissolved in DCM. EDC·HCl (1.2–1.5 equiv) was added and left to form a cloudy solution. Then, the corresponding amine (1.0 equiv) was added, and the reaction was stirred at r.t. The reaction was monitored using TLC or LC–MS. The reaction was quenched with 1 M HCl until pH = 1. The organic phase was washed with saturated aqueous NaCl solution (1 \times) and then dried over anhydrous Na_2SO_4 . The product was filtered, concentrated and purified by column chromatography.

General Procedure A-2: Synthesis of Thioacetate Derivatives 15 and 26 Using Ethylchloroformate as a Coupling Reagent. 3-(Acetylthio)propionic acid (1.2 equiv) was dissolved in tetrahydrofuran (THF) and cooled in an ice bath. Et_3N (1.2 equiv) was added, followed by addition of ClCO_2Et (1.3 equiv). After 5 min, the ice bath was removed, and the mixture was stirred at r.t. for 30 min. The corresponding amine (1.0 equiv) was slowly added. The reaction was monitored using TLC or LC–MS. After the reaction was completed, volatiles were evaporated at reduced pressure, and the crude product was purified using column chromatography or preparative HPLC (H_2O + 0.05% FA/ACN + 0.05% FA 95:5 \rightarrow 5:95).

General Procedure A-3: Synthesis of Thioacetate Derivatives 24 and 25 Using HATU as a Coupling Reagent. 3-(Acetylthio)propionic acid (1.5 equiv), HATU (1.5 equiv), and DIEA (1.5 equiv) were dissolved in DCM. The corresponding amine (1.0 equiv) was added, and the reaction was stirred at r.t. for 2 days. Volatiles were evaporated at reduced pressure, and the crude product was purified using preparative HPLC (H_2O + 0.05% FA/ACN + 0.05% FA 95:5 \rightarrow 5:95).

General Procedure B: Hydrolysis of Thioacetate to Obtain Derivatives 8 and 27–41. Thioacetate (1.0 equiv) was dissolved in methanol or dioxane under an Ar atmosphere, and 2 M aq. solution of NaOH (2.0–3.0 equiv) or solid NaOH (3.0–4.0 equiv) was added. The reaction was stirred at r.t. for 1–2 h. After quenching with 1 M HCl, the product was extracted with EtOAc (3 \times). The combined organic extracts were washed with saturated aqueous NaCl solution, dried over anhydrous Na_2SO_4 , and filtered. The solvent was removed at reduced pressure. Purification was done via flash chromatography. In the case of more polar compounds, instead of quenching the reaction with 1 M HCl, the pH was adjusted to acidic using Amberlite IR-120. After filtration, Amberlite was washed with MeOH (3 \times), the solvent was evaporated, and the product was purified using preparative HPLC (H_2O + 0.05% FA/ACN + 0.05% FA 95:5 \rightarrow 5:95).

General Procedure C: Synthesis of Free Thiols 5–11. Aniline (1.0 equiv) was placed in a crimp vial. The vial was evacuated and flushed with Ar followed by addition of 3-mercaptopropionic acid (1.2–1.5 equiv). The vial was flushed with Ar again and heated to 120 $^\circ\text{C}$ for 5 h. The crude product was purified using reverse-phase flash chromatography (H_2O + 0.1% FA/ACN + 0.1% FA 95:5 \rightarrow 5:95).

General Procedure D: Deprotection of the tert-Butyloxycarbonyl Group to Obtain Compounds 18a and 21a. To a solution of the corresponding Boc-protected compound (1.0 equiv) in DCM was added TFA (5.0–7.0 equiv), and the mixture was stirred at r.t. overnight. Volatiles were evaporated, and the crude product was used in the next step without further purification.

Synthesis of 3-(3-(Acetylthio)propanamido)benzoic Acid (14). Compound **14** was synthesized according to general procedure A-1, using 3-aminobenzoic acid (130 mg, 0.95 mmol), 3-(acetylthio)propionic acid (210 mg, 1.42 mmol), and EDC·HCl (272 mg, 1.42 mmol) in DCM (10 mL). The product was purified using preparative HPLC. The final product was obtained as white powder (62 mg, 25%) ^1H NMR (500 MHz, $\text{DMSO}-d_6$): δ ppm 12.96 (br s, 1H), 10.18 (s, 1H), 8.21 (s, 1H), 7.79 (d, J = 6.6 Hz, 1H), 7.61 (d, J = 7.9 Hz, 1H), 7.41 (t, J = 7.9 Hz, 1H), 3.09 (t, J = 6.8 Hz, 2H), 2.65 (t, J = 6.8 Hz, 2H), 2.33 (s, 3H). ^{13}C NMR (126 MHz, $\text{DMSO}-d_6$): δ ppm 195.5, 169.5, 167.2, 139.4, 131.3, 129.1, 124.1, 123.1, 119.8, 36.0, 30.6, 24.3. HRMS (ESI $^+$) m/z : calcd for $\text{C}_{12}\text{H}_{14}\text{NO}_4\text{S}$ [$\text{M} + \text{H}$] $^+$, 268.06380; found, 268.06381.

Synthesis of 3-(3-Mercaptopropanamido)benzoic Acid (29). Compound **29** was synthesized according to general procedure B, using compound **14** (62 mg, 0.23 mmol) and NaOH (37 mg, 0.92 mmol) in MeOH (2 mL). The product was purified using preparative HPLC. The final product was obtained as white powder (35 mg, 67%). ^1H NMR (500 MHz, $\text{DMSO}-d_6$): δ ppm 12.95 (s, 1H), 10.15 (s, 1H), 8.24 (s, 1H), 7.81 (dd, J = 8.1, 0.9 Hz, 1H), 7.61 (d, J = 7.7 Hz, 1H), 7.42 (t, J = 7.9 Hz, 1H), 2.75 (q, J = 7.2 Hz, 2H), 2.64 (t, J = 6.8 Hz, 2H), 2.40 (t, J = 8.0 Hz, 1H); δ ppm 169.6, 167.2, 139.3, 131.3, 129.0, 124.0, 123.2, 119.8, 40.3, 19.6. HRMS (ESI $^-$) m/z : calcd for $\text{C}_{10}\text{H}_{10}\text{NO}_3\text{S}$ [$\text{M} - \text{H}$] $^-$, 224.03868; found, 224.03814.

Protein Expression and Purification. The expression of IMP-7, VIM-1, and NDM-1 was performed according to the protocol previously described with slight modifications.⁵⁰

In Vitro Inhibition Assays. Activity assays for NDM-1, VIM-1, VIM-2, and IMP-7 were carried out, as previously described.⁵⁰ Final protein concentrations were 0.5 nM (NDM-1), 4.0 nM (VIM-1), and 0.1 nM (IMP-7) in a 50 mM HEPES buffer (pH 7.5, 0.01% Triton X-100). The substrate (Fluorocillin, synthesized as described⁵¹) was dissolved in assay buffer to a final concentration of 888 nM. Test compounds were dissolved and prediluted in DMSO (final concentration: 1%). In a black polystyrol 96-well plate (Corning), a total of 1 μL of the respective inhibitor solution at different

concentrations was incubated with 89 μL of the respective protein dilution in buffer at room temperature for 30 min. 10 μL of substrate solution was added. The readout of the emitted fluorescence was started immediately (45 s for 30 cycles) using a Tecan Infinite F200Pro (Tecan Group Ltd.; excitation at 495 nm and emission at 525 nm). Blank controls were performed without the enzyme. Positive controls were performed with the enzyme but without an inhibitor. The inhibitory activity of each test compound was measured in three independent experiments. For calculation of IC_{50} values, data obtained from measurements with eight different inhibitor concentrations were used. For the evaluation of the sigmoidal dose response equation (variable slope with four parameters), GraphPad Prism 5 (GraphPad Software, La Jolla, CA, USA) was used.

Cytotoxicity Assays. Cytotoxicity assays on HepG2, HEK293, and A549 cells were performed as described previously.⁵²

Selectivity Assays. Selectivity assays on various MMPs and TACE were performed as described previously.^{52,53}

MIC Assays. MICs of imipenem plus compounds against MBL-positive and MBL-negative clinical isolates and/or against transformed *E. coli* strains producing different recombinant MBLs were determined according to a microdilution method established by the Clinical and Laboratory Standards Institute (CLSI).⁵⁴

Time-Kill Kinetics. The antimicrobial activity of imipenem or imipenem + 29 against *K. pneumoniae* producing NDM-1 (T2301) was determined by the time-kill method following CLSI guidelines.⁵⁵ Bacterial suspensions supplemented with imipenem (0.5 \times MIC; 8 mg/L) and/or 29 (128 mg/L) were incubated for various time intervals (0, 2, 4, 6, 8, and 24 h) at 37 $^{\circ}\text{C}$, and viability counts were performed by plating 100 μL onto blood agar plates. Experiments were performed in triplicate. Bactericidal activity was defined as ≥ 3 log killing after 24 h.

Fractional Inhibitory Concentration Index. The checkerboard assay was performed to test for synergy *in vitro*. The microtiter plates were set up with serial doubling dilutions of compounds (2–128 mg/L) and imipenem (0.06–128 or 0.5–512 mg/L). FICIs ≤ 0.5 were defined as synergistic; FICIs from >0.5 to ≤ 1 were defined as an additive; FICIs from 1 to ≤ 4 were defined as indifferent; and FICIs > 4 were defined as antagonistic.⁴⁶

Lipophilicity Determination. Log $D_{7.4}$ was analyzed using an HPLC–MS based method. The retention time of 12 compounds with known log $D_{7.4}$ was determined and plotted toward their log $D_{7.4}$. Linear regression was used to determine the log $D_{7.4}$ of unknown compounds. Analysis was performed using a Dionex Ultimate 3000 HPLC system coupled to a TSQ Quantum Access MAX (Thermo Fisher, Dreieich, Germany) with the following conditions: EC150/2 NUCLEODUR C18 Pyramid column, 5 μM (Macherey Nagel, Düren, Germany); eluent A: 50 mM NH_4OAc pH 7.4, eluent B: acetonitrile, and flow: 0.6 mL/min. The gradient was set to 0–100% B from 0 to 2.5 min, 100% B from 2.5 to 3.0 min, 100–0% B from 3.0 to 3.2 min, and 0% B from 3.2–5.0.

In Vivo Zebrafish Toxicity Assay. Toxicity testing was performed according to the procedure described in the literature with minor modifications using zebrafish embryos of the AB wild-type line at 1 day after fertilization.⁵⁶ Embryos were collected and kept in a Petri dish at 28 $^{\circ}\text{C}$ until the next day in 0.3 \times Danieau's medium (17 mM NaCl, 2 mM KCl, 1.8 mM $\text{Ca}(\text{NO}_3)_2$, 1.5 mM HEPES (pH 7.1–7.3), 0.12 mM MgSO_4 , and 1.2 μM methylene blue). The toxicity assay was performed using a 96-well plate with one embryo per well and 10 embryos per condition. To obtain compound concentrations between 30 and 150 μM , solutions of compounds 8, 39, and 40 were prepared freshly using 0.3 \times Danieau's medium with a final DMSO concentration of 1% (v/v). Single zebrafish embryos were placed in wells and directly incubated in the corresponding compound solutions. Monitoring of developmental defects, heart rate, touch-evoked locomotion response, and survival rate was done daily (up to 120 hpf) *via* microscopy (Table S3). All the described experiments were performed with zebrafish embryos <120 h after fertilization (hpf) and are not classified as animal experiments according to EU Directive 2010/63/EU. Protocols for husbandry and care of adult

animals are in accordance with the German Animal Welfare Act (§11 Abs. One TierSchG).

G. mellonella Infection Model. Larvae of the greater wax moth (*G. mellonella*) infected with a clinical *K. pneumoniae* isolate producing NDM-1 (T2301) were treated with imipenem or compound 29 or both antibiotics. A 10 μL Hamilton syringe was used to inject 10 μL aliquots of the inoculum, that is, approx. 10^5 bacteria, into the haemocoel of each caterpillar *via* the last left proleg. Bacterial colony counts on blood agar were used to confirm the injected cfu. A total of 10 μL of anti-infectives (0.12 μg of imipenem and/or 38.4 μg of cpd. 29) was then administered by injection into a different proleg 30 min thereafter. In total, 16 randomly chosen caterpillars were used for each group of an experiment. For all experiments, two control groups were included consisting of caterpillars that were either injected twice with PBS or that received no injection. Larvae were incubated in Petri dishes at 37 $^{\circ}\text{C}$ and scored daily for survival. Larvae were considered dead if they repeatedly did not respond to touch. Survival kinetics were generated to evaluate differences between treated and untreated caterpillars over a period of 3 days. Experiments were performed independently in triplicate, and data were pooled.

■ ASSOCIATED CONTENT

Supporting Information

The Supporting Information is available free of charge at <https://pubs.acs.org/doi/10.1021/acs.jmedchem.1c01755>.

General experimental procedures; synthesis of all compounds; supporting figures and tables; NMR spectra of final compounds; and LCMS spectra of key compounds (PDF)

Molecular formula strings (CSV)

■ AUTHOR INFORMATION

Corresponding Author

Anna K. H. Hirsch – Helmholtz Institute for Pharmaceutical Research Saarland, (HIPS)—Helmholtz Centre for Infection Research (HZI), 66123 Saarbrücken, Germany; Department of Pharmacy, Saarland University, 66123 Saarbrücken, Germany; Helmholtz International Lab for Anti-infectives, 66123 Saarbrücken, Germany; orcid.org/0000-0001-8734-4663; Email: anna.hirsch@helmholtz-hips.de

Authors

Cansu Kaya – Helmholtz Institute for Pharmaceutical Research Saarland, (HIPS)—Helmholtz Centre for Infection Research (HZI), 66123 Saarbrücken, Germany; Department of Pharmacy, Saarland University, 66123 Saarbrücken, Germany

Jelena Konstantinović – Helmholtz Institute for Pharmaceutical Research Saarland, (HIPS)—Helmholtz Centre for Infection Research (HZI), 66123 Saarbrücken, Germany

Andreas M. Kany – Helmholtz Institute for Pharmaceutical Research Saarland, (HIPS)—Helmholtz Centre for Infection Research (HZI), 66123 Saarbrücken, Germany

Anastasia Andreas – Helmholtz Institute for Pharmaceutical Research Saarland, (HIPS)—Helmholtz Centre for Infection Research (HZI), 66123 Saarbrücken, Germany; Department of Pharmacy, Saarland University, 66123 Saarbrücken, Germany

Jan S. Kramer – Institute of Pharmaceutical Chemistry, Goethe University Frankfurt, 60438 Frankfurt, Germany

Steffen Brunst – Institute of Pharmaceutical Chemistry, Goethe University Frankfurt, 60438 Frankfurt, Germany

Lilia Weizel – Institute of Pharmaceutical Chemistry, Goethe University Frankfurt, 60438 Frankfurt, Germany

Marco J. Rotter – Institute of Pharmaceutical Chemistry, Goethe University Frankfurt, 60438 Frankfurt, Germany

Denia Frank – Institute of Medical Microbiology and Infection Control, University Hospital Frankfurt, 60596 Frankfurt, Germany

Samir Yahiaoui – Helmholtz Institute for Pharmaceutical Research Saarland, (HIPS)—Helmholtz Centre for Infection Research (HZI), 66123 Saarbrücken, Germany; orcid.org/0000-0001-5134-5007

Rolf Müller – Helmholtz Institute for Pharmaceutical Research Saarland, (HIPS)—Helmholtz Centre for Infection Research (HZI), 66123 Saarbrücken, Germany; Department of Pharmacy, Saarland University, 66123 Saarbrücken, Germany; Helmholtz International Lab for Anti-infectives, 66123 Saarbrücken, Germany; orcid.org/0000-0002-1042-5665

Rolf W. Hartmann – Helmholtz Institute for Pharmaceutical Research Saarland, (HIPS)—Helmholtz Centre for Infection Research (HZI), 66123 Saarbrücken, Germany; Department of Pharmacy, Saarland University, 66123 Saarbrücken, Germany; orcid.org/0000-0002-5871-5231

Jörg Haupenthal – Helmholtz Institute for Pharmaceutical Research Saarland, (HIPS)—Helmholtz Centre for Infection Research (HZI), 66123 Saarbrücken, Germany

Ewgenij Proschak – Institute of Pharmaceutical Chemistry, Goethe University Frankfurt, 60438 Frankfurt, Germany; orcid.org/0000-0003-1961-1859

Thomas A. Wichelhaus – Institute of Medical Microbiology and Infection Control, University Hospital Frankfurt, 60596 Frankfurt, Germany; orcid.org/0000-0002-4029-2955

Complete contact information is available at: <https://pubs.acs.org/10.1021/acs.jmedchem.1c01755>

Notes

The authors declare the following competing financial interest(s): C.K., J.K., A.K., S.Y., J.H., R.H., E.P., T.W. and A.K.H.H. are co-inventors on a pending EU patent application EP20 164 855.7 that incorporates methods outlined in this manuscript.

ACKNOWLEDGMENTS

The authors would like to acknowledge and thank Simone Amann, Jeannine Jung, Selina Wolter, and Dennis Jener for their work with analytical assays. A.K.H.H. gratefully acknowledges funding from the Helmholtz-Association's Initiative and Networking Fund, and J.K. acknowledges funding by the Alexander von Humboldt Foundation. E.P. thanks Deutsche Forschungsgemeinschaft (DFG, Heisenberg-Professur PR1405/7-1) for financial support.

ABBREVIATIONS

A549, lung carcinoma cell line; DCM, dichloromethane; DMEM, Dulbecco's modified Eagle medium; FICI, fractional inhibitory concentration index; HDAC, histone deacetylase; HEK293, embryonal kidney cell line; HepG2, hepatocellular carcinoma cell line; IC₅₀, half maximal inhibitory concentration; LasB, *P. aeruginosa* elastase; MBL, metallo- β -lactamase; MIC, minimum inhibitory concentration; MTC, maximum tolerated concentration; MMP, human matrix

metalloprotease; SAR, structure–activity relationship; THF, tetrahydrofuran

REFERENCES

- (1) McGeary, R. P.; Tan, D. T.; Schenk, G. Progress toward Inhibitors of Metallo- β -Lactamases. *Future Med. Chem.* **2017**, *9*, 673–691.
- (2) Richardson, L. A. Understanding and Overcoming Antibiotic Resistance. *PLoS Biol.* **2017**, *15*, No. e2003775-5.
- (3) Hoffman, P. S. Antibacterial Discovery: 21st Century Challenges. *Antibiotics* **2020**, *9*, 213.
- (4) Meini, M.-R.; Llarrull, L. I.; Vila, A. J. Overcoming Differences: The Catalytic Mechanism of Metallo- β -Lactamases. *FEBS Lett.* **2015**, *589*, 3419–3432.
- (5) Worthington, R. J.; Melander, C. Overcoming Resistance to β -Lactam Antibiotics. *J. Org. Chem.* **2013**, *78*, 4207–4213.
- (6) Mojica, M. F.; Bonomo, R.; Fast, W. B1-Metallo-Beta-Lactamases: Where Do We Stand? *Curr. Drug Targets* **2016**, *17*, 1029–1050.
- (7) Ambler, R. P. The Structure of β -Lactamases. *Philos. Trans. R. Soc. London, Ser. B* **1980**, *289*, 321–331.
- (8) Bush, K.; Bradford, P. A. Interplay between β -Lactamases and New β -Lactamase Inhibitors. *Nat. Rev. Microbiol.* **2019**, *17*, 295–306.
- (9) Bush, K.; Jacoby, G. A. Updated Functional Classification of β -Lactamases. *Antimicrob. Agents Chemother.* **2010**, *54*, 969–976.
- (10) Ball, M.; Boyd, A.; Ensor, G. J.; Evans, M.; Golden, M.; Linke, S. R.; Milne, D.; Murphy, R.; Telford, A.; Kalyan, Y.; Lawton, G. R.; Racha, S.; Ronsheim, M.; Zhou, S. H. Development of a Manufacturing Route to Avibactam, a β -Lactamase Inhibitor. *Org. Process Res. Dev.* **2016**, *20*, 1799–1805.
- (11) Bebrone, C. Metallo- β -Lactamases (Classification, Activity, Genetic Organization, Structure, Zinc Coordination) and Their Superfamily. *Biochem. Pharmacol.* **2007**, *74*, 1686–1701.
- (12) Bush, K.; Bradford, P. A. β -Lactams and β -Lactamase Inhibitors: An Overview. *Cold Spring Harbor Perspect. Med.* **2016**, *6*, a025247.
- (13) Green, V. L.; Verma, A.; Owens, R. J.; Phillips, S. E. V.; Carr, S. B. Structure of New Delhi Metallo- β -Lactamase 1 (NDM-1). *Acta Crystallogr., Sect. F: Struct. Biol. Cryst. Commun.* **2011**, *67*, 1160–1164.
- (14) Toussaint, K. A.; Gallagher, J. C. β -Lactam/ β -Lactamase Inhibitor Combinations: From Then to Now. *Ann. Pharmacother.* **2015**, *49*, 86–98.
- (15) Wade, N.; Tehrani, K. H. M. E.; Bröchle, N. C.; Haren, M. J.; Mashayekhi, V.; Martin, N. I. Mechanistic Investigations of Metallo- β -Lactamase Inhibitors: Strong Zinc Binding Is Not Required for Potent Enzyme Inhibition. *ChemMedChem* **2021**, *16*, 1651–1659.
- (16) Somboro, A. M.; Osei Sekyere, J.; Amoako, D. G.; Essack, S. Y.; Bester, L. A. Diversity and Proliferation of Metallo- β -Lactamases: A Clarion Call for Clinically Effective Metallo- β -Lactamase Inhibitors. *Appl. Environ. Microbiol.* **2018**, *84*, No. e00698-18.
- (17) Papp-Wallace, K. M.; Bonomo, R. A. New β -Lactamase Inhibitors in the Clinic. *Infect. Dis. Clin.* **2016**, *30*, 441–464.
- (18) Liu, B.; Trout, R. E. L.; Chu, G.-H.; McGarry, D.; Jackson, R. W.; Hamrick, J. C.; Daigle, D. M.; Cusick, S. M.; Pozzi, C.; De Luca, F.; Benvenuti, M.; Mangani, S.; Docquier, J.-D.; Weiss, W. J.; Pevear, D. C.; Xerri, L.; Burns, C. J. Discovery of Taniborbactam (VNRX-5133): A Broad-Spectrum Serine- and Metallo- β -Lactamase Inhibitor for Carbapenem-Resistant Bacterial Infections. *J. Med. Chem.* **2020**, *63*, 2789–2801.
- (19) Fast, W.; Sutton, L. D. Metallo- β -Lactamase: Inhibitors and Reporter Substrates. *Biochim. Biophys. Acta, Proteins Proteomics* **2013**, *1834*, 1648–1659.
- (20) Lima, L. M.; Silva, B. N. M. d.; Barbosa, G.; Barreiro, E. J. β -Lactam Antibiotics: An Overview from a Medicinal Chemistry Perspective. *Eur. J. Med. Chem.* **2020**, *208*, 112829.
- (21) Ju, L.-C.; Cheng, Z.; Fast, W.; Bonomo, R. A.; Crowder, M. W. The Continuing Challenge of Metallo- β -Lactamase Inhibition: Mechanism Matters. *Trends Pharmacol. Sci.* **2018**, *39*, 635–647.

- (22) Parkova, A.; Lucic, A.; Krajnc, A.; Brem, J.; Calvopiña, K.; Langley, G. W.; McDonough, M. A.; Trapencieris, P.; Schofield, C. J. Broad Spectrum β -Lactamase Inhibition by a Thioether Substituted Bicyclic Boronate. *ACS Infect. Dis.* **2020**, *6*, 1398–1404.
- (23) Rotondo, C. M.; Wright, G. D. Inhibitors of Metallo- β -Lactamases. *Curr. Opin. Microbiol.* **2017**, *39*, 96–105.
- (24) Jobin, P. G.; Butler, G. S.; Overall, C. M. New Intracellular Activities of Matrix Metalloproteinases Shine in the Moonlight. *Biochim. Biophys. Acta, Mol. Cell Res.* **2017**, *1864*, 2043–2055.
- (25) Dufour, A.; Overall, C. M. Missing the Target: Matrix Metalloproteinase Antitargets in Inflammation and Cancer. *Trends Pharmacol. Sci.* **2013**, *34*, 233–242.
- (26) McGeary, R. P.; Tan, D. T.; Schenk, G. Progress toward Inhibitors of Metallo- β -Lactamases. *Future Med. Chem.* **2017**, *9*, 673–691.
- (27) Goto, M.; Takahashi, T.; Yamashita, F.; Koreeda, A.; Mori, H.; Ohta, M.; Arakawa, Y. Inhibition of the Metallo- β -Lactamase Produced from *Serratia marcescens* by Thiol Compounds. *Biol. Pharm. Bull.* **1997**, *20*, 1136–1140.
- (28) Meng, Z.; Tang, M.-L.; Yu, L.; Liang, Y.; Han, J.; Zhang, C.; Hu, F.; Yu, J.-M.; Sun, X. Novel Mercapto Propionamide Derivatives with Potent New Delhi Metallo- β -Lactamase-1 Inhibitory Activity and Low Toxicity. *ACS Infect. Dis.* **2019**, *5*, 903–916.
- (29) Tehrani, K. H. M. E.; Martin, N. I. Thiol-Containing Metallo- β -Lactamase Inhibitors Resensitize Resistant Gram-Negative Bacteria to Meropenem. *ACS Infect. Dis.* **2017**, *3*, 711–717.
- (30) Mollard, C.; Moali, C.; Papamicael, C.; Dambon, C.; Vessilier, S.; Amicosante, G.; Schofield, C. J.; Galleni, M.; Frère, J.-M.; Roberts, G. C. K. Thiomandelic Acid, a Broad Spectrum Inhibitor of Zinc β -Lactamases. Kinetic and Spectroscopic Studies. *J. Biol. Chem.* **2001**, *276*, 45015–45023.
- (31) Li, N.; Xu, Y.; Xia, Q.; Bai, C.; Wang, T.; Wang, L.; He, D.; Xie, N.; Li, L.; Wang, J.; Zhou, H.-G.; Xu, F.; Yang, C.; Zhang, Q.; Yin, Z.; Guo, Y.; Chen, Y. Simplified Captopril Analogues as NDM-1 Inhibitors. *Bioorg. Med. Chem. Lett.* **2014**, *24*, 386.
- (32) Klingler, F.-M.; Wichelhaus, T. A.; Frank, D.; Cuesta-Bernal, J.; El-Delik, J.; Müller, H. F.; Sjuts, H.; Göttig, S.; Koenigs, A.; Pos, K. M.; Pogoryelov, D.; Proschak, E. Approved Drugs Containing Thiols as Inhibitors of Metallo- β -Lactamases: Strategy to Combat Multidrug-Resistant Bacteria. *J. Med. Chem.* **2015**, *58*, 3626–3630.
- (33) Büttner, D.; Kramer, J. S.; Klingler, F.-M.; Wittmann, S. K.; Hartmann, M. R.; Kurz, C. G.; Kohnhäuser, D.; Weizel, L.; Brüggerhoff, A.; Frank, D.; Steinhilber, D.; Wichelhaus, T. A.; Pogoryelov, D.; Proschak, E. Challenges in the Development of a Thiol-Based Broad-Spectrum Inhibitor for Metallo- β -Lactamases. *ACS Infect. Dis.* **2018**, *4*, 360–372.
- (34) Yahiaoui, S.; Voos, K.; Hauptenthal, J.; Wichelhaus, T. A.; Frank, D.; Weizel, L.; Rotter, M.; Brunst, S.; Kramer, J. S.; Proschak, E.; Ducho, C.; Hirsch, A. K. H. N-Aryl Mercaptoacetamides as Potential Multi-Target Inhibitors of Metallo- β -Lactamases (MBLs) and the Virulence Factor LasB from *Pseudomonas aeruginosa*. *RSC Med. Chem.* **2021**, *12*, 1698–1708.
- (35) Kany, A. M.; Sikandar, A.; Hauptenthal, J.; Yahiaoui, S.; Maurer, C. K.; Proschak, E.; Köhnke, J.; Hartmann, R. W. Binding Mode Characterization and Early in Vivo Evaluation of Fragment-Like Thiols as Inhibitors of the Virulence Factor LasB from *Pseudomonas aeruginosa*. *ACS Infect. Dis.* **2018**, *4*, 988–997.
- (36) Brown, D. G.; May-Dracka, T. L.; Gagnon, M. M.; Tommasi, R. Trends and Exceptions of Physical Properties on Antibacterial Activity for Gram-Positive and Gram-Negative Pathogens. *J. Med. Chem.* **2014**, *57*, 10144–10161.
- (37) Liu, Y.; Chen, C.; Sun, L.-Y.; Gao, H.; Zhen, J.-B.; Yang, K.-W. Meta-Substituted Benzenesulfonamide: A Potent Scaffold for the Development of Metallo- β -Lactamase ImiS Inhibitors. *RSC Med. Chem.* **2020**, *11*, 259–267.
- (38) Richter, M. F.; Drown, B. S.; Riley, A. P.; Garcia, A.; Shirai, T.; Svec, R. L.; Hergenrother, P. J. Predictive Compound Accumulation Rules Yield a Broad-Spectrum Antibiotic. *Nature* **2017**, *545*, 299–304.
- (39) Richter, M. F.; Hergenrother, P. J. The Challenge of Converting Gram-Positive-Only Compounds into Broad-Spectrum Antibiotics. *Ann. N.Y. Acad. Sci.* **2019**, *1435*, 18–38.
- (40) Van Lint, P.; Libert, C. Chemokine and Cytokine Processing by Matrix Metalloproteinases and Its Effect on Leukocyte Migration and Inflammation. *J. Leukocyte Biol.* **2007**, *82*, 1375–1381.
- (41) Sternlicht, M. D.; Werb, Z. How Matrix Metalloproteinases Regulate Cell Behavior. *Annu. Rev. Cell Dev. Biol.* **2001**, *17*, 463–516.
- (42) Sbardella, D.; Fasciglione, G. F.; Gioia, M.; Ciaccio, C.; Tundo, G. R.; Marini, S.; Coletta, M. Human Matrix Metalloproteinases: An Ubiquitarian Class of Enzymes Involved in Several Pathological Processes. *Mol. Aspects Med.* **2012**, *33*, 119–208.
- (43) Park, H. I.; Jin, Y.; Hurst, D. R.; Monroe, C. A.; Lee, S.; Schwartz, M. A.; Sang, Q.-X. A. The Intermediate S1' Pocket of the Endometase/Matrilysin-2 Active Site Revealed by Enzyme Inhibition Kinetic Studies, Protein Sequence Analyses, and Homology Modeling. *J. Biol. Chem.* **2003**, *278*, 51646–51653.
- (44) Chakraborty, C.; Sharma, A. R.; Sharma, G.; Lee, S.-S. Zebrafish: A Complete Animal Model to Enumerate the Nanoparticle Toxicity. *J. Nanobiotechnol.* **2016**, *14*, 1–13.
- (45) MacRae, C. A.; Peterson, R. T. Zebrafish as Tools for Drug Discovery. *Nat. Rev. Drug Discovery* **2015**, *14*, 721–731.
- (46) Doern, C. D. When Does 2 plus 2 Equal 5? A Review of Antimicrobial Synergy Testing. *J. Clin. Microbiol.* **2014**, *52*, 4124–4128.
- (47) Bei, Y. Myocardial extraction from suckling rats HHS public access. *Physiol. Behav.* **2017**, *176*, 139–148.
- (48) Pereira, M. F.; Rossi, C. C.; da Silva, G. C.; Rosa, J. N.; Bazzolli, D. M. S. *Galleria mellonella* as an Infection Model: An in-Depth Look at Why It Works and Practical Considerations for Successful Application. *Pathog. Dis.* **2020**, *78*, 1–15.
- (49) Tsai, C. J.-Y.; Loh, J. M. S.; Proft, T. *Galleria mellonella* Infection Models for the Study of Bacterial Diseases and for Antimicrobial Drug Testing. *Virulence* **2016**, *7*, 214–229.
- (50) Proschak, A.; Kramer, J.; Proschak, E.; Wichelhaus, T. A. Bacterial Zincophore [S,S]-Ethylenediamine-N,N'-Disuccinic Acid Is an Effective Inhibitor of MBLs. *J. Antimicrob. Chemother.* **2018**, *73*, 425–430.
- (51) Rukavishnikov, A.; Gee, K. R.; Johnson, I.; Corry, S. Fluorogenic Cephalosporin Substrates for β -Lactamase TEM-1. *Anal. Biochem.* **2011**, *419*, 9–16.
- (52) Hauptenthal, J.; Baehr, C.; Zeuzem, S.; Piiper, A. RNase A-like Enzymes in Serum Inhibit the Anti-Neoplastic Activity of siRNA Targeting Polo-like Kinase 1. *Int. J. Cancer* **2007**, *121*, 206–210.
- (53) Konstantinović, J.; Yahiaoui, S.; Alhayek, A.; Hauptenthal, J.; Schönauer, E.; Andreas, A.; Kany, A. M.; Müller, R.; Köhnke, J.; Berger, F. K.; Bischoff, M.; Hartmann, R. W.; Brandstetter, H.; Hirsch, A. K. H. N-Aryl-3-Mercaptosuccinimides as Antivirulence Agents Targeting *Pseudomonas aeruginosa* Elastase and *Clostridium collagenases*. *J. Med. Chem.* **2020**, *63*, 8359–8368.
- (54) Weinstein, M. P.; Patel, J. B.; Burnhman, C.-A.; Zimmer, B. L. Clinical and Laboratory Standards Institute Methods for Dilution Antimicrobial Susceptibility Tests for Bacteria That Grow Aerobically Standard, Approval CDM-A. *Methods for Dilution Antimicrobial Susceptibility Tests for Bacteria That Grow Aerobically*; Clinical Laboratory Standards Institute (CLSI), 2018; p 91.
- (55) CLSI. *M26-A Methods for Determining Bactericidal Activity of Antimicrobial Agents*; Clinical & Laboratory Standards Institute, Approved Guideline This Document Provides Procedures for Determining the Lethal Activity of Antimicrobial Agents, September, 1999.
- (56) Maes, J.; Verlooy, L.; Buenafe, O. E.; de Witte, P. A. M.; Esguerra, C. V.; Crawford, A. D. Evaluation of 14 Organic Solvents and Carriers for Screening Applications in Zebrafish Embryos and Larvae. *PLoS One* **2012**, *7*, No. e43850-9.

Supporting Information

***N*-Aryl mercaptopropionamides as broad-spectrum inhibitors of metallo-beta-lactamases**

Cansu Kaya^{1,2}, Jelena Konstantinović¹, Andreas M. Kany¹, Anastasia Andreas^{1,2}, Jan S. Kramer³, Steffen Brunst³, Lilia Weizel³, Marco J. Rotter³, Denia Frank⁴, Samir Yahiaoui¹, Rolf Müller^{1,2,5}, Rolf W. Hartmann^{1,2}, Jörg Haupenthal¹, Ewgenij Proschak³, Thomas A. Wichelhaus⁴, Anna K.H. Hirsch^{1,2,5*}

¹Helmholtz Institute for Pharmaceutical Research Saarland, (HIPS) – Helmholtz Centre for Infection Research (HZI), Campus E8.1, 66123 Saarbrücken, Germany

²Department of Pharmacy, Saarland University, Campus E8.1, 66123 Saarbrücken, Germany

³Institute of Pharmaceutical Chemistry and Institute of Biochemistry, Goethe University Frankfurt, Max-von-Laue-Straße 9, 60438 Frankfurt, Germany

⁴Institute of Medical Microbiology and Infection Control, University Hospital Frankfurt, Paul-Ehrlich-Straße 40, 60596 Frankfurt, Germany

⁵Helmholtz International Lab for Anti-infectives, Campus E8.1, 66123 Saarbrücken, Germany

*Email: anna.hirsch@helmholtz-hips.de

Table of Contents

1. General Experimental Procedures	S2
2. Synthesis of All Compounds	S4
3. Supporting Figures and Tables	S17
4. NMR Spectra of Final Compounds.....	S23
5. LCMS Spectra of Key Compounds.....	S45

1. General Experimental Procedures

General Procedure A-1: Synthesis of thioacetate derivatives 12–14, 16–18 and 19–23 using EDC·HCl as coupling reagent.

3-(Acetylthio) propionic acid (1.2–1.5 eq) was placed in a vial and dissolved in DCM. EDC·HCl (1.2–1.5 eq) was added and left to form a cloudy solution. Then, the corresponding amine (1.0 eq) was added, and the reaction was stirred at r.t. The reaction was monitored using TLC or LC-MS. The reaction was quenched with 1 M HCl until pH=1. The organic phase was washed with saturated aqueous NaCl solution (1x) and then dried over anh. Na₂SO₄. The product was filtered and concentrated. Purification was done by column chromatography.

General Procedure A-2: Synthesis of thioacetate derivatives 15 and 26 using ethylchloroformate as coupling reagent.

3-(Acetylthio) propionic acid (1.2 eq) was dissolved in THF and cooled in an ice-bath. Et₃N (1.2 eq) was added, followed by addition of ClCO₂Et (1.3 eq). After 5 minutes, the ice-bath was removed, and the reaction was stirred at r.t. for 30 minutes. The corresponding amine (1.0 eq) was slowly added. The reaction was monitored using TLC or LC-MS. After the reaction was completed, volatiles were evaporated under reduced pressure, and the crude product was purified using column chromatography or preparative HPLC (H₂O+0.05%FA / ACN+0.05%FA 95:5 → 5:95)

General Procedure A-3: Synthesis of thioacetate derivatives 24 and 25 using HATU as coupling reagent.

3-(Acetylthio) propionic acid (1.5 eq), HATU (1.5 eq) and DIEA (1.5 eq) were dissolved in DCM. The corresponding amine (1.0 eq) was added, and the reaction was stirred at r.t. for 2 days. Volatiles were evaporated under reduced pressure, and the crude product was purified using preparative HPLC (H₂O+0.05%FA/ACN+0.05%FA 95:5 → 5:95).

General Procedure B: Hydrolysis of thioacetate to obtain derivatives 8 and 27–41.

Thioacetate (1.0 eq) was dissolved in methanol or dioxane under an Ar atmosphere, and 2 M aq. solution of NaOH (2.0–3.0 eq) or solid NaOH (3.0–4.0 eq) was added. The reaction was stirred at r.t. for 1–2 h. After quenching with 1 M HCl, the product was extracted with EtOAc (3×). The combined organic extracts were washed with saturated aqueous NaCl solution, dried over anh. Na₂SO₄ and filtered. The solvent was removed under reduced pressure. Purification was done via flash chromatography. In case of more polar compounds, instead of quenching the reaction with 1 M HCl, pH was adjusted to acidic using Amberlite IR-120. After filtration, Amberlite was washed with MeOH (3x), the solvent was evaporated, and the product was purified using preparative HPLC (H₂O+0.05%FA/ACN+0.05%FA 95:5 → 5:95).

General Procedure C: Synthesis of free thiols 5–11

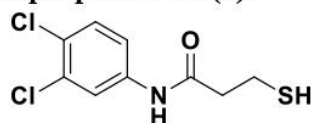
Aniline (1.0 eq) was placed in a crimp vial. The vial was evacuated and flushed with Ar followed by addition of 3-mercaptopropionic acid (1.2–1.5 eq). The vial was flushed with Ar again and heated to 120 °C for 5 h. The crude product was purified using reverse phase flash chromatography (H₂O+0.1%FA/ACN+0.1%FA 95:5 → 5:95).

General Procedure D: Deprotection of tert-butyloxycarbonyl group to obtain compounds 18a and 21a

To a solution of corresponding Boc-protected compound (1.0 eq) in DCM TFA (5.0–7.0 eq) was added and the reaction was stirred overnight at r.t. Volatiles were evaporated, and the crude product was used in the next step without further purification.

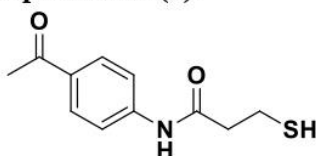
2. Synthesis of All Compounds

N-(3,4-Dichlorophenyl)-3-mercaptopropanamide (5).



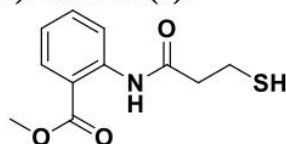
Compound **6** was synthesized according to general procedure C, using 3,4-dichloroaniline (150 mg, 1.25 mmol) and 3-mercaptopropionic acid (330 μ L, 3.75 mmol). The product was purified by reverse phase flash chromatography ($\text{H}_2\text{O}+0.1\%\text{FA}/\text{ACN}+0.1\%\text{FA}$ 95:5 \rightarrow 5:95). The final product was obtained as white solid (120 mg, 51%). ^1H NMR (500 MHz, $\text{DMSO}-d_6$) δ ppm: 10.27 (s, 1H), 8.00 (d, $J = 2.4$ Hz, 1H), 7.56 (d, $J = 8.8$ Hz, 1H), 7.47 (dd, $J = 8.8, 2.4$ Hz, 1H), 2.77–2.71 (m, 2H), 2.66–2.62 (m, 2H), 2.45–2.40 (m, 1H). ^{13}C NMR (126 MHz, $\text{DMSO}-d_6$) δ ppm: 169.9, 139.1, 131.0, 130.7, 124.5, 120.2, 119.1, 40.3, 19.5. HRMS (ESI $^-$) m/z calcd. for $\text{C}_9\text{H}_8\text{Cl}_2\text{NOS}$ $[\text{M}-\text{H}]^-$ 247.97091, found 247.97091.

N-(4-Acetylphenyl)-3-mercaptopropanamide (6).



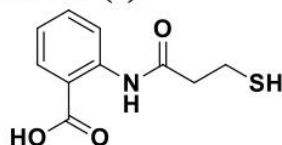
Compound **7** was synthesized according to general procedure C, using methyl 4'-aminoacetophenone (150 mg, 1.09 mmol) and 3-mercaptopropionic acid (145 μ L, 1.64 mmol). The product was purified by flash chromatography (Hex/EtOAc, 7:3). The final product was obtained as white solid (30 mg, 15%). ^1H NMR (500 MHz, $\text{DMSO}-d_6$) δ ppm: 10.31 (s, 1H), 7.92 (d, $J = 8.7$ Hz, 2H), 7.73 (d, $J = 8.7$ Hz, 2H), 2.52 (s, 3H), 2.77–2.73 (m, 2H), 2.69–2.66 (m, 2H), 2.44–2.41 (m, 1H). ^{13}C NMR (126 MHz, $\text{DMSO}-d_6$) δ ppm: 196.5, 170.0, 143.4, 131.6, 129.5, 118.3, 40.4, 26.4, 19.5. HRMS (ESI $^-$) m/z calcd. for $\text{C}_{11}\text{H}_{12}\text{NO}_2\text{S}$ $[\text{M}-\text{H}]^-$ 222.05942, found 222.05882.

Methyl 2-(3-mercaptopropanamido)benzoate (7).



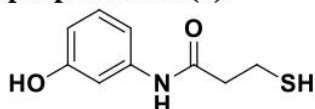
Compound **8** was synthesized according to general procedure C, using methyl 2-aminobenzoate (400 mg, 2.64 mmol) and 3-mercaptopropionic acid (346 μ L, 3.97 mmol). The product was purified by flash chromatography (Hex/EtOAc, 7:3). The final product was obtained as white solid (118 mg, 19%). ^1H NMR (500 MHz, $\text{DMSO}-d_6$) δ ppm: 10.59 (s, 1H), 8.22 (d, $J = 8.2$ Hz, 1H), 7.90 (dd, $J = 7.9, 1.53$ Hz, 1H), 7.60 (t, $J = 7.8$ Hz, 1H), 7.20 (t, $J = 7.6$ Hz, 1H), 3.85 (s, 3H), 2.78–2.74 (m, 2H), 2.71–2.68 (m, 2H), 2.49–2.46 (m, 1H). ^{13}C NMR (126 MHz, $\text{DMSO}-d_6$) δ ppm: 169.5, 167.5, 139.3, 133.9, 130.5, 123.3, 121.4, 118.2, 52.4, 41.1, 19.6. HRMS (ESI $^+$) m/z calcd. for $\text{C}_{11}\text{H}_{14}\text{NO}_3\text{S}$ $[\text{M}+\text{H}]^+$ 240.06889, found 240.06851.

2-(3-Mercaptopropanamido) benzoic acid (**8**).



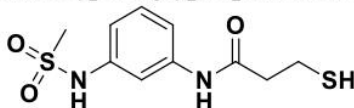
Compound **8** was synthesized according to general procedure B, using compound **8** (54 mg, 0.23 mmol) and 1 M aq. NaOH solution (13 mL, 0.46 mmol) in dioxane (5 mL). The final product was obtained in quantitative yield. ^1H NMR (500 MHz, DMSO- d_6) δ ppm: 13.61 (br s, 1H), 11.12 (s, 1H), 8.47 (d, $J = 7.8$ Hz, 1H), 7.97 (dd, $J = 7.9, 1.6$ Hz, 1H), 7.61–7.57 (m, 1H), 7.17–7.13 (m, 1H), 2.78–2.73 (m, 2H), 2.71–2.68 (m, 2H), 2.49–2.47 (m, 1H). ^{13}C NMR (126 MHz, DMSO- d_6) δ ppm: 169.5, 169.2, 140.6, 134.0, 131.1, 122.8, 120.1, 116.7, 41.5, 19.5. HRMS (ESI $^-$) m/z calcd. for $\text{C}_{10}\text{H}_{10}\text{NO}_3\text{S}$ [$\text{M}-\text{H}$] $^-$ 224.03868, found 224.03838.

N-(3-Hydroxyphenyl)-3-mercaptopropanamide (**9**).



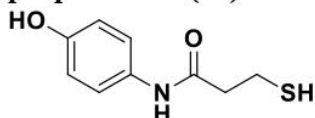
Compound **9** was synthesized according to general procedure C, using 3-aminophenol (200 mg, 1.83 mmol) and 3-mercaptopropionic acid (240 μL , 2.75 mmol). The product was purified by flash chromatography (Hex/EtOAc, 7:3). The final product was obtained as white solid (144 mg, 40%). ^1H NMR (500 MHz, DMSO- d_6) δ ppm: 9.81 (s, 1H), 9.34 (s, 1H), 7.18 (t, $J = 1.9$ Hz, 1H), 7.05 (t, $J = 8.0$ Hz, 1H), 6.94 (br d, $J = 8.3$ Hz, 1H), 6.43 (dd, $J = 7.9, 1.98$ Hz, 1H), 2.73 (q, $J = 7.0$ Hz, 2H), 2.60 (t, $J = 6.9$ Hz, 2H), 2.36 (t, $J = 8.0$ Hz, 1H). ^{13}C NMR (126 MHz, DMSO- d_6) δ ppm: 169.2, 157.6, 140.1, 129.3, 110.2, 109.8, 106.2, 40.3, 19.7. HRMS (ESI $^+$) m/z calcd. for $\text{C}_9\text{H}_{12}\text{NO}_2\text{S}$ [$\text{M}+\text{H}$] $^+$ 198.05832, found 198.05809.

3-Mercapto-*N*-(3-(methylsulfonamido)phenyl)propanamide (**10**).



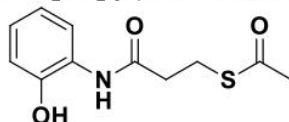
Compound **10** was synthesized using general procedure C, using methyl *N*-(3-aminophenyl) methanesulfonamide (90 mg, 0.48 mmol) and 3-mercaptopropionic acid (64 μL , 0.72 mmol). The product was purified using reverse phase column chromatography. The final product was obtained as white solid (23 mg, 19%). ^1H NMR (500 MHz, DMSO- d_6) δ ppm: 10.03 (s, 1H), 9.74 (s, 1H), 7.53 (t, $J = 2.0$ Hz, 1H), 7.39–7.34 (m, 1H), 7.23 (t, $J = 8.1$ Hz, 1H), 6.89–6.84 (m, 1H), 2.97 (s, 3H), 2.73 (q, $J = 7.0$ Hz, 2H), 2.64–2.60 (m, 2H), 2.41–2.33 (m, 1H). ^{13}C NMR (126 MHz, DMSO- d_6) δ ppm: 169.4, 139.9, 138.7, 129.5, 114.54, 114.45, 110.3, 40.3, 30.7, 19.6. HRMS (ESI $^-$) m/z calcd. for $\text{C}_{10}\text{H}_{13}\text{N}_2\text{O}_3\text{S}_2$ [$\text{M}-\text{H}$] $^-$ 273.03730, found 273.03727.

N-(4-Hydroxyphenyl)-3-mercaptopropanamide (**11**).



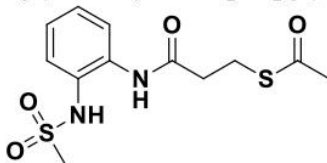
Compound **11** was synthesized according to general procedure C, using 4-aminophenol (152 mg, 1.37 mmol) and 3-mercaptopropionic acid (177.6 μ L, 1.64 mmol). The product was purified using column chromatography (Hex/EtOAc, 7:3). The final product was obtained as white solid (145 mg, 53%). ^1H NMR (500 MHz, DMSO- d_6) δ ppm: δ 9.68 (br s, 1H), 9.14 (s, 1H), 7.37–7.31 (m, 2H), 6.71–6.64 (m, 2H), 2.74–2.70 (m, 2H), 2.56 (t, J = 6.9 Hz, 2H), 2.34 (t, J = 8.0 Hz, 1H). ^{13}C NMR (126 MHz, DMSO- d_6) δ ppm: 168.5, 153.2, 130.8, 120.9, 115.0, 40.1, 19.8. HRMS (ESI $^+$) m/z calcd. for $\text{C}_9\text{H}_{12}\text{NO}_2\text{S}$ [$\text{M}+\text{H}$] $^+$ 198.05832, found 198.05832.

S-(3-((2-Hydroxyphenyl)amino)-3-oxopropyl) ethanethioate (12).



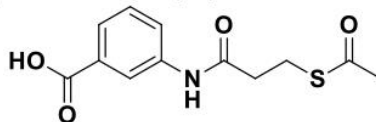
Compound **12** was synthesized according to general procedure A-1, using 2-aminophenol (150 mg, 1.37 mmol), 3-(acetylthio) propionic acid (305 mg, 2.06 mmol) and EDC HCl (395 mg, 2.06 mmol) in DCM (10 mL). The product was purified using column chromatography (Hex/EtOAc, 7:3). The final product was obtained as white solid (272 mg, 80%). ^1H NMR (500 MHz, CDCl_3) δ ppm: 8.42 (s, 1H), 7.65 (s, 1H), 7.16–7.12 (m, 1H), 7.06–7.01 (m, 2H), 6.90–6.85 (m, 1H), 3.24 (t, J = 6.9 Hz, 2H), 2.78 (t, J = 6.9 Hz, 2H), 2.37 (s, 3H). ^{13}C NMR (126 MHz, CDCl_3) δ ppm: 196.6, 171.0, 148.8, 127.5, 125.4, 122.3, 120.7, 120.1, 37.1, 30.8, 25.0. MS (ESI $^-$) m/z 238.97 [$\text{M}-\text{H}$] $^-$, 198.05 [$\text{M}-\text{Ac}+\text{H}$] $^-$.

S-(3-((2-(Methylsulfonamido)phenyl)amino)-3-oxopropyl)ethanethioate (13).



Compound **13** was synthesized according to general procedure A-1, using *N*-(2-aminophenyl) methanesulfonamide (220 mg, 1.18 mmol), 3-(acetylthio) propionic acid (262 mg, 1.77 mmol) and EDC HCl (339 mg, 1.77 mmol) in DCM (10 mL). The product was purified by column chromatography (DCM/MeOH, 95:5). The final product was obtained as white solid (100 mg, 30%). ^1H NMR (500 MHz, DMSO- d_6) δ ppm: 9.47 (s, 1H), 8.81 (s, 1H), 7.59 (d, J = 7.5 Hz, 1H), 7.38 (d, J = 7.6 Hz, 1H), 7.25–7.16 (m, 2H), 3.09 (t, J = 6.8 Hz, 2H), 2.94 (s, 3H), 2.71 (t, J = 6.7 Hz, 2H), 2.34 (s, 3H). ^{13}C NMR (126 MHz, DMSO- d_6) δ ppm: 195.5, 170.1, 131.8, 129.5, 126.2, 125.65, 125.57, 124.9, 35.7, 30.6, 24.3. HRMS (ESI $^+$) m/z calcd. for $\text{C}_{12}\text{H}_{17}\text{N}_2\text{O}_4\text{S}_2$ [$\text{M}+\text{H}$] $^+$ 317.06242, found 317.06000.

3-(3-(Acetylthio)propanamido)benzoic acid (14).

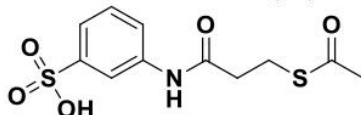


Compound **14** was synthesized according to general procedure A-1, using 3-aminobenzoic acid (130 mg, 0.95 mmol), 3-(acetylthio) propionic acid (210 mg, 1.42 mmol) and EDC HCl (272 mg, 1.42 mmol) in DCM (10 mL). The product was purified using preparative HPLC. Final product was obtained as white powder (62 mg, 25%) ^1H NMR (500 MHz, DMSO- d_6) δ ppm:

S6

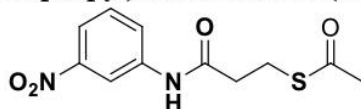
12.96 (br s, 1H), 10.18 (s, 1H), 8.21 (s, 1H), 7.79 (d, $J = 6.6$ Hz, 1H), 7.61 (d, $J = 7.9$ Hz, 1H), 7.41 (t, $J = 7.9$ Hz, 1H), 3.09 (t, $J = 6.8$ Hz, 2H), 2.65 (t, $J = 6.8$ Hz, 2H), 2.33 (s, 3H). ^{13}C NMR (126 MHz, DMSO- d_6) δ ppm: 195.5, 169.5, 167.2, 139.4, 131.3, 129.1, 124.1, 123.1, 119.8, 36.0, 30.6, 24.3. HRMS (ESI $^+$) m/z calcd. for $\text{C}_{12}\text{H}_{14}\text{NO}_4\text{S}$ $[\text{M}+\text{H}]^+$ 268.06380, found 268.06381.

3-(3-(Acetylthio)propanamido)benzenesulfonic acid (15).



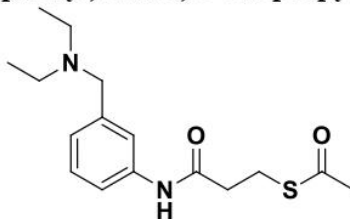
Compound **15** was synthesized according to the general procedure A-2, using 3-aminobenzenesulfonic acid (75 mg, 0.43 mmol), 3-(acetylthio) propionic acid (77 mg, 0.52 mmol), Et_3N (72 μL , 0.52 mmol) and ClCO_2Et (55 μL , 0.58 mmol) in THF (5 mL). The reaction was stirred at r.t. overnight. The product was purified using preparative HPLC. The final product was obtained as a colorless oil (65.5 mg, 50%). ^1H NMR (500 MHz, DMSO- d_6) δ ppm: 10.03 (s, 1H), 7.82–7.79 (m, 1H), 7.61–7.59 (m, 1H), 7.29–7.20 (m, 2H), 3.07 (t, 2H, $J = 6.9$ Hz), 2.61 (t, $J = 6.8$ Hz, 2H), 2.31 (s, 3H). ^{13}C NMR (126 MHz, DMSO- d_6) δ ppm: 195.4, 169.1, 148.7, 138.4, 128.0, 120.4, 119.1, 116.5, 35.9, 30.6, 24.3. MS (ESI $^+$) m/z 303.95 $[\text{M}+\text{H}]^+$.

S-(3-((3-Nitrophenyl)amino)-3-oxopropyl) ethanethioate (16).



Compound **16** was synthesized according to the general procedure A-1, using 3-nitroaniline (250 mg, 1.81 mmol), 3-(acetylthio) propionic acid (322 mg, 2.17 mmol) and EDC HCl (416 mg, 2.17 mmol) in DCM (15 mL). The product was purified using column chromatography (Hex/EtOAc, 7:3). The final product was obtained as off-yellow solid (315 mg, 65%). ^1H NMR (500 MHz, DMSO- d_6) δ ppm: 10.47 (s, 1H), 8.62–8.59 (m, 1H), 7.92–7.84 (m, 2H), 7.59 (t, $J = 8.2$ Hz, 1H), 3.09 (t, $J = 6.9$ Hz, 2H), 2.68 (t, $J = 6.9$ Hz, 2H), 2.32 (s, 3H). ^{13}C NMR (126 MHz, DMSO- d_6) δ ppm: 169.9, 148.0, 140.0, 130.2, 125.0, 117.8, 113.1, 36.0, 30.5, 24.1. MS (ESI $^-$) m/z 267.10 $[\text{M}-\text{H}]^-$.

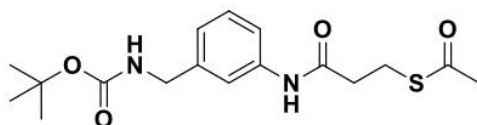
S-(3-((3-((Diethylamino)methyl)phenyl)amino)-3-oxopropyl) ethanethioate (17).



Compound **17** was synthesized according to the general procedure A-1, using 3-((diethylamino)methyl) aniline (200 mg, 1.12 mmol), 3-(acetylthio) propionic acid (199.5 mg, 1.35 mmol) and EDC HCl (259 mg, 1.35 mmol) in DCM (15 mL). The product was purified using preparative HPLC. The final product was obtained as transparent oil (303.8 mg, 88%). ^1H NMR (500 MHz, DMSO- d_6) δ ppm: 10.02 (s, 1H), 7.59 (br s, 1H), 7.52–7.47 (m, 1H), 7.24 (t, $J = 7.9$ Hz, 1H), 7.06–7.01 (m, 1H), 3.65 (s, 2H), 3.07 (t, $J = 6.9$ Hz, 2H), 2.64–2.55 (m, 6H), 2.31

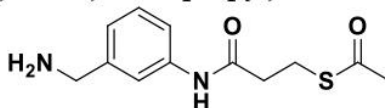
(s, 3H), 1.02 (t, $J = 7.1$ Hz, 6H). ^{13}C NMR (126 MHz, DMSO- d_6) δ ppm: 195.4, 169.1, 139.1, 128.6, 124.0, 119.7, 118.1, 56.4, 46.0, 35.9, 30.6, 24.3, 10.8. MS (ESI $^+$) m/z 309.20 $[\text{M}+\text{H}]^+$.

S-(3-((3-(((tert-Butoxycarbonyl)amino)methyl)phenyl)amino)-3-oxopropyl) ethanethioate (18).



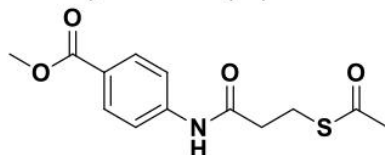
Compound **18** was synthesized according to general procedure A-1, using *tert*-butyl (3-aminobenzyl) carbamate (134 mg, 0.60 mmol), 3-(acetylthio) propionic acid (134 mg, 0.91 mmol) and EDC·HCl (173 mg, 0.91 mmol) in DCM (15 mL). The final product was obtained as off-white solid (134 mg, 63%). ^1H NMR (500 MHz, DMSO- d_6) δ ppm: 9.96 (s, 1H), 7.46 (s, 1H), 7.45–7.31 (m, 2H), 7.22 (t, $J = 7.8$ Hz, 1H), 6.90 (d, $J = 7.6$ Hz, 1H), 4.07 (d, $J = 6.2$ Hz, 2H), 3.07 (t, $J = 6.8$ Hz, 2H), 2.62 (t, $J = 6.9$ Hz, 2H), 2.32 (s, 3H), 1.39 (s, 9H). ^{13}C NMR (126 MHz, DMSO) δ ppm: 195.4, 172.7, 169.1, 155.8, 140.8, 139.0, 128.6, 121.8, 117.6, 117.5, 43.4, 35.9, 28.3, 26.4, 24.3. MS (ESI $^+$) 353.07 m/z $[\text{M}+\text{H}]^+$.

S-(3-((3-(Aminomethyl)phenyl)amino)-3-oxopropyl) ethanethioate (18a).



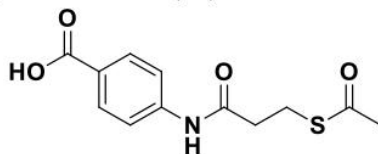
Compound **18a** was synthesized according to general procedure D, using compound **18** (123 mg, 0.33 mmol) and TFA (133 μL , 1.67 mmol) in DCM (5 mL). The crude product was used for the next step without further purification. The final product was obtained as off-white oil in quantitative yield (138 mg). ^1H NMR (500 MHz, CD_3OD) δ ppm: 7.86 (s, 1H), 7.43–7.35 (m, 2H), 7.18 (m, 1H), 4.09 (s, 2H), 3.20 (t, $J = 6.9$ Hz, 2H), 2.70 (t, $J = 6.9$ Hz, 2H), 2.32 (s, 3H). ^{13}C NMR (126 MHz, CD_3OD) δ ppm: 197.1, 172.1, 140.5, 135.1, 130.7, 125.5, 121.7, 121.7, 44.4, 37.5, 30.4, 25.6. HRMS (ESI $^-$) m/z calcd. for $\text{C}_{12}\text{H}_{15}\text{N}_2\text{O}_2\text{S}$ $[\text{M}-\text{H}]^-$ 251.08597, found 251.08593.

Methyl 4-(3-(acetylthio)propanamido)benzoate (19).



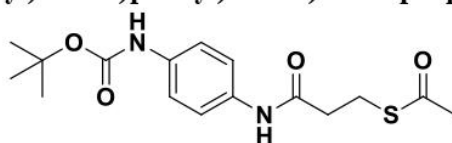
Compound **19** was synthesized according to general procedure A-1, using methyl 4-aminobenzoate (91 mg, 0.60 mmol), 3-(acetylthio) propionic acid (134 mg, 0.90 mmol) and EDC·HCl (173 mg, 0.60 mmol) in DCM (10 mL). The product was purified using column chromatography (Hex/EtOAc, 7:3). The final product was obtained as white solid (50 mg, 29%) ^1H NMR (500 MHz, DMSO- d_6) δ ppm: 10.32 (s, 1H), 7.91–7.89 (m, 2H), 7.71–7.69 (m, 2H), 3.82 (s, 3H), 3.08 (t, $J = 6.8$ Hz, 2H), 2.68 (t, $J = 6.8$ Hz, 2H), 2.33 (s, 3H). ^{13}C NMR (126 MHz, DMSO- d_6) δ ppm: 195.4, 169.8, 165.8, 143.4, 130.3, 124.0, 118.4, 51.9, 36.1, 30.5, 24.1. HRMS (ESI $^+$) m/z calcd. for $\text{C}_{13}\text{H}_{16}\text{NO}_4\text{S}$ $[\text{M}+\text{H}]^+$ 282.07945, found 282.07697.

4-(3-(Acetylthio)propanamido)benzoic acid (**20**).



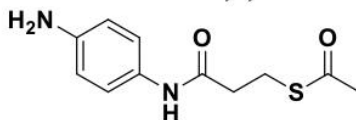
Compound **20** was synthesized according to general procedure A-1, using 4-aminobenzoic acid (129 mg, 0.73 mmol), 3-(acetylthio) propionic acid (210 mg, 1.09 mmol) and EDC·HCl (270 mg, 1.09 mmol) in DCM (10 mL). The product was purified using preparative HPLC. The final product was obtained as white powder (200 mg, 79%). ¹H NMR (500 MHz, DMSO-*d*₆) δ ppm: 12.68 (br s, 1H), 10.29 (s, 1H), 7.90–7.85 (m, 2H), 7.70–7.65 (m, 2H), 3.08 (t, *J* = 6.8 Hz, 2H), 2.67 (t, *J* = 6.8 Hz, 2H), 2.33 (s, 3H). ¹³C NMR (126 MHz, DMSO-*d*₆) δ ppm: 195.4, 169.4, 167.2, 139.2, 131.3, 129.0, 124.0, 123.1, 119.8, 35.9, 30.5, 24.2. HRMS (ESI⁻) *m/z* calcd. for C₁₂H₁₂NO₄S [M-H]⁻ 266.04925, found 266.04928.

S-(3-((4-((*tert*-Butoxycarbonyl)amino)phenyl)amino)-3-oxopropyl) ethanethioate (**21**).



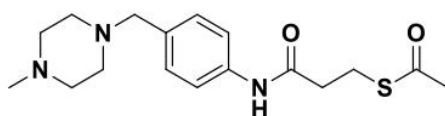
Compound **21** was synthesized according to the general procedure A-1, using *tert*-butyl (4-aminophenyl)carbamate (250 mg, 1.20 mmol), 3-(acetylthio) propionic acid (213.5 mg, 1.44 mmol) and EDC HCl (276 mg, 1.44 mmol) in DCM (15 mL). The final product was obtained as off-white solid (357 mg, 88%). The product was used in the next step without further purification. ¹H NMR (500 MHz, DMSO-*d*₆) δ ppm: 9.83 (s, 1H), 9.22 (br s, 1H), 7.45–7.40 (m, 2H), 7.37–7.30 (m, 2H), 3.06 (t, 2H, *J* = 6.9 Hz), 2.58 (t, 2H, *J* = 6.9 Hz), 2.31 (s, 3H), 1.45 (s, 9H). ¹³C NMR (126 MHz, DMSO-*d*₆) δ ppm: 195.4, 168.6, 152.8, 134.9, 133.5, 119.5, 118.4, 78.8, 35.8, 30.5, 28.1, 24.3. MS (ESI⁺) *m/z* 339.2 [M+H]⁺.

4-(3-(Acetylthio)propanamido)benzenaminium-2,2,2-trifluoroacetate (**21a**).



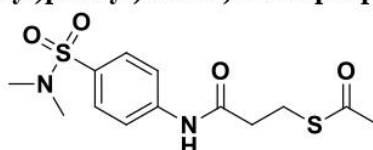
Compound **21a** was synthesized according to the general procedure D, using compound **21** (150 mg, 0.44 mmol) and TFA (250 μL, 3.10 mmol) in DCM (3 mL). The final product was obtained in the form of TFA salt as pale orange oil (156.1 mg, 100%). The product was used in the next step without further purification. ¹H NMR (500 MHz, DMSO-*d*₆) δ ppm: 10.09 (s, 1H), 7.60 (d, *J* = 8.8 Hz, 2H), 7.18 (d, *J* = 8.8 Hz, 2H), 3.98 (br s, 3H), 3.06 (t, *J* = 6.8 Hz, 2H), 2.62 (t, *J* = 6.8 Hz, 2H), 2.31 (s, 3H). ¹³C NMR (126 MHz, DMSO-*d*₆) δ ppm: 195.4, 172.7, 169.3, 158.3 (q, *J*_{C-F} = 34.3 Hz), 138.2, 127.4, 123.0, 120.0, 35.9, 30.5, 24.2. ¹⁹F NMR (470 MHz, DMSO-*d*₆) δ ppm: -74.58. MS (ESI⁺) *m/z* 239.1 [M+H]⁺.

S-(3-((4-((4-Methylpiperazin-1-yl)methyl)phenyl)amino)-3-oxopropyl) ethanethioate (**22**).



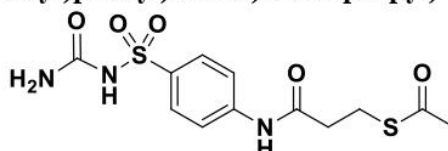
Compound **22** was synthesized according to general procedure A-1, using 4-((4-methylpiperazin-1-yl)methyl)aniline (115 mg, 0.56 mmol), 3-(acetylthio) propionic acid (124 mg, 0.84 mmol) and EDC·HCl (161 mg, 0.84 mmol) in DCM (10 mL). The product was purified using preparative HPLC. The final product was obtained as colorless oil (115 mg, 61%). ¹H NMR (500 MHz, DMSO-*d*₆) δ ppm: 9.95 (s, 1H), 7.57 (d, *J* = 8.5 Hz, 2H), 7.19 (d, *J* = 8.5 Hz, 2H), 3.38 (s, 2H), 3.07 (t, *J* = 6.8 Hz, 2H), 2.61 (t, *J* = 6.8 Hz, 2H), 2.54 (s, 8H), 2.32 (s, 3H), 2.18 (s, 3H). ¹³C NMR (126 MHz, DMSO-*d*₆) δ ppm: 195.4, 169.0, 137.8, 132.8, 129.2, 118.8, 61.5, 54.5, 52.1, 45.4, 35.9, 30.5, 24.3. HRMS (ESI⁺) *m/z* calcd. for C₁₇H₂₆N₃O₂S [M+H]⁺ 336.17402, found 336.17407.

S-(3-((4-(*N,N*-Dimethylsulfamoyl)phenyl)amino)-3-oxopropyl) ethanethioate (23).



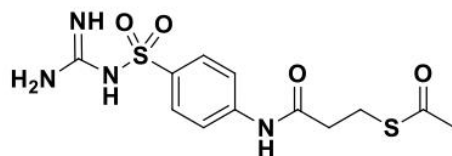
Compound **23** was synthesized according to general procedure A-1, using 4-amino-*N,N*-dimethylbenzenesulfonamide (110 mg, 0.54 mmol), 3-(acetylthio) propionic acid (122 mg, 0.82 mmol) and EDC·HCl (158 mg, 0.82 mmol) in DCM (10 mL). The product was purified using reversed phase column chromatography. The final product was obtained as white solid (70 mg, 38%). ¹H NMR (500 MHz, DMSO-*d*₆) δ ppm: 10.43 (s, 1H), 7.84–7.79 (m, 2H), 7.71–7.66 (m, 2H), 3.09 (t, *J* = 6.7 Hz, 2H), 2.69 (t, *J* = 6.7 Hz, 2H), 2.56 (s, 6H), 2.33 (s, 3H). ¹³C NMR (126 MHz, DMSO-*d*₆) δ ppm: 195.4, 170.0, 143.0, 128.9, 128.3, 118.8, 37.6, 36.1, 30.6, 24.1. HRMS (ESI⁺) *m/z* calcd. for C₁₃H₁₉N₂O₄S₂ [M+H]⁺ 331.07807, found 331.07523.

S-(3-((4-(*N*-Carbamoylsulfamoyl)phenyl)amino)-3-oxopropyl) ethanethioate (24).



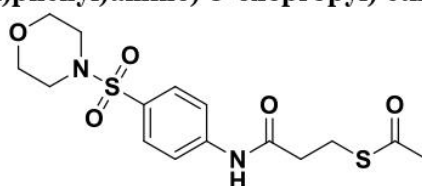
Compound **24** was synthesized according to the general procedure A-3, using 4-amino-*N*-carbamoylbenzenesulfonamide (350 mg, 1.62 mmol), 3-(acetylthio) propionic acid (361.4 mg, 2.44 mmol), HATU (927.8 mg, 2.44 mmol) and DIEA (425 μL, 2.44 mmol) in DCM (15 mL). The product was purified using preparative HPLC. The final product was obtained as white solid (317.4 mg, 56%). ¹H NMR (500 MHz, DMSO-*d*₆) δ ppm: 10.46 (s, 1H), 10.40 (s, 1H), 7.84–7.79 (m, 2H), 7.78–7.71 (m, 2H), 6.34 (br s, 2H), 3.08 (t, *J* = 6.8 Hz, 2H), 2.67 (t, *J* = 6.8 Hz, 2H), 2.32 (s, 3H). ¹³C NMR (126 MHz, DMSO-*d*₆) δ ppm: 195.3, 169.9, 152.1, 143.0, 133.9, 128.5, 118.4, 36.0, 30.5, 24.0. MS (ESI⁺) *m/z* 346.04 [M+H]⁺.

S-(3-((4-(*N*-Carbamimidoylsulfamoyl)phenyl)amino)-3-oxopropyl) ethanethioate (25).



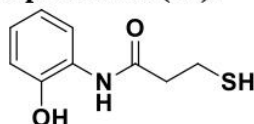
Compound **25** was synthesized according to the general procedure A-3, using 4-amino-*N*-carbamimidoylbenzenesulfonamide (250 mg, 1.17 mmol), 3-(acetylthio) propionic acid (259.4 mg, 1.75 mmol), HATU (665.4 mg, 1.75 mmol) and DIEA (300 μ L, 1.75 mmol) in DCM (10 mL). The product was purified using preparative HPLC. The final product was obtained as white solid (229.5 mg, 57%). ^1H NMR (500 MHz, DMSO- d_6) δ ppm: 10.24 (s, 1H), 7.69–7.63 (m, 4H), 6.65 (br s, 4H), 3.07 (t, $J = 6.9$ Hz, 2H), 2.65 (t, $J = 6.8$ Hz, 2H), 2.32 (s, 3H). ^{13}C NMR (126 MHz, DMSO- d_6) δ ppm: 195.4, 169.6, 158.0, 141.3, 138.8, 126.6, 118.4, 36.0, 30.5, 24.1. MS (ESI $^+$) m/z 345.1 [M+H] $^+$.

S-(3-((4-(Morpholinyl)sulfonyl)phenyl)amino)-3-oxopropyl) ethanethioate (26).



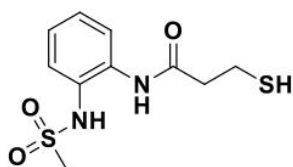
Compound **26** was synthesized according to the general procedure A-2, using 4-(morpholinyl)sulfonamide (100 mg, 0.41 mmol), 3-(acetylthio) propionic acid (73.4 mg, 0.50 mmol), Et $_3$ N (70 μ L, 0.50 mmol) and ClCO $_2$ Et (50 μ L, 0.54 mmol) in THF (5 mL). The reaction was stirred at r.t. for 7 days. The product was purified using column chromatography (Hex/EtOAc, 6:4 \rightarrow 4:6). The final product was obtained as white foam (84.9 mg, 55%). ^1H NMR (500 MHz, DMSO- d_6) δ ppm: 10.44 (s, 1H), 7.82 (d, $J = 8.9$ Hz, 2H), 7.67 (d, $J = 8.7$ Hz, 2H), 3.64–3.58 (m, 4H), 3.08 (t, $J = 6.8$ Hz, 2H), 2.85–2.78 (m, 4H), 2.69 (t, $J = 6.8$ Hz, 2H), 2.32 (s, 3H). ^{13}C NMR (126 MHz, DMSO- d_6) δ ppm: 195.4, 170.0, 143.3, 129.0, 128.0, 118.8, 65.2, 45.9, 36.1, 30.5, 24.1. MS (ESI $^+$) m/z 243.92 [M+H] $^+$.

***N*-(2-Hydroxyphenyl)-3-mercaptopropanamide (27).**



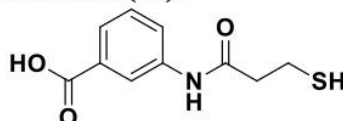
Compound **27** was synthesized according to general procedure B, using compound **12** (87 mg, 0.36 mmol) and NaOH (57 mg, 1.44 mmol) in MeOH (2 mL). The final product was obtained pure without any purification as off-white solid in quantitative yield (75 mg). ^1H NMR (500 MHz, DMSO- d_6) δ ppm: 9.72 (s, 1H), 9.28 (s, 1H), 7.74–7.71 (m, 1H), 6.95–6.91 (m, 1H), 6.86–6.84 (m, 1H), 6.77–6.73 (m, 1H), 2.76–2.69 (m, 4H), 2.38–2.34 (m, 1H). ^{13}C NMR (126 MHz, DMSO- d_6) δ ppm: 169.8, 147.8, 126.2, 124.6, 122.4, 118.9, 115.7, 30.7, 19.9. HRMS (ESI $^+$) m/z calcd. for C $_9$ H $_{12}$ NO $_2$ S [M+H] $^+$ 198.05832, found 198.05842.

3-Mercapto-*N*-(2-(methylsulfonyl)phenyl)propanamide (28).



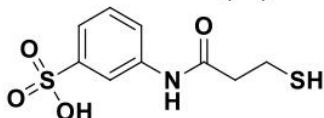
Compound **28** was synthesized according to general procedure B, using compound **13** (30 mg, 0.10 mmol) and 2 M NaOH aq. solution (95 μ L, 0.19 mmol) in MeOH (5 mL). The product was purified using preparative HPLC. The final product was obtained as white solid (27 mg, 33%). ^1H NMR (500 MHz, CDCl_3) δ ppm: 8.06 (s, 1H), 7.75 (d, $J = 7.9$ Hz, 1H), 7.36 (d, $J = 7.9$ Hz, 1H), 7.32 (td, $J = 7.8, 1.4$ Hz, 1H), 7.24–7.22 (m, 1H), 6.74 (s, 1H), 3.03 (s, 3H), 2.94–2.89 (m, 2H), 2.76 (t, $J = 6.5$ Hz, 2H), 1.75 (t, $J = 8.4$ Hz, 1H). ^{13}C NMR (126 MHz, CDCl_3) δ ppm: 170.3, 133.3, 128.4, 128.2, 126.8, 126.7, 124.8, 41.2, 39.6, 20.4. HRMS (ESI $^-$) m/z calcd. for $\text{C}_{10}\text{H}_{13}\text{N}_2\text{O}_3\text{S}_2$ $[\text{M}-\text{H}]^-$ 273.03730, found 273.03734.

3-(3-Mercaptopropanamido)benzoic acid (29).



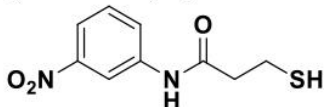
Compound **29** was synthesized according to general procedure B, using compound **14** (62 mg, 0.23 mmol) and NaOH (37 mg, 0.92 mmol) in MeOH (2 mL). The product was purified using preparative HPLC. The final product was obtained as white powder (35 mg, 67%). ^1H NMR (500 MHz, $\text{DMSO}-d_6$) δ ppm: 12.95 (s, 1H), 10.15 (s, 1H), 8.24 (s, 1H), 7.81 (dd, $J = 8.1, 0.9$ Hz, 1H), 7.61 (d, $J = 7.7$ Hz, 1H), 7.42 (t, $J = 7.9$ Hz, 1H), 2.75 (q, $J = 7.2$ Hz, 2H), 2.64 (t, $J = 6.8$ Hz, 2H), 2.40 (t, $J = 8.0$ Hz, 1H). δ ppm: 169.6, 167.2, 139.3, 131.3, 129.0, 124.0, 123.2, 119.8, 40.3, 19.6. HRMS (ESI $^-$) m/z calcd. for $\text{C}_{10}\text{H}_{10}\text{NO}_3\text{S}$ $[\text{M}-\text{H}]^-$ 224.03868, found 224.03814.

3-(3-Mercaptopropanamido)benzenesulfonic acid (30).



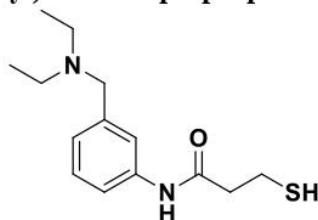
Compound **30** was synthesized according to the general procedure B, using compound **15** (40.4 mg, 0.13 mmol) and NaOH (21.3 mg, 0.53 mmol) in MeOH (3 mL). After workup with Amberlite, the product was purified using preparative HPLC. The final product was obtained as colorless oil (17.9 mg, 51%). ^1H NMR (500 MHz, $\text{DMSO}-d_6$) δ ppm: 9.99 (s, 1H), 7.82–7.79 (m, 1H), 7.64–7.60 (m, 1H), 7.28–7.20 (m, 2H), 2.77–2.71 (m, 2H), 2.62 (t, $J = 6.9$ Hz, 2H), 2.37 (t, $J = 8.0$ Hz, 1H). ^{13}C NMR (126 MHz, $\text{DMSO}-d_6$) δ ppm: 169.3, 148.8, 138.5, 127.9, 120.3, 119.0, 116.6, 40.3, 19.7. HRMS (ESI $^-$) m/z calcd. for $\text{C}_9\text{H}_{10}\text{NO}_4\text{S}_2$ $[\text{M}-\text{H}]^-$ 260.00567, found 260.00568.

3-Mercapto-N-(3-nitrophenyl)propanamide (31).



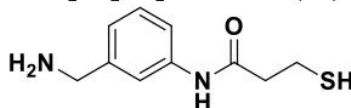
Compound **31** was synthesized according to the general procedure B, using compound **16** (97.7 mg, 0.36 mmol) and NaOH (44 mg, 1.09 mmol) in MeOH (5 mL). After workup with Amberlite, the product was purified using preparative HPLC. The final product was obtained as off-yellow solid (58 mg, 70%). ¹H NMR (500 MHz, DMSO-*d*₆) δ ppm: 10.47 (s, 1H), 8.66–8.63 (m, 1H), 7.92–7.87 (m, 2H), 7.60 (t, *J* = 8.2 Hz, 1H), 2.78–2.73 (m, 2H), 2.70–2.66 (m, 2H), 2.44 (t, *J* = 8.0 Hz, 1H). ¹³C NMR (126 MHz, DMSO-*d*₆) δ ppm: 170.2, 148.0, 140.2, 130.2, 125.0, 117.7, 113.1, 40.4, 19.5. HRMS (ESI⁻) *m/z* calcd. for C₉H₉N₂O₃S [M-H]⁻ 225.03394, found 225.03348.

***N*-(3-((Diethylamino)methyl)phenyl)-3-mercaptopropanamide (32).**



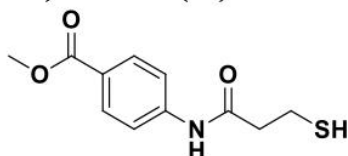
Compound **32** was synthesized according to the general procedure B, using compound **17** (150 mg, 0.49 mmol) and NaOH (77.8 mg, 1.94 mmol) in MeOH (8 mL). After workup with Amberlite, the product was purified using preparative HPLC. The final product was obtained as transparent oil (30 mg, 23%). ¹H NMR (500 MHz, DMSO-*d*₆) δ ppm: 10.04 (s, 1H), 7.66 (br s, 1H), 7.55–7.52 (m, 1H), 7.27 (t, *J* = 7.7 Hz, 1H), 7.09–7.06 (m, 1H), 3.76 (br s, 2H), 2.74 (q, *J* = 7.2 Hz, 2H), 2.68–2.60 (m, 6H), 2.38 (t, *J* = 7.9 Hz, 1H), 1.07 (t, *J* = 7.1 Hz, 6H). ¹³C NMR (126 MHz, DMSO-*d*₆) δ ppm: 169.4, 139.2, 128.7, 124.2, 120.0, 118.4, 56.1, 46.0, 40.2, 19.7, 10.4. HRMS (ESI⁺) *m/z* calcd. for C₁₄H₂₃N₂OS [M+H]⁺ 267.15256, found 267.15256.

***N*-(3-(Aminomethyl)phenyl)-3-mercaptopropanamide (33).**



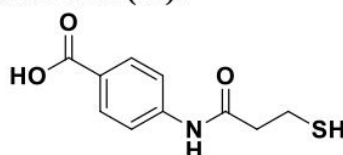
Compound **33** was synthesized according to general procedure B, using compound **18a** (138 mg, 0.55 mmol) and NaOH (86 mg, 2.18 mmol) in MeOH (3 mL). The product was purified using preparative HPLC. The final product was obtained as colorless oil (52 mg, 45%). ¹H NMR (500 MHz, DMSO-*d*₆) δ ppm: 10.10 (s, 1H), 7.77 (s, 1H), 7.46 (d, *J* = 8.7 Hz, 1H), 7.33 (t, *J* = 7.9 Hz, 1H), 7.11 (d, *J* = 7.6 Hz, 1H), 3.94 (s, 2H), 2.74 (t, *J* = 6.7 Hz, 2H), 2.64 (t, *J* = 6.7 Hz, 2H), 2.52–2.51 (m, 1H). ¹³C NMR (126 MHz, DMSO-*d*₆) δ ppm: 169.5, 139.3, 135.7, 128.9, 123.4, 120.2, 119.0, 42.8, 40.2, 19.7. HRMS (ESI⁺) *m/z* calcd. for C₁₀H₁₃N₂OS [M+H]⁺ 211.08996, found 211.09000.

Methyl 4-(3-mercaptopropanamido)benzoate (34).



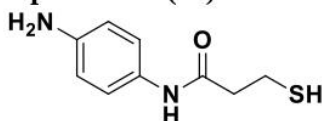
Compound **34** was synthesized according to general procedure B, using compound **19** (50 mg, 0.17 mmol) and 2 M NaOH aq. solution (177 μ L, 0.35 mmol) in MeOH (3 mL). The product was purified using reverse phase column chromatography. The final product was obtained as white solid (12 mg, 45%). ^1H NMR (500 MHz, CDCl_3) δ ppm: 10.32 (s, 1H), 7.92–7.90 (m, 2H), 7.77–7.72 (m, 2H), 3.82 (s, 3H), 2.75 (t, $J = 6.7$ Hz, 2H), 2.69–2.66 (m, 2H), 2.42 (br s, 1H). ^{13}C NMR (126 MHz, CDCl_3) δ ppm: 170.0, 165.8, 143.5, 130.3, 123.8, 118.4, 51.9, 40.4, 19.5. HRMS (ESI $^-$) m/z calcd. for $\text{C}_{11}\text{H}_{12}\text{NO}_3\text{S}$ $[\text{M}-\text{H}]^-$ 238.05433, found 238.05409.

4-(3-Mercaptopropanamido)benzoic acid (**35**).



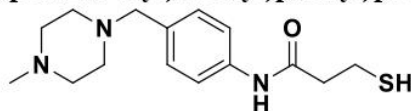
Compound **35** was synthesized according to general procedure B, using compound **20** (76 mg, 0.28 mmol) and NaOH (44 mg, 1.13 mmol) in MeOH (1.5 mL). The product was purified using preparative HPLC. The final product was obtained as white powder (61 mg, 95%). ^1H NMR (500 MHz, $\text{DMSO}-d_6$) δ ppm: 12.70 (br s, 1H), 10.27 (s, 1H), 7.89–7.87 (m, 2H), 7.71–7.69 (m, 2H), 2.74 (m, 2H), 2.67 (m, 2H), 2.40 (t, $J = 7.9$ Hz, 1H). ^{13}C NMR (126 MHz, $\text{DMSO}-d_6$) δ ppm: 169.9, 166.9, 143.1, 130.4, 125.1, 118.3, 40.4, 19.5. HRMS (ESI $^-$) m/z calcd. for $\text{C}_{10}\text{H}_{10}\text{NO}_3\text{S}$ $[\text{M}-\text{H}]^-$ 224.03868, found 224.03821.

N-(4-Aminophenyl)-3-mercaptopropanamide (**36**).



Compound **36** was synthesized according to the general procedure B, using compound **21a** (105.6 mg, 0.44 mmol) and NaOH (71 mg, 1.77 mmol) in MeOH (5 mL). After workup with Amberlite, the product was purified using preparative HPLC. The final product was obtained as colorless oil (35 mg, 40%). ^1H NMR (500 MHz, $\text{DMSO}-d_6$) δ ppm: 9.78 (s, 1H), 7.75–7.03 (m, 4H), 6.81 (d, $J = 8.8$ Hz, 2H), 2.75–2.69 (m, 2H), 2.58 (t, $J = 6.8$ Hz, 2H), 2.35 (t, $J = 7.9$ Hz, 1H). ^{13}C NMR (126 MHz, $\text{DMSO}-d_6$) δ ppm: 168.9, 135.3, 133.7, 120.4, 118.8, 40.4, 19.8. HRMS (ESI $^+$) m/z calcd. for $\text{C}_9\text{H}_{13}\text{N}_2\text{OS}$ $[\text{M}+\text{H}]^+$ 197.07431, found 197.07443.

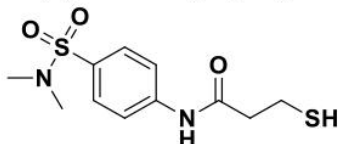
3-Mercapto-*N*-(4-((4-methylpiperazin-1-yl)methyl)phenyl)propanamide (**37**).



Compound **37** was synthesized according to general procedure B, using compound **22** (57 mg, 0.17 mmol) and NaOH (100 mg, 0.38 mmol) in MeOH (1 mL). The product was purified using preparative HPLC. The final product was obtained as colorless oil (28 mg, 56%). ^1H NMR (500 MHz, CDCl_3) δ ppm: 7.63 (s, 1H), 7.48 (d, $J = 8.5$ Hz, 2H), 7.24 (s, 2H), 3.50 (s, 2H), 2.89

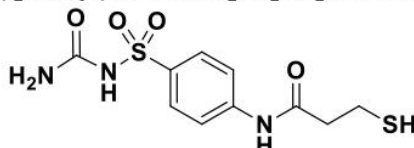
(t, $J = 6.6$ Hz, 2H), 2.80–2.57 (m, 8H), 2.69 (t, $J = 6.6$ Hz, 2H), 2.45 (s, 3H), 1.70 (s, 1H). ^{13}C NMR (126 MHz, CDCl_3) δ ppm: 169.2, 137.1, 133.4, 130.0, 120.0, 62.1, 54.1, 51.5, 44.7, 41.4, 20.4. HRMS (ESI⁺) m/z calcd. for $\text{C}_{15}\text{H}_{24}\text{N}_3\text{OS}$ $[\text{M}+\text{H}]^+$ 294.16345, found 294.16324.

***N*-(4-(*N,N*-Dimethylsulfamoyl)phenyl)-3-mercaptopropanamide (38).**



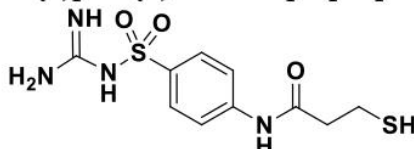
Compound **38** was synthesized according to general procedure B, using compound **23** (70 mg, 0.21 mmol) and 2 M NaOH aq. solution (212 μL , 0.42 mmol) in MeOH (2 mL). The product was purified using preparative HPLC. Final product was obtained as white solid (56 mg, 91%). ^1H NMR (500 MHz, $\text{DMSO-}d_6$) δ ppm: 10.40 (s, 1H), 7.85–7.82 (m, 2H), 7.70–7.62 (m, 2H), 2.76–2.73 (m, 2H), 2.70–2.66 (m, 2H), 2.57 (s, 6H), 2.43–2.40 (m, 1H). ^{13}C NMR (126 MHz, $\text{DMSO-}d_6$) δ ppm: 170.2, 143.2, 128.9, 128.3, 118.9, 40.5, 37.7, 19.6. HRMS (ESI⁻) m/z calcd. for $\text{C}_{11}\text{H}_{15}\text{N}_2\text{O}_3\text{S}_2$ $[\text{M}-\text{H}]^-$ 287.05295, found 287.05295.

***N*-(4-(*N*-Carbamoylsulfamoyl)phenyl)-3-mercaptopropanamide (39).**



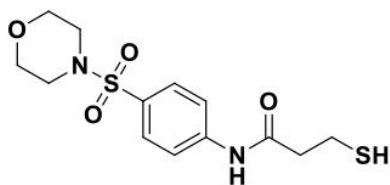
Compound **39** was synthesized according to the general procedure B, using compound **24** (80 mg, 0.23 mmol) and NaOH (28 mg, 0.70 mmol) in MeOH (5 mL). After workup with Amberlite, the product was washed with H_2O (3x). Final product was obtained as white solid (46.1 mg, 65%). ^1H NMR (500 MHz, $\text{DMSO-}d_6$) δ ppm: 10.46 (br s, 1H), 10.39 (s, 1H), 7.84–7.80 (m, 2H), 7.79–7.75 (m, 2H), 6.37 (br s, 2H), 2.78–2.72 (m, 2H), 2.70–2.65 (m, 2H), 2.42 (t, $J = 8.0$ Hz, 1H). ^{13}C NMR (126 MHz, $\text{DMSO-}d_6$) δ ppm: 170.1, 152.1, 143.2, 133.9, 128.5, 118.5, 40.4, 19.5. HRMS (ESI⁻) m/z calcd. for $\text{C}_{10}\text{H}_{12}\text{N}_3\text{O}_4\text{S}_2$ $[\text{M}-\text{H}]^-$ 302.02747, found 302.02731.

***N*-(4-(*N*-Carbamimidoylsulfamoyl)phenyl)-3-mercaptopropanamide (40).**



Compound **40** was synthesized according to the general procedure B, using compound **25** (80 mg, 0.23 mmol) and NaOH (28 mg, 0.70 mmol) in MeOH (5 mL). After workup with Amberlite, the product was obtained pure as off-white solid (22 mg, 32%). ^1H NMR (500 MHz, $\text{DMSO-}d_6$) δ ppm: 10.24 (s, 1H), 7.71–7.65 (m, 4H), 6.66 (br s, 4H), 2.77–2.71 (m, 2H), 2.68–2.63 (m, 2H), 2.40 (t, $J = 8.0$ Hz, 1H). ^{13}C NMR (126 MHz, $\text{DMSO-}d_6$) δ ppm: 169.8, 158.0, 141.5, 138.8, 126.6, 118.4, 40.3, 19.5. HRMS (ESI⁻) m/z calcd. for $\text{C}_{10}\text{H}_{13}\text{N}_4\text{O}_3\text{S}_2$ $[\text{M}-\text{H}]^-$ 301.04345, found 301.04337.

3-Mercapto-*N*-(4-(morpholinosulfonyl)phenyl)propanamide (41).



Compound **41** was synthesized according to the general procedure B, using compound **26** (80 mg, 0.22 mmol) and NaOH (26 mg, 0.64 mmol) in MeOH (5 mL). After workup with Amberlite, the product was purified using preparative HPLC. The final product was obtained as white solid (45 mg, 63%). ^1H NMR (500 MHz, DMSO- d_6) δ ppm: 10.44 (s, 1H), 7.86 (d, $J = 8.7$ Hz, 2H), 7.68 (d, $J = 8.8$ Hz, 2H), 3.63–3.59 (m, 4H), 2.84–2.80 (m, 4H), 2.77–2.73 (m, 2H), 2.71–2.66 (m, 2H), 2.43 (br s, 1H). ^{13}C NMR (126 MHz, DMSO- d_6) δ ppm: 170.2, 143.4, 129.0, 127.9, 118.8, 65.3, 45.9, 40.4, 19.5. HRMS (ESI $^-$) m/z calcd. for $\text{C}_{13}\text{H}_{17}\text{N}_2\text{O}_4\text{S}_2$ $[\text{M}-\text{H}]^-$ 329.06352, found 329.06381.

3. Supporting Figures and Tables

Figure S1. Proposed binding modes of compounds **8**, **29**, and **35** to IMP-7. The structure of IMP-7 was generated through manual mutation and energy minimization of the IMP-1 structure in complex with a mercapropoxy carboxylate inhibitor (PDB code 1DD6, Concha et al, *Biochemistry*, 39 (15), 4288–4298). Docking was performed using default settings from MOE 2019.0102 and the best pose was subjected to energy minimization.

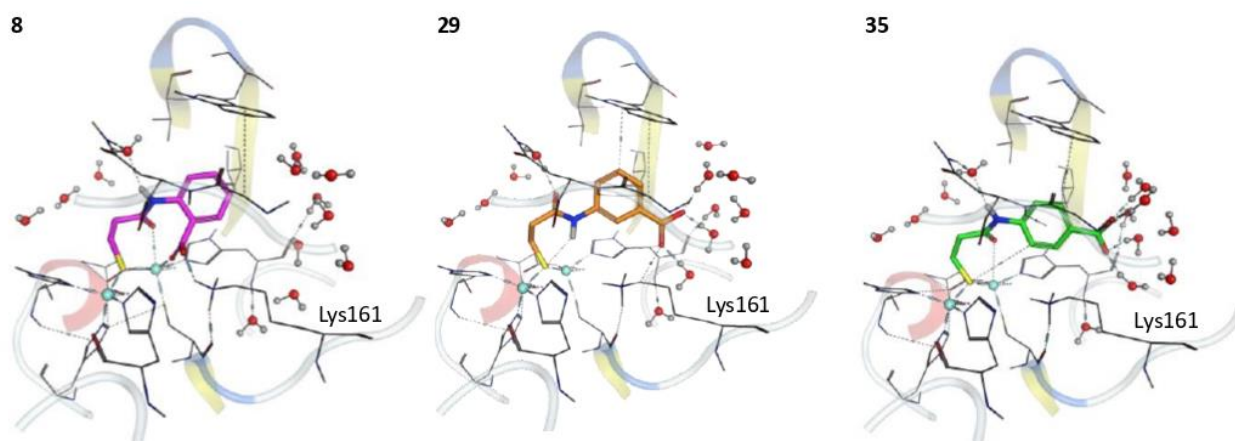


Table S1. Percent inhibition of LasB at 100 μM by inhibitors **5**, **29**, **34** and **39**.

Compound	% inh. of LasB @100 μM
5	55.8
29	9.2
34	26.5
39	19.7

Table S2. Intrinsic antimicrobial activity of eight selected compounds against four different transformants.

Isolates	MIC [mg/L]							
	6	8	29	30	33	38	39	40
<i>E. coli</i> NDM-1	>1024	>1024	>1024	>1024	>1024	>1024	>1024	>1024
<i>E. coli</i> VIM-1	1024	n.d.	>128	>128	>128	>128	>128	>128
<i>E. coli</i> IMP-1	1024	n.d.	>128	>128	>128	>128	>128	>128
<i>P. aeruginosa</i> VIM-2	>1024	n.d.						

Table S3. Zebrafish-embryo toxicity results for three compounds **8**, **39** and **40**.

Compounds	Conc. (µM)	2 dpf	3 dpf	4 dpf	5 dpf	Final Survival rate %
8	150	OK	OK, 2 malf.	OK, 2 malf.	OK, 2 malf.	100
	100	OK	OK, 2 malf.	OK, 2 malf.	OK, 2 malf.	100
	50	OK	OK, 1 malf.	OK, 1 malf.	OK, 1 malf.	100
	30	OK	OK, 1 malf.	OK, 1 malf.	OK, 1 malf.	100
39	150	OK	OK, 1 malf.	OK, 1 malf.	OK, 1 malf.	100
	100	OK	OK	OK	OK	100
	50	OK	OK, 1 malf.	OK, 1 malf.	OK, 1 malf.	100
	30	OK	OK	OK	OK	100
40	150	OK	OK, 1 malf.	OK, 1 malf.	OK, 1 malf.	100
	100	OK	OK	OK	OK	100
	50	OK	OK	OK	OK	100
	30	OK	OK, 1 malf.	OK, 1 malf.	OK, 1 malf.	100
Danieau's ctrl	-	OK	OK, 1 malf., 1 dead	OK	OK	90
DMSO ctrl	-	OK	OK, 1 malf.	OK	OK	100

malf. = body curvature

impaired dev. = impaired development, pericardial edema

For 10–20% of larvae (1–2 larvae out of 10) a curvature of the body was observed when incubated in compound **8**. For compounds **39** and **40** the body curvature was detected in maximum 10% of larvae. A comparable ratio of malformation was also found in the control groups (with only Danieau's medium or 1% DMSO). Therefore, observed body malformation in larvae incubated in compound can be considered as not related to compound treatment.

Table S4. Retention time t_R and corresponding $\log D_{7.4}$ values of control compounds.

Compounds	t_R^a	$\log D_{7.4}$
Salicylic Acid	1.86	-2.11
Atenolol	1.85	-1.82
Furosemide	2.13	-1.02
Caffeine	1.98	-0.07
Antipyrin	2.18	0.38
Chloramphenicol	2.38	1.14
Propranolol	2.50	1.26
Carbamazepine	2.58	1.54
Nifedipine	2.87	3.17
Loratadine	3.36	4.40
Bifonazol	3.31	4.77
Clotrimazol	3.38	5.21

^aRetention time in min.

Table S5. Antimicrobial activity of imipenem with selected compounds against *E. coli* NDM-1 (T2359).

Inhibitor Conc.	Imipenem MIC (mg/L)						
	8	29	30	33	35	39	40
-	128	128	128	128	128	128	128
+ 128 µg/mL	2	≤0,5	2	64	8	16	16
+ 64 µg/mL	8	2	32	128	32	64	64
+ 32 µg/mL	16	8	128	128	128	128	128
+ 16 µg/mL	64	64	128	128	128	128	128
+ 8 µg/mL	64	64	128	128	128	128	128
+ 4 µg/mL	64	128	128	128	128	128	128
+ 2 µg/mL	n.d.	128	128	128	128	128	128

Table S6. Antimicrobial activity of imipenem with selected compounds against *E. coli* VIM-1 (T2544).

Inhibitor Conc.	Imipenem MIC (mg/L)					
	29	30	33	35	39	40
-	32	64	32	32	32	32
+ 128 µg/mL	16	4	2	2	0.5	1
+ 64 µg/mL	32	8	8	8	8	2
+ 32 µg/mL	32	32	16	16	16	4
+ 16 µg/mL	32	32	32	32	16	16
+ 8 µg/mL	32	64	32	32	32	16
+ 4 µg/mL	32	64	32	32	32	16
+ 2 µg/mL	32	64	32	32	32	16

Table S7. Antimicrobial activity of imipenem with selected compounds against *E. coli* IMP-1 (T2360).

Inhibitor Conc.	Imipenem MIC (mg/L)					
	29	30	33	35	39	40
-	1	2	2	2	2	2
+ 128 µg/mL	1	0.5	1	0.5	0.5	0.5
+ 64 µg/mL	0.5	1	1	1	0.5	0.5
+ 32 µg/mL	1	1	1	1	1	1
+ 16 µg/mL	2	1	1	1	1	1
+ 8 µg/mL	0.5	2	2	1	1	2
+ 4 µg/mL	0.5	2	2	1	2	2
+ 2 µg/mL	1	2	2	5	2	2

Table S8. Intrinsic antimicrobial activity of compound **29** against eleven clinical isolates expressing various MBL and non-MBL carbapenemases.

Isolates	Compound 29 MIC (mg/L)
<i>E. coli</i> NDM-7 (T2239)	>256
<i>K. pneumoniae</i> NDM-1 (T2301)	>256
<i>E. cloacae</i> NDM-1 (T2311)	>256
<i>S. marcescens</i> NDM-1 (T2352)	>256
<i>E. coli</i> NDM-5 (T2351)	>256
<i>E. cloacae</i> VIM-1 (T2353)	>256
<i>P. aeruginosa</i> VIM-1 (T2357)	>256
<i>P. aeruginosa</i> IMP-1 (T2325)	>256
<i>E. cloacae</i> GIM-1 (T2218)	>256
<i>A. baumannii</i> OXA-23 (T2434)	>256
<i>E. coli</i> KPC-2 (T2435)	>256

Chapter 3: Concluding Remarks and Outlook

As described in the introduction section, antivirulence therapy is considered as an effective method to lower the selective pressure on pathogenic bacteria by targeting their extracellular virulence factors. The first part of this thesis was focused on the discovery and synthesis of inhibitors of ColH and LasB, two extracellular zinc-containing enzymes that play vital roles in the pathogenicity of the resistant bacteria *Clostridium histolyticum* and *Pseudomonas aeruginosa*, respectively.

For the sake of clarity, the compound codes are opted from each chapter, referring to the respective manuscript they are part of.

In designing inhibitors of LasB, we first opted a substrate-based fragment merging approach on a previously identified hit structure compound **4** *N*-(3,4-dichlorophenyl)-2-mercaptoacetamide ($IC_{50} = 6.6 \pm 0.3 \mu M$). Rationalization of the binding mode of this new class, α -benzyl-*N*-aryl mercaptoacetamides, was achieved with a co-crystal structure of LasB in complex with compound **7d**. Even though it was co-crystallized in the same binding pocket like our previous hit structure compound **4**, unlike this molecule, di-chloro motif was shown to be not beneficial for the inhibitory activity.

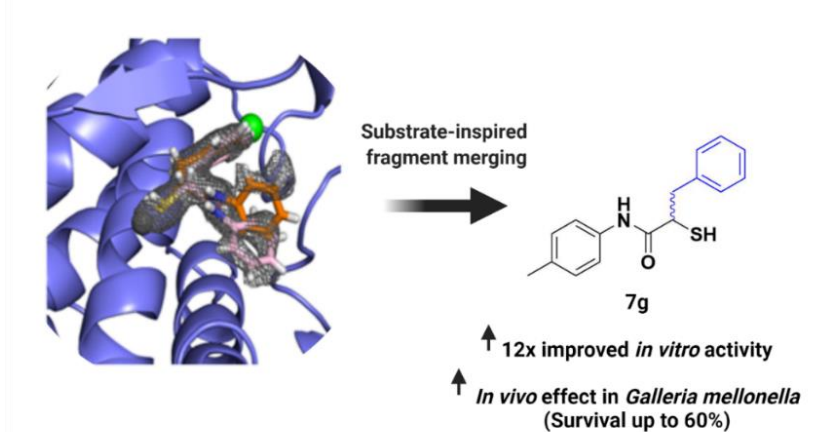


Figure 3.1: Schematic representation of the substrate-inspired fragment merged strategy. The figure is reprinted with permission from *Angew. Chem. Int. Ed.* **2022**, *61*, e202112295.

By optimizing the compound **7d** with a small structure activity study, we identified compound **7g**, substituted with a methyl group on *para*-position, with a 12-fold increase in activity ($IC_{50} = 0.48 \pm 0.04 \mu M$) restoring the selectivity over human matrix metalloproteins (Figure 3.1). We were able to rationalize this extraordinary boost in activity by the interactions of the benzyl

group in the binding pocket, namely the interaction of *para*-methyl group with surrounding leucine residue (Leu 197). The increase in potency against LasB with this class of compounds also translated into an *in vivo* effect and our compound **7g** increased the survival rate of the *Galleria Mellonella* larvae up to 60% after three days of incubation. Overall, we demonstrated the importance of applying fragment-merging/linking strategies on fine-tuning of the potency of the inhibitors of this important target.

Following this successful approach, we extended the chemical space of these class of inhibitors by exploring the effect of different substituents on both *N*-aryl and the benzyl ring. Given the fact that the *para*-position was the most beneficial for activity, we designed and synthesized seven derivatives, all of which bear substituents on *para*-position of the *N*-aryl ring.

Interestingly, electron-withdrawing groups did not demonstrate a beneficial effect with respect to activity, and electron-donating groups such as methoxy or hydroxyl only maintained the activity of compound **7d**. Nevertheless, the exploration of different substituents provided a deeper understanding of the nature of the binding pocket. For example, the *N*-arylamide group in the S1` pocket is stabilized by H-bonding and hydrophobic interactions. To further improve these core interactions, we performed a molecular docking study to replace the *N*-aryl ring with heterocycles differing in size and substituents.

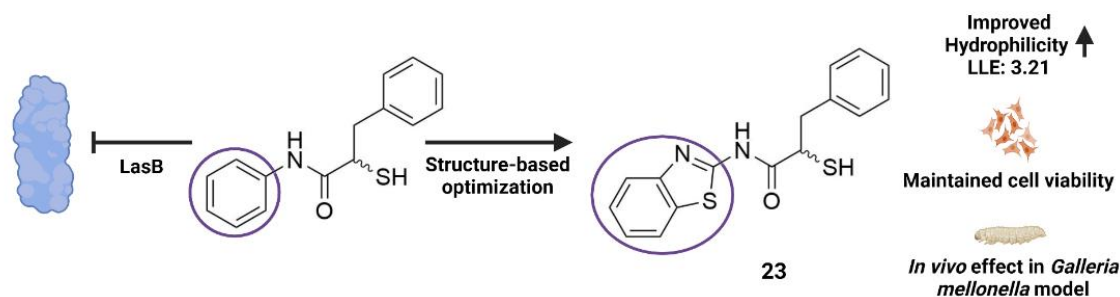


Figure 3.2 Schematic representation of the structure-based design strategy. The figure is reused with permission from *ACS Infectious Diseases* 2022 8 (5), 1010–1021 DOI: 10.1021/acsinfecdis.1c00628.

Although no notable improvement in the activity was observed with these nine additional heterocyclic derivatives, selected compounds such as **13** and **23** (Figure 3.2) showed a restored activity and selectivity over human MMPs compared to compound **7g**. They also maintained the cell viability and demonstrated an *in vivo* effect in *Galleria Mellonella* model. These results

validated our inhibitors as potential candidates to block the pathogenicity of *P. aeruginosa* and improved the LLE of our compounds.

In the next part of the thesis, screening of a halogen-enriched fragment library with several bio-orthogonal methods against peptidase domain of extracellular target ColH yielded a hit fragment compound **4** with a low micromolar activity ($IC_{50} = 117 \pm 5 \mu M$). Crystallization of 4-chloroisatin with ColH-PD revealed an interesting observation that unlike most metalloprotease inhibitors, the fragment was not directed to the zinc cation on the active site.

Considering the potential interactions on the binding pocket, we realized different growing directions of the fragment and explored these separately to demonstrate the effect of different modifications on the inhibitory activity. Eight of the derivatives were commercially available and therefore was purchased whereas 27 of them were synthesized.

Rationalization of the binding modes of the predicted structures were performed through docking in the crystal structure. Among 35 derivatives, a two-fold improvement against ColH-PD activity with compound **6** ($IC_{50} = 44 \pm 2 \mu M$) is achieved which can be considered as a significant improvement given the small size of the molecule.

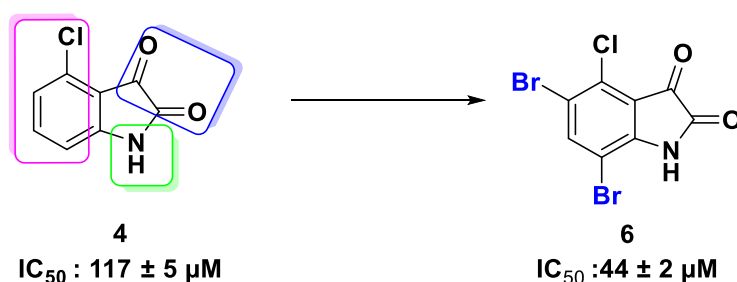


Figure 3.3 Chemical structure and IC_{50} value of the hit fragment compound **4** and the optimized fragment compound **6**.

Given that the identified fragment is quite small, further growing strategies are crucial for improving the potency. Nevertheless, our efforts successfully highlighted the importance of applying fragment-based strategies on antivirulence targets for designing and developing novel pathoblockers.

In the final part of the thesis, we identified a series of *N*-aryl mercaptoacetamides as inhibitors of several class B1 metallo-beta-lactamases. The discovery of this class was achieved through the design of a merged inhibitor structure inspired by a previously identified hit structure and

recently discovered *N*-aryl mercaptopropionamides inhibiting both several class B1 MBLs and LasB.

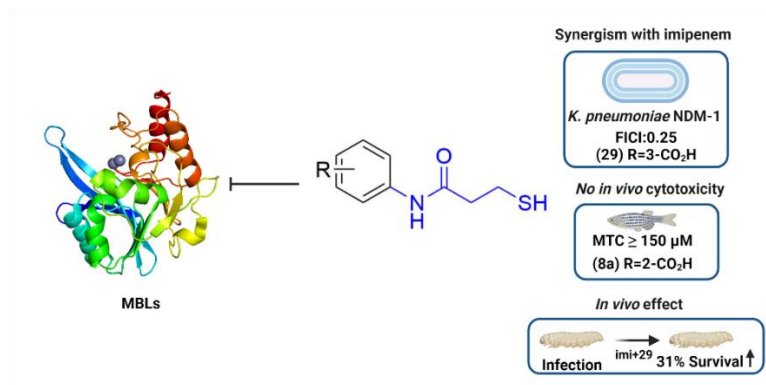
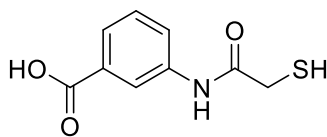


Figure 3.4 Schematic representation of *N*-aryl mercaptopropionamides as inhibitors of MBLs. The figure is reprinted with permission from *Journal of Medicinal Chemistry* **2022** 65 (5), 3913– 3922 DOI: 10.1021/acs.jmedchem.1c01755

Our aim was to increase the hydrophilicity of the substituents on the *N*-aryl ring, thereby increasing their hydrophilicity, as the position of β -lactamases in Gram-negative bacteria in the periplasm constitutes a problem of permeability. Consequently, measuring the $\log D_{7.4}$ value of our inhibitors in a HPLC–MS based assay enabled us to select some inhibitors fulfilling several parameters such as low $\log D_{7.4}$, high selectivity, and high potency for further evaluation.

We observed that the increase in hydrophilicity of the substituents on the *N*-aryl ring did not always correlate to the increase in their potency as some compounds demonstrating the lowest $\log D_{7.4}$ values were not potent inhibitors of some of the selected class B1 MBLs (IMP-7, VIM- 1, NDM-1).

Among six selected structures, compound **29** showed a synergistic effect with imipenem against *E. coli* producing NDM-1. It also showed a concentration-dependency and reduced the MIC values at their highest concentration up to 256-fold.



29

IC_{50} (NDM-1) = $4.0 \pm 0.0 \mu\text{M}$

IC_{50} (IMP-7) = $6.4 \pm 0.6 \mu\text{M}$

IC_{50} (VIM-1) = $1.2 \pm 0.0 \mu\text{M}$

$\log D_{7,4}$: -0.96

Figure 3.5 Structure of compound **29** and its inhibitory activity against three different ClassB1 MBLs.

A two-dimensional checkerboard analysis of compound **29** against a clinical *K. pneumoniae* isolate producing NDM-1 indicated the synergism of the hit compound **29** when combined with imipenem with a fractional inhibitory concentration index (FICI) value of 0.25, verifying the rescue effect of our inhibitor. The synergistic effect and the time-kill studies shown by inhibitor **29** also translated to an *in vivo* effect in *K. pneumoniae* producing NDM-1 in a *Galleria mellonella* infection model, demonstrating the potential of this structural motif in filling the increasing void for clinically approved MBL inhibitors.

Outlook

The results described in this thesis present important milestones in designing anti-infectives with novel modes of action for both resistant Gram-positive and Gram-negative bacteria. These milestones can pave the way for overcoming upcoming challenges in obtaining selective and potent inhibitors.

Future perspectives for each of the projects presented can be summarized as follows:

LasB:

- Screening the inhibitory activities of different zinc-binding groups to overcome the stability issues associated with free thiol group.
- Screening of the identified hits against other potential human off-targets to enhance the selectivity profile of the identified inhibitors.
- Further optimization of the physicochemical properties of the identified class to improve the lipophilic ligand efficacy (LLE).

ColH:

- Structure-based growing of the optimized fragment and parent fragment in the binding pocket of ColH-PD.
- Exploration of different zinc-binding groups to grow the identified fragment in the direction of the zinc group on active site.

MBLs:

- Identifying binding mode of this class by a co-crystal structure.
- Further optimization of the chemical class to improve the selectivity against several off-targets.
- Increasing hydrophilicity further while checking the experimental $\log D_{7.4}$ values of the inhibitors.
- Exploration of the synergistic effect of identified inhibitors in combination with different β -lactam antibiotics or against different isolates.
- Performing additional *in vivo* studies to demonstrate the potential of this class of compounds as successful MBL inhibitors.

References

- (1) Ventola, C. L. The Antibiotic Resistance Crisis: Causes and Threats. *P T J.* **2015**, *40* (4), 277–283. <https://doi.org/Article>.
- (2) Bank, W. Drug-Resistant Infections. *Drug-Resistant Infect.* **2017**. <https://doi.org/10.1596/26707>.
- (3) World Health Organization. No Time To Wait: Securing the Future From Drug-Resistant Infections Report To the Secretary-General of the United Nations https://www.who.int/antimicrobial-resistance/interagency-coordination-group/IACG_final_report_EN.pdf?ua=1 (accessed Oct 23, 2021).
- (4) Martínez, O. F.; Cardoso, M. H.; Ribeiro, S. M.; Franco, O. L. Recent Advances in Anti-Virulence Therapeutic Strategies with a Focus on Dismantling Bacterial Membrane Microdomains, Toxin Neutralization, Quorum-Sensing Interference and Biofilm Inhibition. *Front. Cell. Infect. Microbiol.* **2019**, *9* (APR), 1–24. <https://doi.org/10.3389/fcimb.2019.00074>.
- (5) Kaya, C.; Walter, I.; Alhayek, A.; Shafiei, R.; Jézéquel, G.; Andreas, A.; Konstantinović, J.; Schönauer, E.; Sikandar, A.; Hauptenthal, J.; Müller, R.; Brandstetter, H.; Hartmann, R. W.; Hirsch, A. K. H. Structure-Based Design of α -Substituted Mercaptoacetamides as Inhibitors of the Virulence Factor LasB from *Pseudomonas Aeruginosa*. *ACS Infect. Dis.* **2022**. <https://doi.org/10.1021/acsinfecdis.1c00628>.
- (6) Lopetuso, L. R.; Scaldaferrri, F.; Petito, V.; Gasbarrini, A. Commensal Clostridia: Leading Players in the Maintenance of Gut Homeostasis. *Gut Pathog.* **2013**, *5* (1), 1–8. <https://doi.org/10.1186/1757-4749-5-23>.
- (7) Hatheway, C. L. Toxigenic Clostridia. *Clin. Microbiol. Rev.* **1990**, *3* (1), 66–98. <https://doi.org/10.1128/cmr.3.1.66-98.1990>.
- (8) Hagihara, M.; Ariyoshi, T.; Kuroki, Y.; Eguchi, S.; Higashi, S.; Mori, T.; Nonogaki, T.; Iwasaki, K.; Yamashita, M.; Asai, N.; Koizumi, Y.; Oka, K.; Takahashi, M.; Yamagishi, Y.; Mikamo, H. Clostridium Butyricum Enhances Colonization Resistance against Clostridioides Difficile by Metabolic and Immune Modulation. *Sci. Rep.* **2021**, *11* (1), 1–15. <https://doi.org/10.1038/s41598-021-94572-z>.
- (9) Eckhard, U.; Huesgen, P. F.; Brandstetter, H.; Overall, C. M. Proteomic Protease Specificity Profiling of Clostridial Collagenases Reveals Their Intrinsic Nature as Dedicated Degradors of Collagen. *J. Proteomics* **2014**, *100*, 102–114. <https://doi.org/10.1016/j.jprot.2013.10.004>.
- (10) Matsushita, O.; Okabe, A. Clostridial Hydrolytic Enzymes Degrading Extracellular Components. *Toxicon* **2001**, *39* (11), 1769–1780. [https://doi.org/10.1016/S0041-0101\(01\)00163-5](https://doi.org/10.1016/S0041-0101(01)00163-5).
- (11) Oshima, N.; Narukawa, Y.; Takeda, T.; Kiuchi, F. Collagenase Inhibitors from *Viola Yedoensis*. *J. Nat. Med.* **2013**, *67* (1), 240–245. <https://doi.org/10.1007/s11418-012-0665-8>.
- (12) Schönauer, E.; Kany, A. M.; Hauptenthal, J.; Hüsecken, K.; Hoppe, I. J.; Voos, K.; Yahiaoui, S.; Elsässer, B.; Ducho, C.; Brandstetter, H.; Hartmann, R. W. Discovery of

- a Potent Inhibitor Class with High Selectivity towards Clostridial Collagenases. *J. Am. Chem. Soc.* **2017**, jacs.7b06935. <https://doi.org/10.1021/jacs.7b06935>.
- (13) Ilies, M.; Banciu, M. D.; Scozzafava, A.; Ilies, M. A.; Caproiu, M. T.; Supuran, C. T. Protease Inhibitors: Synthesis of Bacterial Collagenase and Matrix Metalloproteinase Inhibitors Incorporating Arylsulfonylureido and 5-Dibenzo-Suberenyl/Suberyl Moieties. *Bioorganic Med. Chem.* **2003**, *11* (10), 2227–2239. [https://doi.org/10.1016/S0968-0896\(03\)00113-5](https://doi.org/10.1016/S0968-0896(03)00113-5).
- (14) Kany, A. M.; Sikandar, A.; Yahiaoui, S.; Hauptenthal, J.; Walter, I.; Empting, M.; Köhnke, J.; Hartmann, R. W. Tackling *Pseudomonas Aeruginosa* Virulence by a Hydroxamic Acid-Based LasB Inhibitor. *ACS Chem. Biol.* **2018**, *13* (9), 2449–2455. <https://doi.org/10.1021/acscchembio.8b00257>.
- (15) Schönauer, E.; Kany, A. M.; Hauptenthal, J.; Hüsecken, K.; Hoppe, I. J.; Voos, K.; Yahiaoui, S.; Elsässer, B.; Ducho, C.; Brandstetter, H.; Hartmann, R. W. Discovery of a Potent Inhibitor Class with High Selectivity toward Clostridial Collagenases. *J. Am. Chem. Soc.* **2017**, *139* (36), 12696–12703. <https://doi.org/10.1021/jacs.7b06935>.
- (16) Voos, K.; Schönauer, E.; Alhayek, A.; Hauptenthal, J.; Andreas, A.; Müller, R.; Hartmann, R. W.; Brandstetter, H.; Hirsch, A. K. H.; Ducho, C. Phosphonate as a Stable Zinc-Binding Group for “Pathoblocker” Inhibitors of Clostridial Collagenase H (ColH). *ChemMedChem* **2021**. <https://doi.org/10.1002/cmdc.202000994>.
- (17) Davis, B. J.; Roughley, S. D. Fragment-Based Lead Discovery; 2017; pp 371–439. <https://doi.org/10.1016/bs.armc.2017.07.002>.
- (18) de Souza Neto, L. R.; Moreira-Filho, J. T.; Neves, B. J.; Maidana, R. L. B. R.; Guimarães, A. C. R.; Furnham, N.; Andrade, C. H.; Silva, F. P. In Silico Strategies to Support Fragment-to-Lead Optimization in Drug Discovery. *Front. Chem.* **2020**, *8* (February), 1–18. <https://doi.org/10.3389/fchem.2020.00093>.
- (19) Li, Q. Application of Fragment-Based Drug Discovery to Versatile Targets. *Front. Mol. Biosci.* **2020**, *7* (August), 1–13. <https://doi.org/10.3389/fmolb.2020.00180>.
- (20) Hubbard, R. E.; Murray, J. B. Experiences in Fragment-Based Lead Discovery; 2011; pp 509–531. <https://doi.org/10.1016/B978-0-12-381274-2.00020-0>.
- (21) Scott, D. E.; Coyne, A. G.; Hudson, S. A.; Abell, C. Fragment-Based Approaches in Drug Discovery and Chemical Biology. *Biochemistry* **2012**, *51* (25), 4990–5003. <https://doi.org/10.1021/bi3005126>.
- (22) Bollag, G.; Hirth, P.; Tsai, J.; Zhang, J.; Ibrahim, P. N.; Cho, H.; Spevak, W.; Zhang, C.; Zhang, Y.; Habets, G.; Burton, E. A.; Wong, B.; Tsang, G.; West, B. L.; Powell, B.; Shellooe, R.; Marimuthu, A.; Nguyen, H.; Zhang, K. Y. J.; Artis, D. R.; Schlessinger, J.; Su, F.; Higgins, B.; Iyer, R.; D’Andrea, K.; Koehler, A.; Stumm, M.; Lin, P. S.; Lee, R. J.; Grippo, J.; Puzanov, I.; Kim, K. B.; Ribas, A.; McArthur, G. A.; Sosman, J. A.; Chapman, P. B.; Flaherty, K. T.; Xu, X.; Nathanson, K. L.; Nolop, K. Clinical Efficacy of a RAF Inhibitor Needs Broad Target Blockade in BRAF-Mutant Melanoma. *Nature* **2010**, *467* (7315), 596–599. <https://doi.org/10.1038/nature09454>.
- (23) Zimmermann, M. O.; Lange, A.; Wilcken, R.; Cieslik, M. B.; Exner, T. E.; Joerger, A. C.; Koch, P.; Boeckler, F. M. Halogen-Enriched Fragment Libraries as Chemical Probes for Harnessing Halogen Bonding in Fragment-Based Lead Discovery. *Future Med. Chem.* **2014**, *6* (6), 617–639. <https://doi.org/10.4155/fmc.14.20>.

- (24) Heidrich, J.; Sperl, L. E.; Boeckler, F. M. Embracing the Diversity of Halogen Bonding Motifs in Fragment-Based Drug Discovery-Construction of a Diversity-Optimized Halogen-Enriched Fragment Library. *Front. Chem.* **2019**, *7* (FEB). <https://doi.org/10.3389/fchem.2019.00009>.
- (25) Wilcken, R.; Liu, X.; Zimmermann, M. O.; Rutherford, T. J.; Fersht, A. R.; Joerger, A. C.; Boeckler, F. M. Halogen-Enriched Fragment Libraries as Leads for Drug Rescue of Mutant P53. *J. Am. Chem. Soc.* **2012**, *134* (15), 6810–6818. <https://doi.org/10.1021/ja301056a>.
- (26) Jerabek-Willemsen, M.; André, T.; Wanner, R.; Roth, H. M.; Duhr, S.; Baaske, P.; Breitsprecher, D. MicroScale Thermophoresis: Interaction Analysis and Beyond. *J. Mol. Struct.* **2014**, *1077*, 101–113. <https://doi.org/10.1016/j.molstruc.2014.03.009>.
- (27) Wienken, C. J.; Baaske, P.; Rothbauer, U.; Braun, D.; Duhr, S. Protein-Binding Assays in Biological Liquids Using Microscale Thermophoresis. *Nat. Commun.* **2010**, *1* (1), 100. <https://doi.org/10.1038/ncomms1093>.
- (28) Kany, A. M.; Sikandar, A.; Haupenthal, J.; Yahiaoui, S.; Maurer, C. K.; Proschak, E.; Köhnke, J.; Hartmann, R. W. Binding Mode Characterization and Early in Vivo Evaluation of Fragment-Like Thiols as Inhibitors of the Virulence Factor LasB from *Pseudomonas Aeruginosa*. *ACS Infect. Dis.* **2018**, *4* (6), 988–997. <https://doi.org/10.1021/acsinfecdis.8b00010>.
- (29) Stura, E. A.; Wilson, I. A. Applications of the Streak Seeding Technique in Protein Crystallization. *J. Cryst. Growth* **1991**, *110* (1–2), 270–282. [https://doi.org/10.1016/0022-0248\(91\)90896-D](https://doi.org/10.1016/0022-0248(91)90896-D).
- (30) Kabsch, W. XDS. *Acta Crystallogr. Sect. D Biol. Crystallogr.* **2010**, *66* (2), 125–132. <https://doi.org/10.1107/S0907444909047337>.
- (31) Evans, P. R.; Murshudov, G. N. How Good Are My Data and What Is the Resolution? *Acta Crystallogr. Sect. D Biol. Crystallogr.* **2013**, *69* (7), 1204–1214. <https://doi.org/10.1107/S0907444913000061>.
- (32) Smart, O. S.; Womack, T. O.; Flensburg, C.; Keller, P.; Paciorek, W.; Sharff, A.; Vonnrhein, C.; Bricogne, G. Exploiting Structure Similarity in Refinement: Automated NCS and Target-Structure Restraints in BUSTER. *Acta Crystallogr. Sect. D Biol. Crystallogr.* **2012**, *68* (4), 368–380. <https://doi.org/10.1107/S0907444911056058>.
- (33) Adams, P. D.; Afonine, P. V.; Bunkóczi, G.; Chen, V. B.; Davis, I. W.; Echols, N.; Headd, J. J.; Hung, L.-W.; Kapral, G. J.; Grosse-Kunstleve, R. W.; McCoy, A. J.; Moriarty, N. W.; Oeffner, R.; Read, R. J.; Richardson, D. C.; Richardson, J. S.; Terwilliger, T. C.; Zwart, P. H. PHENIX : A Comprehensive Python-Based System for Macromolecular Structure Solution. *Acta Crystallogr. Sect. D Biol. Crystallogr.* **2010**, *66* (2), 213–221. <https://doi.org/10.1107/S0907444909052925>.
- (34) Emsley, P.; Lohkamp, B.; Scott, W. G.; Cowtan, K. Features and Development of Coot. *Acta Crystallogr. Sect. D Biol. Crystallogr.* **2010**, *66* (4), 486–501. <https://doi.org/10.1107/S0907444910007493>.

Appendix: Conference Contributions

“Fragment-based design of inhibitors of ColH from *Clostridium Histolyticum*”

Oral Presentation:

Kaya C., Hamsparth T., Kany A.M., Schönauer E., Hauptenthal J., Yahiaoui S., Brandstetter H., Hartmann R.W, Hirsch A.K.H. 7th RSC-BMCS Fragment-based drug discovery, March 2019, Cambridge, UK

Poster Presentation:

Kaya C., Hamsparth T., Kany A.M., Schönauer E., Hauptenthal J., Yahiaoui S., Brandstetter H., Hartmann R.W, Hirsch A.K.H. 7th RSC-BMCS Fragment-based drug discovery, March 2019, Cambridge, UK

“Design, synthesis and Biological evaluation of ColH from *Clostridium Histolyticum*”

Oral Presentation:

Kaya C., Kany A.M., Schönauer E., Sikandar A., Hauptenthal J., Yahiaoui S., Maurer C. K., Empting M., Hüsecken K., Hoppe I.J., Voos K., Ducho C., Köhnke J., Brandstetter H., Hartmann R.W, Hirsch A.K.H. Summer Symposium of the Graduate School Natural Product Research Saarland University, July 2018, Saarbrücken, Germany

Poster Presentation:

Kaya C., Kany A.M., Schönauer E., Sikandar A., Hauptenthal J., Yahiaoui S., Maurer C. K., Empting M., Hüsecken K., Hoppe I.J., Voos K., Ducho C., Köhnke J., Brandstetter H., Hartmann R.W, Hirsch A.K.H. International HIPS Symposium, June 2018, Saarbrücken, Germany

“N-Aryl mercaptopropionamides as broad-spectrum inhibitors of metallo-beta-lactamases”

Oral Presentation:

Kaya C., Yahiaoui S., Kany A.M., Hauptenthal J., Kramer J.S., Brunst S., Proschak E., Wichelhaus T.A., Hartmann R.W., Hirsch A.K.H. 17th Annual PhD Retreat HZI, November 2020, Braunschweig, Germany

Poster Presentation:

Kaya C., Yahiaoui S., Kany A.M., Hauptenthal J., Kramer J.S., Brunst S., Proschak E., Wichelhaus T.A., Hartmann R.W., Hirsch A.K.H. Annual Meeting, September 2019, Heidelberg, Germany